SYNTHESIS AND CHARACTERIZATION OF FUNCTIONAL MATERIALS FOR ENERGY APPLICATIONS

Thesis

Submitted for the Award of the Degree
of
Doctor of Philosophy

In
Applied Physics

Submitted By
Krishan Pal
Enrollment No. 054/12

Under the supervision of
Dr. Khem Bahadur Thapa

Department of Applied Physics
School for Physical Sciences
Babasaheb Bhimrao Ambedkar University
(A Central University)
Lucknow -226025, U.P. (India)

2021

Dedicated to
My Parents and
Teachers

DECLARATION

I, **Mr. Krishan Pal**, hereby declare that this Doctoral Research Work Thesis entitled **"SYNTHESIS AND CHARACTERIZATION OF FUNCTIONAL MATERIALS FOR ENERGY APPLICATIONS"** is my own work carried out under the guidance of **Dr. Khem Bahadur Thapa,** Department of Applied Physics, School for Physical Sciences, Babasaheb Bhimrao Ambedkar University, (A Central University), Lucknow-226025, Uttar Pradesh, India. The matter embodied in this thesis is written by me and has not been submitted to any other university for award of any other Degree or Diploma. This thesis is essentially free from all kinds of plagiarism.

Krishan pal.

(Krishan Pal)

Date: 03/09/2021

Place: LUCKNOW

CERTIFICATE

This is to certify that the thesis titled **"SYNTHESIS AND CHARACTERIZATION OF FUNCTIONAL MATERIALS FOR ENERGY APPLICATIONS"** submitted by **Mr. Krishan Pal** is an original research work and has not been previously submitted in part or full for the award of any other degree or diploma to this or any other university.

The thesis submitted to Babasaheb Bhimrao Ambedkar University satisfies all the requirements as stipulated in the *Doctor of Philosophy (Ph.D.) regulations- 1999 as amended in 2008/2010/2013* and it is fit for submission and evaluation for the award of the degree of Doctor of Philosophy of the University.

Supervisor
Dr. Khem Bahadur Thapa
Department of Physics
Babasaheb Bhimrao Ambedkar University
Lucknow-226025

Date: 03/09/2021

Head of the Department

विभागाध्यक्ष
Head
भौतिकी विभाग
Deptt. of Physics
बाबा साहेब भीमराव अम्बेडकर विश्वविद्यालय
Baba Saheb Bhimrao Ambedkar University
लखनऊ - 226025 उ० प्र० भारत
Lucknow - 226025, U.P., India

ACKNOWLEDGEMENT

First and foremost, praises and thanks to God, the Almighty, for giving me the chance to avail this opportunity and His constant blessings throughout my research work to complete the research successfully.

I would like to express my deep and sincere gratitude to my supervisor **Dr. Khem B. Thapa**, Department of Applied Physics, School for Physical Sciences, Babasaheb Bhimrao Ambedkar University, Lucknow who gave me the golden opportunity to research this wonderful topic. I always debtful for his invaluable suggestions, enthusiasm, and constant encouragement, during my Ph.D. work. His dynamic vision, sincerity, outstanding supervision, inspiration, motivation, and undying patience have deeply inspired me. Throughout my Ph.D, he gave sound advice, good teaching, and a lot of good ideas, which have been highly encouraging. His profound knowledge and aptitude towards science have made me think rationally about my future goals as a physicist. I could not have imagined having a better advisor, mentor, and most importantly such a kind-hearted person for my Ph.D. life.

I extended my grateful thanks to **Prof. Bal Chandra Yadav,** Head, Department of Physics, for providing me the necessary and all kinds of departmental facilities.

Besides my advisor, I must like to show my immense gratitude towards faculty members **Prof. Devesh Kumar, Dr. Anil Kumar Yadav**, **Dr. Ramesh Chandra**, and **Dr. Devendra Singh** for their excellent guidance, constant encouragement, and cooperation, during this work. Their expertise was invaluable in formulating the research questions and methodology.

I would like to express my special thanks to further express my profound gratitude to Research Scholar, for his constant support and guidance throughout my research work. My completion of Ph.D. work could not have been accomplished without the full support of him.

I would likes to acknowledge my labmates **Dr. Asish Kumar** and **Ms. Abhisikta Bhaduri** for their relentless support .

I would like to acknowledge the assistance of all research scholars of our department but special thanks to **Dr. Samiksha Sikarwar**, **Ms. Priyanka**

Chaudhary, Mr. Dheeraj Kumar Maurya, Dr. Narinder Kumar, Mr. Diptarka Roy, who gave me encouragement for doing my work and also for writing thesis. I also acknowledge to research scholars **Dr. Nitu Yana and Dr. Lovekush** from MANIT Bhopal MP, **Dr. Kapil Guleria** from University of Bhopal MP, **Ms. Neha Sharma** from IISER Pune Maharstra for encouraging support to enhance my research carrier. I had very useful discussions with them on both academic and non-academic matters and also I had enjoyable time with them.

I acknowledge to University grant commission UGC NEW DELHI, for providing me financial support from Rajiv Gandhi National fellowship (RGNF) **F1-17.1/2015-16/RGNF-2015-17-SC-UTT-25301**.

I sincerely thank all teaching and non-teaching staff members of department of Physics for their valuable and timely help throughout my work.

Besides, I do not find words to express my deepest appreciation to my godlike parents **Mr. Jwala Prasad** and **Mrs. Kishori Devi**. You are always there for me in all situations of my Ph.D. life. My family members **Dr. Naresh Kumar, Mrs. Beena Kumar, Mr. Hariom Singh, Mrs. Jagveer Devi, Dr. Pawan Kumar, Dr. Suman Kumar** gave me uncondtional supports and guidance to my life during Ph.D. course. I sweet thanks to **Preeti Singh, Prakhyati Singh, Pragati singh, Rudrakshi Singh and Pari**, whose give me supports and appreciation me to be happy and healthy environment, at critical situation in my life. Without their unwavering support and blessings, I could not think of my completion of Ph.D. work.

Krishan Pal

LIST OF PUBLICATIONS

Published manuscripts

[1] **Krishan Pal**, Pawan Singh, Abhishikta Bhaduri and Khem B. Thapa, Current challenges and future prospects for a highly efficient (> 20%) kesterite CZTS solar cell: A review, ***Sol. Energy Mater. & Sol. Cells.,*** 196, 138–156, 2019.

[2] **Krishan Pal**, Khem B. Thapa, and Abhisikta Bhaduri, A Review on the Current and Future Possibilities of Copper-Zinc Tin Sulfur Thin Film Solar Cell to Increase More Than 20% Efficiency, ***Adv. Sci. Eng. Med***., 10, 1-7, 2018.

[3] Shweta, **Krishan Pal** and Khem B. Thapa, Synthesis and characterization of ZnO nano-particles for solar cell application by the cost effective co-precipitation method without any surfactants, ***AIP Conf. Proc.,*** 2142, 030008-1–030008-4, 2019.

[4] **Krishan Pal,** Dheeraj Kumar Maurya, Priyanka Chaudhary, Khem Bahadur Thapa, and Bal Chandra Yadav, Co-precipitation Synthesis with a Variation of the Sulphur Composition of Kesterite Phase Cu_2ZnSnS_4 (CZSS) without Annealing, ***Process, J. Phys. Sci.,*** 32(2), 27–39, 2021.

[5] Pawan Singh, Khem B Thapa , Narinder Kumar, **Krishan Pal** and Devesh Kumar, Graphene layers on semi-finite 1D asymmetric periodic structure of Si/Glass materials with defect of nematic liquid crystal for a sensor device, ***Mater. Res. Exp.***, 6, 066209, 2019.

[6] Varsha Gautam, **Krishan Pal**, Narendra Kumar, DR G N Pandey, Bhuvneshwer Suthar, Khem B. Thapa, Sant P. Ojha, Low cost synthesis of ZnO nano-particles, and characterization study for the device of water disinfection, ***AIP Conf. Proc.,*** 2220(1), 020170, 2020.

[7] Roshni Maurya, Pawan Singh, Prabal P. Singh, **Krishan Pal**, Girijesh N. Pandey, and Khem B. Thapa, Absorption and bandwidth properties of graphene based 1D-photonic crystal for THz devices, ***AIP Conf. Proc.,*** 2220, 020084, 2020.

[8] Asish Kumar, Pawan Singh, **Krishan Pal**, Narendra Kumar, Khem B. Thapa, Broadband reflector of 1D photonic crystal containing TiO_2/SiO_2 material at visible region, ***AIP Conf. Proc.,*** 2220(1), 020068, 2020.

[9] Pawan Singh, **Krishan Pal**, Khem B. Thapa, Narinder Kumar, Devesh Kumar, First edition, Advances in Photonic Crystals and Devices: Embedded Liquid Crystal Defect with Graphene Layers in Asymmetric One-Dimensional Photonic Crystal as Sensor Application, ISBN:9781351029421, ***CRC Press,*** Boca Raton Florida, 2019.

COMMUNICATED MANUSCRIPTS

[1] **Krishan Pal**, Priyanka Chaudhary, Ravi Kant Tripathi, Sumit Tiwari, and Khem B. Thapa, B. C. Yadav, Non-toxic, low cost, stable, and auto-cleaned visible photodetector of Tin (II) Sulphide (SnS) nanoflakes for commercial application, ***Mater. Chem. & Phys***., August 2021.

[2] **Krishan Pal**, Ravi K. Tripathi, Khem B. Thapa, Non-peel-off and recombination reducing JABS layer into the hetero-junction Cu_2ZnSnS_4 solar cell: A new approach, ***Asia-Pacific Journal of Science and Technology***, August 2021.

[3] Priyanka Chaudhary, Arpit Verma, Akash Mishra, **Krishan Pal**, E. Ranjith Kumar, B. C. Yadav, Khem B. Thapa, Surbhi Mishra, D. K. Diwedi, Preparation of carbon quantum dot using bike pollutant: Evalution of structural, optical and moister sensing properties, ***Mater. Sci. & Eng.,*** July 2021.

INVITED-TALK/ CONFERENCES/ WORKSHOPS/ POSTER PRESENTATION/ PRIZE

1. Oral presentation in **“International Conference on Nanoscience and Nanotechnology (ICNN-2017)”** organized by BBA, University Lucknow, Uttar Pradesh, India, held on September 22-24, 2017.
2. Poster presentation in **“International Conference on Structure and dynamics of Biomolecules (SDBM-2017)”** organized by D.D.U. Gorakhpur, Uttar Pradesh, India, held on January 27-28, 2017.
3. Participate in workshop, **“Recent Advances and Fundamentals of Nanomaterials for application in the photonics (RAFNAP-2017)”** organized by NIT Durgapur, West Bengal, India, held on February 15-19, 2017.
4. Poster presentation in **“1st North Indian Science Congress NISC-2018, International Conference on Science and Technology for Sustainable Future”** organized by BBA, University Lucknow, Uttar Pradesh, India, held on January 10-11, 2018.
5. Consolation prize for best poster presentation in **“1st North Indian Science Congress NISC-2018, International Conference on Science and Technology for Sustainable Future”** honoured by BBA, University Lucknow, Uttar Pradesh, India, held on January 10-11, 2018.
6. Poster presentation in “**National Conference on Soft Matter**” organized by D.D.U. Gorakhpur, Uttar Pradesh, India, held on March 27-28, 2018.
7. Oral Presentation in **“Sukhsm padarth avam avchatan urja”** organized by BBA, University Lucknow, Uttar Pradesh, India, held on February 1-3 2019.
8. Poster presentation in “**International Conference on Advances in Basic Sciences (ICABS19)**” organized by G.D.C. Memorial college, Bahal (Bhiwani), Hariyana, India, held on February 7-9. 2019.
9. Participate in workshop, **“Sukhsm Padarth avam Sambadh Chatan Urja par online ratsriya sangoshthi”** organized by organized by BBA, University Lucknow, Uttar Pradesh, India, held on September 27-29, 2020.

10. Oral presentation in **“INTERNATIONAL WEBINAR ON NANOSCIENCE & NANOTECHNOLOGY-2020 (IWNN-2020)”** organized by BBA, University Lucknow, Uttar Pradesh, India, held on November 27-29, 2020.
11. Online Short Invited Talk in “**Fifth International Online Conference on Reuse and Recycling of Materials (Polymers, Wood, Paper, Leather, Glass, Metals, Ceramics, Semi Conductors, Water etc) and their products (ICRM – 2020)**” organized by Mahatma Gandhi University Kottayam, Kerala, India, held on December 11-13, 2020.

PREFACE

Modern civilization is fully dependent on materials. Materials influence our daily life of every segment of transportation, housing, clothing, telecommunication, food production, etc. Earlier civilizations have been designated by the level of the development of their materials such as the Stone Age, Bronze Age, and Iron Age**.** The twenty first century is an era of technological development of functional and smart materials for sustainable energy applications. Researchers in materials science and engineering under *Science, Technology, Engineering and Mathematics* are looking at functional materials of metals and alloys, polymers, ceramics and composites as energy materials. The energy materials based on nanostructured functional materials are developing and considering the best materials for the manufacture of sustainable energy devices. To meet the demand for low cost and eco-friendly sustainable energy, energy materials and their new technologies are needed to be developed. Today, researchers around the world are focusing on the development of efficient and cost effective energy devices to meet the challenge of increasing energy demand. In addition to this, the energy devices must be fabricated in such a way that such devices are to be for environmental friendly. In this direction, new methods are being explored to convert solar energy into electrical energy by photovoltaic (PV) solar cells, which is the best way to obtain plentiful sustainable energy. The design and manufacture of PV solar cells are being used as the low cost and eco-sustainable devices. To develop innovative approaches, researchers are striving to engineer the low-cost, bearable and highly efficient equipment using abundant materials. Therefore, we have also attempted to study how functionalized ZnO, SnS, CZTS materials using abundant materials are synthesized by low-cost synthesis processes. Based on the literature survey of functional materials for energy devices, we focused our study on the selection of functional materials (FMs) containing environmentally friendly, non-toxic, and low-cost constituent elements as well as environmentally friendly synthesis methods.

The brief introduction of the functional materials for synthesis and characterization for potential applications in chapter first. Here, we have given the study of the historical background of functional materials especially energy materials, and also their technical development in the field of Materials Science and Engineering. This chapter mainly focuses on the photovoltaic functional materials such as CZTS, SnS, ZnO, CdS, etc., and also describes the CZTS phases, electronic band structures, and important parameters to enhance the photovoltaic efficiency. CZTS is an I_2-II-IV-VI_4 group functional material. The various types of effective parameters in photovoltaic applications are discussed and resoluted the hurdles of efficiency of solar cells problems. Besides this, we also try to find out the issues of the Kesterite materials based on the structure, band structure, electronic structure and studied how to get more than 20% efficiency of solar cells using the different buffer layers.

Synthesis methods and Characterization techniques for energy materials are discussed in chapter second. The synthesis methods especially Co-precipitation Spray Pyrolysis and Hydrothermal/Solvothermal methods are described and explained that how these methods are suitable to synthesis the functional nanomaterials for photovoltaic purposes.

Chapters three and four deal with the synthesis of functional material II-VI and I_2-II-IV-VI_4 (ZnO and Cu_2ZnSnS_4) nanomaterial are synthesised by copriciptation without any surfactants and characterise the materials for window layer and absorber layer in solar cell applications. In the synthesis mechanism, the functional materials are synthesized without any surfactants and vacuum/noble gases, which makes it an economically low-cost method in comparison to the other methods. The spherical NMs of CZTS has enhanced the solar energy conversion and this is an appropriate property for photovoltaic materials. These chapters suggests that the ZnO and CZTS powders without any surfactant are beneficial for commercial productions as well.

Synthesis and characterization of functional material (IV-VI) SnS for energy applications is discussed chapter five. The SnS NMs by low-cost precipitation method, thin-film is fabricated with help of the self-made spray pyrolysis method. The first time, the grown thin films by SPM method are found to have hydrophobic and scratchproof nature of SnS nano flakes. The synthesis of SnS thin film for photodetector by the SPM route has found with low response/recovery time in comparison to the CVD route The stability of the SnS photodetector is also found to be stable for around one year. The SnS thin film also resolves the usual problem of thermionic and diffusion losses, and recombination; and SnS thin film can be used as a

JABS layer in the hetero-junction device with structure Ag/ARC/Al-ZnO/i-ZnO/CdS/**SnS**/CZTS/ITO.

Conclusion and future prospects of this research work has been discussed in chapter six. In this chapter, we suggests that the functional materials can be used to resolve the issues of stoichiometry phase, toxic environment, time taking processes, and cost of materials and synthesis methods. Among these problems, thermionic and diffusion loss, and recombination, are also resolved by selecting suitable functional materials and techniques. For the synthesis of the suitable functional materials, we have explained the synthesis methods having low cost and suitable characterization techniques for the as-synthesize and their applications in fabricating energy devices.

My studies reveal that the CPT and SPT are the best synthesis methods for the low-cost, high efficient and eco-friend functional nanomaterials (ZnO, CZTS and SnS) for optical and electronic devices. The photovoltaic solar cells and hydrophobic photodetectors may be fabricated with these elements and synthesis methods. This technology may also be adopted to industry for mass production of the photovoltaic solar cells and hydrophobic photodetectors, because the ratio of the performance and the cost of the material may be high by choosing the low cost, non-toxic and eco-friendly elements, and ecofriendly synthesis processes for structural modification.

LIST OF FIGURES

LIST OF TABLES

TABLE OF CONTENTS

Chapter 1 Introduction

Page No.

Chapter 2 Synthesis Methods and Characterization Techniques for Functional Materials Page No.

Chapter-3 Synthesis and Characterization of II-VI group (ZnO) Functional Material without any Surfactant for Photovoltaic Applications

Chapter 4 Functional Material (I_2-II-IV-VI_4) Cu_2ZnSnS_4 Synthesis without Vacuum Annealing for Photovoltaic Applications

Chapter-5 Synthesis and Characterization of Functional Material (IV-VI) SnS for Energy Applications Page No.

Chapter-6 Conclusions and Future Prospects **Page No.**

CHAPTER 1

Introduction

Chapter 1

Introduction

1.1 Introduction

Modern civilization is fully dependent on materials. Materials influence our daily life of every segment of transportation, housing, clothing, telecommunication, food production, etc. Earlier civilizations have been designated by the level of the development of their materials such as the Stone Age, Bronze Age, and Iron Age**.** From time to time, we discovered materials and techniques for producing materials that had superior properties than to those of natural ones. These new developing materials were potteries and various metals and alloys. The modified characteristics of materials were not the relatively recent times that scientists came to understand the relationships between the structural elements of materials and their properties. Today, more than three lakhs of different materials have evolved with rather specialized characteristics that meet the needs of our modern society and materials are included metals, metallic oxides and chalcogenides, plastics, glasses, and fibers, etc. These materials are functionalized with the other materials in terms of the structures to enhance the properties of materials as per their requirement.

In this chapter, we have given the study of the historical background of functional materials (FMs) especially energy materials and also their technical development in the field of materials science and engineering. Materials Science and Engineering (MSE) have played a vital role in the development of advanced materials devices by modification of the compositions and their structures.

1.2 Functional Materials

Functional materials (FMs) are characterized as those materials, which have particular native properties and functions of their functional property like ferroelectricity, piezoelectricity, and magnetism or energy storage and optics for ultrafast devices. FMs are found in all classes of ceramics, metals, polymers, and organic molecules as well as composite materials. Functional materials are often used in electromagnetic applications from kHz to THz and the plasmonic properties of metals at optical frequencies assume particular importance in many applications from sensors to metatronics. The particular native properties of the functional materials have been used in energy devices such as electro and magneto-caloric materials, energy storage, and solar harvesting functional materials. Therefore, today all types of materials viz. ceramics, metals, polymers, and hybrid materials are considered the advanced materials as the functional materials **[1]**. Now, we discuss the classification of the function materials in MSE.

Figure 1.1: Classification of functional materials based on applications.

1.3 Classification of Functional Materials

In materials science, there are different ways of classification of materials such as applications basis, solid materials basis and structure-properties basis. Based on groups that possess different structures and properties, materials are categorized into five groups as Metals and Alloys, Ceramics & Glass-ceramics, Polymers (plastics), Semiconductors, Composite materials **[2]**. Based on the functional classifications, the materials are classified on their performances like mechanical (structural), biological, electrical, magnetic, and optical that are the most important functional properties of the materials. The classification of FMs based on applications is shown in **Fig. 1.1.** The energy conversion PV cells and energy storage devices based on functional materials have been already developed such as amorphous silicon (a:Si:H), Cadmium Telluride, Tin Sulphide (SnS), Cadmium Sulphide (CdS), Copper Indium Gallium Selenide (CIGSe), Copper Zinc Tin Sulphur (CZTS), Copper Zinc Tin Selenide (CZTSe), Copper Tin Sulphide (CTS), etc. But today researchers are looking forward to low cost, high efficiency and eco-friendly devices based on functional materials. The energy materials and nanotechnology of the functional materials may fulfill the needs of human beings in modern civilization.

1.4 Energy Materials and Nanotechnology

Researchers are trying to understand the physics and chemistry of materials by study large and complex structures. In this process, a fundamental building block in the structure is the key parameter to know the functional properties. These new structures are designed by the constituent's atomic displacement and formed a new shape of FMs. Due to this arrangement of atom's position or a certain shape of crystallites, the mechanical, electrical, magnetic, and other properties of FMs are changed and modified and the characteristics of such materials are termed as "nanotechnology". The word nano prefixes 1nm to 100nm of the structural dimensions of the crystallites that are characterized by microscopy techniques **[3].** From nanometer to micrometer scale dimensions, new materials with molecular or atomic precision are broadly discovered for electrochemical energy conversions, catalysis, nano-electronics, and bio-engineering to molecular recognitions and self-assembly of nanostructures. The synthesis of such nanomaterials is done by two methods: "***bottom-up and top-down***". These two methods are used to synthesis the functional nanomaterials The functional nanomaterials convert one form of energy to another form of energy and such FMs are used in renewable energy conversion e.g. high performance Photovoltaic (PV) devices. The universe has lots of energy sources on the earth in the form of renewable and non-renewable energy sources.

1.5 Energy Sources on Earth

According to U.S. primary energy consumption of the energy source in 2019, the global energy consumption is about 100.2 quadrillion British thermal units (BTU) **[4].** The historical features of average total energy consumption development at the global are shown in **Fig. 1.2**, It predicts that the Renewable, Nuclear, Petroleum, Natural gas, Coal energy sources are the major energy sources on earth.

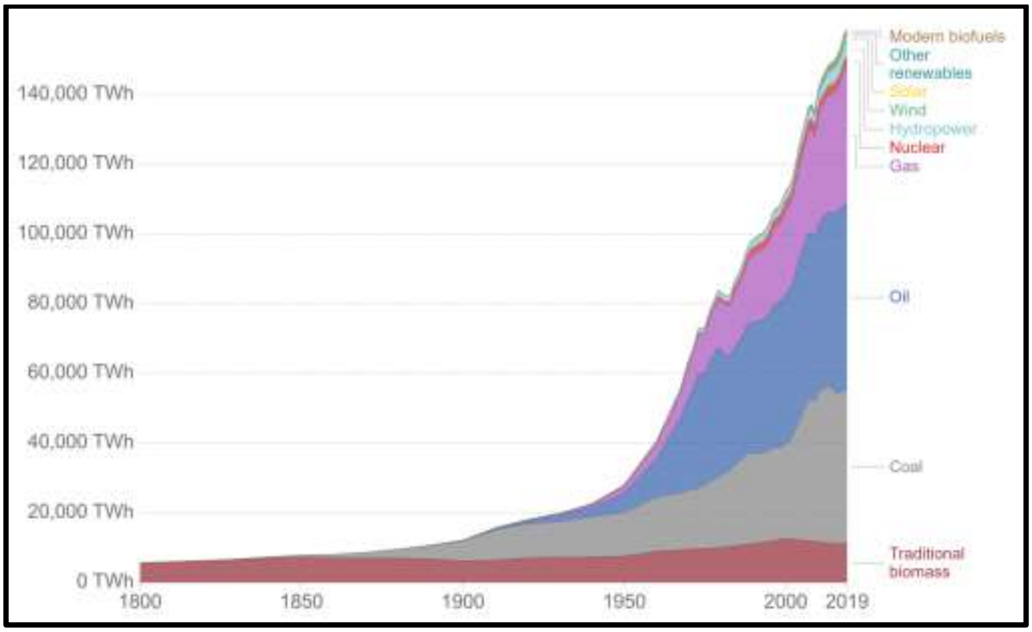

Figure 1.2: The historical energy consumption from 1950 to 2020, [*Source: Vaclav Smile, Energy Transitions: Global and National Perspectives. & BP Statistical Review of World Energy, 2017, copyright permission]*.

This data also confirms that the demand for renewable energy sources consumption has grown exponentially in comparison to other non-renewable energy sources. The availability of renewable sources are sufficient on earth in the form of the sun, wind, water, air, etc. These renewable energies are not popular in daily use in lack of efficient conversion devices. But the sun energy is harnessing by a photovoltaic device and this device is based on the functional nanomaterials, which is also called energy nanomaterials energy devices.

1.5.1 Photovoltaic Cell

The Photovoltaic (PV) cell is a device to generating the electric current (direct) from the solar light using semiconductor nanomaterials/functional nanomaterials. When light is illuminated on the surface of the semiconductor material, excitons (electron-hole pair) are generated and separated the electron-hole from valance band to conduction band by the photon energy. This effect is known as "photoelectric effect" **[5].** In 1839, firstly Becquerel measured the light-dependent voltage (photovoltaic effect) **[6].** In 1954, some researchers of the Bell Laboratory, USA, discovered the *pn*-junction diode semiconductor and accidentally they measured the voltage diode in the ordinary light **[7].** After one year, the same group identified the silicon (Si) *pn*-junction solar cell with 6% efficiency, which was recorded as the highest efficiency in PV cells. In 1960, Nobel laureate Shockley and Queisser established a theoretically fundamental *pn*-junction solar cell with 33% efficiency in the visible spectrum **[8].** This hypothesis was based on the energy band gap of *pn*-junction, illuminated spectrum of light, and thermodynamic parameters.

In 1963, Cusano fabricated a thin film of Cadmium Telluride (CdTe) with 6% efficiency **[9].** After this synthesis of Cadmium Telluride, the US satellite program used to power the satellite with this efficiency of PV cell. At that time photovoltaic was the most demanding field for the space mission. In 1970, Nobel laureates Alferov designed a heterojunction photovoltaic cell, which was a new idea for the hetero-junction nanomaterials [**10].** In 1973, IBM, USA developed GaAs heterostructure with 13% efficiency **[11].** In the same year, another event, *Cherry Hill conference, New Jersey USA*, held and the US government support to the US Department of energy organization, for photovoltaic research. This year consider as the scientific evaluation in renewable energy **[5].** In 1980, the solar industries started to manufacture the PV modules of Si *pn*-junction in the USA, JAPAN, and EUROPE. From 1990, Arco Solar, USA Company, started to commercialize the PV cells based on Crystalline Si, amorphous Si, and $CuInSe_2$, etc.

In the PV operation, the photoelectron generations are generated where PV cell or solar cell is fabricated a junction of the doped semiconductors (p-type and n-type). Every semiconductor materials of the solar cells obey and require the following processes for conversion of the solar energy into the electrical energy;

(i) The incident illuminated photon’s must have 1.1-2.0 eV energy.

(ii) The generation of the electron hole-pairs.

(iii) The separation of the electron-hole pairs before the recombination.

(iv) The collection of the photo-generated charges by the metallic contacts or electrode.

The quanta or energy of photons are the part of the sunlight spectrum that is distributed in a range of energy. When photons have substantial threshold energy, free conduction electrons flick from the valance band to the conduction band and produce a “band gap energy”. During this process, bonds break and free to move in a new energy band (conduction band). The schematic diagram mechanism of PV cell for electricity conduction in illumination is shown in **Fig. 1.3**.

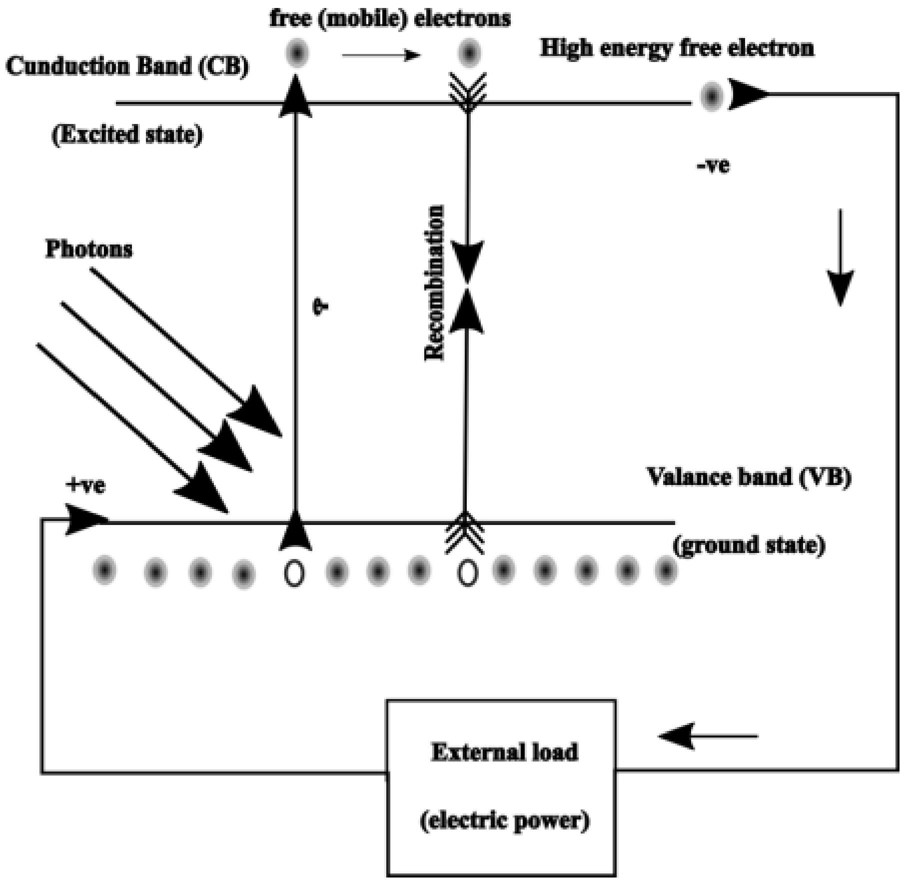

Figure 1.3: Schematic diagram of a solar cell with electronic conduction in a semiconductor in illumination of light.

The **Fig. 1.3** shows that most of the electrons participate in electricity conduction but some of them lose their energy and go to lower energy level. These electrons have the maximum chance to recombine with holes. Carriers recombination may happen through the different modes. The radiative, non-radiative, Shockley-Read-Hall (SRH) recombination are the main hurdles in a photovoltaic cell for electricity generation [**13**]. For instant, semiconductor PV cells are fabricated of the *pn*-junction, called the mind of the solar cell, and the junction has electronic asymmetry. Due to asymmetry of electrons and holes in the opposite direction across the junction in the illumination of light, in this process, a current flows in the short-circuiting lead **[13].** The role of the *pn*-junction in the solar cell will be explained in the next section.

1.5.2 Solar Cell

A solar cell is a large number of panels of PV cells. The solar cell is also an electrical device, which is used to convert optical energy into electrical energy by electronic properties of the semiconductor material. The characteristics of the solar cell are dark current (I_D), short circuit current (J_{SC}), open circuit voltage (V_{OC}), fill factor (FF), which are directly dependent on illumination of light and property of semiconductor materials. For a simple conventional solar cell designing, *p*-type semiconductor material is deposited on a metallic substrate, after that, n-type materials are fabricated on that film carefully without any diffusion. In last, a metallic electrode is fabricated on the n-type materials layer for PV device formation. These electrodes cover film 15% area only for passing the light. However, some researchers reported that the antireflection coating in the remaining 85% area uses to eliminate the problem of reflection. A simple schematic representation diagram is shown in **Fig. 1.4**.

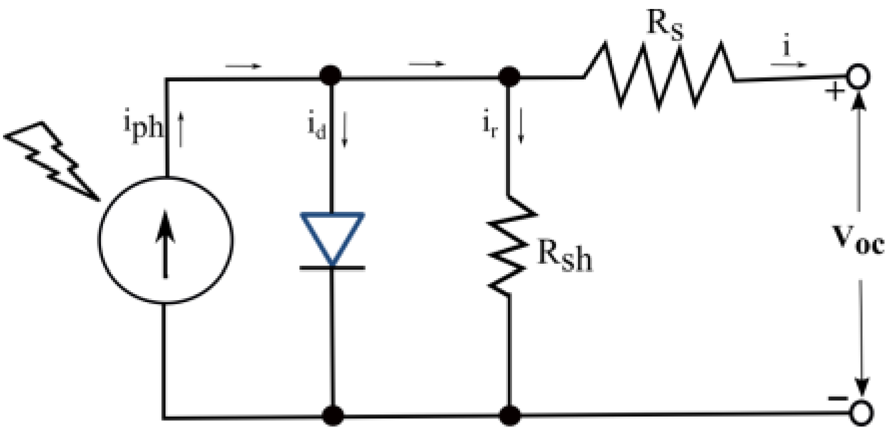

Figure 1.4: A simple representation of schematic circuit diagram of the solar cell (In this, R_s is series resistance and R_{sh} is shunt resistance).

From the above schematic circuit diagram of solar cell [**14**], the load current is given as;

$$i = i_{ph} - i_d - i_r \tag{1.1}$$

where I_{ph} is photocurrent, i_d is diode current and i_r is the current through shunt resistance.

1.5.2.1 Working Principle of Solar Cell: The schematic circuit diagram of a *pn*-junction solar cell is shown in **Fig. 1.5** where the n-type region has negative charge carriers (e^-) in the majority and positive charge carriers (h^+) in minority and the *p*-type region has vice-versa. Generally, *n*-type layer is a thin comparison to the p-type layer, because light can penetrate easily into a thin layer. The penetration depends directly upon the wavelength because the energy of the photons is inversely proportional to the wavelength of the light **[5]**. This energy is given as;

$$E = hc/\lambda \tag{1.2}$$

where h is the plank's constant, c is the speed of light, λ is the wavelength of light. Long-wavelength photon has small energy, which can easily cross the *n*-type layer to reach the *p*-type region.

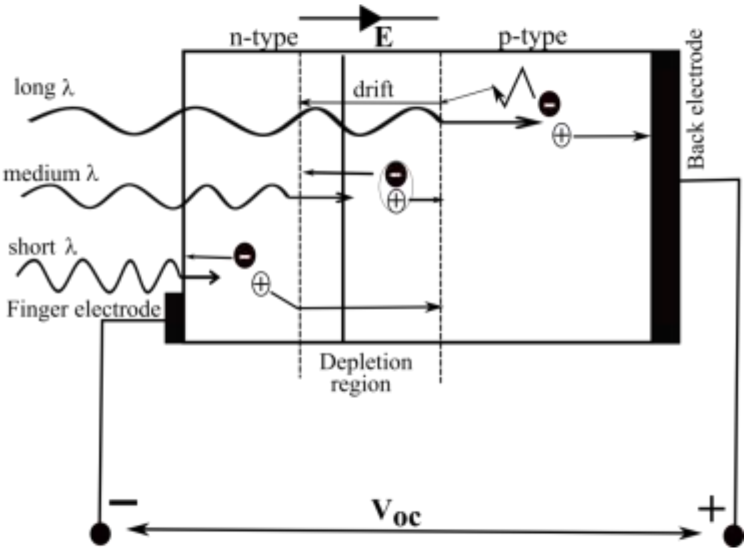

Figure 1.5: Principle operation diagram of the *pn*-junction solar cell.

The e^- and h^+ pairs are generated after illumination. In the depletion area, e^- and h^+ combines, and ions of opposite charge are collected at the junction and formed an electric field. This electric field works to push the electrons to *n*-type region and the holes to the *p*- type region. Metal electrodes collect these charge carriers on both sides of the solar cell. To recombine these charge carriers, the external load is applied in which the current is flowing.

1.5.2.2 I-V Characteristics of Solar Cell: The I-V characteristic of the solar cell is the output i.e. the superposition of the I-V curve in the absence of light (dark state) and presence of light (bright state) **[15].** The I-V curve is generated by the solar cell output in the absence of light (dark current) and the presence of light (photocurrent). The open-circuit voltage (V_{oc}) is given as; $\boldsymbol{V_{oc} = \frac{kT}{q} ln \frac{I_{sc}}{I_0}}$, where I_{sc} is the short circuit current ($I_{sc} >> I_o$) and the general expression for the current production in the solar cell is given as $\boldsymbol{I = I_{sc} - I_0 \left(e^{\frac{qV}{kT}} - 1\right) - I_d}$, where I_d is the diode saturation current **[5].** The solar cell efficiency (η) is given as;

$$\eta = \frac{FF.I_{sc}.V_{oc}}{Power_{incident}} \qquad (1.3)$$

The solar cell efficiency (η) is directly affected with the three important parameters viz. short circuit current (I_{sc}), open-circuit voltage (V_{oc}), and fill factor (FF). These parameters of PV device are determined from the illuminated I-V characteristics, which directly affect the solar cell conversion efficiency (η). The short-circuit current (I_{sc}) is flowed through externally when electrodes are short-circuited in the device. The I_{sc} directly depends upon the illumination light photons flux density. When electrodes of the solar cells are not connected externally, then the charges are collected on the electrodes in the illumination light. A voltage difference is generated on the electrodes, called open-circuit voltage (V_{oc}) and the maximum voltage of the solar cell is found in the forward bias. The V_{oc} depends on the photo-generated current density that is given as;

$$V_{oc} = \frac{kT}{q} \ln\left(\frac{J_{ph}}{J_0} - 1\right) \qquad (1.4)$$

and V_{oc} directly depends on the saturation current (J_0) and the photo-generated current (J_{ph}). However, the saturation current (J_0) depends upon the recombination of the solar cell. The fill factor (FF) is the ratio between the maximum powers to the minimum power which is given as;

$$\text{FF} = \frac{\text{Power output}}{\text{Incident power}} = \frac{J_{mp}V_{mp}}{J_{sc.}I_{sc}}. \qquad (1.5)$$

Based on the working principle and I-V characteristics of the solar cells. The cells are formed by different materials. From micro scale to nano scale, the development of photovoltaic cells are categorised into four generations.

1.6 Generations of Solar Cells

In the materials science, we have to show that the rate of perform and cost always high for sustain the device. So, high performance and low cost of the PV devices are the two key parameters for categrorise to development of the solar cells. Generally, solar cells progresses are categorized into four generations solar cell:

1.6.1 First Generation Solar Cell (1G)

Generally, Si-based solar cells are considered the first generation solar cells and such cells cover more than 80% market of the photovoltaic industry [**16].** The monocrystalline, polycrystalline, amorphous and hybrid silicon solar cells are also considered in this generation. The material’s cost is high and performance is low due to thickness of the devices and recombination reasons.

1.6.2 Second Generation of Solar Cell (2G)

In this generation, the thickness of the device is reduced to less than 2µm and called the thin-film solar cell. Non-silicon-based *pn*-junction solar cells are thin-film solar cells which are fabricated by CdTe, CIGS, CZTS, CdS, and PbS, etc. materials. These materials are more absorber comparison to silicon. That’s why solar cells of these types of materials have probability to enhance the performance but their are some challenges in these cells like use of rare earth elements, high production cost and hazardous fabrication process. Using earth-abundant materials, reducing production cost, and eco-friendly fabrication process, the researchers are trying to resolve these problems and enhancing the efficiency of the photo photovoltaic cells.

1.6.3 Third Generation of Solar Cell (3G)

In this generation, a new variety of materials such as carbon nanotubes (CNTs), silicon nanowires, quantum dots (QDs) are considered. The nano inks are used as thin film deposition for photovoltaic cells and polymers, organic dyes, and conductive plastics materials are also used for photo cells .

1.6.4 Fourth Generation of Solar Cell (4G)

Flexible and foldable solar cells belong to this generation solar cell e.g. 4G polymer solar cells **[17].** In this generation, the hole transport layer of the inorganics materials is used to enhance the photovoltaic activity.

Now, we review the functional materials for the photovoltaic cell to keep in mind that the solar cell must be low cost, less time-consuming in synthesis and eco-friendly devices. Such photovoltaic cells can be used to fabricate in 2G solar cells.

1.7 Review of Literature

The energy crisis is the most captivating problem in this world for the 21st century. Coal, Oil, Gas are three main energy sources that fulfill 80% demand of the energy consumption of the world **[18].** Only twenty percent of the world's energy consumption fulfil by renewable energy sources. According to the Impact report 2019 on renewable energy **[19],** Tesla’s solar roof plans have come to a revolutionary change in the energy industries. Indeed, many governments of the world want pollution-free vehicles and the renewable energy in the source can be achieved the target. The idea behind it is to utilize solar energy, which is easily available, directly accessible on earth freely and it will save the earth’s atmosphere from pollution. Solar energy is incident directly $1.2\text{x}10^5$ Tera Watt (TW) on the whole earth **[20].** The amount of energy is varied from place to place, time to time, and weather-to-weather due to the orbitory and spinning motion of sun and earth **[21].** The photon intensity versus wavelength graph of the energy spectrum for solar insolation is shown in **Fig. 1.6.** The **Fig. 1.6** shows that UV- Visible wavelength range has the maximum intensity of the photons in the insolation light. The intensity of photon is a parameter to enhance the absorption of the materials, which is constantly varied. Shockley-Queisser is already theoretically proposed that single-junction solar cells have 33% energy conversion characteristic in UV-Visible light [**8**].

The emerging new technology of photovoltaic cells prefers to form a device with cost-effective, long durable, and high efficiency. This has been observed that 1st generation solar cells have no more probability to increase the efficiency because silicon is less absorptive material. To increase the absorption, 2nd generation solar cells based on inorganic materials are useful, which is described in the next section of this chapter.

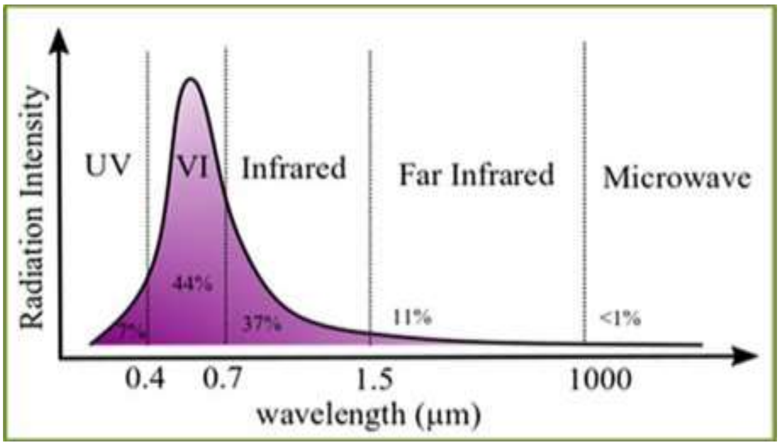

Figure 1.6: Radiation intensity versus wavelength of photons with the percentage in the solar spectrum.

1.7.1 Inorganic Energy Materials for Solar Cell

In second generation *pn*-junction solar cells, lots of organic and inorganic materials are considered to enhance the photovoltaic property. The main components of such cells are absorber, buffer, window and anti-reflection coating (ARC), and metallic electrodes. The Graphene, MXenes, and CNTs, etc. organic materials are also used to fabricating the efficiency of solar cells. Metallic electrode materials Silver (Ag), Gold (Au), Nickel (Ni), Aluminum (Al), and sometimes Al+Ni are used in photovoltaic cells because these materials have high work function and high mobility free electrons **[22**]. More than 30% of light is reflected from the silicon solar cell surface. Using antireflection coating (ARC) layers the reflection is reduced and increased the absorption of light. The photovoltaic performance is enhanced by using ARC of SiO_2, ZnO, TiO2, SiN_x, MgF_2, which has high anti-reflection and transparent properties in window layer of solar cell[**23, 24].** The MgF_2 layer has a wide bandgap and it is used in CIGS solar cells and improved photocurrent density (J_{ph}) by 6.8% in comparison to without ARC [**25].** Generally, single-layer antireflection coatings is not capable of covering the solar range of the solar spectrum because multilayers cover the wide band of spectrum. So, the double layer of MgF_2/SiN_x is used to cover the solar range and wide bandgap with transparent property **[26].** In the double-layer antireflection coating, higher (2.2~2.6) to lower (1.3~1.6) refractive index has used at the bottom layer to upper layers **[27].** Other than ARC layer in a solar cell, there are window layer, buffer layer, junction absoption (JABS) layer, the absorber layer, and metallic contacts which are discuss below;

1.7.1.1 Window Layer: The window layer is used to reduce the recombination and put below the antireflection layer because incident photons are absorbed by this layer. The window layer has a wide bandgap (~ 2.6 eV) of oxide materials such as Sn, In, Zn, and Cd metals oxide. Hence, the window layer is made of several metal oxides, which are transparent and suitable for band structure in the solar cells. For instance, ZnO and Al:ZnO are frequently used materials in the window layers **[28].** The window layer has a small thickness (60nm ~ 80nm) compared to the absorber layer to reduce series resistance in solar cell devices.

1.7.1.2 Buffer Layer: The buffer layer is used to reduce the recombination at the junction interface. Generally, buffer layer of CdS, ZnS, etc. are used as the n-type semiconductor of Kesterite solar cells for most probably the highest efficiency. The toxic CdS buffer layer material is replaced with the Zinc oxysulfide (Zn(O,S)) in CIGS-based solar cells, which is a promising non-toxic n-type material [**29, 30**]. Because Zn(O,S) has a suitable conduction band offset (CBO) in the p-n junction interface band structure of solar cells [**31, 32**]. The tunability of the band is the special characteristic of the buffer layer. The “cliff” type band i.e. Ec (absorber) > Ec (buffer) in the energy band diagram forms interfacial recombination [**30, 33, 34**]. The spike type structure E_c (absorber) < E_c (buffer) in the energy band diagram that blocks photocurrent collection for CBO larger than 0.5 eV [**35, 36**]. Recently, the buffer layer material CdS is formed “spike” type band structure in the Kesterite solar cells, and Kesterite CZTSSe (p-Type) heterojunction solar cells have been reported the 12.6% efficiency due to spike type structure while CIGS solar cells have already been reported the 22.6% efficiency.

1.7.1.3 Junction-Absorber (JABS) Layer: JABS layer is an interfacial layer between the buffer and absorber layers in hetero-junction solar cells. This layer is used to resolve the cliff-type problems, which role-play the recombination losses at the junction in the Kesterite solar cells. The thin layer of Carbon nanotubes (CNTs), Graphenes, MXenes, SnS nano-flakes can be used as JABS layers because these organic materials are the unique feature of the breathing mode of cylindrical and 2-D type molecules. The breathing characteristics of molecules can control illumination in the range of the wavelength of photons and increase the absorption, reducing the heating and reflection. Another best solution is SnS (indirect bandgap) nano-flakes for preventing the recombination losses, which traps the light and increases the absorption coefficients.

1.7.1.4 Absorber Layer: The absorber layer of chalcogenide materials is used in *pn*-junction solar cells to enhance the concentration of charge carriers because the absorber layer has a high absorption coefficient (α) more >10^4. The form of chalcogenide materials is $CuXA_2$ (where X= In, Sn, Ga, Al; A = S, Se, Te), which are mostly used for photovoltaic purpose **[37]**. There are several absorber layers for solar cells but some of them are discussed here:

1.7.1.4 (a) Cadmium Telluride (CdTe): CdTe is a photovoltaic material because it has a large absorption coefficient (>10^4cm^{-1}) **[38],** direct bandgap (1.45eV) [**39**]. CdS heterojunction type of solar cell device had the highest efficiency of 22.1% [**40**], but it has a drawback of the toxicity of the CdTe due to issue of the telluride scarcity.

1.7.1.4 (b) Cu(InGa)Se$_2$ (CIGS): CIGS is chalcopyrite semiconductors like $CuInS_2$, $CuIn_xGa_{1-x}Se2$, CuInSe2, etc. and CIGS is suitable for PV applications having direct band gaps and high optical absorption coefficients. In 1974, first time, CdS/$CuInSe_2$ junction solar cell was fabricated and about 4.5% efficiency of CIGS was reported [**41, 42**]. Today, the quaternary compound $Cu_2InGaSe_4$ (CIGS) is the best commercialized chalcopyrite reported with 22.6% efficiency [**43**].

1.7.1.4 (c) Tin Sulfide (SnS): SnS is IV-VI group FMs with high absorber, earth-abundant, non-toxic and suitable optical band gap for optoelectronic purposes. It is a layered structure compound similar to the CNTs or Graphene [**44**] and is used as an absorber layer (p-type). The power conversion efficiency of the SnS p-type absorber layer solar cells is 32% that is the highest efficiency compared to silicon solar cells **[45]**. The functional material SnS has an indirect band gap in thin film and a direct band gap in thick film form.

1.7.1.4 (d) Kesterite Cu_2ZnSnS_4 (CZTS or CZSS): Kesterite solar cells are proposed to solve the challenges of CIGS cell technology. The challenging problems in CIGS are using rare lelements, toxicity, non-ecofriendly methods. In its solutions, Indium is replaced with Zn and Sn earth-abundant materials. First time, the CZTS material-based photovoltaic cell was reported in 1988 and fabricated the CZTS photovoltaic device with 0.7% efficiency in 1996 **[46].** The record efficiency of CZTS material-based photovoltaic cells with 12.6% was reported in 2014, which is the highest in pure Kesterite form **[47]**.

1.7.2 Kesterite Structure

The Kesterite CZTS is a quaternary compound, which is derived from parents group II-VI Zinc blende compounds. The II-VI group semiconductor functional material, ME (M = Cd, Zn, Hg; E = S, Se, Te) Zinc blende compound is functionalized with II-group atom substituted by two atoms: one atom of I-group and one atom of III-group atom. The functionalized compound is formed ternary I-III-VI$_2$ semiconductor i.e. CuInS$_2$ chalcopyrite.

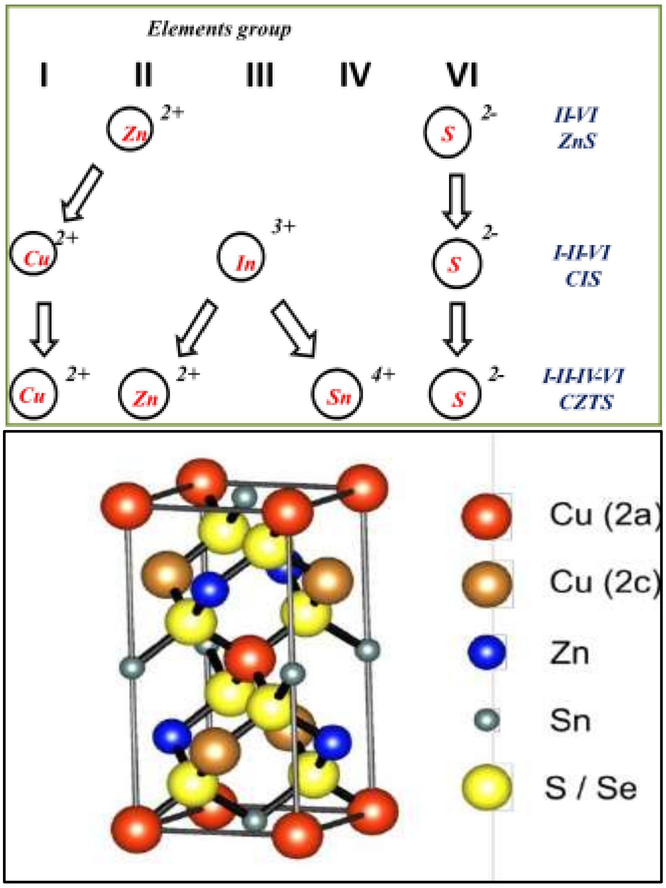

Figure 1.7: (a) Schematic diagram of progression of Kesterite materials from II-VI to I-II-IV-VI compound, and (b) The functional material I-II-IV-VI (Kesterite) unit cell CZTS.

The scarcity and rare earth element with availability ~0.049 ppm only on earth of the atom Indium of the III-group is a crucial issue. So, III group atom Indium (6+) is replaced by I-group atom Zinc (+2) and II group atom Tin (+4) and formed I_2-II-IV-VI_4 compound. The functional material compound I_2-II-IV-VI_4 is quaternary compound and has one form Kesterite Cu_2ZnSnS_4 [**48**]. The functionalized quaternary compound from II-VI to I_2-II-IV-VI_4 is shown in **Fig. 1.7 (a).**

The Cu_2ZnSnS_4 crystallizes are classified into two main phases: (i) Kesterite (KS, space group $I\bar{4}m$), (ii) Stannite (ST, space group I2m) which are observed by the experiments **[49-52].** The first principle study shows that the Kesterite is the more stable compound as compared to the mono-crystalline Cu_2ZnSnS/Se_4 stannite structure and found that the stannite phase has slightly higher energy than the Kesterite **[53].** The copper and zinc atoms are in an alternate position (d-wick-off position) of the space group; and there is an equal probability to take alternate statistically occupied positions in KS form of CZTS [**54].**

The most energetically favorable structure of CZTS was accepted to be the Kesterite structure is shown in **Fig. 1.7 (b).** The **Fig. 1.7 (b)** shows that there are two alternating cationic planes: one with Sn and Cu, and another with Cu and Zn. The S and Se anionic planes separate these cationic planes. There may be the oxidation probability by the constituent elements i.e. Cu^+, Zn^{2+}, Zn^{4+}, and S/Se^{2-}. Chen et al. [**55]** analyzed the bandgap of all probable defects of $Cu_2ZnSnSe_4$ and estimated levels by density functional theory (DFT) simulations**.** It also confirms that the Kesterite structure is more stable than the Stannite structure **[56, 57].** More study on the variation of S and Se quantities, the lattice parameters variation is shown in **Tab. 1.1**.

Table 1.1: The lattice constant and the bandgap of CZTS and CZTSe in the tetragonal unit cell of the Kesterite structure:

Compound	**Conductivity**	**a (A^0)**	**c (A^0)**	**Band gap (eV)**	**Ref.**
Sulphide	p-type	5.427	10.840	1.5	[58]
Selenide	p-type	5.40	10.846	1.0	[59]

Tab. 1.1 shows that the CZTSe has a large size in comparison to CZTS because Se has large size in comparison to S. More comparative study of the chalcogenide materials like CZTS, CZTSe, CZTSSe, CIGS, CIGSe are reviewed with various parameters which are helpful to photovoltaic study in **Tab. 1.2.**

Table 1.2: The comparative study of chalcogenide materials for a photovoltaic cell:

Properties	**CZTS**	**CZTSe**	**CZTSSe**	**CIGS**	**CIGSe**	**Ref.**
Lattice constants (a, c) A^0	a=5.427, b=10.840	a=5.40, b=10.846	a=5.40 b=10.846	*a* = 5.6-5.8, *c* = 11.0-11.5	*a* = 5.6-5.8, *c* = 11.0-11.5	[58, 59]
Space group	$I\bar{4}$/I42m	$I\bar{4}$/I42m	$I\bar{4}$/I42m	$I\bar{4}2d$	$I\bar{4}2d$	
Crystal structure	Tetragonal	Tetragonal	Tetragonal	Tetragonal	Tetragonal	[60, 61]
Density (gm/cm^3)	4.56	4.56	4.56	5.7	5.7	[60]
Bandgap (eV)	1.4-1.5	1.0	1.4-1.5	1.0-1.7	1.0-1.7	[61, 62]
Crystal energy (meV/atom)	2.86	2.86	2.86	--	--	[63]
Absorption coeff. (cm^{-1})	10^4	10^4-10^5	10^4-10^5	10^4-10^5	10^4-10^5	[62]
Carrier concentrations (cm^{-1})	10^{15}-10^{20}	10^{15}-10^{20}	10^{15}-10^{20}	10^{17-18}	10^{17-18}	[64]
Carriers lifetime majority/minority (ns)	15/2.5	15/2.5	15/2.5	250	--	[65]
Current density (mA/cm^2)	10^{-6}-10^{-3}	10^{-6}-10^{-3}	10^{-6}-10^{-3}	10^{-8}	--	[66]
Melting point (^{0}C)	990	990	990	1,070-990	1,070-990	[67]
Efficiency (%)	8.4	10.1	12.6	22.6	--	[68-70]

Tab.1.2 shows that the maximum properties e.g. bandgap, crystal structure, absorption coefficient, carrier concentrations and lattice parameters of the Kesterite are similar to the CIGS. However, CIGS based solar cells are already commercialized in the market. Beside these, the charge carrier concentration and current density of the Kesterite are slightly better than the CIGS, which is the positivity in CZTS for photovoltaic. The main factor of the high efficiency of CIGS is the charge carrier's lifetime (~250 ns). The lifetime of the charge carrier's shows very low recombination rate in the illumination. On the other hand, CZTS has a very low charge carrier lifetime (2.5/15 ns) and showed the very high recombination rate. The major problem of this single phase CZTS is resolved by single phase synthesis of pure CZTS materials. After that CZTS could be the counterpart of the CIGS. For this, the physical, chemical and structural properties of the CZTS are compared with the CIGS as well as the others compounds like CIGSe, CZTSe, and CZTSSe, as tabled in **Tab. 1.2.** The CZTS based photovoltaic cell has low efficiency, but this can be enhanced by the modification of structure and phase.

The kesterite has the crystalline structure within the Cu–Zn layers with a disorder at z = ¼, and ¾, which is experimentally observed **[71]**. The KS and ST structure shows the tetragonal structure with different arrangements of Cu and Zn lattice positions. The KS-type structure has the cation layers Cu-Sn, Cu-Zn, Cu-Sn, and Cu-Zn alternate at z = 0, ¼, ½, and ¾, respectively, whereas Zn-Sn layers alternate with Cu-Zn layers in the stannite-type structure. In KS and ST-type structures, Sn and S are occupied the same lattice positions and formed a certain phase.

1.7.3 Phase of Kesterite

The synthesis of single phase of quaternary chalcogenide compound (I_2-II-IV-VI_4) is a complicated task because of the existence of the multi phases in the form of secondary and ternary phases. These phases influence the histrionics change in the property of the Kesterite.

In the synthesis of the CZTS, some phases are found like quaternary (Cu_2ZnSnS_4), ternary (Cu_2SnS_3), binary compounds (CuS, ZnS, SnS, Cu_2S, SnS_2). The properties of secondary and ternary phases like electronic, optical and structural, etc. are compered with the properties of quaternary phase CZTS in **Tab. 1.3**. The effects of these parameters on solar devices are described in **Tab. 1.3**.

Table 1.3: The comperative characteristics of the secondary, ternary and Kesterite phases are given below ***[72]***:

Properties	**CZTS**	**ZnS**	**CuS**	**Cu_2S**	**SnS_2**	**Cu_2SnS_3**
Band gap (eV)	1.4-1.5	3.54-3.68	1.55	1.21	2.2	0.98-1.35
Structural properties	Kesterite type $I\bar{4}$	Sphalerite & Wurtzite $I\bar{4}3m$	Hexagonal crystal	Chalcocite	Rhombo-hedral	Cubic and Tetragonal
Electrical properties	Semi-conductor, p-type	Insulator, p-type	*p*-type	metal like, highly defective	*n*-type	*p*-type
Effect on solar cell	Absorbing material	Active area/ photocurrent reduce	Positive response	Short the solar cell	*n*-type, forms diode and barrier for carrier collection	Affect carrier Collection at electrode/ V_{oc}
Removal of Secondary phases		ZnS:HCl, ZnSe: ($KMnO_4+H_2SO_4$) / Na_2S Etching	KCN	KCN	KCN Etching	KCN Etching

Tab. 1.3 shows that binary phase ZnS is the major problem because it is generally formed during synthesis at low temperature and insulator type (Bandgap ≥3 eV) phase. To optimize the suitable phase for photovoltaic purposes, it is compulsory to take one parameter constant and varying other parameters **[73].** Several research works have been done on the Kesterite with the variation of the composition of the element, temperature, and pressure **[72].** The variation of these parameters affects the performance of solar cell because these effects are reduced the recombination loss, and increased the charge carriers by the defects formation inside the materials. Hence, the growth of the single-phase of Kesterite can control some phases and defects by the limitations of elements composition ratio Cu/(Zn + Sn) and Zn/Sn. There are two

ways: (i) either Cu poor or (ii) Cu rich, that is considered for better performance of the solar cell because it changes the composition ratio.

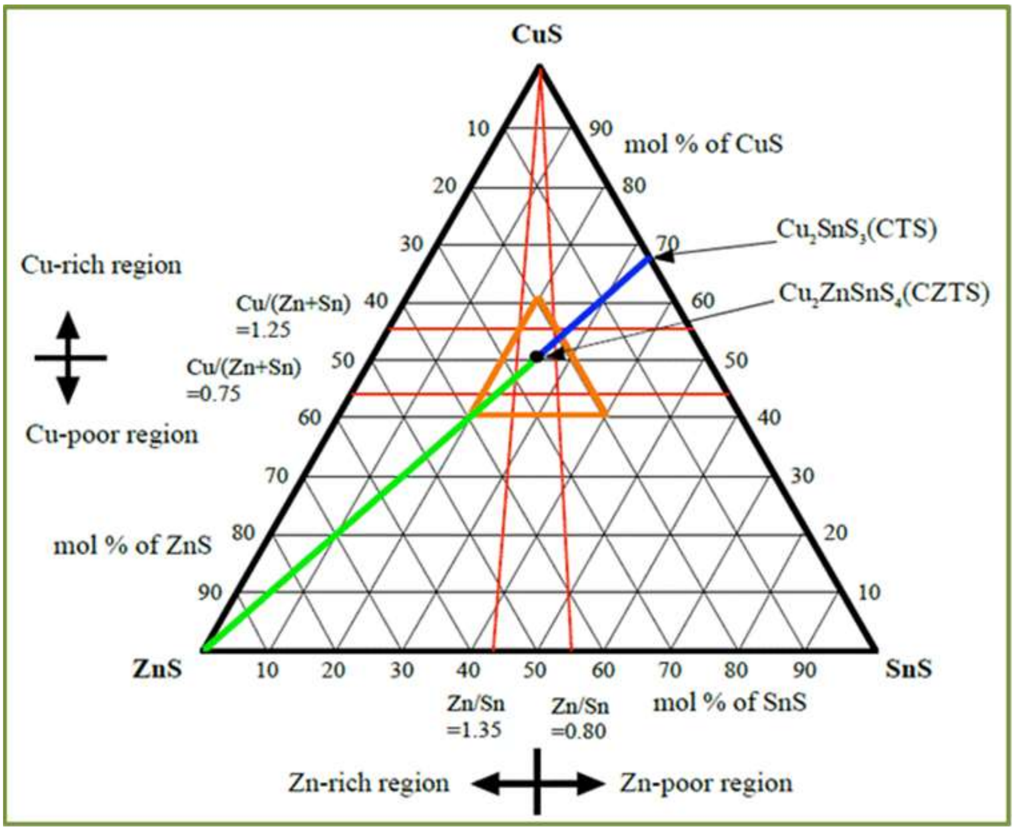

Figure 1.8: Phase diagram of the CZTS pseudo-ternary system is consists of CuS, ZnS, SnS with a ratio of 50:25:25, respectively.

The single-phase formation of Kesterite is found in the narrow range of chemical energy, $-0.4<\mu_{Cu}<0$, where phase space is studied by the first principle method **[74-76].** For the stability of CZTS, the formation energy of Kesterite must be −4.21eV and the formation energy of the most probable secondary phase (ZnS) is −1.75 eV. Mostly, the copper defect vacancies with the Cu-poor and Zn-rich conditions are associated with high-efficiency devices. Mitzi et al. **[77]** recommended the conditions of Cu-poor and Zn-rich for the growth of world record highly efficient CZTS,Se device under the equilibrium conditions. Kategri et al. **[78]** investigated the pseudo-ternary phase diagram of the Cu_2ZnSnS_4 system to grow the formation of the Kesterite family and proposed CZTS has a high dependency on composition and temperature and improved the performance of the photovoltaic devices. The pseudo-ternary phase diagram is shown in **Fig. 1.8**.

1.7.4 Electronic Band Structure of Kesterite

The CZTS contains eight electrons around each anion ($4xS^{2-}$) and forms the four covalent bonds with a closed valence shell of cations (Cu or Zn or Sn). The whole system shows a complete system of the quaternary molecule, which has a particular electronic band structure. The electronic band structure has the different density of states for different structure. The density of states of CZTZ and CZTSe are analyzed [**79]** and shown the electronic band structure of CZTS and CZTSe are shown in **Fig 1.9.** The **Fig. 1.9** shows the four symmetry directions of CZTS band structure similar to the CIGS,Se band structure and the dashed lines at zero energy level denotes to the valence band maximum energy. The shifting of electron's atomic energy levels in the CZTS is due to electromagnetic interaction between the electron's magnetic dipole and make the spin-orbit coupling. The spin-orbit interaction represented by the different energy bands, but the index of the bands ($j=v_1$, v_2, v_3, and c_1) refers to spin-independent bands, where c_1 represents the lowest conduction band or conduction band minimum (CBM) and v_1 represents the topmost valance band or valance band maximum (VBM). The chain of explanation of the band structure for I_2-II-IV-VI_4 (CZTS) was found the results with the following points **[80]**:

- The quaternary compound I_2-II-IV-VI_4 semiconductors have the direct bandgap at the Γ-point (the calculated bandgap energy shown in **Tab. 1.4**).
- The top valence band (VBM) has an anti-bonding component of p-d orbital hybridization between the VI-group anions and I-group cations.
- The bottom conduction band (CBM) has an anti-bonding component of s-s and s-p orbital hybridization between the IV-group cation and VI-group anion.

Table 1.4: The calculated Γ-point band-gap energy (E_g) of Kesterite and Stannite:

Methods	CZTS Kesterite (eV)	CZTS stannite (eV)	CZTSe Kesterite (eV)	CZTSe stannite (eV)
GGA+QP	1.56	1.42	1.05	0.89
HSE06	1.47	1.27	0.90	0.70
GW_0	1.57	1.40	0.72	0.85

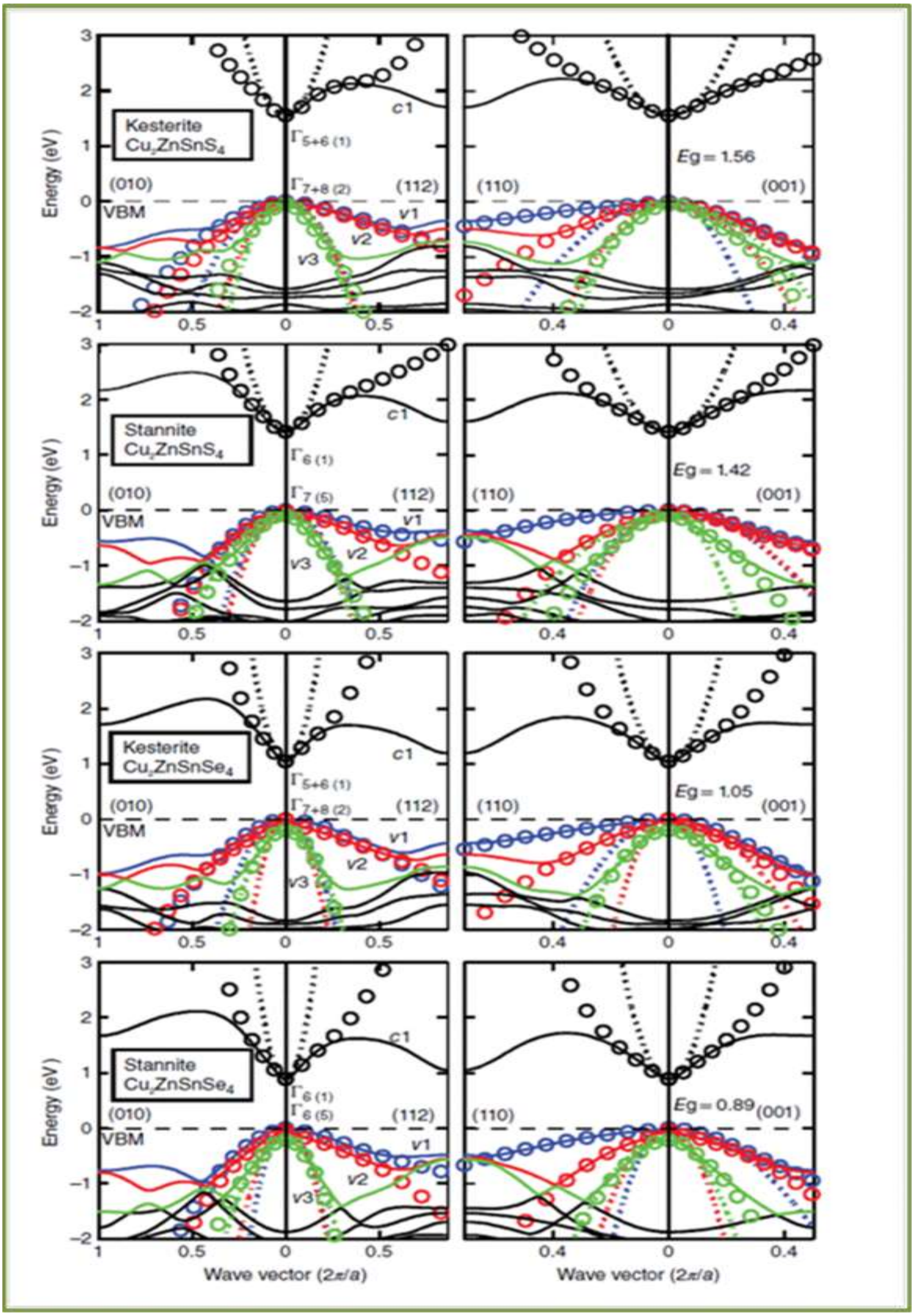

Figure 1.9: The electronic band structure E_j (k) of the Kesterite and Stannite structures of CZTS and CZTSe along with four symmetry directions.

When the IV-group cations change from Si to Sn, the band gaps of CZTS are decreased and identified by GGA, GGA+HSE, HSE functional method as shown in **Fig. 1.10.** These analyzed results support well with bandgap determination by the various measurement techniques **[81-86].**

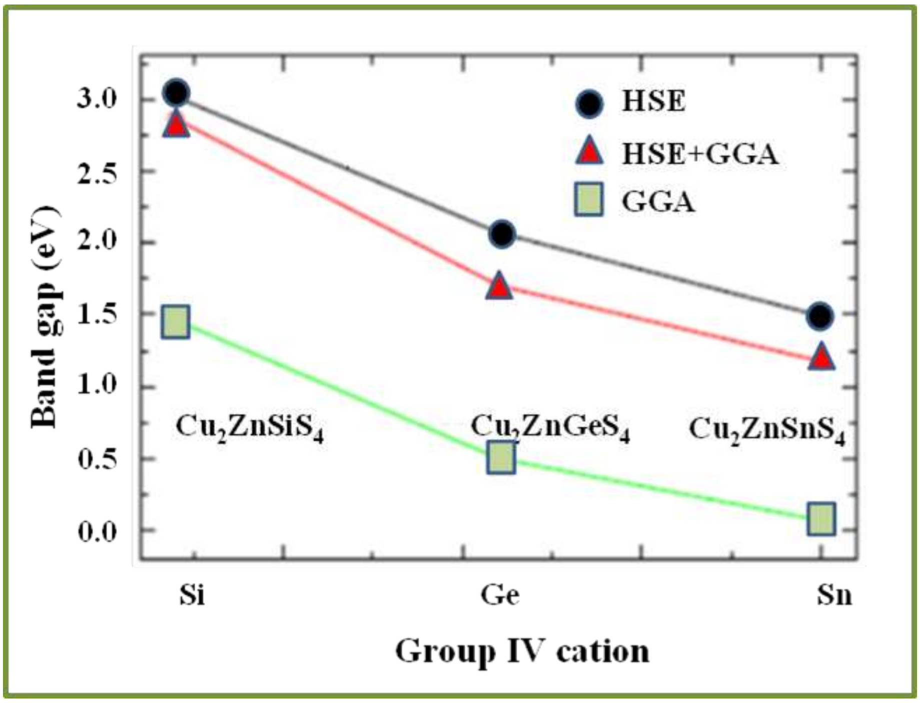

Figure 1.10: The study bandgap variation of Kesterite $Cu_2Zn\text{-}IV\text{-}S_4$ with IV-group cations change from Si to Sn.

The electronic parameter (bandgap) is obtained by the semi-local functional PW91 [**87].** The hybrid functional theory of Hartree-Folk approximation [HF] is used for quantitative estimation of the changing bandgap with the HSE (Heyd-Scuseria-Ernzerhof) and the screening constant (omega=0.11Bohr^{-1}) **[87, 88].** The energy exchange-correlation is given as;

$$E_{xc}^{HSE}(\omega) = \frac{1}{4}E_x^{Fock,SR} + \frac{3}{4}E_x^{PBE,SR} + E_x^{PBE,LR} + E_C^{PBE} \qquad (1.5)$$

In the eqn. (1.5), the first term represents “the exchange component of electron-electron interaction (in short-range or Fock exchange energy); and second, third, fourth terms are the “the exchange energies in short-range”, “the exchange energies in long”, “direct exchange energy”, respectively. These parameters are calculated by the Generalized Gradient Approximation (GGA) density functional. The calculated energy band gaps of CZTS and CZTSe are matched with the experimental results [**85, 89, 90].**

Chen et al. [**87**] explained the energy stability in the band gaps, which are followed as:

(i) The Kesterite has lower energy than the stannite and the Wurtzite (WZ) Kesterite has also lower energy than the Wurtzite stannite.

(ii) The Kesterite structure is more stable than the stannite (Cu_2Cd-IV-S_4 series exception case in the Stannite).

The energy difference between Kesterite and Stannite becomes smaller monotonically as IV-group cations changes from Si to Sn element.

1.7.5 Developement of Kesterite Solar Cell

In 1988, first time, Ito and Nakazawa **[91]** declared the photovoltaic effect in CZTS and found an open-circuit voltage (V_{oc}=165 mV). In 2001, Friedlander and Kategri et al. **[92, 93]** reported the conversion efficiencies with 2.3% and 2.63%, respectively**.** In 2008, the Kategri group reported the improved efficiency of the Kesterite (*pn*-junction) solar cells by 6.3% through the optimization on annealing in the sulfur atmosphere **[94].** In 2010, Todorov et al. **[95]** reported that CZTS,Se based solar cells has 9.6% efficiency. In 2014, the efficiency of the Kesterite CZTS,Se-based thin-film solar cells was reported 12.6% [**96].** The total progress of the highest conversion efficiencies of Kesterite in lustrum timing is shown in **Fig. 1.11**.

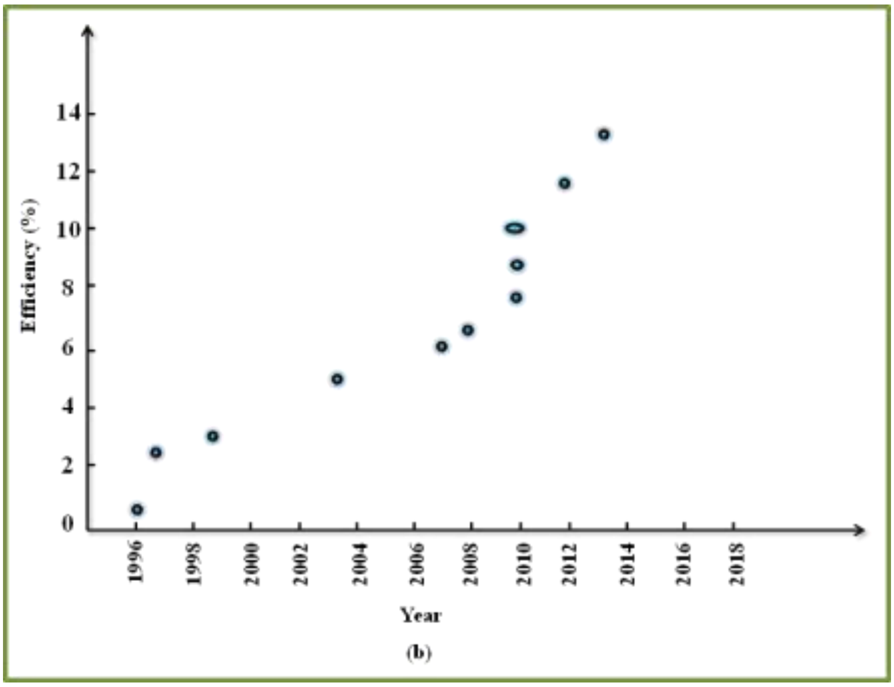

Figure 1.11: Total progression of Kesterite solar cell efficiency from 1996 to 2018.

The highest efficiency of CZTS/Se was reported by joint research of the IBM, Tokyo Ohka Kogyo (TOK) and Newport Corporation verified independently **[97-101]**. The current highest conversion efficiencies of the Kesterite has been reported by different synthesis methods are shown in **Tab. 1.5**.

Table 1.5: The current highest reported conversion efficiencies of Kesterite solar cell synthesis by different methodis shown with V_{oc} open-circuit voltage, J_{sc} current densities, and fill factor (FF):

Methods	Materials	Voc (mV)	J_{sc} (mA/cm^2)	FF	Conv. effi. (%)	Time	Ref.
CBD method (non-vacuum)	CZTS	610	17.9	62.0	6.67	2008	[102]
Thermal evaporation (vacuum)	CZTS	661	19.5	65.8	8.84	2011	[103]
Spin coating (Vacuum)	CZTSe	422.8	38.7	61.9	10.1	2012	[104]
Electro-deposition (Non-vacuum)	CZTSe	390.0	35.3	58.0	8.0	2014	[105]
Hydrazine- slurry method (vacuum)	CZTSSe	513.4	35.2	69.8	12.6	2014	[68]
Spray Pyrolysis method (non-vacuum)	CZTSSe	-	-	-	5.1	2014	[106]

Larramona et al. **[107]** reported 5.0% efficiency of the CZTS solar cell by spray pyrolysis method, in which non-vacuum technique was used. The non-vacuum spray pyrolysis method is used to synthesize the oxide and sulfide because this method is very cheap, easily available, and having some advanced properties in the film like high roughness surface of film, easily grow the multilayers in the controlled thickness. The conversion efficiency of pure sulfur based on the sprayed Kesterite is shown in **Tab. 1.6.** Some important parameters in spray method are carrier gas, spray atmosphere, substrate temperature, and annealing condition. These parameters can change the characteristics of Kesterite material.

Table 1.6: The highest conversion efficiency of pure Sulphur based sprayed Kesterite:

Spray type/ key	**Precursors/ solvent/ carrier gas**	**Substrate temperature [^{0}C]/ etching**	**Annealing condition**	**J_{sc} (mA/cm^2)**	**Voc (mV)**	**FF (%) Area (cm^2)**	**Eff. [%]**	**R_s/ R_{sh} (Ω cm^2)**	**Ref.**
Pneumatic XY robotics	$CuCl_2$,$ZnCl_2$, $SnCl_4$, NaHS/ water+ethanol/ N_2 (glove box)	300^{0}C/ HCl (8%)	N_2; 525^{0}C, 15min+H_2S; 525^{0}C, 60min	19	630	50 0.25	5	4/ 300	[108]
Pneumatic / (8nm)	$CuCl_2$, $ZnCH_3COOH$, $SnCl_4$, NH_3CSNH_3/ water/ air (air)	331	331, 30min	8.3	430	52	1.8	9.7/ 252	[109]
Pneumatic /	$CuCl_2$, $ZnCH_3COOH$, $SnCl_4$, NH_3CSNH_3/ water/ Ar (Ar box)	360/ KCN (1%)	Ar, S+Sn+580 ^{0}C, 30min	9.8	421	34.3 0.09	1.4	18/ 89	[110]
Pneumatic / Ar and Ar+H_2 carrier gas	$CuCl_2$, $ZnCH_3COOH$, $SnCl_4$, NH3CSNH$_3$/ water/ Ar (Ar)	220 KCN (1%)	Ar, S+Sn+580 ^{0}C, 30min	10.7	407	33 0.09	1.4	17/ 70.8	[111]
Pneumatic	$CuCl_2$,	350 KCN	Ar,	10.3	356	32.5	1.2	16/	[108]

/	$ZnCH_3COOH$, $SnCl_4$, NH_3CSNH_3/ water/ Ar (Ar)	(1%)	S+Sn+580 ^{0}C, 30min			0.09		61	
Pneumatic /	$CuCl_2$, $ZnCH_3COOH$, $SnCl_4$, NH_3CSNH_3/ water/ Ar (Ar)	450 KCN (1%)	Ar, S+Sn+580 ^{0}C, 30min	7.5	361	37.1 0.09	1	15	[112]
Pneumatic /	$CuCl_2$, $ZnCH_3COOH$, $SnCl_4$, NH_3CSNH_3/ water/ $Ar+H_2$ (Air)	220 KCN (1%)	Ar, S+Sn+580 ^{0}C 30min	10.7	407	33	1.4	17.3/ 70.8	[113]

After study the **Tab.1.6,** we have investigated that the conversion efficiency is directly related to open-circuit voltage, current density, fill factor, series resistance. More study to these types of parameters for CZTS photovoltaic efficiency are discussed in the next section.

1.7.6 CZTS Solar Cell Efficiency

The solar cell efficiency depends on open-circuit voltage (V_{oc}), current density (J_{sc}), and fills factor (FF). The CZTS solar cell efficiency parameter open-circuit voltage (V_{oc}) is urged by carrier generation and recombination near the charge-separating junction in solar cell and played a dominant role as shown in **Fig. 1.12**. The CdS/CZTSSe solar cell has a conversion efficiency of approximately 12.6% **[8].** Hence, researcher understands the junction characteristics, current collection, and recombination mechanisms in the current generation of devices have deliberated the fault deficit in the efficiency of the solar cell.

In the Kesterite solar cells, the “junction characteristics”, “current collection” and “recombination mechanisms” parameters are modified by changing in parameters:

"composition of element/defects and generated granaries", "substrate temperature", "annealing", "sulpherization", "concentration", "pH of salt's solution" and "interface carrier recombination center". These parameters directly affect to bandgap, radiative and non-radiative recombination. The CZTS has a direct bandgap of 1.1-1.6eV, radiative and non-radiative recombination having a high absorption coefficient in the visible energy range. Some of them parameters of CZTS for photovoltaic cells are discussed below:

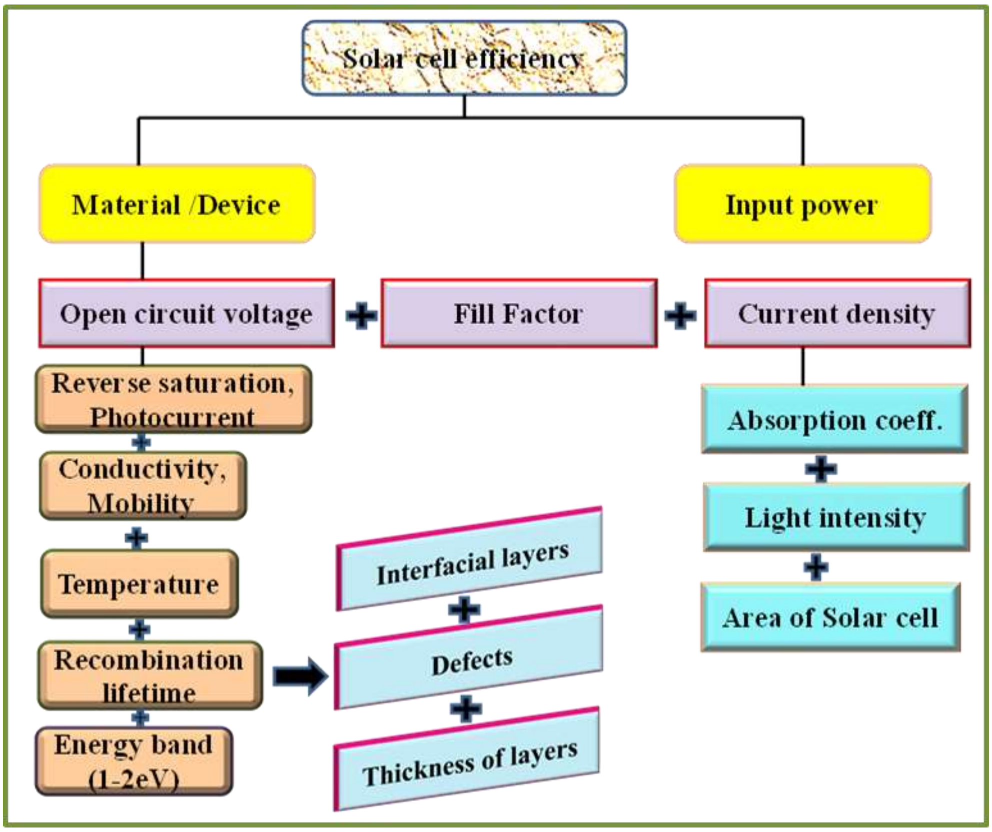

Figure 1.12: Development of conversion efficiency of Kesterite thin-film solar cells with efficiency parameters.

1.7.6.1 Variation in composition of the constituent elements: The variation in composition parameter is directly correlated to the characteristics of material structure. The variation in constituent elements quantitatively (Cu poor and Zn rich ratio) effect Kesterite structure improves the photovoltaic efficiency **[114]**. This relation in constituent elements composition versus efficiency is shown in **Fig. 1.13** and the highest efficiency of the CZTS cell is achieved within the range of 0.80-0.90 for Cu/(Zn + Sn) and 1.2–1.3 for Zn/Sn ratio. Sahayraja et al. **[115]** announced that the particle size increases with increasing the Cu/(Zn+Sn))= 0.80–0.90 and Zn/Sn=1.2-1.3 ratio and found grain size up to ≥ 1 μm.

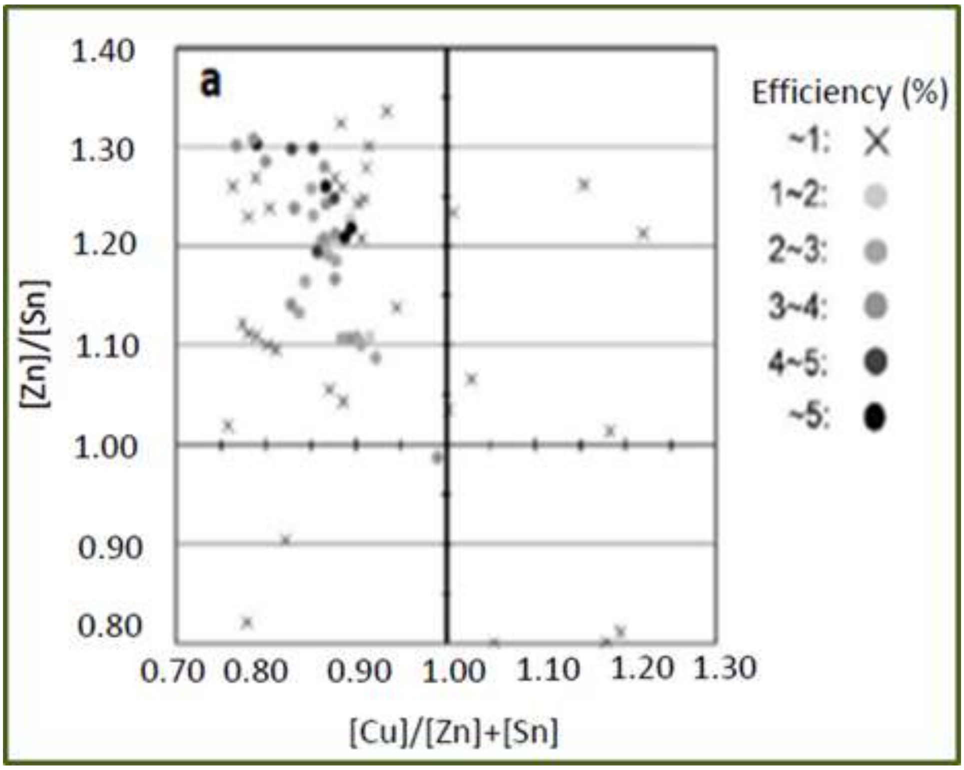

Figure 1.13: The elemental composition versus efficiency of Kesterite solar cells.

The ratio of Cu/In and Cu/(In+Ga) in Kesterite (CIS, CIGS,) is reported the highest efficiency that is the best applicable for photovoltaic cells **[116-119].** The whole discussion of the parameter and its effects on characteristics are discussed in **Tab. 1.7.**

Table 1.7: The role of constituent elements composition ratio in the Kesterite characterization analysis:

Methods/ Materials	Precursor Salts/ Solvents/ Temperature	Ratio Cu/(Zn+Sn) or Zn/Sn	Characterization	Applications	Ref.
Co-evaporation / CZTSe	Cu, ZnSe, Sn, Se/ $T_{sub.}$=623^{0}K , $T_{an.}$=723^0 K	0.85-1.15	• 0.90-1.10 • Single-phase • Polycrystalline • Kesterite • The intensity of	----	[120]

			(112) increased • FWHM decrease • Bandgap and resistivity (23-0.02Ohm-cm) decreased with ratio increases • Grain size decreases with ratio decreases • Grains densely packed and roughness 3–5 nm in Cu-poor • a=0.568 nm, c=1.138 nm		
Multilayer of precursors by e-evaporation / CZTS	ZnS, Sn, Cu/ $T_{sulf}=550^0$ C with Nitrogen (1 hour)	0.813-0.659	• a=5.432 and c=10.835 Angstrom. • Anti-sites Zn_{Sn} or Cu_{Sn}, $Sn_{Zn,}$ and V_{Sn} vacancy defects • Intensities tell Stannite phase absent • Average grain size • The energy gap (1.47-1.63 eV) increases with the ratio of Tin • The density of acceptor defects V_{Sn}, Cu_{Sn}, and Zn_{Sn} anti-sites reduced Tin content	---	[121]
RF co-sputtering/	Cu, ZnS, Sn, SnS/ flow rate: 50	0.75-1.25,	• Optimum band gap=1.5 eV	Solar cell	[122]

CZTS	sccm, Ar gas: pressure= 0.5 Pa, Sub. Rotation= 20 rpm, Pre-sputter time=3 min, T_{an}=580^0 C (5^0 C/mnt)	0.80-1.35	• Abs. coef.=10^{-4}cm^{-1} • Pseudo-ternary CuS-ZnS-SnS phase diagram		
Spray Pyrolysis/ CZTS	Cupric chloride, Zinc Acetate, Stannic Chloride, Thiourea/ pH: 3.0, 4.5, 5.5/ T_{sub}=643 K, spray rate 12 ml/min,	0.90-1.32	• Polycrystalline • Non-stoichiometric (pH=3) • Band gap=1.45eV • a = 0.542nm, c = 1.085nm • Resistivity =0.1-2.9 Ωcm	---	[123]
Vacuum evaporation / CZTS	Cu, Zn, Sn, S salts, T_{sub}=550^{0}C,	0.82-1.06, 1.1	• Grain size ≥1 µm increased • Resistivity decreased (2.5×10^{-1}-7.0×10^{-3})Ωcm • Better crystallinity with increasing ratio	Solar cell	[124]
Sol-Gel/ CZTS	Copper acetate monohydrate, Zinc acetate dihydrate, Tin chloride die-hydrate, DW, ammonium acetate, N_2 and H_2S (5%) at 500^0 C for 1 hour	0.73-1.0, 1.15	• Amount of Zn or Sn decreased with increasing Cu ratio • The grain size increased as the ratio decreased • The bandgap (1.62-1.40)eV • Cu/(Zn+Sn)=0.80 exhibit the highest effici.	Solar cell (2.03%)	[125]

			due to the large grains		
Spray pyrolysis/ CZTS	CuCl$_2$, Zn(CH$_3$CO$_2$)$_2$ SnCl$_4$, SC(NH$_2$)$_2$/ T$_{sub}$=450°C, air Pressure=20,000Pa, Spray deposition rate=3ml/min (20min time)	0.73-1.0	• Increasing temperature (^{o}C) helps grain size growth (550° C - 580°C) • CTS, CZTS phases • Low-frequency band presented • Low resistivity with high ZnS binary phase concentration	Solar cell (0.49%)	[126]
Multilayer precursors by e-beam evaporation / CZTS	ZnS, Sn, Cu, T$_{sub}$=150, multiple layers structure: ZnS/Cu/Sn/ZnS/Cu/Sn/ZnS	0.92-0.75	• Transmittance wavelength range (250-2500 nm) • Spurious phases (Cu$_{(2-x)}$S, Cu$_x$Sn$_y$S$_z$, Sn$_x$S$_y$) • Band gap 1.48-1.62eV • Bandgap shrinkage with the increase of the [Cu]/[Sn] ratio defect-induced on the bandgap • Shrinkage acceptor defects (V$_{Sn}$, Cu$_{Sn}$, and Zn$_{Sn}$ anti-sites) created by reduced Tin content • Density and the energy gap is		[127]

			not influenced by the Zn content but influenced [Sn]/[Cu] ratio		
Co-evaporation / AZTSe	Ag, Zn, Sn, Se/ T_{sub}=150^0 C, T_{annl}=500^0 C, Thickness-2µm, Etching by KCN (1M) for 3 min/ pressure =10^{-9} Torr	Ag/Sn = 1.50-1.85, Zn/Sn = 1.03- 1.15	• Ag-poor (smaller grains) • ZnSe, Ag_2Se, Ag_8SnSe_6 secondary phases • Carrier density (~1012 /cm^3) and electron mobility (~100 cm^2/V.s) • The PL intensity reduced on increasing Sn (decreasing the Ag/Sn ratio) increase average grain size • Minimize non-radiative recombination • Prevent bandgap • Narrowing or the formation of deep defects on high Ag/Sn ratio	Solar cell	[128]

After study the **Tab. 1.7**, the suitable constituent elements composition ratio is Cu-poor and Zn-rich that would be laid 0.80–0.90 for Cu/(Zn +Sn), 1.1–1.3 for Zn/Sn, and 1.6 for Cu/Sn to get the high-efficiency Kesterite solar cells.

1.7.6.2 Role of Defects in Kesterite: The lattice defect is an important parameter to reduce the loss of electron-hole pairs by recombination and the role of defect is a feasible parameter for photovoltaic semiconductor devices. The defects are identified in the form of vacancies, anti-sites, interstitials, and defect complexes, which are indicated in **Tab. 1.8**. The defects also generate the shallow donor and acceptor levels, and mid-gap and deep trap state between the band gaps of the Kesterite [**129].**

Table 1.8: The defect, ionization level, and impacts on solar cell description are given below:

Type of defects	**Ionization level of Defects**	**Formation Energy (eV)**	**Impact on CZTS solar cell**
V_{Cu}	1 Acceptor (-)	0.02	Ionized from (0/0) to -1 state and transition level ε(-/0) forms the shallow state (favorable)
V_{Zn}	2 Acceptor (2-)	---	Deep levels (unfavorable)
V_{Sn}	4 Acceptor (4-)	---	Deep levels (unfavorable)
$V_{S/Se}$	1 Donor (-)	---	Mid-gap state (unfavorable)
Cu_{Zn}	1 Acceptor (-)	≥0.02	Deeper than V_{Cu} (favorable)
Zn_{Cu}	1 Donor (-)	---	The shallow level near the conduction band (unfavorable)
Cu_{Sn}	1 Acceptor (1-)	---	Deep and multi-levels (unfavorable)
Sn_{Cu}	2 Donor (2+)	---	Deep level and mid-gap state (unfavorable)
Zn_{Sn}	2 Acceptor (2-)	---	Deep levels (unfavorable)
Sn_{Zn}	2 Donor (2+)	---	Mid-gap states (unfavorable)
Cu_i	1 Donor (2+)	---	Shallow states near conduction band (unfavorable)
Zn_i	2 Donor (2+)	---	Mid-gap states (unfavorable)
Stoichiometry defect: $Cu_{Zn+}Zn_{Cu}$,	---	≥2	$Cu_{Zn+}Zn_{Cu}$ low impact on optoelectronic properties and another decrease the bandgap 0.3

Cu_{Sn}+Sn_{Cu}, Zn_{Sn}+ Sn_{Zn}			eV
Non-stoichiometry defect: (V_{Cu}+Zn_{Cu}), (V_{Zn}+Sn_{Zn}), (Zn_{Sn}+2Zn_{Cu}), (2Cu_{Zn}+Sn_{Sn})	---	~0.3-0.6	Significant impact and responsible for local variation in chemical potential

The V_{Cu}, Cu_{Zn} and Cu_{Zn}+Zn_{Cu} defects in CZTS are feasible to improve the characteristics but the other defects (i.e. V_{Zn}, V_{Sn}, V_S, V_{Se}) are unfavorable. The defect V_{Cu} is the vacancy of the Cu atom that generates the displacement of the atom in the unit cell of the CZTS. Similarly, other vacancies also generate the displacement of the related atoms. When the Cu atom displaces by the Zn atom in the CZTS, then anti-site defect Cu_{Zn} is generated and similarly, other anti-site defects are also generated. However, when two anti-site defects combine then they make defect complexes [**130-132].** These defects have a special ionization level due to which the number of a charge carrier or conductivity (p-type) and recombination are affected as V_S and V_{Se} form the mid-gap states while the V_{Zn} and V_{Sn} form the deep levels and midgap states within the bandgap range and Cu_{Zn} and Zn_{Cu} form the shallow acceptor and donor levels, respectively [**133**]. The anti-site Sn_{Zn} forms the two midgap states and interstitials Cu_i, Zn_i form the shallow donor level.

The ratio Cu/(Zn+Sn) and Zn/Sn enhance the characteristics due to the formation of the anti-site defects V_{Cu} and Cu_{Zn}, and affects the p-type conductivity of CZTS [**134].** The shallow donors of Zn_{Cu} defects ionizes to positive charge and behaves like an electron sink and hole barrier in CZTSSe solar cell. This defect creates inhomogeneity and increases the electron recombination as well as the open-circuit voltage. The limited V_{oc} is controlled by deep-level recombination centers in the bulk interface and grain boundary [**135, 136]**. The defect (V_{Cu}+Zn_{Cu}) helps in the transportation of charge in CZTS,Se because the defect repels the majority charge carriers (holes) and collects the electrons to the n-type buffer layer that can be created by the Cu poor and Zn rich condition **[137]**. But V_{oc} reduces in CZTSSe devices due to defects by the recombination centers at interfaces and grain boundaries in the bulk material. The point defect creates bandgap fluctuations due to non-uniform chemical stoichiometry **[136]**. Some defects like Zn_{Sn}, O_{Se}, Na_i, at the grain boundaries create the barrier for holes and help to transport the electrons through the grain boundaries **[138, 139].**

1.7.6.3 Temperature Effects on Kesterite: The substrate temperature and annealing or sulpherisation are other parameters that affect electronic properties of Kesterite. In the annealing process, lattices are mismatched in CZTS, and diffusion of atoms is created across the interface. The effect of temperature investigate at room temperature (R_t) to 450°C and the crystalline structure of the Kesterite is found at 370°C **[140]**. The grain size is increased with increasing temperature.

From the review literature of temperature effect on Kesterite structure, the spray pyrolysis method at 340–410°C temperature is suitable for the synthesized of Kesterite where the annealing temperature of Kesterite is 460–580°C. These temperature ranges are proposed for better results to improve the qualities of the absorber layer of the CZTS. But the secondary phases, defects, and $Mo(S/Se)_2$ layers are created between the absorber and Mo metallic layer. However, the Sn and S elements are evaporated at this temperature. So, these elements needs to create non-stoichiometric CZTS film at high temperature. Hence, balanced stoichiometry is obtained by controlling the temperature and the ratio of the constituent elements like Cu, Zn, Sn, S, Se are taken.

Mkawi et al. **[141]** studied the chemical composition of the CZTS thin-film misbalanced of increasing the annealing temperature 460–580°C, where the resultant phase of the CZTS is misbehaved. Zhou et al. [**142**] proposed that the absorption coefficient varies with temperature and photon energy. Hence, the oxide type impurities of the CZTS thin film can be removed by annealing at high temperatures and the elements have sufficient energy to form the proper structure. But in this process, the sulfur is also evaporated. To resolve this problem, the inert atmosphere (Argon or Nitrogen) or hydrogen sulfide (H_2S) is required for the synthesis of CZTS during the annealing.

1.7.6.4 Energy Loss at Interface in Heterojunction Solar Cell: The phase impurity and the poor interface quality increase the energy loss and reduce the performance of the solar cell efficiency in the heterojunction device. So, the interface quality can be improved using the interfacial layer or JABS layer, where the JABS layer sandwitches between the buffer and absorber layer. As we know that, the physics of solar cell

efficiency is directly dependent on the open-circuit voltage (V_{oc}), short circuit current density (J_{sc}), and fill factor (FF). The open-circuit voltage (Voc) is reduced by the interface recombination of the device. To elucidate the open-circuit voltage deficit, the mechanism of the carrier recombination is analyzed by the equation below:

$$V_{oc} = \frac{E_A}{q} - \frac{AkT}{q}\ln\frac{J_{00}}{J_L} \tag{1.6}$$

where E_A=activation energy for recombination, A=ideality factor, q=electronic charge, k=Boltzman constant, J_{00}=reverse saturation current density, and J_L=photocurrent density **[143]**.

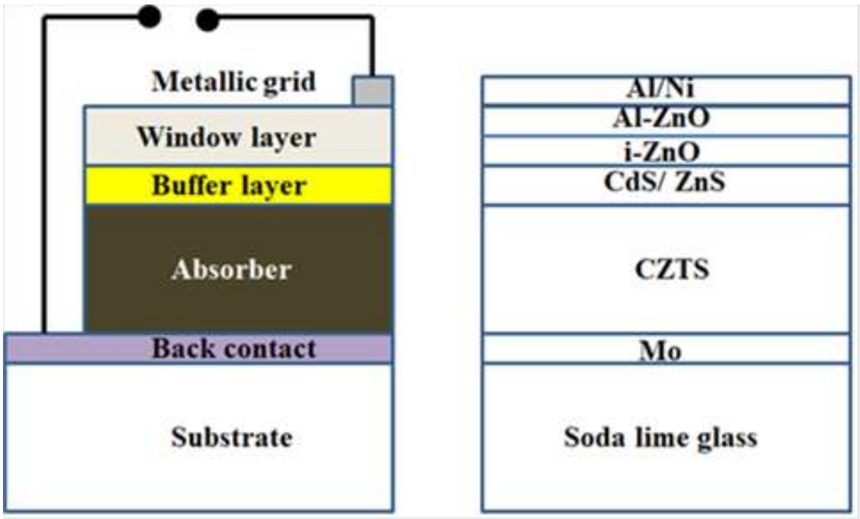

Figure 1.14: The schematic diagram of the heterojunction device structure of the CZTS solar cell.

The heterojunction device structure of the CZTS solar cell is shown in **Fig. 1.14**. Secondary phases and defects are created at the interfaces by the inter diffusion of the materials. The annealing does the inter-diffusion and the secondary phases create like Cu_2S at CdS/CZTS and ZnS and SnS_2 at CZTS/Mo interfaces **[144-146].** However, the Cd is diffused into CZTS, and Zn and S are diffused into the CdS layer. As a result, the band alignment is switched at CdS and CZTS interfaces and makes the “cliff type” structure in the band alignments due to which carrier transport disrupts and loses the energy **[147].** Another reason for energy loss is the MoS_2 or $MoSe_2$ layers. In the sulfurization process, MoS_2 or $MoSe_2$ layer is created at the CZTS and Mo interfaces, and this process is very difficult to increasing the efficiency of the solar cell **[148-150].** But the layers affect the open-circuit voltage due to the shifting band alignment between CZTS and Mo interface **[151].**

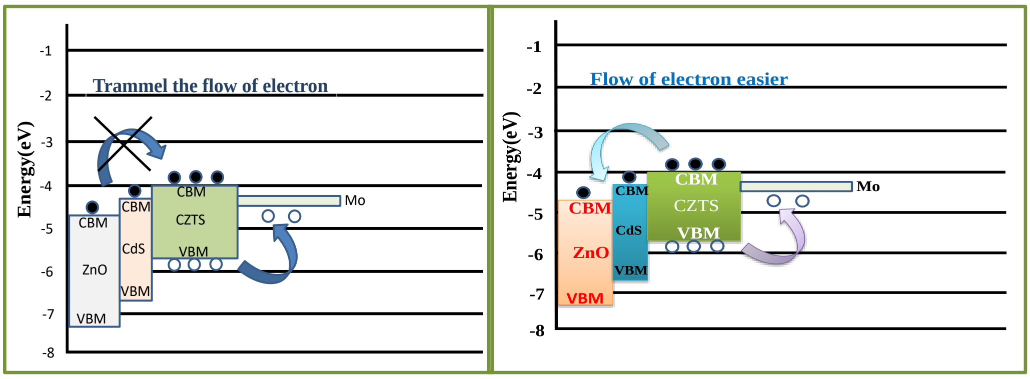

Figure 1.15: Behavior of conduction electron in heterojunction device band structure.

1.7.6.5 CdS and CZTS Interface: The CdS (n-type) and the CZTS (p-type) layers form a p-n junction in the metal grids in the form of AlZnO/i-ZnO/CdS/CZTS/Mo/SLG for fabrication of a solar device, where Al: ZnO is the aluminum-doped zinc oxide. The *pn-* junction of the CdS and CZTS interface is the interested research work because the maximum charge carriers losses near the interface are due to the recombination and the band offset on the transportation of charge carriers. There are two types of recombination/band offset that are formed: (i) ***spike*** and (ii) ***cliff***. Scheer et al. **[152]** explained that the spike barrier is trammel and it is restricted to flow of electrons from CZTS to CdS. As a result, V_{oc} of the device increases. The cliff type barrier or negative band offset helps to flow electrons from CZTS to CdS and as result, the J_{sc}, V_{oc}, and FF enhance [**153**]. The mechanism of the charge carrier's transport across the potential barrier is explained in **Fig. 1.15.**

The "cliff type" structure and "spike type" structure are observed in CdS/CZTS interface and CdS/CZTS,Se interface respectively **[154, 155]**. Tajima et al. [**156]** estimated the conduction band offset (CBO) at the CdS/CZTS interface by the valance band offset (VBO). The X-ray photoelectron spectroscopy is used to measure the energy bandgap. The flat band conduction band minimum (CBM) was reported which shown in **Fig. 1.15**. This condition helps to charge transportation smoothly at the junction CdS/CZTS interface.

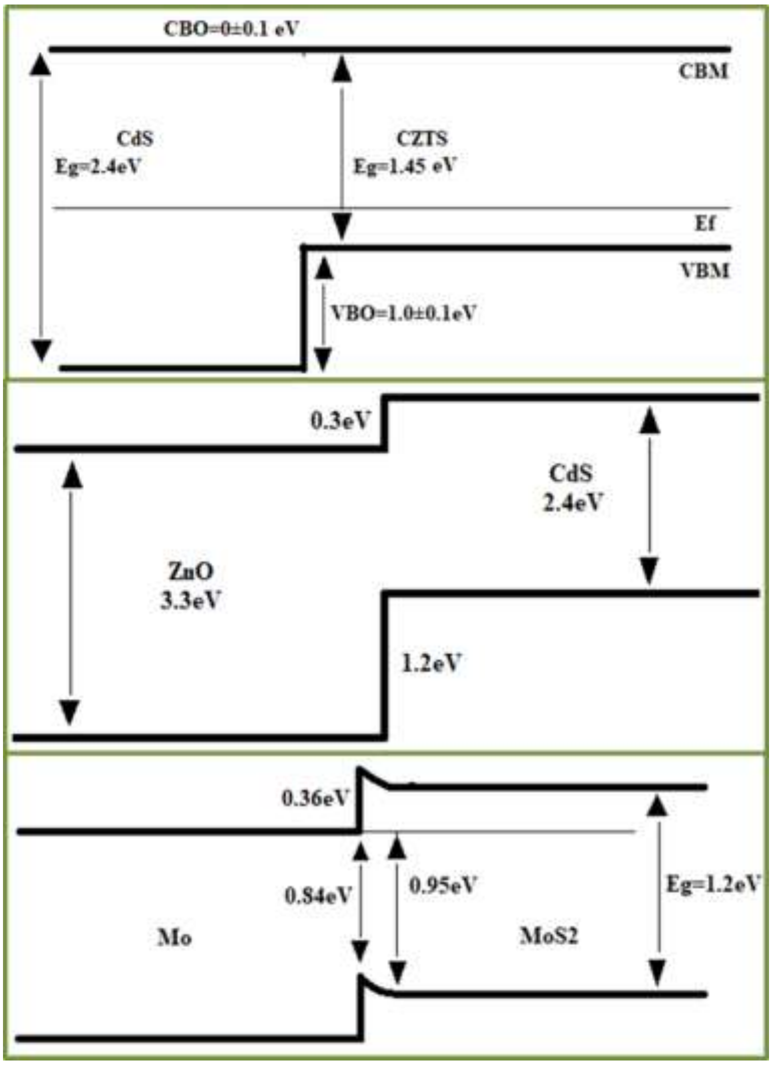

Figure 1.16: The state of conduction band offset (CBO) at junction Mo:MoS_2, ZnO:CdS, CdS:CZTS.

1.7.6.6 ZnO/CdS Interface: To enhance the efficiency of the Kesterite solar cell, i-ZnO/Al: ZnO, In2O3, ZnSnO, GaP materials are used as a window layer. Such materials are highly conductive having a wide optimal bandgap and are highly transparent in the desired spectrum **[157, 158**]. These layers are used in the CZTS and CIGS solar cells. Janotti et al. [**159]** analyzed that i-ZnO/Al: ZnO is the best window layer and showed a positive response such as improved V_{oc} for the solar cell application [**160]**. The band alignment of the ZnO and CdS interface is investigated for the CIGS absorber **[161]**. The band alignment is explained the charge carrier's transportation as shown in **Fig. 1.16**. But another investigation shown the flat band offset as CBO=0.1±0.15eV and VBO=−0.96 ± 0.15eV, which supports the charge transportation at the interface **[162**].

1.7.6.7 CZTS and Mo interface: The charge collection point/electrode is the charge carrier loss in the device of the solar cell. This is the deleterious effect to enhance the efficiency of a solar cell because V_{oc} is affected. So, lots of metallic-coated substrates are used to collect the charges. The metals W, Mo, ITO, FTO, Cr, V, Ti, Mn, Au, Ni, Ag, Pt, Nb, etc. are used to collect the charge carriers as the electrode [**163**]. Mostly, Mo is used in high-efficiency solar cells such as CIS, CIGS because it has ohmic contact, good adhesion, and formed the diffusion barrier layer $(MoS/Se)_2$ **[164, 165]**. Hence, the Mo metal is used in the Kesterite solar cell that may increase the open-circuit voltage (V_{oc}). Scragg et al. **[165]** observed that if the electrodeposited CZTS/Mo/SLG film is annealed/sulfurized, at 550 °C, then the thickness of the film is increased with the increasing time and the decreasing temperature, where grain size also reduces the film thickness **[166].** The thickness of the MoS_2 layer was helpful in the device performance if TiN layer is used **[167, 168]**. The band offset CBO is 0.36 eV at the Mo/MoS_2 interface as shown in **Fig. 1.16** [**169]**.

Currently, there are some intermediate layers used to improve the back contact of the CZTS solar cell. These intermediate layers are taken like TiN, Silver, Bismuth, Carbon, ZnO, Al_2O_3, TiB_2 at the CZTS and Mo interface, etc. The coating of these materials is applied on the substrate in the nanometer range. The intermediate layer TiN was deposited in the CZTS and Mo interface by a sputtering process, and the efficiency of 5.5% with 621 mV open-circuit voltage, 18.71mA/cm^2 current density and 47.1% fill factor of the CZTS solar cell was reported [**150]**. The CZTSe with TiN layer has also been reported with an efficiency of 8.9%, 385 mV open-circuit voltage, 42.60mA/cm^2 current density, and fill factor 54.2% **[149]**.

If the 10nm thickness of the ZnO layer is used in between Mo and CZTS layers, the efficiency is also enhanced from 2.5% to 6.0% due to the reduction of the series resistance (R_s) [**170]**. Liu et al. [**171]** reported the enhancement of the efficiency of the solar cell from 1.13% to 4.3% with decreasing the voids and the thickness of the MoS_2. Some researchers suggested that MoS_2 is beneficial for the high efficiency of Kesterite solar cells but others researchers were against such type of fabrication. Hence, there are lots of investigations required to justify the mechanism of MoS_2 at the interface of CZTS, where MoS_2 is beneficial or not.

1.7.7 Future of the Kesterite Solar Cell

The big challenge for the low-cost Kesterite (CZTS/CZTSe/CZTS, Se) solar cell is to enhance the conversion efficiency. The main reason for the low efficiency of Kesterite (CZTS) solar cells is the high loss of charge carriers by the recombination during charge transportation and the charge collection at the electrode. The charge carriers loss affect directly by the interfacial layer between the absorber and the buffer layers and the absorber and the metallic contacts. As discuss earlier that CdS is the best buffer layer for the CIGS solar cell, but it is not suitable for the CZTS,Se solar cell because the recombination timing of the CZTS,Se solar cell at the interface is very low as compared to the CIGS solar cell. The main reason for low recombination in the CdS/CZTS interface is Cd diffusion in the absorber layer at the time of solar cell fabrication. The interface of CdS/CZTS has a spike type band offset with 0.4 eV energy **[172].** Hence, it is required to develop a suitable buffer layer for replacing the CdS layer, i.e. appropriate function interfacial layer between the buffer and the absorber. The carbon nanotube (CNT) is the best solution to the above-discussed problem. The cylindrical molecules of CNTs have been already shown valuable applications for electronics, optics, nanotechnology, and another field of materials science because the CNTs have a unique feature-breathing mode of cylindrical type molecules. The feature of the nanotube structure is to make fine-tuning through the narrow selectivity of the wavelength of emission and can be detected by light. Due to the breathing mode of the cylindrical molecules of the carbon nanotubes (CNT), the CNT may be the suitable interfacial layer to reduce the recombination between the absorber and the buffer layers. Similarly, Graphene nano layer may also be the another best solution for this problem.

The Mo(S_2/Se_2) layer is another hurdle for the efficiency enhancement of the Kesterite solar cell. The Mo interface plays a vital role in the enhancement of the Kesterite solar cell because it has maximum series resistance. The Mo(S_2/Se_2) layer is formed often in the Kesterite solar cell during the annealing process. Hence, two points are clearly concluded that (i) avoid annealing process of the solar cell after the complete fabrication of the device, and (ii) remove the Mo metal by the high work function metal such as Ni (5.22), NiO (>5.2), Pd (5.22), Pt (5.64) **[[173, 174].** Here, the fabrication of the device without annealing may be a wonderful investigation because this process avoids the formation of MoS_2/Se_2 layer and is helpful to short out the energy loss problem. The diffusion of the metallic salts across the interfaces in the absorber layer is helpful to have a high work function. In the presence of the high work function layer, all charge carriers (holes) must be collected in the electrode in the right manner to enhance the efficiency of the solar cell. This charge collection phenomenon form the ohmic contact with the Kesterite solar cell and have more probability to extract the charge carriers.

1.8 Objectives of Thesis

Based on the literature survey of the functional materials for energy devices, we focus our study on the selection of functional materials having eco-friendly, non-toxic, and low-cost constituent elements and ecofriendly synthesis methods. After selection of the constituents for compositions and synthesis methods, the XRD, EDS, FESEM/SEM, UV-Visible and I-V characteristics use to characterize the as-synthesized functional materials and study the electronic and optical properties of the FMs for energy application. These characteristics study of the energy materials are used to enhance the efficiency of the photovoltaic solar cell, photodetector, etc. The photo parameters properties and I-V characteristics are investigated to understand the photodetector mechanism.

1.9 Organization of the Thesis

This presented thesis is organized into six chapters. The content of each chapter is given below:

First chapter gives a brief introduction of the functional materials, synthesis, characterization, and potential applications. Here, we have given the study of the historical background of functional materials (FMs) especially energy materials, and also their technical development in the field of Materials science and Engineering (MSE). MSE has played a crucial role in the development of advanced materials devices by modification in the structures of materials for different applications in solid-state physics, and these materials are known as functional materials in MSE. This chapter mainly focuses on the photovoltaic functional materials such as CZTS, SnS, ZnO, CdS, etc., and also describes the CZTS phases, electronic band structures, and important parameters to enhance the photovoltaic efficiency. CZTS is an I_2-II-IV-VI_4

group functional material. The literature survey of the Kesterite materials is the main part of this chapter that presents the brief history of the photovoltaic properties of Kesterite solar cells and their effective parameters for high efficiency. These various types of effective parameters in photovoltaic applications are discussed briefly and resoluted the hurdles of efficiency of solar cells problems. Besides this, we also try to find out the issues of the Kesterite materials based on the structure, band structure, electronic structure and studied how to get more than 20% efficiency of solar cells using the different buffer layers.

Second chapter deals with the synthesis methods and characterization techniques for energy materials. The synthesis methods especially Co-precipitation Spray Pyrolysis and Hydrothermal/Solvothermal methods are described and it is explained that how these methods are suitable to synthesis the functional nanomaterials for photovoltaic devices. These synthesis methods must usually of low cost, less time consuming and eco-friendly. The synthesized functional materials are analyzed by X-Ray diffraction (XRD), UV-Visible (UV-VIS) Spectroscopy, and Scanning Electron Microscopy (SEM) / Field Emission Scanning Electron Microscopy (FESEM), Energy Dispersive X-Ray Spectroscopy, X-Ray Photoelectron Spectroscopy (XPS), etc. Besides this, brief studies of the photovoltaic nanomaterials are also included in this chapter, which suggests the basic motivation to work in this field.

Third chapter includes the synthesis of ZnO nanomaterial without any surfactants and characterization for window layer in solar cell applications. Scanning electron microscope (SEM), X-ray diffraction (XRD), and Energy Dispersive X-ray spectroscopy (EDS) are the necessary characterization techniques used for the confirmation of the shapes and sizes of ZnO nanoparticles. The study of powder ZnO nanoparticles is the versatile application in a window layer of the third-generation solar cell, and such powder is also beneficial for commercial productions as well.

Fourth chapter deals with the synthesis and characterization of functional material (I_2-II-IV-VI_4) viz. Cu_2ZnSnS_4 without vacuum annealing for solar cell absorber layer application, which is a low-cost and less-time consuming and ecofriendly co-precipitation method. In the synthesis mechanism, the functional materials are synthesized without any surfactants and vacuum/noble gases, which makes it an economically low-cost method in comparison to the other methods. The novelty of this work is the synthesis of spherical CZTS nanomaterials without any sulpherization/vacuum/inert annealing. The surface-to-volume ratio of the spherical CZTS nanomaterials has enhanced the solar energy conversion and this is an appropriate property for photovoltaic materials. The characteristic results of the CZTS show them best materials for photovoltaic devices. However, the thin film of the CZTS nanomaterials is the economically cheapest and the suitable material for Kesterite solar cells applications.

Chapter five contains the synthesis and characterization of functional material (IV-VI) SnS for energy applications. After synthesis of the SnS nanomaterials by low-cost Co-precipitation method, thin-film is fabricated with help of the self-made spray pyrolysis method (SPM). The first time, the grown thin films by SPM method are found to have hydrophobic and scratchproof nature of SnS nano flakes. The synthesis of SnS thin film for photodetector by the SPM route has found with low response/recovery time in comparison to the CVD route The stability of the SnS photodetector is also found to be stable for around one year. The SnS thin film also resolves the usual problem of thermionic and diffusion losses, and recombination; and SnS thin film can be used as a JABS layer in the hetero-junction device with structure Ag/ARC/Al-ZnO/i-ZnO/CdS/**SnS**/CZTS/ITO.

Chapter six gives the brief conclusions and future prospects of the research work presented in the thesis. In this chapter, we discuss how the functional materials can be used to resolve the issues of stoichiometry phase, toxic environment, time taking processes, and cost of materials and synthesis methods. Among these problems, thermionic and diffusion loss, and recombination, are also resolved by selecting suitable functional materials and techniques. For the synthesis of the suitable functional materials, we have explained the synthesis methods having low cost and suitable characterization techniques for the as-synthesize and their applications in fabricating energy devices. Besides this, the prospects of the photovoltaic nanomaterials are also included in this chapter, which suggests that, if we follow the low-cost synthesis routes, then we can fabricate low cost, less time consuming, and eco-friendly photovoltaic devices. In this way, functional materials may be cheap and best for energy device fabrications. In addition to this, such studies give basic motivation to the researchers to look their research work into the field of using functional materials as the energy materials.

If researchers adopt the co-precipitations to synthesize the materials like ZnO for window layer and CZTS for absorber layer, the results of the Kesterite structure based photovoltaic devices will be competing for the champion results of the conventional photovoltaic devices and such devices have cheap, non-toxic, and ecofriendly features. The researchers can also adopt the simple thin-film spray pyrolysis method for SnS hydrophobic photodetector with the best photo response and recovery time. This simple method may also be used in the mass production of devices.

References:

[1] M. F. Ashby and D. R. H. Jones, Engineering Materials1: An Introduction to Their Properties and Applications, *Published by Elsevier Ltd.*, Butterworth-Heinemann, Woburn, UK, 2005.

[2] P. L. Mangonon, The Principles of Materials Selection for Engineering Design, *Upper Saddle River,* NJ: Prentice-Hall PTR, Paramus, 1999.

[3] Jr. W. D. Callister and D. G. Rethwisch, Materials Science and Engineering: An Introduction, *John Wiley & Sons*, ISBN-13: 978-0-471-73696-7, USA, 2007.

[4] https://www.eia.gov/energyexplained/us-energy-facts/data-and-statistics.php, 2020.

[5] A. Luque and S. Hegedus, Handbook of photovoltaic science and Engineering, *John Wiley and Sons Ltd*, The Atrium, Southern Gate, Chichester, West Sussex England, 2003.

[6] E. Becquerel, Mémoire sur les effets électriques produits sous linfluence des rayons solaires, *Comptes Rendus* 9, 561-567, 1839.

[7] D. Chapin, C. Fuller and G. Pearson, A New Silicon p-n Junction Photocell for Converting Solar Radiation into Electrical Power, *J. Appl. Phy*., 25, 676-677, 1954.

[8] W. Shockley and H. Queisser, Detailed Balance Limit of Efficiency of *pn*-Junction Solar Cells, *J. Appl. Phys.*, 32, 510-519, 1961.

[9] D. Cusano, CdTe solar cells and photovoltaic heterojunctions in II–VI compounds, *sol. Stat. Elect.*, 6, 217-232, 1963.

[10] Z. I. Alferov, The history and future of semiconductor heterostructures, *Semiconductors,* 32, 1-14, 1998.

[11] A. Luque and S. Hegedus, Handbook of Photovoltaic Science and Engineering, *John Wiley & Sons Ltd*, ISBN 0-471-49196-9, The Atrium, Southern Gate, Chichester, West Sussex PO19 8SQ, England, 2003.

[12] I. Pelant, J. Valenta, Luminescence of disordered semiconductors, Luminescence Spectroscopy of Semiconductors, *Oxf. Uni. Press.*, New York, 2012.

[13] M. A. Green, Solar cells: operating principles, technology, and system applications, *Englewood Cliffs, NJ, Prentice-Hall, Inc.,*United States, 1982.

[14] K. D. Jäger, O. Isabella, A. H. M. Smets, R. A. C. M. M. V. Swaaij and M. Zeman, Solar energy: fundamentals, technology, and systems, *Cambridge: UIT Cambridge,* ISBN: 9781906860738, United Kingdom, 2016.

[15] E. Y. Shvets, S. L. Khrypko, and E. I. Zubko, Investigation of methods used in calculations of solar cell parameters, *Rad.s Commun. Syst*. 52, 16-23, 2009.

[16] M. T. Kibria, A. Ahammed, S. M. Sony, F. Hossain and S. U. Islam, A Review: Comparative studies on different generation solar cells technology, *Proceedings of 5th International Conference on Environmental Aspects of Bangladesh, ICEAB,* 2014, doi:http://benjapan.org/ICEAB/proceedingsICEAB14/i14%20p33.pdf.

[17] K. D. G. Imalka Jayawardena, L. J. Rozanski, C. A. Mills, M. J. Beliatis, N. A. Nismy and S. R. P. Silva, Inorganics-in-Organics: recent developments and outlook for 4G polymer solar cells, *Nanoscale*, 5, 8411-8427, 2013.

[18] V. Smile, Energy Transitions: Global and National Perspectives & BP Statistical Review of World Energy, *Praeger Publishers Inc,* ISBN 978-1440853241**,**
Westport, New York, 2017.

[19] https://www.tesla.com/ns_videos/2019-tesla-impact-report.pdf_2021

[20] A. Muratoglu and M. I. Yuce, World energy outlook and place of renewable resources, *Int. J. Sci. and Tech. Rech.*, 1 10–17, 2015.

[21] K. Wang, R. E. Dickinson, Contribution of solar radiation to decadal temperature variability over land, *Proc. Natl. Acad. Sci.* U.S.A., 110, 14877–14882, 2013.

[22] H. B. Michaelson, The work function of the elements and its periodicity, *J. Appl. Phys.*, 48, 4729–4733, 1977.

[23] G. Antoine, A. S. Glaude, P. Neveu and L. Thomas, Comprehensive simulation and optimization of porous SiO_2 anti-reflective coating to improve glass solar transmittance for solar energy applications, *Sol. Energ. Mat. Sol. Cells*, 182, 166-177, 2018.

[24] N. Boukortt and S. Patane, High-Efficiency Cu(In1−xGax)Se_2 Solar Cell Investigation with Single Layer Antireflection Coating of MgF2. *2nd International Conference on Smart Grid and Renewable Energy (SGRE)*, Doha, Qatar, 1-5, 2019. https://doi.org/ 10.1109/SGRE46976.2019.9020702..

[25] N. Rezaei, O. Isabella, Z. Vroon and M. Zeman, Optical optimization of a multi-layer wideband anti-reflection coating using porous MgF_2 for sub-micron-thick CIGS solar cells, *Sol. Energ.*, 177, 59-67, 2019.

[26] S. K. Dhungel, J. Yoo, K. Kim, S. Jung, S. Ghosh, and J. Yi, Double-Layer Antireflection Coating of MgF_2/SiN_x for Crystalline Silicon Solar Cells, *J. Korean Phys. Soc.: JKPS,* 49(3), 885-889, 2006.

[27] S. E. Lee, S. W. Choi and J. Yi, Optical properties of ZnO/MgF_2 bilayer thin films prepared by PVD technique, *Thin Solid Films,* 376, 208, 2000.

[28] E. R. Rwenyagila, B. A. Tuffour, M. G. Z. Kana, O. A. Ojo, W. O. Soboyejo, Optical properties of ZnO/Al/ZnO multilayer films for large-area transparent electrodes, *J. Mater. Res.*, 29(24), 912-2920, 2014.

[29] B. W. Sanders and A. Kitai, Atomic Layer Deposition of Zn(O,S) Alloys Using Diethylzinc with H_2O and H_2S: Effect of Exchange Reactions, *Chem. Mater*. 4, 1005-1011, 1992.

[30] S. Merdes, R. Saez-Araoz, A. Ennaoui, J. Klaer, M. C. Lux-Steiner, and R. Klenk, Recombination mechanisms in highly efficient thin film Zn(S,O)/Cu(In,Ga)S_2Zn(S,O)/Cu(In,Ga)S_2 based solar cells, *Appl. Phys. Lett.,* 95, 213502, 2009.

[31] P. Sinsermsuksakul, K. Hartman, S. B. Kim, J. Heo, L. Sun, H. H. Park, R. Chakraborty, T. Buonassisi and R. G. Gordon, Enhancing the efficiency of

SnS solar cells via band-offset engineering with a zinc oxysulfide buffer layer, *Appl. Phys. Lett.*, 102, 053901, 2013.

[32] C. Persson, C. Platzer-Bjorkman, J. Malmstrom, T. Torndahl, and M. Edoff, Strong Valence-Band Offset Bowing of ZnO1−xSx Enhances p-Type Nitrogen Doping of ZnO-like Alloys, *Phys. Rev. Lett.* 97, 146403, 2006.

[33] T. Minemoto, T. Matsui, H. Takakura, Y. Hamakawa, T. Negami, Y. Hashimoto, T. Uenoyama, and M. Kitagawa, *Sol. Energ. Mat. Sol. Cell.*, 67, 83-88, 2001.

[34] M. Niemegeers, Burgelman, and A. Devos, *Applied Physics Letters*, 67, 843-845, 1995.

[35] J. Poortmans and V. Arkhipov, Thin-film solar cells: fabrication, characterization, and applications., Hoboken, *NJ:John Wiley* & *Sons Inc.*, Chichester, England, 2007.

[36] Y. Kim, W. Lee, D. R. Jung, J. Kim, S. Nam, H. Kim, and B. Park, Optical and electronic properties of post-annealed ZnO:Al thin films, *Appl. Phys. Lett.*, 96, 171902, 2010.

[37] W. V. D. Stam, A. C. Berends and C. d. M. Donega, Prospects of Colloidal Copper Chalcogenide Nanocrystals, *Chem. Phys. Chem.*, 17(5), 559-81, 2016.

[38] Z. Bai, J.Yang, D. Wang, Thin-film CdTe solar cells with an absorber layer thickness in micro-and sub-micrometer scale, *Appl. Phys. Lett.*, 99(14), 143502, 2011.

[39] N. Romeo, A. Bosio, A. Romeo, An innovative process is suitable to produce high-efficiency CdTe/CdS thin-film modules, *Sol. Energy Mater. Sol. Cells*, 94(1), 2-7, 2010.

[40] http://investor.firstsolar.com/releasedetail.cfm?ReleaseID=956479, 23 February 2016.

[41] S. Wagner, J. L. Shay, P. Migliorato and H. M. Kasper, $CuInSe_2$/CdS heterojunction photovoltaic detectors, *Appl. Phys. Lett.*, 25(8), 434-435, 1974.

[42] L. L. Kazmerski, F. R. White, and G. K. Morgan, Thin-film CuInSe2/CdS heterojunction solar cells. *Appl. Phys. Lett.*, 29(4), 268-270, 1976.

[43] P. Jackson, R. Wuerz, D. Hariskos, E. Lotter, W. Witte and M. Powalla, Effects of heavy alkali elements in Cu(In,Ga)Se_2 solar cells with efficiencies up to 22.6%, *Phys. Status Solidi RRL*, 10(8), 593-586, 2016.

[44] N. K. Reddy, M. Devika and E. S. R. Gopal, Review on Tin (II) Sulfide (SnS) Material: Synthesis, Properties, and Applications, *Crit. Rev. Solid State & Mater. Sci.*, 40:359–398, 2015.

[45] P. K. Nair, A. R. Garcia-Angelmo, M. T. S. Nair, Cubic and orthorhombic SnS thin-film absorbers for tin sulfide solar cells. *Phys. Status Solidi A.*, 213 (1): 170–177, 2016.

[46] D. B Mitzi, O. Gunawan, T. K Todorov, and D. Aaron, R. Barkhouse, Prospects and performance limitations for Cu-Zn-Sn-S-Se photovoltaic technology. Philosophical Transactions of the Royal Society of London A: Mathematical, *Physical and Engineering Sciences*, 371(1996), 20110432, 2013.

[47] W. Wang, M. T. Winkler, O. Gunawan, T. Gokmen, T. K. Todorov, Y. Zhu, and D. B. Mitzi, Device characteristics of CZTSSe thin-film solar cells with 12.6% efficiency, *Adv. Energy Mater.*, 4(7):1301465–n/a, ISSN 1614-6840, 2014.

[48] S. Giraldo, Z. Jehl, M. Placidi, V. I. Roca, E. Saucedo, A. P. Rodríguez, Progress and Perspectives of Thin Film Kesterite Photovoltaic Technology: A Critical Review, *Adv. Energy Mater.*, 31(16), 1806692, 2019.

[49] J. S. Seol, S. Y. Lee, J. C. Lee, H. D. Nam and K. H. Kim, Electrical and optical properties of Cu_2ZnSnS_4 thin films prepared by rf magnetron sputtering process. *Sol. Energy Mater. Sol. Cells*, 75(1), 155-162, 2003.

[50] T. Tanaka, T. Nagatomo, D. Kawasaki, M.Nishio, Q. Guo, A. Wakahara and H. Ogawa, Preparation of Cu_2ZnSnS_4 thin films by hybrid sputtering. Journal of *Phys. Chem. of Solids*, 66(11), 1978-1981, 2005.

[51] S. R. Hall, J. T. Szymanski, and J. M. Stewart, Kesterite, (Cu<2)(Zn, Fe) (SnS< 4), and stannite, (Cu<2)(Fe,Zn)(SnS<4), structurally similar but distinct minerals. *Canad Mineral*, 16(2), 131-137, 1978.

[52] S. Schorr, Structural aspects of adamantine like multinary chalcogenides, *Thin Solid Films*, 515 (15), 5985-5991, 2007.

[53] I. D. Olekseyuk, L. D. Gulay, I. V. Dydchak, L. V. Piskach, O. V. Parasyuk, O. V. Marchuka, Single crystal preparation and crystal structure of the Cu_2Zn/Cd, Hg/$SnSe_4$ compounds, *J. Alloy. Comp.*, 340, 141–145, 2002.

[54] A. Nateprov, V. C. Kravtsov, G. Gurieva, S. Schorr, Single-crystal X-ray structure investigation of $Cu_2ZnSnSe_4$, *Surf. Eng. Appl. Electrochem.*, 49, 423–426, 2013.

[55] S. Bourdais, C. Choné, B. Delatouche, A. Jacob, G. Larramona, C.Moisan, A. Lafond, F. Donatini, G. Rey, S. Siebentritt, A. Walsh, G. Dennler, Is the Cu/Zn disorder the main culprit for the voltage deficit in kesterite solar cells?, *Adv. Energy Mater.*, 6(12), 1502276, 2016.

[56] S. Chen, X. G. Gong, A. Walsh, and S. H. Wei, Crystal and electronic band structure of Cu_2ZnSnX_4 (X=S and Se) photovoltaic absorbers: first-principles insights. *Appl. Phys. Lett.*, 94(4), 41903, 2009.

[57] J. Paier, R. Asahi, A. Nagoya, and G. Kresse, Cu_2ZnSnS_4 as a potential photovoltaic material: a hybrid Hartree-Fock density functional theory study, *Phys. Rev. B*, 79 (11), 115126, 2009.

[58] JCPDS Card: 26-0575.

[59] H. Wang, Progress in thin-film solar cells based on Cu_2ZnSnS_4, *Int. J. Photo energy*, 2011, 801292–801302, 2011.

[60] L. Guen, W. S. Glaunsinger, Electrical, Magnetic and EPR studies of the quaternary chalcogenide $Cu_2AIIBIVX_4$ prepared by iodine transport, *J. Solid State Chem.*, 35, 10–21, 1980.

[61] T. Tinoco, C. Rincon, M. Quintero, G. S. Perez, Phase diagram and optical energy gaps for CuInyGa1−ySe_2 alloys, *Phys. Status Solidi*, 124, 427–434, 1991.

[62] X. Zhang, G. Guo, C. Ji, K. Huang, C. Zha, Y. Wang, L. Shen, A. Gupta and N. Bao, Efficient thermolysis route to monodisperse Cu_2ZnSnS_4 nanocrystal with controlled shape and structure, *Sci. Rep.*, 4, 5086–5093, 2014.

[63] S. Chen, X. G. Gong, A. Walsh, S. H. Wei, Crystal and electronic band structure of Cu_2ZnSnX_4 (X=S and Se) photovoltaic absorbers: first-principles insights, *Appl. Phys. Lett.,* 94, 041903–041907, 2009.

[64] K. Ito, Copper Zinc Tin Sulfide-Based Thin Film Solar Cells, first ed., *John Wiley and Sons Ltd.*, Chichester, West Sussex, United Kingdom, 2015.,

[65] O. V. Galan, J. A. A. Arvizu, Y. Sanchez, M. E. Rodriguez, E. Saucedo, D. S. Jimenez and M. Titsworth, Route towards low cost-high efficiency second generation solar cells: current status and perspectives, *J. Mater. Sci. Mater. Electron*., 26, 5562–5572, 2014.

[66] A. Fairbrother, E. Saucedo, X. Fontane, V. Izquierdo-Roca, D. Sylla, M. E Rodriguez, F. A. P. Adugalo, O. V. Galan and A. P. Rodriguez, Preparation of 4.8% Efficiency CZTS Based Solar Cell by a Two-step Process, *Photovoltaic Specialists Conference (PVSC),* 2012, 002679–002684, 2012.

[67] H. Matsushita, T. Ichikawa, A. Katsui, Structural, thermodynamical and optical properties of Cu_2-II-IV-VI_4 quaternary compounds, *J. Mater. Sci.,* 40, 2003–2005, 2005.

[68] W. Wang, M. T. Winkler, O. Gunawan, T. Gokmen, T. K. Todorov, Y. Zhu and D. B. Mitzi, Device characteristics of CZTSSe thin-film solar cells with 12.6% efficiency, *Adv. Energy Mater.,* 4, 1301465–1301470, 2014.

[69] P. Jackson, R. Wuerz, D. Hariskos, E. Lotter, W. Witte and M. Powalla, Cover Picture: effects of heavy alkali elements in Cu(In, Ga)Se_2 solar cells with efficiencies up to 22.6%, *Phys. Status Solidi R,* 10, 583–586, 2016.

[70] B. Shin, O. Gunawan, Y. Zhu, N.A. Bojarczuk, S. J. Chey, S. Guha, Thin-film solar cell with 8.4% power conversion efficiency using an earth-abundant Cu_2ZnSnS_4 absorber, *Prog. Photovolt.,* 21, 72–76, 2011.

[71] N. Kamoun, H. Bouzouita, B. Rezig, Fabrication and characterization of Cu_2ZnSnS_4 thin films deposited by spray pyrolysis technique, *Thin Solid Films,* 515, 5949–5952, 2007.

[72] K. Pal, P. Singh, A. Bhaduri and K.B. Thapa, Current challenges and future prospects for a highly efficient (> 20%) kesterite CZTS solar cell: A review, *Sol. Energy Mater. Sol. Cells,* 196, 138–156, 2019.

[73] T. M. Friedlmeier, N. Wieser, T. Walter, H. Dittrich and H. W. Schock, Heterojunctions based on Cu_2ZnSnS_4 and $Cu_2ZnSnSe_4$ thin films, *Proceedings of the 14th European Photovoltaic Specialists Conference, Barcelona,* 1242–1245, 1997.

[74] S. Chen, X. G. Gong, A. Walsh and S. H. Wei, Defect physics of the Kesterite thin-film solar cell absorber Cu2ZnSnS4, *Appl. Phys. Lett.*, 96, 021902–021906, 2010.

[75] A. Walsh, S. Chen, S. H. Wei, X. G. Gong, Kesterite of the thin-film solar cell: advances of materials modeling Cu2ZnSnS4, *Adv. Energy Mater.*, 2, 400–409, 2012.

[76] A. Nagoya, R. Asahi, R. Wahl, G. Kresse, Defect formation and phase stability of Cu_2ZnSnS_4 photovoltaic material, *Phys. Rev. B,* 81, 113202-113206, 2010.

[77] D. Mitzi, O. Gunawan, T. Todorov, K. Wang, S. Guha, The path towards a high-performance solution-processed kesterite solar cell, *Sol. Energy Mater. Sol. Cell.*, 95, 1421, 2011.

[78] H. Katagiri, K. Jimbo, M. Tahara, H. Araki, K. Oishi, The influence of the composition ratio on CZTS-based thin-film solar cells, *Mater. Res. Soc. Symp. Proc.*, 1165, 2009.

[79] K. Ito, Copper Zinc Tin Sulfide-Based Thin Film Solar Cells, first ed., *John Wiley and Sons Ltd.,* Chichester, West Sussex, United Kingdom, 2015.

[80] S. Chen, A. Walsh, Y. Luo, J. H. Yang, X. G. Gong and S. H. Wei, Wurtzite derived polytypes of kesterite and Stannite quaternary chalcogenide semiconductors, *Phys. Rev. B,* 82, 195203–195211, 2010.

[81] J. O. Jeon, K. D. Lee, L. S. Oh, S. W. Seo, D. K. Lee, H. Kim, J. Jeong, M. J. Ko, B. S. Kim, H. J. Son, J. Y. Kim, Highly efficient copper–zinc–tin–

selenide (CZTSe) solar cells by electrodeposition, *Chem. Sus. Chem.*, 7, 1073-1077, 2014.

[82] N. Nakayama and K. Ito, Sprayed films of stannite Cu_2ZnSnS_4, *Appl. Surf. Sci.*, 92, 171–175, 1996.

[83] N. Kamoun, H. Bouzouita, B. Rezig, Fabrication and characterization of Cu_2ZnSnS_4 thin films deposited by spray pyrolysis technique, *Thin Solid Films,* 515, 5949–5952, 2007.

[84] F. Gao, S. Yamazoe, T. Maeda, K. Nakanishi and T. Wada, Structural and optical properties of In-free $Cu_2ZnSn(S, Se)_4$ solar cell materials, *Jpn. J. Appl. Phys*., 51, 1–5, 10NC29, 2012.

[85] S. Ahn, S. H. Jung, J. Y. Gwak, A. Cho, K. Shin, K. Yoon, D. Y. Park, H. Cheong, J. H. Yun, Determination of bandgap energy (Eg) of $Cu_2ZnSnSe_4$ thin films: on the discrepancies of reported band gap values, *Appl. Phys. Lett.* 97, 1–3 021905, 2010.

[86] R. Haight, A. Barkhouse, O. Gunawan, B. Shin, M. Copel, M. Hopstaken and D. B. Mitzi, Band alignment at the $Cu_2ZnSn(SxSe1–x)_4$/CdS interface, *Appl. Phys. Lett.,* 98, 253502-253506, 2011.

[87] S. Chen, A. Walsh, Y. Luo, J. H. Yang, X. G. Gong, S. H. Wei, Wurtzite derived polytypes of kesterite and Stannite quaternary chalcogenide semiconductors, *Phys. Rev. B*, 82, 195203-195211, 2010.

[88] J. Paier, M. Marshman, K. Hummer, G. Kresse, I. C. Gerber, J. G. Angyan, Screened hybrid density functionals applied to solids, *J. Chem. Phys*., 124, 154709-154723, 2006.

[89] S. Chen, X. G. Gong, A. Walsh, S. H. Wei, Crystal and electronic band structure of Cu_2ZnSnX_4 (X=S and Se) photovoltaic absorbers: first-principles insights, *Appl. Phys. Lett.*, 94, 041903–041907, 2009.

[90] J. Paier, R. Asahi, A. Nagoya and G. Kresse, Cu_2ZnSnS_4 as a potential photovoltaic material: a hybrid Hartree-Fock density functional theory study, *Phys. Rev. B*, 79, 115126–115134, 2009.

[91] K. Ito and T. Nakazawa, Electrical and optical properties of Stannite-type quaternary semiconductor thin films, *Jpn. J. Appl. Phys*., 27, 2094–2097, 1988.

[92] T. M. Friedlmeier, N. Wieser, T. Walter, H. Dittrich and H. W. Schock, Heterojunctions based on Cu_2ZnSnS_4 and $Cu_2ZnSnSe_4$ thin films, *Proceedings of the 14th European Photovoltaic Specialists Conference, Barcelona*, 1242–1245, 1997.

[93] H. Katagiri, Kotoe Saitoh, Tsukasa Washio, Hiroyuki Shinohara, Tomomi Kurumadani, Shinsuke Miyajima, Development of thin-film solar cell-based on Cu_2ZnSnS_4 thin films, *Sol. Energy Mater. Sol. Cells*, 65, 141–148, 2001.

[94] H. Kategori, Kazuo Jimbo, S. yamada, T. kamimura,W. S. maw, T. fukano, T. Ito, T. motohiro, Enhanced conversion efficiencies of Cu_2ZnSnS_4-based thin-film solar cells by using the preferential etching technique, *APEX 1*, 041201–041202, 2008.

[95] T. K. Todorov, K. B. Reuter, D. B. Mitzi, High-efficiency solar cell with earth-abundant liquid-processed absorber, *Adv. Energy Mater.*, 22, E156–E157, 2010.

[96] W. Wang, M. T. Winkler, O. Gunawan, T. Gokmen, T. K. Todorov, Y. Zhu, D. B. Mitzi, Device characteristics of CZTSSe thin-film solar cells with 12.6% efficiency, *Adv. Energy Mater*, 4, 1301465–1301470, 2014.

[97] L. Yao, J. Ao, M.J. Jeng, J. Bi, S. Gao, G. Sun, Q. He, Z. Zhou, Y. Sun, L.B. Chang, A CZTSe solar cell with 8.2% power conversion efficiency fabricated using electrodeposited Cu/Sn/Zn precursor and a three-step selenization process at low Se pressure, *Sol. Energy Mater. Sol. Cells*, 159, 318-324, 2017.

[98] S. Giraldo, T. Thersleff, G. Larramona, M. Neuschitzer, P. Pistor, K. Leifer, A. Perez-Rodriguez, C. Moisan, G. Dennler, E. Saucedo, $Cu_2ZnSnSe_4$ solar cells with 10.6% efficiency through innovative absorber engineering with Ge superficial nanolayer, *Prog. Photovoltaics*, 24, 1359–1367, 2016.

[99] G. Zoppi, I. Forbes, R. W. Miles, P. J. Dale, J. J. Scragg and L. M. Peter, $Cu_2ZnSnSe_4$ Thin-film solar cells produced by selenization of magnetron sputtered precursors, *Prog. Photovolt.*, 17, 315–319, 2009.

[100] S. Bag, O. Gunawan, T. Gokmen, Y. Zhu, D. B. Mitzi, Hydrazine-Processed Gesubstituted CZTSe solar cells, *Chem. Mater.*, 24, 4588–4593, 2012.

[101] S. A. Kissin, A Reinvestigation of the Stannite (Cu_2FeSnS_4)-kesterite (Cu_2ZnSnS_4) pseudo-binary system, *Can. Mineral.*, 27, 689–697, 1989.

[102] S. A. Nadi, P. Chelvanathan, Z. Zakaria, M. M. Alam, Z. A. Alothman, K. Sopian, N. Amin, Post-deposition annealing effect on Cu_2ZnSnS_4 thin films grown at different substrate temperature, *Int. J. Photoenergy*, 2014, 589027–589034, 2014.

[103] Shin, O. Gunawan, Y. Zhu, N.A. Bojarczuk, S.J. Chey and S. Guha, Thin-film solar cell with 8.4% power conversion efficiency using an earth-abundant Cu_2ZnSnS_4 absorber, *Prog. Photovolt.*, 21, 72–76, 2011.

[104] J. Paier, M. Marshman, K. Hummer, G. Kresse, I.C. Gerber and J.G. Angyan, Screened hybrid density functionals applied to solids, *J. Chem. Phys.*, 124, 154709–154723, 2006.

[105] J. O. Jeon, K. D. Lee, L. S. Oh, S. W. Seo, D. K. Lee, H. Kim, J. H. Jeong, M. J. Ko, B. S. Kim, H. J. Son and J. Y. Kim, Highly efficient copper–zinc–tin–selenide (CZTSe) solar cells by electrodeposition, *Chem. Sus. Chem.*, 7, 1073–1077, 2014.

[106] X. Zeng, K. F. Tai, T. Zhang, C. W. John Hoa, X. Chen, A. Huan, T. C. Sum and L. H. Wong, $Cu_2ZnSn(S,Se)_4$ kesterite solar cell with 5.1% efficiency using spray pyrolysis of aqueous precursor solution followed by selenization, *Sol. Energy Mater. Sol. Cells,* 124, 55–60, 2014.

[107] G. Larramona, S. Bourdais, A. Jacob, C. Chone, T. Muto, Y. Cuccaro, B. Delatouche, C. Moisan, D. Pere, G. Dennler, Efficient Cu_2ZnSnS_4 solar cells spray-coated from a hydro-alcoholic colloid synthesized by the instantaneous reaction, *RSC Adv.*, 4, 14655–14662, 2014.

[108] O. V. Galan, J. A. Andrade-Arvizu, Y. Sanchez, M. E. Rodriguez, E. Saucedo, D. Seuret-Jimenez and M. Titsworth, Route towards low cost-high efficiency second generation solar cells: current status and perspectives, *J. Mater. Sci. Mater. Electron.*, 26, 5562–5572, 2014.

[109] V. G. Rajeshmon, N. Poornima, C. S. Kartha, K. P. Vijayakumar, Modification of optoelectronic properties of sprayed In_2S_3 thin-film diffusion for application as a buffer layer in CZTS based solar cell, *J. Alloy. Comp.*, 553, 239–244, 2013.

[110] O. V. Galan, M. Caurel, M. E. Rodriguez, D. J. Olarte, M. A. Frutis, E. Saucedo, Electrical properties of sprayed Cu_2ZnSnS_4 thin films and its relation with secondary phase formation and solar cell performance, *Sol. Energy Mater. Sol. Cells*, 132, 557–562, 2013.

[111] M. Espindola Rodriguez, D. Sylla, Y. Sanchez, S. L. opez-Marino, X. Fontane, J. Lopez-Garcıa, M. Placidi, A. Perez-Rodrıguez, O. Vigil-Galan, and E. Saucedo, Pneumatically sprayed Cu_2ZnSnS_4 films under Ar and Ar–H_2 atmosphere, *J. Phys. D Appl. Phys*., 47, 245101-245108.

[112] O. Vigil-Galan, Maykel Courel, M. Espindola-Rodriguez, V. Izquierdo Roca, E. Saucedo, A. Fairbrother, Toward a high Cu_2ZnSnS_4 solar cell efficiency processed by spray pyrolysis method, *J. Renew. Sustain. Energy*, 5, 053137-053152, 2013.

[113] M. E. Rodriguez, D. Sylla, Y. Sanchez, S. Lopez-Marino, X. Fontane, J. Lopez-Garca1, M. Placidi, A. Perez-Rodrıguez, O. Vigil-Galan and E. Saucedo, Pneumatically sprayed Cu_2ZnSnS_4 films under Ar and Ar–H_2 atmosphere, J. *Phys. D Appl. Phys.*, 47, 245101-245109, 2014.

[114] H. Katagiri, K. Jimbo, W. S. Maw, K. Oishi, M. Yamazaki, H. Araki, A. Takeuchi, Development of CZTS-based thin-film solar cells, *Thin Solid Films* 517, 2455–2460, 2009.

[115] S. Sahayaraj, G. Brammertz, M. Buffiere, M. Meuris, J. Vleugels and J. Poortmans, Effect of Cu content and temperature on the properties of $Cu_2ZnSnSe_4$ solar cells, *EPJ Photovoltaics*, 7, 70304–70313, 2016.

[116] J. Piekoszewski, J. J. Loferski, R. Beaulieu, J. Beall, B. Roessler and J. Shewchun, RF sputtered $CuInSe_2$ thin films, *Sol. Energy Mater*., 2, 363–372, 1980.

[117] R. Noufi, R. Axton, C. Herrington and S. K. Deb, Electronic properties versus composition of thin films of $CuInSe_2$, *Appl. Phys. Lett*., 45, 668–670, 1984.

[118] J. Tuttle, D. Albin, J. Goral, C. Kennedy and R. Noufi, Effects of composition and substrate temperature on the electro-optical properties of thin-film $CuInSe_2$ and $CuGaSe_2$, *Sol. Cell.*, 24, 67–79, 1988.

[119] I. Repins, M.A. Contreras, B. Egaas, C. DeHart, J. Scharf, C. L. Perkins, B. To and Romenel Noufi, 19.9%-efficient ZnO/CdS/$CuInGaSe_2$ solar cell with 81.2% fill factor, *Prog. Photovoltaic*, 16, 235–239, 2008.

[120] G. S. Babu, Y. B. Kishore Kumar, P. U. Bhaskar and V. S. Raja, Effect of Cu/(Zn+Sn) ratio on the properties of co-evaporated $Cu_2ZnSnSe_4$ thin films, *Sol. Energ. Mat. Sol. C.*, 94, 221-226, 2010.

[121] C. Malerba, C. L. A. Ricardo, M. Valentini, F. Biccari, M. Muller, L. Rebuffi, E. Esposito, P. Mangiapane, P. Scardi, and A. Mittiga, Stoichiometry effect on Cu_2ZnSnS_4 thin films morphological and optical properties, *J. Renew. Sust. Energ.*, 6, 011404-12, 2014.

[122] H. Katagiri, K. Jimbo, M. Tahara, H. Araki and K. Oishi, The influence of the composition ratio on CZTS-based thin-film solar cells, *Mater. Res. Soc. Symp. Proc.*, 01, 1165, 2009.

[123] Y. B. K. Kumar, G. S. Babu, P. U. Bhaskar, S. S. Vanjari, Effect of starting-solution pH on the growth of Cu_2ZnSnS_4 thin films deposited by spray pyrolysis, *Physica Status Solidi A*, 206, 1525–1530, 2009.

[124] T. Tanaka, A. Yoshida, D. Saiki, K. Saito, Q. Guo, M. Nishio and T. Yamaguchi, Influence of composition ratio on properties of Cu_2ZnSnS_4 thin films fabricated by co-evaporation, *Thin Solid Films*, 518, S29–S33, 2010.

[125] K. Tanaka, Y. Fukui, N. Moritake, H. Uchiki, Chemical composition dependence of morphological and optical properties of Cu_2ZnSnS_4 thin films deposited by sol-gel sulfurization and Cu_2ZnSnS_4 thin-film solar cell efficiency, *Sol. Energ. Mat. Sol. C.*, 95, 838-842, 2011.

[126] M. E. Rodriguez, M. Placidi, O. V. Galan, V. I. Roca, X. Fontane, A. Fairbrother, et al., Compositional optimization of photovoltaic grade Cu_2ZnSnS_4 films grown by pneumatic spray pyrolysis, *Thin Solid Films*, 535, 67–72, 2013.

[127] C. Malerba, F. Biccari, C. Leonor A. Ricardo, M. Valentini, R. Chierchia, M. Muller, A. Santoni, E. Esposito, P. Mangiapane, P. Scardi and A. Mittig, CZTS stoichiometry effects on the band gap energy, *J. Alloy. Comp.*, 582, 528–534, 2014.

[128] T. Gershon, K. Sardashti, Y. S. Lee, O. Gunawan, S. Singh, D. Bishop, A. C. Kummel and R. Haight, Compositional effects in $Ag_2ZnSnSe_4$ thin films and photovoltaic devices, *Acta. Mater.*, 126, 383-388, 2017.

[129] S. Chen, J. H. Yang, X. G. Gong, A. Walsh and S. H. Wei, Intrinsic point defects and complexes in the quaternary kesterite semiconductor Cu_2ZnSnS_4, *Phys. Rev. B*, 81, 245204, 2010.

[130] H. Katagiri, K. Saitoh, T. Washio, H. Shinohara, T. Kurumadani and S. Miyajima, Development of thin-film solar cell based on Cu_2ZnSnS_4 thin films, *Sol. Energ. Mat. Sol. C.*, 65, 141-148, 2001.

[131] R. A. Wibowo, W. S. Kim, E. S. Lee, B. Munir and K. H. Kim, Single-step preparation of quaternary $Cu_2ZnSnSe_4$ thin films by RF magnetron sputtering from binary chalcogenide targets, *J. Phys. Chem. Solids*, 68, 1908-1913, 2007.

[132] T. Tanaka, T. Nagatomo, D. Kawasaki, M. Nishio, Q. X. Guo, A. Wakahara, A. Yoshida and H. Ogawa, Preparation of Cu_2ZnSnS_4 thin films by hybrid sputtering, *J. Phys. Chem. Solids*, 66, 1978-1981, 2005.

[133] S. Chen, A. Walsh, X. G. Gong and S. H. Wei, Classification of lattice defects in the kesterite Cu_2ZnSnS_4 and $Cu_2ZnSnSe_4$ earth-abundant solar cell absorbers, *Adv. Energy Mater.*, 25, 1522-1539, 2013.

[134] M. Kumar, A. Dubey, N. Adhikari, S. Venkatesan and Q. Qiao, Strategic review of secondary phases, defects, defect-complexes in kesterite CZTS-Se solar cells, *Energ. Environ. Sci.*, 8, 3134-3159, 2015.

[135] T. K. Todorov, J. Tang, S. Bag, O. Gunawan, T. Gokmen, Y. Zhu and D. B. Mitzi, Beyond 11% Efficiency: Characteristics of State-of-the-Art $Cu_2ZnSn(S, Se)_4$ Solar Cells, *Adv. Energy Mater.*, 3, 34-38, 2013.

[136] A. Polizzotti, I. L. Repins, R. Noufi, S. H. Wei, D. B. Mitzi, The state and future prospects of kesterite photovoltaics, *Energ. Environ. Sci.*, 6, 3171-3182, 2013.

[137] S. Y. Chen, X. G. Gong, A. Walsh and S. H. Wei, Defect physics of the kesterite thin-film solar cell absorber Cu_2ZnSnS_4, *Appl. Phys. Lett.*, 96, 021902-3, 2010.

[138] W. J. Yin, Y. L. Wu, S. H. Wei, R. Noufi, M. M. Al-Jassim, and Y. F. Yan, Engineering Grain Boundaries in $Cu_2ZnSnSe_4$ for Better Cell Performance: A First-Principle Study, *Adv. Energy Mater.*, 4, 1300712-7, 2014.

[139] W. M. Haynes, D. R. Lide and T. J. Bruno, Handbook of Chemistry and Physics: A Ready-reference Book of Chemical and Physical Data, *CRC Press*, New York, 1969.

[140] S. A. Nadi, P. Chelvanathan, Z. Zakaria, M. M. Alam, Z. A. Alothman, K. Sopian and N. Amin, Post-deposition Annealing Effect on Cu_2ZnSnS_4 Thin Films Grown at Different Substrate Temperature, *Int. J. Photoenergy*, 2014 589027-589034, 2014.

[141] E. M. Mkawi, K. Ibrahim, M. K. M. Ali, K. M. A. Saron, M. A. Farrukh, Nageh K. Allam, Influence of substrate temperature on the properties of electrodeposited kesterite Cu_2ZnSnS_4 (CZTS) thin films for photovoltaic applications, *J. Mater. Sci. Mater.*, 26, 222-228, 2015.

[142] S. Zhou, R. Tan, X. Jiang, X. Shen, W. Xu, W. Song, Growth of CZTS thin films by sulfurization of sputtered single-layered Cu–Zn–Sn metallic precursors from an alloy target, *J. Mater. Sci. Mater. Electron.*, 24, 4958–4963, 2013.

[143] O. Gunawan, T. K. Todorov, D. B. Mitzi, Loss mechanisms in hydrazine-processed $Cu_2ZnSn(Se, S)_4$ solar cells, *Appl. Phys. Lett.*, 97, 233506-3, 2010.

[144] T. Kato, H. Hiroi, N. Sakai, S. Muraoka, H. Sugimoto, Characterization of front and back interfaces on Cu_2ZnSnS_4, *Thin-Film Solar Cells*, EU. PVSEC., 2236-2239, 2012.

[145] J. T. Watjen, J. J. Scragg, T. Ericson, M. Edoff and C. Platzer-Bjorkman, Secondary compound formation revealed by transmission electron microscopy at the Cu_2ZnSnS_4/Mo interface, *Thin Solid Films*, 535, 31-34, 2013.

[146] N. Muhunthan, O. P. Singh, M. Thakur, P. Karthikeyan, D. Singh, M. Saravanan, V. Singh, Interfacial Properties of CZTS Thin Film Solar Cell, *Sol. Energy*, 2014, 1-8, 2014.

[147] T. Kato, H. Hiroi, N. Sakai, H. Sugimoto, Characterization of Front and Back Interfaces on Cu_2ZnSnS_4 Thin-Film Solar Cells, *PSECE*, 2125-2127, 2013.

[148] K. J. Yang, J. H. Sim, B. Jeon, D. H. Son, D. H. Kim, S. J. Sung, D. K. Hwang, S. Song, D. B. Khadka and J. Kim, Effects of Na and MoS_2 on Cu_2ZnSnS_4 thin-film solar cell, *Prog. Photovoltaics*, 23, 862-873, 2015.

[149] B. Shin, Y. Zhu, N. A. Bojarczuk, S. J. Chey and S. Guha, Control of an interfacial $MoSe_2$ layer in $Cu_2ZnSnSe_4$ thin-film solar cells: 8.9% power conversion efficiency with a TiN diffusion barrier, *Appl. Phys. Lett.*, 101, 053903-4, 2012.

[150] J. J. Scragg, T. Kubart, J. T. Watjen, T. Ericson, M. K. Linnarsson and C. Platzer-Bjorkman, Effects of Back Contact Instability on Cu_2ZnSnS_4 Devices and Processes, Chem. Mater., 25, 3162-3171, 2013.

[151] B. Shin, N. A. Bojarczuk, and S. Guha, On the kinetics of $MoSe_2$ interfacial layer formation in chalcogen-based thin-film solar cells with molybdenum back contact, *Appl. Phys. Lett.*, 102, 091907-3, 2013.

[152] R. Scheer and H. W. Schock, First ed., Chalcogenide Photovoltaics: Physics, Technologies, and Thin Film Devices, *John Wiley and Sons*, Halle (Saale), Germany, 2011.

[153] M. Gloeckler and J. Sites, Efficiency limitations for wide-band-gap chalcopyrite solar cells, *Thin Solid Films*, 480:481, 241-245, 2005.

[154] A. Santoni, F. Biccari, C. Malerba, M. Valentini, R. Chierchia and A. Mittiga, Valence band offset at the CdS/Cu_2ZnSnS_4 interface probed by x-ray photoelectron spectroscopy, *J. Phys. D Appl. Phys.*, 46, 175101-5, 2013.

[155] R. Haight, A. Barkhouse, O. Gunawan, B. Shin, M. Copel, M. Hopstaken and D. B. Mitzi, Band alignment at the $Cu_2ZnSn(S_xSe_{1-x})_4$ /CdS interface, *Appl. Phys. Lett.,* 98, 253502-3, 2011.

[156] S. Tajima, K. Kataoka, N. Takahashi, Y. Kimoto, T. Fukano, M. Hasegawa and H. Hazama, Direct measurement of band offset at the interface between CdS and Cu_2ZnSnS_4 using hard X-ray photoelectron spectroscopy, *Appl. Phys. Lett.,* 103 243906-4, 2013.

[157] J. Keller, J. Lindah, M. Edoff, L. Stolt and T. Torndahl, Potential gain in photocurrent generation for Cu (In, Ga) Se_2 solar cells by using In_2O_3 as a transparent conductive oxide layer, *Prog. Photovoltaics,* 24, 102–107, 2016.

[158] K. H. Huang, J. G. Yu, C. P. Kuo, R. M. Fletcher, T. D. Osentowski, L. J. Stinson, M. G. Craford and A. S. H. Liao, Twofold efficiency improvement in high-performance AlGaInP light-emitting diodes in the 555-620nm spectral region using a thick GaP window layer, *Appl. Phys. Lett.*, 61, 1045-1047, 1992.

[159] A. Janotti and C. G. V. d. Walle, Fundamentals of zinc oxide as a semiconductor, *Rep. Prog. Phys.,* 72, 126501-29, 2009.

[160] U. Rau and M. Schmidt, Electronic properties of ZnO/CdS/Cu(In, Ga)Se_2 solar cells aspects of hetero-junction formation, *Thin Solid Films,* 387, 141-146, 2001.

[161] M. Ruckh, D. Schmid and H. W. Schock, Photoemission studies of the ZnO/CdS interface, *J. Appl. Phys.,* 76, 5945-5948, 1994.

[162] L. Weinhardt, C. Heske, E. Umbach, T. Niesen, S. Visbeck and F. Karg, Band alignment at the i-ZnO/CdSi-ZnO/CdS interface in Cu(In, Ga)(S, Se)$_2$Cu(In, Ga)(S, Se)$_2$ thin-film solar cells, *Appl. Phys. Lett*., 84, 3175-3177, 2004.

[163] K. Orgassa, H. W. Schock and J. H. Werner, Alternative back contact materials for thin-film Cu(In, Ga)Se_2 solar cells, *Thin Solid Films,* 431, 387-391, 2003.

[164] L. Assmann, J. Bernede, A. Drici, C. Amory, E. Halgand, M. Morsli, Study of the Mo thin films and Mo/CIGS interface properties, *Appl. Surf. Sci.*, 246, 159-166, 2005.

[165] J. J. Scragg, J. T. Watjen, M. Edoff, T. Ericson, T. Kubart, C. P. Bjorkman, A Detrimental Reaction at the Molybdenum Back Contact in $Cu_2ZnSn(S, Se)_4$ Thin-Film Solar Cells, *J. Am. Chem. Soc.*, 134, 19330-19333, 2012.

[166] Y. Feng, T. K. Lau, G. Cheng, L. Yin, Z. Li, H. Luo, Z. Liu, X. Lu, C. Yang, X. Xiao, A low-temperature formation path toward highly efficient Se-free Cu_2ZnSnS_4 solar cells fabricated through sputtering and sulfurization, *Cryst. Eng. Comm.*, 18, 1070-1077, 2016.

[167] K. J. Yang, J. H. Sim, B. Jeon, D. H. Son, D. H. Kim, S. J. Sung, D. K. Hwang, S. Song, D. B. Khadka and J. Kim, Effects of Na and MoS_2 on Cu_2ZnSnS_4 thin-film solar cell, *Prog. Photovolt.*, 23, 862-873, 2015.

[168] T. P. Dhakal, S. Harvel, M. van Hest, Glenn Teeter, Back Contact Band Offset Study of Mo-CZTS Based Solar Cell Structure by Using XPS/UPS Techniques, *IEEE 42nd Photovoltaic Specialist Conference (PVSC)*, 1-4, 2015, doi: 10.1109/PVSC.2015.7355623.

[169] J. J. Scragg, T. Kubart, J. T. Watjen, T. Ericson, M. K. Linnarsson and C. Platzer-Bjorkman, Effects of Back Contact Instability on Cu_2ZnSnS_4 Devices and Processes, *Chem. Mater.*, 25, 3162-3171, 2013.

[170] S. L. Marino, M. Placidi, A. P.Tomas, J. Llobet, V. I. Roca, X. Fontane, A. Fairbrother, M. E. Rodriguez, D. Sylla and A. P. Rodriguez, Inhibiting the absorber/Mo-back contact decomposition reaction in $Cu_2ZnSnSe_4$ solar cells: the role of a ZnO intermediate nanolayer, *J. Mater. Chem. A*, 1, 8338-8343, 2013.

[171] X. Liu, H. Cui, W. Li, N. Song, F. Liu, G. Conibeer and X. Hao, Improving Cu_2ZnSnS_4 (CZTS) solar cell performance by an ultrathin ZnO intermediate layer between CZTS absorber and Mo back contact, *Phys. Status Solidi RRL*, 8, 966-970, 2014.

[172] T. Minemoto, T. Matsui, H. Takakura, Y. Hamakawa, T. Negami, Y. Hashimoto, T. Uenoyama, M. Kitagawa, Theoretical analysis of the effect of

conduction band offset of window/CIS layers on the performance of CIS solar cells using device simulation, *Sol. Energy Mater. Sol. Cells*, 67, 83-88, 2001.

[173] J. Holzl, F. K. Schulte, H. Wagner, 1st ed., Solid Surface Physics, *Springer Verleg*, Berlin, Germany, 1979.

[174] J. C. Riviere, M. Green, Marcel Dekker, Solid State Surface Science, Springer, ISBN-10: 3662158094, New York, USA, 1969.

[175] H. B. Michaelson, The work function of the elements and its periodicity, *J. Appl. Phy.*, 48, 4729-4733, 1977.

CHAPTER 2

Synthesis Methods and Characterization Techniques for Functional Materials

Chapter 2

Synthesis Methods and Characterization Techniques for Functional Materials

2.1 Introduction

As we know that the renewable energy is the main source of energy in coming days. Therefore, the renewable energy attracts its importance progressively among the people and researchers. There are several ways to convert the renewable energy into useful energy in the field of nanoscience and nanotechnology. The utilization of nanotechnology can enhance the electrical energy from solar energy via opto-electronic devices like photovoltaic cells, light emitting diodes, and photodetectors, ets. Due to the ability of voltage generation and current density of functional materials (FMs), the solar cell is regarded as the most promising opto-electronic device for solar energy conversion. The opto-electronic devices are made of nanomaterials especially FMs with advanced characteristics. The synthesis of FMs by nanotechnology can improve the performance and reduce the cost of devices. The improved performance and reduced cost of FM nanomaterials or nanoparticals (NPs) can be used in solar energy conversion devices. So, nanotechnology is also being used to modify the crystal structure at nano scale in which the ratio of performance to cost always becomes high for energy applications like photovoltaic/solar cells. Nowadays, 40% of the solar energy utilizes via renewable energy devices where the hetero-junction photovoltaic (PV) devices are widly used. The hetero-junction PV devices are fabricated by several different methods.

In this chapter, we study the cost-effective and eco-friendly synthesis methods like co-precipitation, spray pyrolysis and hydrothermal methods for FMs, and the characterization analysis of as-synthesized FMs via characterization tools. In the characterization tools, x-ray diffraction (XRD), X-Ray photoelectron spectroscopy (XPS), scanning electron microscope (SEM), field effect scanning electron microscope (FESEM), Raman spectroscopy, UV-Visible, I-V characterisation technique, etc. are used to investigate the properties of FMs for energy materials application.

2.2 Role of Functional Nanomaterials in the Energy Application

Several applications of FMs have been proposed already, but in 1958, the first time, functional nanomaterials were used practically to powering satellites as the photovoltaic (PV) solar cell **[1]**. But the low efficiency and extravagant cost of the devices are two key parameters in the PVs that reduced the interest in the application of FMs. The solution of these two problems is resolved by the nanoscience and nanotechnology approaches in material scinence and its innovations in photovoltaic solar cells increase the demand of the FMs. The semiconductor or metallic nanomaterials have formed high performance and long durable devices because properties of the nanomaterials depend on their processing of the structures. The structures and compositions of nanomaterials are used to control the performance and cost of the device. The metallic nanomaterials e.g. copper NPs (≤50nm) change the behavior of ductility comparison to bulk form. The change in the structure of the magnetic nanomaterials exhibited the superparamagnetism property. The quantum confinement effects are present in the semiconductor quasi particles e.g. quantum wells, quantum wires, and quantum dots., and surface plasmon resonances effects present in metal nanomaterials. The dimensionality of a semiconductor is directly corelated to the level of electron density. So, two dimension (2-D) semiconductors are behaved as ***quantum well*** because free electrons restrict in one dimension in thin film. Researchers have also demonstrated that the absorption of solar radiation is much greater in nanomaterials thin-film based PV devices than continuous sheets of bulk material based PV devices. Because nanoparticles are smaller and can absorb a greater amount of solar radiation.

In this chapter, we discuss the synthesis methods of functional nanomaterials to control the cost and performance of the photovoltaic based solar cells. The nanoparticles (NPs), nanowires (NWs), nanocrystals (NCs), quantum dots (QDs) are the differents shapes of the nanomaterials, which play a vitol role in generating photo excited charge carriers. These photo-excited charge carriers are helpful to enhance the efficiency of solar cells **[2]**. In the metallic-based photovoltaic device, the photon absorption property enhances the PV solar devices due to surface plasmon effects (SPE) in metallic nanomaterials. The surface plasmons, in the depletion region interface, are the electrons-holes oscillations that are created generally between the two different materials. The conflict of “effective carrier’s collections” and “high absorption of incident light” are resolved by the metal nanoparticles absorption layer in the PV devices. The reason behind it is the scattering and concentrations of the light mechanisms and surface plasmon polaritons (SPPs) in the nanomaterials. The phenomenon of light concentration in the devices is due to the localized field of surface plasmons surrounding the particles and supported the higher absorption of photons [**3**]. If the metallic nanomaterials are used underneath the bottom interfaces between the absorbers layers, then the nanomaterials convert the incident light into SPPs. In this phenomenon, the electromagnetic waves travel along with the surface the interface of the layers. At the plasmon resonance frequency of the metallic particles, the SSPs are greater than the dimensions of the metallic particles that is the reason for the enhancement of the absorption [**3**]. The nanomaterials are implanted into the bulk form to gain light absorption with the excited surface plasmons. Hence, the concentrated incident energy is localized to the surface plasmons field. This energy is induced to produce more photo-excited electron-hole pairs. The nanomaterials have different sizes for the photovoltaic solar cells due to their dimensions and they are categorised into zero Dimension nanomaterials, One Dimension nanomaterials, two Dimension nanomaterials and Three dimension nanomaterials.

2.2.1 Zero-Dimensional (0-D) Nanomaterials

As we have discussed that the nanotechnology of nanomaterials is the main technique to reduce the size of the materials. Due to quantum confinement, the nanomaterials are used to enhance the charge carrier’s generation of the photovoltaic solar cell and to reduce the photo absorptions. The excited single pair of electron-hole is generated by one absorbed photon and such generations of charge carriers are increased the solar cell efficiency up to maximum 33% that is called the Shockley Queisser limit [**4].** The Shockley Queisser limit can be achieved the high efficiency with help of the quantum dots or 0-D nanomaterials by the simple generation of excitons [**5].**

As we know that the high-energy photo-excited carriers are dissipated very fast in bulk-size semiconductor materials, due to the inelastic scattering of carriers-phonons. The best solution to this problem is quantum dots, which can slow down to photo-excited carries dissipation. The discrete energy levels in quantum dot (QD) extremly lower the rate of the dissipation process allow the extra energy to generate a new pair of excitations. The variation in bandgap can be achieved by adjusting the nanomaterials sizes of QD **[6]**. The examples of QDs are Lead Sulphide, Selenide and Telluride, Cadmium Selenide, and Indium Phosphide, etc. The quantum dots of Lead sulphide, Selenide and Telluride, Cadmium Selenide, and Indium Phosphide, etc. demonstrate the multiple excitons generation effects [**7-12].**

2.2.2 One-Dimensional (1-D) Nanomaterials

Nano-tubes (NTs), nanorods (NRs) and nanowires (NWs) belong to one-dimensional (1-D) nanomaterials, and such nanostructures promise to increase energy-density and cycling-life of energy for energy application. **Fig. 2.1** shows the exact dimensions of materials. The optical loss is reduced by the field concentration effect of nanomaterials. The NWs have an absorption cross-section greater than the physical cross-section. **[13]**. The enhancing effect in arrays NWs is produced by using a higher refractive index. This enhancing effect exhibits a cavity effect or light trapping by the multiple reflections from the boundaries of wires to enhance efficiency **[14].**

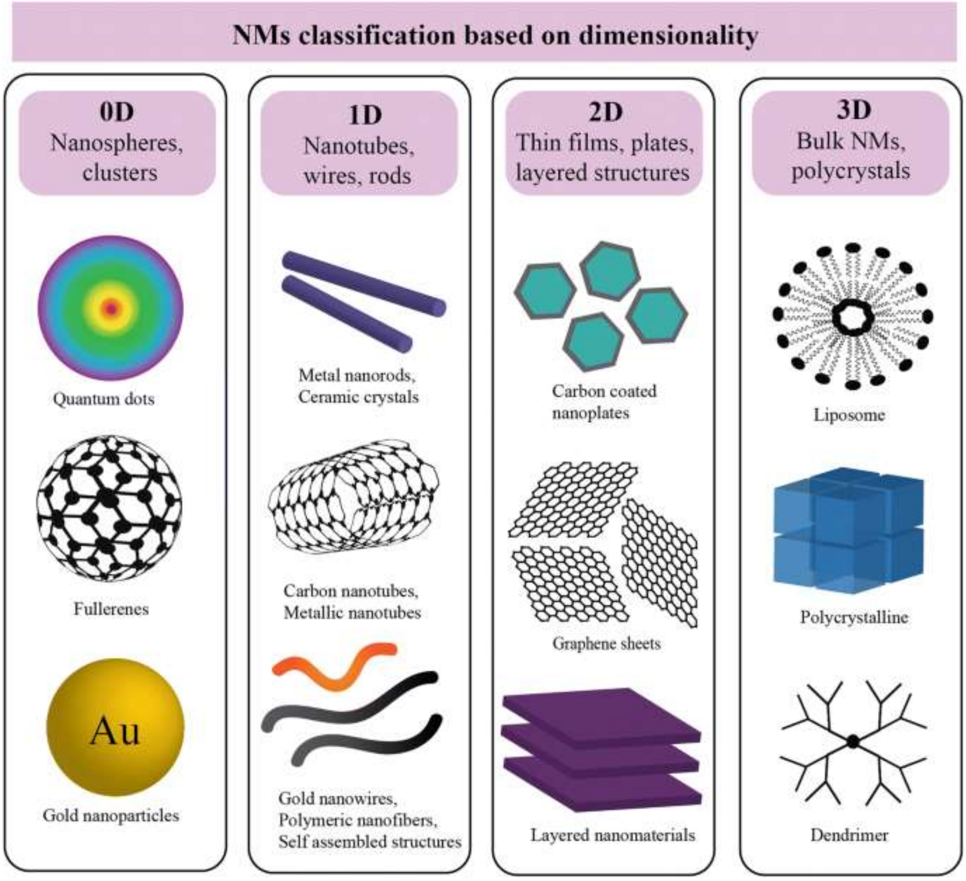

Figure 2.1: The classification of nanomaterials based on dimensionality: 0D, 1D, 2D, 3D.

To get the best results, the incident light wavelength's order should be the same range of "diameter" and "pitch of the nanowire" arrays and the dimensions of the nanowires. 1-D functional nanomaterials can be applied in PV devices with various multipurpose designs. An array of such unit cells can arise plane with resin or spin-on-glass (SOG). The upper surface of the NWs can be exposed by etching or chemical-mechanical machining to allow contact with the transparent conducting oxide such as Indium tin oxide (ITO) **[15].**

2.2.3 Two-Dimensional (2-D) Nanomaterials

This type of nanostructures are mainly used in thin-film solar cells because of their smaller size in materials and electron transport characteristics, which results in high-performance devices. The energy density of 2-D nanomaterials varies constantly, which is the main feature of the thin-film and 2-D nanomaterials may be most probably engineered on the wafer shape or thin film. The interlayer space between the layers is manipulated by the non-layered materials and is known as 2-D nano-fluidic channels. These nanomaterials can also be engineered into different sized porous structures for energy storage and catalytic applications purposes.

There are several techniques such as spray pyrolysis, dip coating, and electrodeposition. to fabrication the 2-D nanomaterials. The thin film, plates, and layered structures can be synthesized by spray pyrolysis methods, which is a simple and cost-effective method. In spray pyrolysis deposition, a metallic thin-film of the nanomaterials can be formed on a substrate in nanometers size for photovoltaic application purposes. At high temperature, the heating substrate induces agglomeration by surface tension and an array of hemispherical nanoparticles with considered sizes. These types of structures are suitable for the plasmonic light trapping phenomenon.

A template technique could allow greater control over nanoparticle fabrication **[16].** The Si is commonly used material in current for profitable PV devices. The Si is extensively used in the electronics industry for the etching process. These are the main advantages of Si wafers. For this requirement of an ordered array of Si NWs, there is a prototype mask required for the dry etching process **[17].**

2.2.4 Three-Dimensional (3-D) Nanomaterials

This type of structured material is rarely used for photovoltaic purposes because the 3-D nanometer scale of the nanomaterials for the solar device is very expensive. This type of materials are used in first generatons of solar cells. So, 3-D nanomaterials have not been applied in the field of photovoltaic energy conversion applications.

2.3 Synthesis Methods

There are several methods are used to synthesize the nanomaterials for example ***top-down*** and ***bottom-up*** approaches. We choose some selective methods to keep in mind, easily feasible synthesis of nanomaterials with abundant and rcofriendly elements. Hence, we have followed three synthesis methods as;

2.3.1 Coprecipitation Method

The co-precipitation (CPM) method is a method of precipitate of materials, which is generally soluble under the employed conditions. The CPM is also known as the controlled precipitation method, which is a basic route of a wet-chemical method for the creation of nanomaterials. In this method, the precursors are inorganic salts that are decomposed in di ionized (DI) water as a solvent to get a homogeneous solution. Generally, metal oxides are synthesized in an open atmosphere; and metal sulfides may also be synthesized in an inert atmosphere by this method. Metal oxides synthesis flowchart is given below in **Fig. 2.2 [18].** In this method, the insoluble products are found under the high saturation condition.

The nucleation growth of the nanomaterials form a lot of small particles, which are agglomerated rapidly to each other. The size, shape, and morphology of the products in the Co-precipitation method are affected by Ostwald ripening and agglomeration processes. In the next step, the supersaturation condition is the necessary condition to produce precipitation in the wet-chemical method. Besides this, pH, temperature, and concentration of solutions are the factors that influence the shape, size, and morphology of the nanomaterials **[19].** After precipitation, the next step is filtration and then washing off the yields/products. In the last step, the calcination process is used to change hydroxides into oxides having finite crystal structures. In this process, NaOH, NH_3, NH_4OH, and Na_2CO_3 are used as a precipitating agents. The surfactants work the avoiding agglomeration and use to control the particle size of the nanomaterials **[20].**

The strengths of the CPM method is a simple and fast method**,** controlled particle size and composition**;** additions to this, there are several prospects to modify the particle surface state, and overall similarity**.** We can control the particle size by “changing the temperature of reaction” and “surface functionalization”.

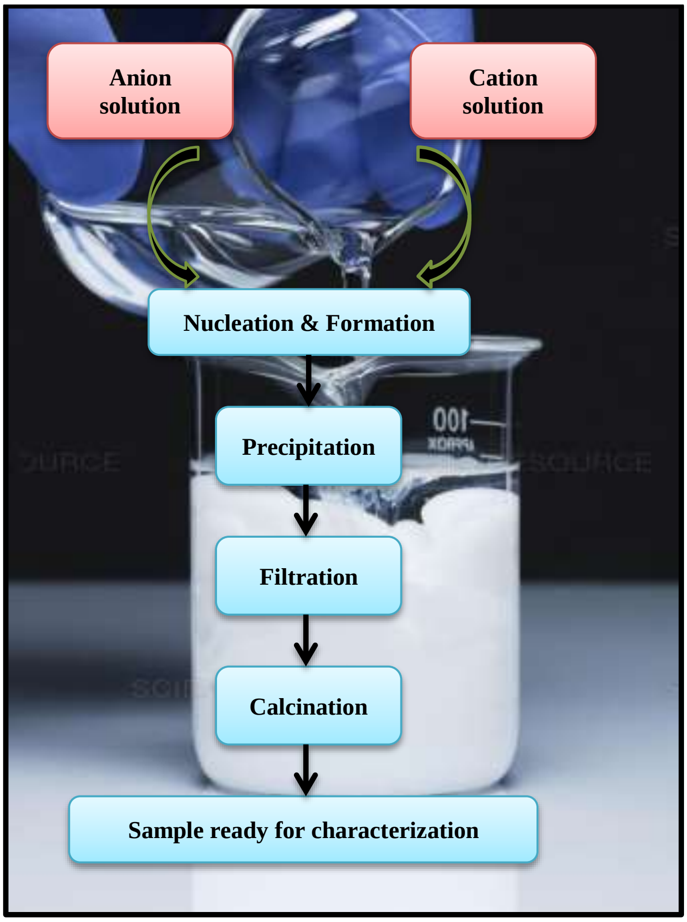

Figure 2.2: Schematic co-precipitation method flow chart diagram of image view.

The CPM method does not involve the use of any organic solvents in the synthesis process but has limitations such as contaminations get precipitated with the by-product. If the reactants vary with different precipitation rates, the synthesis of the nanoparticles does not get in the well-shapes **[21].** Hence, the top-down approach, in the next synthesis method, discuss to resolve these types of problems i.e. the spray pyrolysis method (SPM).

2.3.2 Spray Pyrolysis Method

The spray pyrolysis method (SPM) is a simple, less time-consuming and cheapest method for thin-film deposition. The SPM has a lot of advantages related to the coating technique, which is used in layered devices like solar cells, photodetectors, sensors, solid oxide fuel cells, etc. This process produces oxide (e.g. Y_2O_3, stabilized zirconia, Al_2O_3, MgO), and sulfide (in inert/sulfide-atmosphere) thin films of high quality at rather low costs. This method delivers the capability to deposit the thin layers on various substrates such as soda-lime glass (SLG), a metallic substrate, fiber substrate, etc. The formation of the oxides layers on the surface of the heated substrate is very homogeneous and good adhesive with the substrate during pyrolysis process. The thin-film morphology is controlled by the substrate temperature, distance of the nozzle to substrate, and concentration of the solvent parameters in this method. The surface of the thin-film is rough and more porous at high temperatures and the cracked films are found at low temperatures. The crystallinity of the materials, texture and other physical properties of the deposited films also influence by substrate temperature in this method. Another main parameter like “precursor solution” also affects the morphology and the properties of the deposited films. Keeping in mind the above parameter, we can synthesize the thin-film of the nanomaterials.

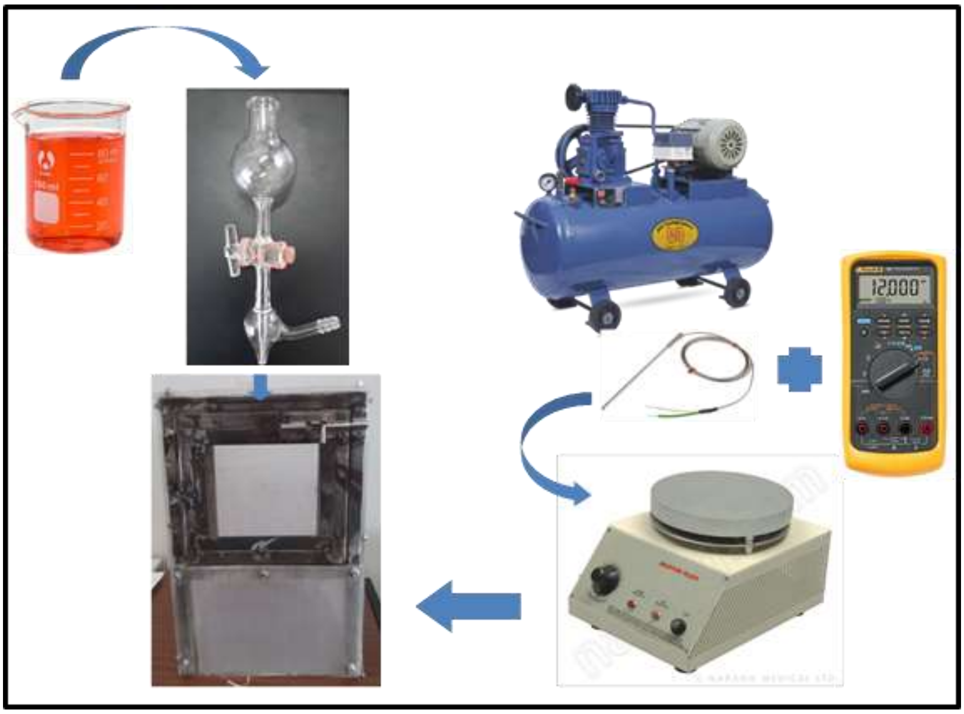

Figure 2.3: Schematic diagram of self-designed spray pyrolysis set-up.

2.3.2.1 Thin-film Deposition: During the film deposition by spray pyrolysis, many processes occur sequentially e.g. precursor solution atomization, droplet transport, and vaporization, spreading on the substrate, drying, and decomposition of the precursor salt as shown in **Fig. 2.4**. These processes improve the film quality from an application requirement point of view. The pyrolysis methode follows three main steps: atomization, transportation of the aerosol, and decomposition of the precursor on the substrate. In the atomization process, droplets are generated from the spray solution by a nozzle with initial velocity towards the substrate. Airblast, ultrasonic, or electrostatic techniques may also be used at this stage. There are various atomizers used to resulting the droplet size, rate of atomization, and initial velocity of the droplets. In this process, the size of the generated droplets depends solely on the fluid charge density level ρ is given as **[22];**

$$r^2 = \left(\frac{-\alpha}{\beta} \right) \frac{3\varepsilon_0}{q\rho}, \qquad (2.1)$$

where $\varepsilon_\circ$=permittivity, q=elementary charge, and $\left(\frac{-\alpha}{\beta} \right)$=1 x 10^{-17} J (constant).

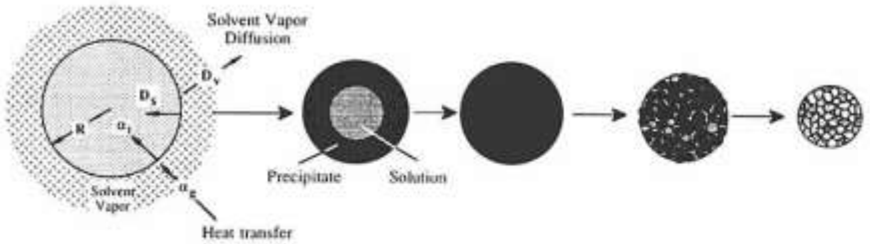

Figure 2.4: Schematic diagram of evaporation precipitation drying decomposition sintering [*Source:* Messing, et al., *J. Amer. Ceram. Society,76, (11), 2707 1993, copyright permission* [**23**]]

Atomization of liquids is the most important parameter to know which type of atomizer is best suited for each application, and it is also important that how the performance of the atomizer is affected by variations in liquid properties and operating conditions. The performance of the atomizer is directly affected by “the variations in liquid properties and operating conditions”, and suggests this that the atomization of liquids is the most important parameter to change the film’s chemical and physical characteristics.

Fig. 2.4 shows the total mechanism of the droplets, in the transportation of the aerosol from the nozzle tip to the substrate surface. But many droplets are carrying precursor atoms without forming a powder to the substrate. Sears et al. **[24]** investigated the mechanism of SnO_2 film growth and studied the effect of Gravitational, electric, thermo-phoretic, and Stokes forces. The above discussion suggests that the fabrication phenomenon on the film is affected by the vapor of droplets that passed close to the hot substrate (just like the CVD phenomenon). The droplet strikes onto the substrate, and forms a powdery deposition. At high temperature, this powdery material is formed a certain shape and size based on the free energy of the molecules at that time.

The substrate temperature is the key parameter and it plays a major role in enhancing the properties of the films. The high temperature of the substrate makes the best crystalline nature in the film **[25, 26].** The size of the grains is determined by “initial nucleation density” and “recrystallization”. At high temperature, the larger size of the grains is increased in the recrystallization process **[27].** During the increase of substrate temperature, the surface of the film is transformed from a crack state to a “dense state” and then to a “porous” state **[28].** The reason for the non-uniformity of the film is the variation of the substrate temperature at different points. The physical and chemical characteristics of the deposited state of the materials are changed, due to the composition ratio of the precursors. The spray pyrolysis experiment is done in an open atmosphere, due to which there is maximum chance to makes the secondary and ternary phases in the film. For instance, SnS is sprayed on the heated substrate, and various phases (Sn_2S_3, SnS_2, SnO_2, etc.) are created and deposited in the film. Hence, we can say that the synthesis of the single phase of the material is very critical in an open atmosphere. Generally, the secondary phases are presented as-synthesized thin film, from lower to higher substrate temperature **[29].**

2.3.2.2 Advantages and Disadvantages of SPM: The SPM has a lot of advantages, along with its simplicity in the synthesis. It is used at a broad level for commercial purposes for the preparation of semiconductor thin films. This SPM method is suitable to dope the films with effectively any elements fraction by dopant adding in the precursor's solution. This method can yield “large-area, high-quality adherent films of uniform thickness”. These two reasons are validated to commercialize this SPM method. So, validation of the advantage of this method is the large area and high quality of target without any vacuum and valid reason for the industrialization of the SPM.

The “film quality” and “thickness of the films” can be controlled easily over a wide range by varying the spray parameters such as spray rate, time, the concentration of the precursor **[27]** The logical advantage of this method is to produce robust free materials at moderate temperature (100^0-500^0 C). In the layered film or wafer, the composition gradients are distributed throughout the film by the composition variation.

There are also few disadvantages of this method for thin-film preparation that film is gained non-uniformity from larger grain to smaller due to uncontrolled spray droplet size. The wastage or unwanted precursors are dopant during the spray deposition and the main disadvantage that it has a very slow deposition rate.

2.3.3 Hydrothermal/ Solvothermal Method

In Hydrothermal method, it is carried out heterogeneous reactions at high temperature (>100^{o}C) and high pressure (1bar) to the aqueous solution for producing the crystallized structure **[30].** Various inorganic materials like metal oxides, chalcogenides, metal-organic frameworks, porous materials, and nanomaterials are synthesized by Hydrothermal method at ambient conditions. The hydrothermal method is based on that premise where the materials are dissolved in aqueous, under excessive temperature as well as pressure conditions. The higher-valence metal oxides are prepared under closed-system in Hydrothermal synthesis [**31].** The Hydrothermal technique for functional nanomaterials is the environmentally benign type method and it is good to control the particle shape and size. This method can be used to grow the materials at high vapor pressure and melting point. Moreover, hydrothermal processing can also be used for producing large and high purity crystalline, single phase, and multi-component oxide materials having well-controlled compositions. The cost of instrumentation is affordable in comparison to other advanced methods. The limitation of the method includes the inability to observe the crystal during its growth **[32]. Fig. 2.5** shows the experimental set-up of the Hydrothermal method containing the “stainless steel lid, bursting disc, Teflon cup, and stainless steel shell”.

Figure 2.5: Schematic representation of Hydrothermal Experimental setup.

The advantages of this Hydrothermal method, as the top-down chemical synthesis, are to attain the transition metal compounds without oxidation states. This method is useful for preparing low-temperature phase materials and metastable compounds, e.g. tellurium iodides (Te_2I and β-TeI) and they have narrow particle size distribution, controlled morphology, and high purity without post-annealing at high temperatures, the crystalline powder is formed. However, the disadvantage of this method is having a limited quantity of synthesized materials. Another disadvantage of this method is that there may blast like a bomb at high temperature and pressure, if negligence is done during the experiment. Solvothermal and Hydrothermal synthesis method are similar, but the only difference is that use of organic solvents like toluene, decalin, and octadecene in the Solvothermal method instead of water in the Hydrothermal synthesis method. The inorganic nanocrystals are prepared extensively by Solvothermal reactions. The “size and shape” of nanocrystals are created by controlling the concentration of precursors solutions and the temperature. So, the size of nanocrystals increases with increasing precursor concentrations. The formation of rod-shaped nanocrystals requires a high chemical potential environment viz. high monomer concentration in solution. Thus, the addition of capping agents such as long-chain alkanethiols, alkylamines, and trioctylphosphine oxide controls the size as well as shape in the Solvothermal synthesis process.

In the whole research work, we have adopted the aforesaid methods to synthesize the nanomaterials of the functional materials. To characterize the nanomaterials, we have characterized the as-synthesized sample with characterization techniques.

2.4 Characterization Techniques

Characterization techniques are used to analysis of the pre-synthesized materials. It is the basic process of materials science to investigate the properties of materials based on the internal structures especially the shape, size, and morphology of the materials. Different–different instruments are used to analyze the properties of the material of the elemental composition, morphology, structure information, shape, size as well as chemical and physical property. UV-Visible (UV-VIS) Spectroscopy and X-Ray Diffraction (XRD), etc. are used to analyze the optical and structural properties of as-synthesised nanomaterials. Scanning Electron Microscopy (SEM) / Field Emission Scanning Electron Microscopy (FESEM) and X-Ray Photoelectron Spectroscopy (XPS), etc. are used to observe the surface morphology and binding enrgy properties.

2.4.1 Diffraction Methods

Nanostructures have attracted enormous interest among science community due to a rapidly development growing class of FMs and growing their applications. Several techniques have been used to characterize the size, crystal structure, elemental composition, and a variety of other physical properties of nanoparticles. In many cases, there are physical properties that can be assessed by more than one technique. The individual strengths and limitations of each technique the choice of the most appropriate method is become more complicated. The diffraction of X-rays from crystals has become invaluable to all areas of materials research. The use of diffraction as a characterization tool becomes almost a century and the field continues to evolve today with new tools continuously enabling new dimensions of characterization. The most traditional uses of diffraction lead to the characterization of crystal structure, phase evolution, particle size, crystallographic texture and lattice strains, and are carried out in all areas of materials research. Hence, some of diffraction methods are discussed below.

2.4.1.1 X-Ray Diffraction: In 1913, the English scientists father and his son Bragg discovered a phenomenon of the “powder X-ray diffraction” of crystal-like by an X-ray beam **[33].** In 1916, first time, German physicists Scherrer and Debye revealed the x-ray diffraction for polycrystalline materials. In the X-ray diffraction phenomenon, wave interference produces, when X-rays interact with a material in a particular reciprocal space then exhibiting periodic and regular structure patterns. The reason behind this interference is the wavelengths delivered by the X-rays are comparable with the interatomic distance of a crystal. The X-rays are diffracted after the strikes from an atomic plane and then they are produced a phase-angle at a certain wavelength. If there is a definite periodicity in the plane, then the diffracted waves in the same specific angle possess a similar phase and generate a resultant interference. Hence, interference are proportional to the number of planes that generate the diffracted wave and allow identifying the structure of studied material. So, XRD is a primary and standard tool to determine the structures of materials these days.

For materials identification, XRD powder method is a simple method to know the nature of the crystalline material. Every substance has characteristic of an X-ray pattern in a crystalline state to identify the crystal phase by this method. These patterns are collected in databases of the Joint Committee on Powder Diffraction Standards (called JCPDS) and grouped index of organic, inorganic, and mineral compounds. There is another information like “size of the crystallite”can be obtained from the XRD pattern using the Debye Scherer formula. So, the crystallite size is analyzed the crystal unit cell by measuring the “extension of the X-ray diffraction of a flat reflection”. The reason behind the broad and narrow peaks in the XRD pattern is due to the periodicity of the crystallite domains in phase reinforces the X-ray diffraction. If the crystals are periodically arranged with defects-free, the X-ray be diffracted at the same angle. If the crystals have non-periodically arranged atoms and a very low degree of frequency viz. the peaks can be broaden. The procedures of the data analysis of the XRD patterns are the following three steps and it use to determine the unknown crystal structure by the XRD data patterns obtaining from diffraction angle versus intensity of the diffracted rays.

- Calculation of “the size” and “shape” of the unit cell by the angular positions of the diffraction peaks.
- Analyze “the number of atoms per unit cell” from the size and shape of the unit cell, the “chemical composition” of the specimen, and its “measured density”
- Deduction of “the atom positions within the unit cell” from the relative intensities of the diffraction peaks

Here, we focus on the first step that study the angular positions of the diffraction peaks, which is used to analyse the shape and size of the crystal strucure.

The indexing of the XRD patterns is important in the diffraction analysis where Miller planes are assigned by each peak during the indexing of the pattern. Here, we are going to give the basic of indexing diffraction patterns in which XRD patterns were obtained from materials like a cubic structure. To analyze the results from the XRD patterns of cubic structure, we follow the following steps as;

- The interplanar spacing distance (*d*) between adjacent planes in the set *(hkl)* of a material with a cubic structure and lattice parameter (*a*), and obtained from the equation:

$$\frac{1}{d^2} = \frac{h^2 + k^2 + l^2}{a^2} \tag{2.2}$$

- On comparing this to Braggs law ($2d \sin\Theta = n\lambda$)

$$\frac{1}{d^2} = \frac{h^2 + k^2 + l^2}{a^2} = \frac{4\sin^2\Theta}{\lambda^2} \tag{2.3}$$

$$\sin^2\Theta = \frac{\lambda^2}{4a^2}\left(h^2 + k^2 + l^2\right) \tag{2.4}$$

$$\sin^2\Theta \propto (h^2 + k^2 + l^2) \tag{2.5}$$

It means as Θ increases, planes with higher Millar indices (*hkl*) diffract with different intencities.

- First reflection is followed due to diffraction from Miller planes (100) i.e. $h^2+k^2+l^2=1$ for primitive cubic plane, (110) i.e. $h^2+k^2+l^2=2$ for body-centered cubic plane, (111) i.e. ($h^2+k^2+l^2=3$) for face-centred cubic lattices. The value of $h^2+k^2+l^2$ can be obtained by dividing the $\sin^2\Theta$ value by the minimum one ($\sin^2\Theta$ value of the first reflection) and multiplying the ratio by the appropriate integer.
- The $\sin^2\Theta$ value is calculated by dividing from the smallest value (first reflection) for all diffraction peaks.
- If these are not an integer, then multiplied by 2 or 3, and found complete integer from the ratio.
- The *hkl* value can be identified from the quadratic forms as listed in **Tab. 2.1.**
- We may also index the diffraction pattern using the ratio of $1/d^2$ value instead of the $\sin^2\Theta$ values, where Θ is a directly measurable quantity.

Table 2.1: Lattice type identification by lattice parameters a,b, & c and *α, β and ϒ* are analysed by (hkl) values:

$h^2+k^2+l^2$	***(hkl)***	**Lattice (*a=b=c; α=β=ϒ*=90°)**
1	100	P
2	110	P, I
3	111	P, F, D
4	200	P, I, F
5	210	P
6	211	P, I
8	220	P, I, F, D
9	300, 221	P
10	310	P, I

11	311	P, F, D
12	222	P, I, F
13	320	P
14	321	P, I
16	400	P, I, F, D
17	410, 322	P
18	411, 330	P, I
19	331	P, F, D
20	420	P, L, F
21	421	P
22	332	P, I
24	422	P, I, F, D
25	500, 430	P
26	510, 431	P, I
27	511, 433	P, F, D
29	520, 432	P
30	521	P, I
32	440	P, I, F, D
33	522, 441	P
34	530, 433	P, I
35	531	P, F, D
36	600, 442	P, I, F
37	610	P
38	611, 532	P, I

40	620	P, I, F, D

(P= Primitive cubic, I= Body-centered cubic, F= Face centered cubic, D= Diamond cubic)

The similar process follows for others FMs like metal, semiconductor, ceramic and advanced composite materials. Hence, we conclude from this table that the selection rules are presented the reflection planes (h, k, l): all integers for Primitive simple cubic (SC), $h+k+l$ is even integers for body centered (BCC), and h, k, l all are even or all odd for Face centered cubic (FCC) (e. g. $h^2+k^2+l^2$ is 1,2,3,4,5,6,8………..for SC, $h^2+k^2+l^2$ is 2,4,6,8,10,12,14,16………..for BCC and $h^2+k^2+l^2$ is 3,4,8,11,12,16………..for FCC)**.**

2.4.1.2 X-ray Photoelectron Spectroscope: The photoelectric effect was discovered by Hertz in 1887 and more explained by Nobel laureate Einstein in 1905 **[34].** P. D. Innes experimented with the coupling of Rontgen tube and Helmholtz coils in 1907 and recorded in a photographic plate that “the electron bands emission depending on their speed” **[35].** When electrons are irradiated with light of a certain wavelength, they are emitted to specific value which depend on their atomic binding forces, which means photoelectrons near the sample surface escape without losing energy through collisions and defact subsequently. The energy are characteristics of the atomic and molecular orbitals are studied from which they are originated. When we select the emitted electrons with high-energy light (X-rays), then each atom generates a characteristic pattern of signals depending on its oxidation state and present amount. The kinetic energy of photoelectrons is differentiated between “the energy of the X-ray photon” and “the binding energy of the electron”.

X-ray photoelectron spectroscopy (XPS) is a low-resolution quantitative method demonstrated by Nobel laureate Siegbahn in 1981 **[36].** This was the first invented electron spectroscopy device for chemical analysis (ESCA). Generally, XPS uses monochromatic X-ray radiation to probe a sample in vacuum. In this method, X-ray photons collide with electrons of the sample and cause the emission of photoelectrons from the sample. The signals correspond to the specific emitted electron configuration for each element. To generate the atomic percentage values, each obtained XPS signal must be corrected by dividing the signal intensity i.e. number of detected electrons by a “relative sensitivity factor” and normalized over the entire detected elements **[33].**

2.4.1.3 Scanning Electron Microscope: A scanning electron microscope (SEM) produces highly magnified and resolved images of a material when a highly focused electron beam is scaned on the surfaces of the material. The SEM gives the information of the material having the chemical compositions and their topology when a highly focused electron beam interacts with atoms of the materials. The two-dimensional scanning beam of SEM on the surface of the materials is used for the surface image formation by collecting the secondary and backscattered electrons.

The upper surface area of the sample is scanned by the electron beam where the high energetic electron lies through the electron gun. The secondary and backscattered electrons are part of electron microscopy technique. A highly energetic electron falls on the sample, and the interaction between the arrangements of the atoms with a beam of electrons is used to investigate the surface of the sample. The morphology images of the sample is visualized on the computer screen through the secondary and backscattered electrons **[37].** Power supply, vacuum system, cooling system, and vibration-free floor, ambient electric and magnetic fields room's infrastructure are the requirement for the SEM. An electron gun, lenses, scanning coils, detectors to collect signals (secondary and backscattered electrons as well as X-ray), sample stage, display/data output devices are the basic components of the SEM. **Fig. 2.6** represents the set-up of SEM. When an electron beam hits the sample, many different types of signals are generated, which are eventually used to observe or analyze the morphology/ topology of the specimen/material. These signals include secondary electrons, backscattered electrons, Auger electrons, X-rays. The SEM uses for revealing the morphology of surface details of the materials**,** high-resolution images**;** detect the compositional difference, and elemental microanalysis (EDX) as well as particle characterization.

Figure 2.6: External view of scanning electron microscope [*Source: USIC, BBAU, copyright permission*].

The advantages of the SEM are high-resolution image**,** fast recognition of existing elements, and the SEM is also supported with other tools like EDX; but SEM has also some limitations with the need for a typically high vacuum**,** destroy sample for further analysis, and need to cut the size of specimen, etc. **[38]. W**ith these limitations of SEM, the SEM analysis is popular among characterize the morphology of the micromaterials and nanomaterials. The field effect electron microscpope FESEM gives high resolution images compere to the SEM. So, FESEM used to investigate the shape and size with the high resolution surface morphology.

The Field Emission Scanning Electron Microscope (FESEM) is a technique to use as microscopy, which is similar to the setup of SEM. The difference between FESEM and SEM is only the electron gun, which is led in the system. The FESEM, JSM 7610F, consists of the Schottky field emission electron gun that makes the use of electric field emission to lower the work function and increase thermionic emission of tungsten. The field emission gun is produced an electron beam and greater current density or brightness. The JSM 7610F FESEM is equipped with the gentle electron beam mode that gives high-resolution images even the low accelerating voltage from 100V to 3.9 kV without damaging the specimen surface. The FESEM is working on Schottky emission affected by the high electric field is employed to the heated metal surface. A tungsten single crystal (tip radius of few hundred nm) coated with ZrO acting as a cathode. The ZrO coating reduces the work function to enhance the emission current at low cathode temperature. Thermo electrons are shielded from the emitter by applying a negative voltage to the suppressor electrode. The advantage of FESEM is that the electron beam current highly stable because the emitter is placed in an ultra-high vacuum of the order of 10^{-7} Pa and it produces a larger probe current **[39].**

2.4.1.4 Energy Dispersive Spectroscope: EDS is also known as energy dispersive X-ray (EDX). Occasionally, it is also termed energy dispersive X-ray microanalysis (EDXMA). This technique is used to investigate the elemental composition of the specimen or sample. The sample may be of any forms such as solid powders, solid thin films, and liquid samples, etc. **[40].** The SEM setup has also been included with the EDX having an extra detector of X-Ray. EDS or EDX is part of X-ray Fluorescence (XRF) spectroscopy where the ejected X-rays from the sample are analyzed to investigate a sample in response to interacting with electrons when the interactions between EM radiation and sample. The basic principle of the EDX is that every atom of a special atomic structure and it is allowed X-rays characteristic of an element of atomic structure to be recognized especially when the interactions between EM radiation and sample **[41].** The electron beam excites an electron in an inner shell and emits electrons from the inner shell when generates an electron-hole by absorbing the energy. The X-ray energy is released from a sample when filling up the hole with the outer electrons, which can be examined through an EDX spectrometer **[42].** The EDX is generally used to investigate the composition of elements in the specimen and it is also given the percentage of oxide of the elements in the sample/material **[43].**

2.4.2 Spectroscopy Techniques

Spectroscopic techniques are used to convey out information of a strong modern analytical framework of the creation of new FMs. It is focused on the development of the physical foundations of new FMs. The main objective of the technique is to analysis the how materials useful for studying the elemental, chemical, and molecular structure, structural completeness of the surface interphase boundaries and nanostructures, and materials metrology. The objective of this technique to analysis of FMs like Auger Electron Spectroscopy (AES), X-ray Photoelectron Spectroscopy (XRF), Secondary Ion Mass Spectrometry (SIMS), Scanning Ion Microscopy (SIM), etc. These techniques belong to modern spectroscopy technique. These modern technoques allows us to investigate elemental, chemical composition, atomic structure, structural completeness of solid surfaces, surface layers, phase boundaries, and nanostructures.

2.4.2.1 Raman Spectroscope: Raman spectroscopy is a fundamental form of molecular spectroscopy **[44, 45].** The structural properties of the molecules are analyzed by vibrational transitions using Infrared (IR) absorption and Raman scattering **[46, 47].** Raman Spectroscopy determines vibrational and rotational energy level spacing from the energy (in terms of wavenumber) shifting of the scattered light. Molecular transition energies are observed by measuring the shifts in the frequency of light scattered when a molecule is subjected to an intense beam of monochromatic light. The discovery of the light scattering phenomenon viz. “Raman effect” was invented in 1928 by Indian Scientist Raman **[48].** Nowadays, this effect is commonly used to study the purity of the molecules by the vibrational states of the molecules. This vibrational study was done in the absence of intense monochromatic light sources, optical components, and detectors. The use of Raman spectroscopy has been used to solve the fundamental and technological problems. The Raman spectroscopy techniqueneeds the high-throughput monochromators and sensitive detectors of laser. The Raman scattering is a phenomenon of two photons event in which polarizability of the molecule changes concerning its vibrational motion of the molecule **[49].** The interaction of the polarizability and incoming radiation of laser creates an induced dipole moment in the molecule. The emitted radiation by the induced dipole moment contains the information of both Rayleigh and Raman scattering.

2.4.2.2 UV-Visible Spectroscope: It is an excellent physical tool where the Ultraviolet, UV-Visible, and near-infra-red (IR) wavelength spectrum are considered for investigation of the optical properties of the incident light. To study the optical properties of the incident light with the sample, the Beer-Lambert law is used to calculate the absorption of the light in terms of the length of the sample and concentration of material in the sample. Generally, the wavelength of the electromagnetic spectrum are 300-400nm for ultraviolet region, 400-765nm for visible region, and 765-3200nm for the near-infra region (IR). This spectroscopy technique is used to study the absorption of liquids, gases as well as solids through radiation **[50].** The absorbance of ultraviolet-visible (UV-Visible) light gives different-different spectra of the FMs and the spectra of the FMs used to study the spectroscopic properties of materials.

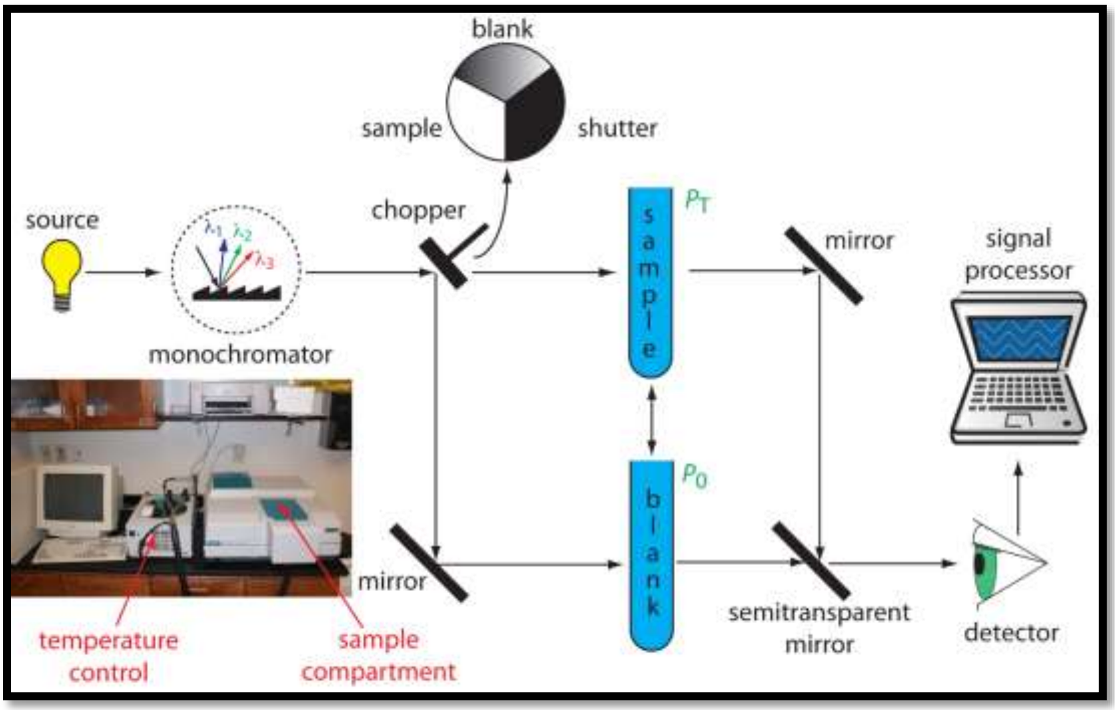

Figure 2.7: Schimatic process of UV-Vis spectroscopy an external view image [*Source: USIC, BBAU, copyright permission*].

The basic principle of UV-Visible spectroscopy is a collision of light with the specimen. When photon energy falls on the specimen, the electrons may be excited from the ground energy state and reached a excited energy state. It shows exciting photons, and sometimes it shows de-excitement, due to the absorbance and emission of light. After this process, the revealed spectrum is observed . UV-Visible spectra is more significant than the energy difference of ground and excited energy state is equivalent to the UV-visible radiation **[51].** The working mechanism of the UV-visible spectrometer is shown in **Fig. 2.7**. UV-Vis spectroscopy is used to calculate the band gap of compounds using absorption spectra of the UV-Vis spectroscopy, which is based on the Tauc-plot **[52].**

2.4.3 I-V Characteristics Technique

The I-V characterstic technique is used to study the property of photodetector to measure the photoparameters via device analyzer (Keithley unit model 6517 B). In this process, a white light source lamp (AM 1.5) of 550 nm wavelength is incident on the film, after that, the voltage is applied onto the electrodes and measured the current in the same electrodes. A self-made drived circuit is used to measure the dark-current and photo-current. The Keithley unit Model 6517 B source meter is used to measure the I-V characteristics of the device. The **Fig. 2.8** shows the process to study the I-V characteristics for SnS nano flakes thin-film.

This chapter concludes the synthesis and characterization methods for Functional materials (FMs). The best synthesis methods for FMs have discussed and also discussed the characterization techniques of as-synthesis of FMs. By these methods, we can propose the FMs for phovoltaic devices. 2-D nanomaterials i.e. thin films are mostly used in the photovoltaic 2nd generation solar cells. The 2-D FMs are already available in the market and these materials are used to fabricate the energy devices. But the cost of such energy devices became very high due to a high cost of synthesis process and use of rare earth elements compositions. Besides this, the complicated and conventional synthesis processes make it time consuming as well as hazardious for environment.

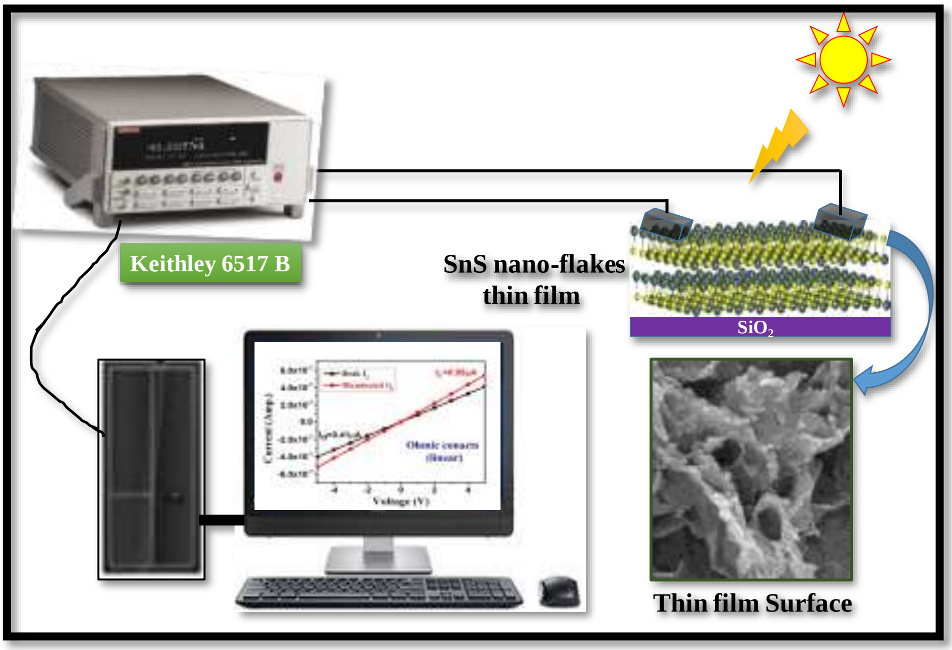

Figure 2.8: The schematic diagram of Keithley (unit model 6517 B) set-up for I-V characteristics measurement.

In this Ph.D. research work, we tried to study, how the energy devices are fabricated with low cost, less-time consuming, eco-friendly method. For this, we have focused on the abundant elements composition and synthesis process of FMs. The XRD, XPS, SEM, FESEM, EDS, UV-Visible, Raman spectroscopy and impedence analyser have used to characterize the as-synthesized FMs for energy device applications.

References:

[1] H. A. Zahl and H. K. Ziegler, Power sources for satellites and space vehicles, *Sol. Energ.*, 4, 32-38, 1960.

[2] L. D. Sio, Active Plasmonic Nanomaterials, *CRC Press Taylor & Francis Group*, ISSN: 13: 978-981-4613-01-9, 6000 Broken Sound Parkway NW, Suite 300 Boca Raton, USA, 2015.

[3] H. A. Atwater and A. Polman, Plasmonics for improved photovoltaic devices, *Nat. Mater.*, 9, 205-213, 2010.

[4] W. Shockley and H. J. Queisser, Detailed balance limit of efficiency of *pn*-junction solar cells, *J. Appl. Phys*., 32, 510–519, 1961.

[5] C. J. Stolle, T. B. Harvey and B. A. Korgel, Nanocrystal photovoltaics: A review of recent progress, *Curr. Opin. Chem. Eng*., 2, 160–167, 2013.

[6] Z. Lin, A. Franceschetti and M. T. Lusk, Size dependence of the multiple exciton generation rates in CdSe quantum dots, *ACS Nano*, 5, 2503–2511, 2011.

[7] S. K. Stubbs, S. J. O. Hardman, D. M. Graham, B. F. Spencer, W. R. Flavell, P. Glarvey, O. Masala, N. L. Pickett and D. J. Binks, Efficient carrier multiplication in InP nanoparticles, *Phys. Rev. B,* 81, 081303-081304, 2010.

[8] R. D. Schaller and V. I. Klimov, High-efficiency carrier multiplication in PbSe nanocrystals: Implications for solar energy conversion, *Phys. Rev. Lett*., 92, 186601-3, 2004.

[9] R. J. Ellingson, M. C. Beard, J. C. Johnson, P. Yu, O. I. Micic, A. J. Nozik, A. Shabaev and A. L. Efros, Highly efficient multiple exciton generation in colloidal PbSe and PbS quantum dots, *Nano Lett.,* 5, 865–871, 2005.

[10] J. E. Murphy, M. C. Beard, A. G. Norman, S. P. Ahrenkiel, J. C. Johnson, P. Yu, O. I. Micic, R. J. Ellingson and A. J. Nozik, PbTe colloidal nanocrystals: Synthesis, characterization, and multiple exciton generation, *J. Am. Chem. Soc.,* 128, 3241–3247, 2006.

[11] M. C. Beard, K. P. Knutsen, P. Yu, J. M. Luther, Q. Song, W. K. Metzger, R. J Ellingson and A. J Nozik, Multiple exciton generation in colloidal silicon nanocrystals, *Nano Lett.*, 7, 2506-2512, 2007.

[12] R. D. Schaller, M. A. Petruska and V. I. Klimov, Effect of electronic structure on carrier multiplication efficiency: Comparative study of PbSe and CdSe nanocrystals, *Appl. Phys. Lett.*, 87, 253102, 2005.

[13] P. Krogstrup, H. I. Jørgensen, M. Heiss, O. Demichel, J. V. Holm, M. Aagesen, J. Nygard and A. F. i Morral, Single-nanowire solar cells beyond the Shockley-Queisser limit, *Nature Photon.*, 7, 306–310, 2013.

[14] T. Nobis, E. M. Kaidashev, A. Rahm, M. Lorenz and M. Grundmann, Whispering gallery modes in nano-sized dielectric resonators with a hexagonal cross-section, *Phys. Rev. Lett.*, 93, 103903, 2004.

[15] P. V. Kamat, Quantum dot solar cells, semiconductor nanocrystals as light harvesters, *J. Phys. Chem. C,* 112, 18737–18753, 2008.

[16] L. D. Sio, Active Plasmonic Nanomaterials, *CRC Press Taylor & Francis Group*, ISSN: 13: 978-981-4613-01-9, 6000 Broken Sound Parkway NW, Suite 300 Boca Raton, USA, 2015.

[17] J. Li, D. Wang, R. R. La Pierre, Advances in III-V Semiconductor Nanowires and Nanodevices, *Bentham Science Publishers*, ISBN: 978-1-60805-415-2, 2011.

[18] M. Khodaei, M. H. Enayati, and F. Karimzadeh, The structure and mechanical properties of Fe_3Al-30 vol.% Al_2O_3 nanocomposite , *J. of Alloy. and Comp.*, 488, 134-137, 2009.

[19] S. Stankic, S. Suman, F. Haque and J. Vidic, Pure and multi-metal oxide nanoparticles: synthesis, antibacterial and cytotoxic properties. *J. of Nan. biotech.,* 14(1), 73, 2016.

[20] B. Reddy, Advances in Nanocomposites: Synthesis, Characterization, and Industrial Applications, *Publish with Intech Open*, ISBN:978-953-51-4497-7, 2011, doi: 10.5772/604.

[21] A. P. Jadhav, C. W. Kim, H. G. Cha, A. U. Pawar, N. A. Jadhav, U. Pal, and Y. S. Kang, Effect of different surfactants on the size control and optical properties of Y_2O_3:Eu3+ nanoparticles prepared by Coprecipitation method, *J. Phys. Chem. C.* 113, 2009.

[22] C. M. Lampkin, Electrochromic materials and devices for energy efficient windows, *Sol. Energ. Mat.*, 11, 1-27, 1984.

[23] Gary L. Messing, Shi-Chang Zhang and Gopal V. Jayanthi, Ceramic Powder Synthesis by Spray Pyrolysis, *J. Amer. Ceram. Society,76, (11), 2707 1993*.

[24] W. M. Sears, M. A. Gee, Mechanics of film formation during the spray pyrolysis of tin oxide, *Thin Solid Films*, 165(1)1:5, 265-277, 1988.

[25] H. H. Affify, S. A. Nasser, S. E. Demian, Influence of substrate temperature on the structural, optical and electrical properties of ZnO thin films prepared by spray pyrolysis, *J. Mater. Sci.: Materials in Electronics*., *Journal of Materials Science: Materials in Electronics*, 2, 152–156, 1991.

[26] A. Goswami, Thin Film Fundamentals, *New Age International (P.) Ltd*, ISBN 13: 9788122408584, India, 1996.

[27] K. L. Chopra, I. Kaur, Thin Film Device Applications, *Springer*, ISBN978-1-4613-3682-2, Boston, MA, 1983.

[28] N.H.J. Stelzer and J. Schoonman, Synthesis of terbia-doped yttria stabilized zirconia thin films by electrostatic spray deposition (ESD), *J. Materials Synthesis, and Proceedings*. 4(6), 429, 1996.

[29] T.H. Sajeesh, K. P. Vijayakumar, and C. S. Kartha, Characterization of p-type thin films prepared using CSP Technique, *MRSI-AGM Conference proceeding*, New Delhi, 2007.

[30] S. Shibata, K. Aoki, T. Yano and M. Yamane, M. Preparation of silica microspheres containing Ag nanoparticles, *J. of sol-gel sci. & Tech.*, 11, 279, 1998.

[31] C.N.R. Rao and K. Biswas, Essentials of Inorganic Materials Synthesis, ISBN 978-1-118-83254-7, *Published by John Wiley & Sons, Inc.*, Hoboken, New Jersey, USA, 2015.

[32] K. Byrappa and T. Adschiri. Hydrothermal technology for nanotechnology." *Progress in Crystal Growth and Characterization of Materials,* 53(2), 117-166, 2007.

[33] L. D. Sio, Active Plasmonic Nanomaterials, *CRC Press Taylor & Francis Group,* 6000 Broken Sound Parkway NW, Suite 300 Boca Raton, FL 33487-2742, U.S., 2016.

[34] T. Wofford, Hertz, Einstein and the photoelectric effect, *Phys. Today*, 61, 5, 10, 2008.

[35] W. Schaaffs, A. E. Sandström, D. H. Tomboulian, P. Kirkpatrick, H. H. PatteeJr. and S. T. Stephenson, Röntgenstrahlen / X-Rays, *Springer, Berlin, Heidelberg*, ISBN:978-3-642-45863-7, 1957.

[36] H. Bluhm, 4 - X-ray photoelectron spectroscopy (XPS) for *in situ* characterization of thin film growth: "In Situ Characterization of Thin Film Growth", G. Koster, G. Rijnders (Eds.), *Woodhead Publishing Ltd*, Cambridge, UK 75-98, 2011

[37] R. Reichelt, Scanning Electron Microscopy In: Hawkes P.W., Spence J.C.H. (eds) *Science of Microscopy. Springer*, New York, NY. 133-2, 2007.

[38] https://www.slideshare.net/JessaArio/scanning-electron-microscopy, 2021.

[39] S. L. Pal, U. Jana, P. K. Manna, G. P. Mohanta, and R. Manavalan, Nanoparticle: an overview of preparation and characterization, *Journal of Applied Pharmaceutical Science*, 1(6), 228–234, 2011.

[40] Sovan L. Pal, U. Jana, P. K. Manna, G. P. Mohanta, R. Manavalan, An Overview Of Preparation And Characterization, *J. Pharam. Sci.*, 6, 228-234, 2011.

[41] S. Stankic S. Suman, F. Haque, J. Vidic, Pure and multi metal oxide nanoparticles: synthesis, antibacterial and cytotoxic properties. *J. Nano-biotech.* 14(1), 73, 2016.

[42] http://www. charfac. umn. edu/instruments/eds_on_sem_primer. pdf, 2021.

[43] L. Reimer, Scanning Electron Microscopy, *Springer-Verlag*, Berlin, J. C. Russ, "Fundamentals of Energy Dispersive X-ray Analysis", Butterworths, London, 1984.

[44] G. Herzberg and B. L. Crawford Jr, Infrared and Raman spectra of polyatomic molecules, *J. Phys. Chem.*, 50(3), 288, 1946.

[45] E. B. Wilson, J. C. Decius and P. C. Cross, Molecular Vibrations: the theory of infrared and Raman vibrational spectra, *New York: McGraw-Hill*, 388, 1955.

[46] J. G. Grasseli and B. J. Bulkin, Analytical Raman spectroscopy, *Wiley*, New York, 1991.

[47] J. R. Ferraro and K. Nakamoto, C. W. Brown, second edition, Introductory Raman spectroscopy, *New York Academic Press*, ISBN: 978-0-12-254105-6, New York, 1994.

[48] C. V. Raman and K. S. Krishnan, A new type of secondary radiation. *Nature*, 121:501, 1828.

[49] I. R. Lewis and G. M. H. Edwards, Handbook of Raman spectroscopy, *Marcel Dekker Inc.*, New York, 2001.

[50] A. P. Jadhav, C. W. Kim, H. G. Cha, A.U. Pawar, N. A. Jadhav, U. Pal and Y. S. Kang, Effect of different surfactants on the size control and optical properties of Y_2O_3:Eu3+ nanoparticles prepared by Coprecipitation method, *J. Physic. Chem. C.* 113, 2009.

[51] V. D. Scott and G Love, Quantitative Electron Probe Microanalysis, *Ellis Horwood*, Chichester, New York,1994.

[52] L. D. Pavia, M. G. Lampman, G. S. Kriz, I. R. Vijaan, Spectroscopy, *CBS Publishers and Distributors*, Washington University, USA,1997.

CHAPTER 3

Synthesis and Characterization of II-VI group (ZnO) Functional Material without any Surfactant for Photovoltaic Applications

Chapter 3

Synthesis and Characterization of II-VI group (ZnO) Functional Material without any Surfactant for Photovoltaic Applications

3.1 Introduction

Renewable energy is an essential energy in this era and it is one such option of energy which is limitless. This energy is directly related to the environment. The scientists and researchers from different streams are working together to make the feasibility of renewable energy for society without harming the environment of the surrounding medium. In the field of renewable energy, enormous advancement has been done in the forms of a different novel device as photovoltaic cells, biofuel, fuel cells, photo-detectors, etc. **[1].** As a source of renewable energy, solar energy fits for an absolute solution to the energy problem to the replacement of carbon-neutral energy. At present, scientific advances in the field of energy sources have materialistic solar devices but such available equipment are costly and also harmful to the environment with 25% efficiency. To fulfill the demand of renewable energy, the solar devices viz. solar cells need to refine and satisfy the challenge of high efficiency, low cost, stability, and ecofriendly **[1].** Currently, a scientific community needs solar cells that have highly efficient, cost-effective and environment-friendly to address the problem of solar energy resources. Many scientists and researchers are synthesizing the different materials to use in efficient solar cells and other solar devices. The synthesized compound or composite materials can be binary, ternary, quaternary and other highly complex materials, and the properties of the materials and their applications also depend on the structure and the composition of the materials as well as the synthesis route of the material, for promising efficient materials to use in solar cells.

The transparent conducting oxides (TCO) films are conductive for electromagnetic (em) waves and electrically conductive for optoelectronic devices such as flat solar panel display. TCO films are made by organic and inorganic materilas and such organic and inorganic TCO films are used for solar cells applications. However, indium tin oxide (ITO) is maximum used in PV devices as a transparent conductive oxides due to low resistance, highly electro and photo conductive and suitable band gap **[2].** Among the different hybrid materials as well as complex materials, ZnO is very easy to fabricate and shows excellent properties to use in different applications including solar devices.

ZnO is a very favorable material for photovoltaic cells due to its salient characteristics of non-toxic, highly stable at normal temperature, low cost, stability as well as easily synthesis with efficient electronic and optical properties **[3-5].** The structure of ZnO shows wurtzite with the distance between the parallel planes of atoms; a=0.325nm, b=0.521nm, excitation binding energy (BE)=60meV, and E_g=3.37eV, which support the excitonic emissions at room temperature **[6-8].** To control the optical properties of ZnO, the researchers have tried to tune the conductivity of ZnO material with doping of oxides **[5].** To obtain the uniform size and shape of ZnO nanomaterials, various synthesis methods have been used like Spray pyrolysis, Thermal decomposition, Sol-Gel, Chemical vapor decomposition (CVD), and Coprecipitation, which obtains suitable shape and size of the nano materials for appropriate application **[9-11].** Among all points of synthesis routes, Coprecipitation method is efficient to yield controllable morphology and reproducibility of nanomaterials using low-cost materials **[12, 13].** ZnO layers can be prepared by a number of methods most often by magnetron sputtering either from group of the same elements or reactively from metal targets. Due to the unique electronic and optical characteristics of ZnO nanoparticles, ZnO has various applications in various electronic and optical devices such as lasers, gas sensors, photocatalysts, nano-generators, biosensors, varistors, photodetectors and acoustic wave devices **[8].**

The hetero-junction PV devices are used to conversion the solar energy into electric charge and fabricated by the combination of two components: (a) Organic semiconductor allocation the light harvesting and generate the electric donar charge, (b) Inorganic semiconductor behave as electron acceptors **[14].** In these types of inorganic PV devices, the electron mobility of ZnO is highly stable in physical and chemical form of materials. Due to this stable characteristic of ZnO, the electron acceptors characteristics in organic semicondoctors are replaced by the electron mobility of ZnO. In inorganic solar cells (ISCs), the total energy generation mechanism is similar to that of the organic solar cell system (OSCs). In this mechanism, the illumination light generates exciton i.e. electrons and holes, and then diffuse to them (donor/acceptor) at interface within a certain length of diffusion **[15].** In the PV devices, the highest occupied molecular orbital (HOMO) and lowest unoccupied molecular orbital (LUMO) gap generated in the band structure at the doner-accepters interface. This interface delivers a dynamic force to the charge carriers to neutralising the binding energy of excitons and detaching them onto two free carriers bia charge transfer. The free charge carriers are transferred to the cathode (positive charge carriers) and anode (negative charge carriers) by the acceptor and donor atoms/molecules in the materials **[3].** The nanoparticles, nanowires and nanorods of ZnO are used as window layer for photovoltaic applications due to high photocurrent density.

In the natural resources of water, the various toxic inorganic substances like F, As, Pb, Cu, Cr, Hg, Sb etc. and organic polluted substances like household wastes, commercial wastes, pesticides and microorganisms are found **[17]**. Besides this the anthropogenic activities like sewage and cosmic activities are caused to contaminant the natural water **[18].** Inorganic waste ingredients in groundwater are the main problems of atmospheric pollutions where inorganic chemicals, carcinogenic organic and infectious pathogens are polluting the ground water day by day. The inorganic pollutants are mainly found for two main reasons: first is a lack of information about the chemicals to be disposed off, and the second is the failure to eliminate anthropogenic pollutants from nature. As a result, the inorganic ingredients in the environment are responsible for the pollution of the ground water because the inorganic ingredients include nitrates, nitrites, fluoride, arsenic, irons, manganeses, lead, mercury, chromium, cadmium, and aluminum are pollutants in the wastewater **[19].** If the impurities of wastewater ingredients need to be removed, then such wastewater is recycled into potable water. The synthesized ZnO nanomaterials are also used in the wastewater treatment applications. The impurities of wastewater ingredients are removed by photocatalytic process of the ZnO nanomaterials. The ZnO nanomaterials absorb light and generate electron-hole pairs. The separation of excited charges carriers transfers to the surface of ZnO nanomaterials photocatalysts produces the redox reactions that is used to remove the impurities from wastewater **[16]**.

In this chapter, we have discussed the synthesis of ZnO nano-material using the Coprecipitation method without any surfactant for window layer in PV devices. The confirmation of shape and size of ZnO nanoparticles can be done by the necessary characterizations like scanning electron microscope (SEM), X-ray diffraction (XRD), UV-Visible and Energy Dispersive X-ray spectroscopy (EDS). Using the above-mentioned characterization tools, we have determined the bandgap, porosity as well as surface morphology of the prepared ZnO nanoparticles. By doping of different appropriate materials in the ZnO nanoparticles, the conductivity of the ZnO nanoparticles can be enhanced **[20].** The recent development of aggregated nanocrystalline ZnO in Dyesensitized solar cells (DSCs) shows a high improvement in the photo conversion efficiency of the ZnO-based DSCs **[21, 22**].

3.2 Experimental Method

The core materials for synthesis of ZnO nanoparticles, have taken the laboratory-grade Zinc acetate (98.5% pure $Zn(CH_3COO)_2.H_2O$) and Sodium hydroxide (98.5% pure NaOH) from Thermo Fisher Scientific Pvt. Ltd. India. The chemical wet methods are adopted to synthesis the desired ZnO nanoparticles.

3.2.1 Synthesis of ZnO Nanomaterials Powder

Using the suitable ratio of core materials, ZnO nanoparticles were synthesized by CPM route without any surfactants. In this synthesis process, $Zn(CH_3COO)_2{\cdot}2H_2O$ (0.2M) and deionized water (DI) were mixed forcefully up to 3hours at 60^{o}C temperature. Further, 150ml solution of distilled water and NaOH (1M) were mixed dropwise at a 1.5ml/minute rate. The filtrate obtained by a white precipitate of solution with pH=9 is washed with DI water and ethanol to filter out unwanted products by precipitate. After the removing unwanted products, the filtrated compound of ZnO was dried for at least 24hours at 80^o temperature. With this described process, we have prepared three samples of ZnO nanoparticles with pure phase compound (sample-A), calcinated the compound at 600^{o}C (sample-B), and annealed compound at 800^{o}C (sample-C). Further, we have characterized the as synthesized samples with different tools to look into the desired application of solar cells.

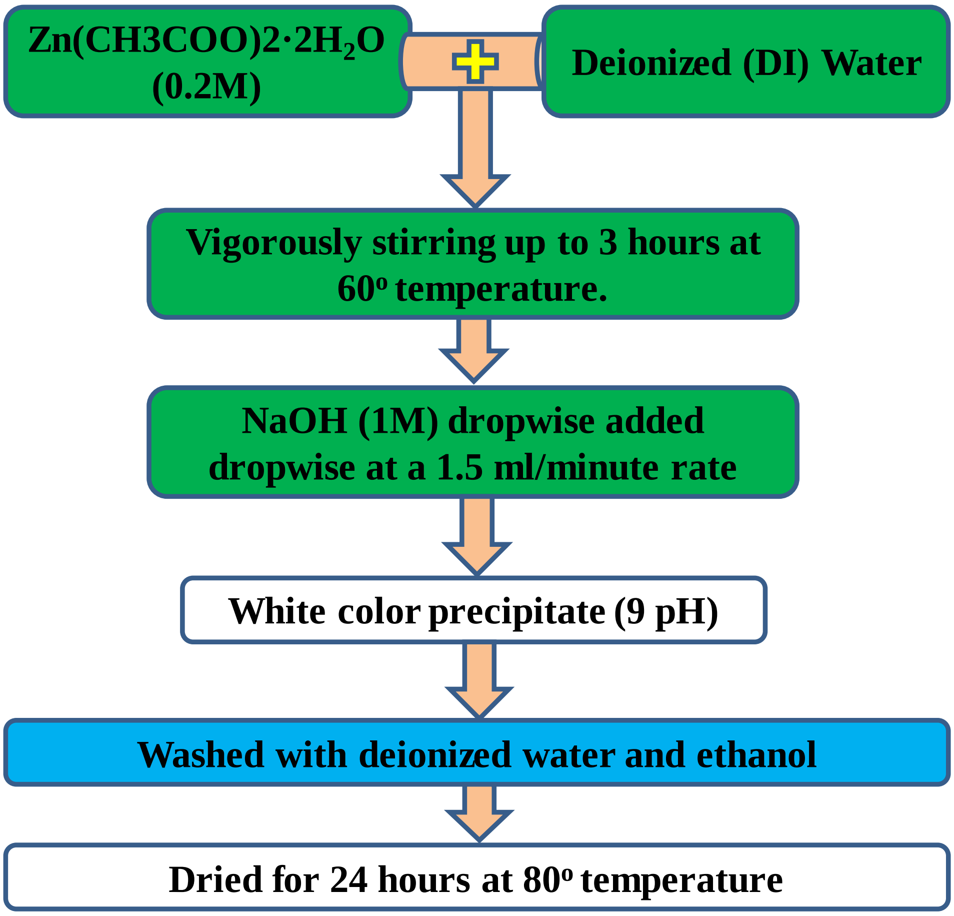

Figure 3.1: The flow chart diagram of ZnO nanomaterials synthesis by Coprecipitation method.

3.2.2 Thin-Film Deposition of ZnO Nanomaterials

To get the best result of surface morphology of the ZnO material by scanning electron microscope, we have fabricated thin-film on the soda lime glass (SLG) substrate. First of all, the SLG substrate was washed by detergent powder and cleaned by an ultrasonic bath in DI water and ethanol mixture and was dried at 80^{o}C in an oven before the deposition of the CZTS solution. The precusrure solution of ZnO was prepared in ethylene glycol (EG) and found a homogeneous dispersed solution after ultra-sonication. The ZnO solution was deposited by drop-casting methods on heated hot plate at 60^{o}C and was repeated this process 3-5times to get the best thickness of the film. The ZnO film was dried on a hot plate at every process of deposition. The surface morphology of the ZnO thin film was analyzed by the scanning electron microscopy (SEM) and results are discussed in the next part in this chapter.

3.3 Results and Discussion

For the desired application of the ZnO nanoparticles, the pre-synthesized ZnO thin film was characterized by using powder X-ray diffraction (XRD) and scanning electron microscope (SEM) methods. XRD method was employed to study the size and shape of prepared materials in the diffraction ranges between 20^o and 80^o (degree) i.e. $20^o \leq 2\theta \leq 80^o$ (degree), with CuK$_\alpha$ monochromatic radiation with wavelength $\lambda = 1.5418\,\overset{o}{A}$. The SEM (JEOL-scanning electron microscope) was used to analyze the surface morphology of ZnO thin film These characterization methods are discussed in the following subsections.

3.3.1 X-Ray Diffraction Ananlysis

As discussed earlier, we have synthesized three samples of the ZnO nanomaterials i.e. without calcinated at room temperature 35^oC (A sample), and calcinated at 600^oC (sample-B) and 800^oC (sample-C). **Fig. 3.1** revealed that the XRD patterns of all three samples of as synthesized ZnO (A=R_t, B=600^oC, and C=800^oC) are strong patterns. These diffraction peaks in the XRD patterns have (100), (002), (101), (102), (110), (103), (112), and (201) planes of ZnO nano material **[23].** Also, wurtzite structures of ZnO nanoparticles of annealed samples were confirmed by JCPDS card no. 36-1451**.** The intense peak values of (100), (002), and (101) crystal planes are found at angle (2θ) in degree 31.75^o, 34.40^o and 36.24°, which is shown in **Fig. 3.2**. Due to absence of any impurity in the as-synthesized samples, the XRD patterns shows by the miller planes of ZnO samples. The obtained diffraction peaks in XRD patterns of ZnO samples get stronger as well as sharper with the higher calcination temperatures. The results reveal to enhance the crystalline nature of prepared materials. Using Debye Scherer method, the average crystalline size of the ZnO nanoparticles is found to be 22.54nm and 28.15nm with lattice parameters a, c as 0.3248nm, c=0.5205nm. The obtained results also support the formerly published paper by Lee et al. **[23].**

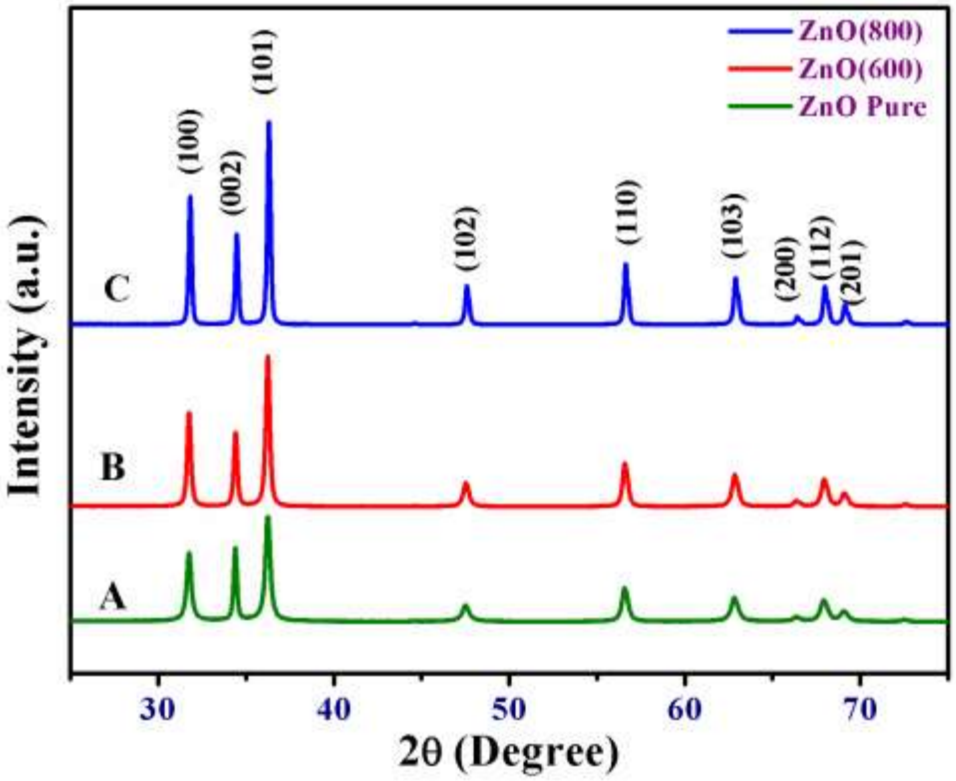

Figure 3.2: XRD patterns of ZnO nanoparticles (a) ZnO at 35°C, (b) ZnO calcinated at 600°C, and (b) ZnO calcinated at 800°C.

3.3.2 Scanning Electron Microscope Analysis

The surface morphology and EDS analysis of ZnO nanoparticles on the glass substrate prepared by Coprecipitation are shown in **Fig. 3.3.** The surface morphology in **Fig. 3.3** shows only the spherical and rod shape of the ZnO nanoparticles and the absence of other sizes and shapes of the nanoparticles. As-prepared thin films are micro-porous and rough, that indicating the absorption of electromagnetic radiation in solar cell applications. In addition, EDS analysis of the synthesized ZnO material at the atomic scale is given in the **Tab. 3.1.** This analysis shows the strong peaks of zinc and oxygen in as synthesized ZnO nanoparticles. At room temperature without calcinate sample of ZnO comprises 73.70% of Oxygen and 26.30% of Zinc. After calcination, Zn ratio is increased with calcinate temperature.

Table 3.1: EDS analysis of Zinc oxide nanoparticles at various calcinated temperatures:

Elements present	Amount Ratio (R_t =35°C)	Amount Ratio (T=600°C)	Amount Ratio (T=800°C)
O	73.70%	63.02%	69.99%
Zn	26.30%	36.98%	30.01%
Total amount percentage=	100%	100%	100%

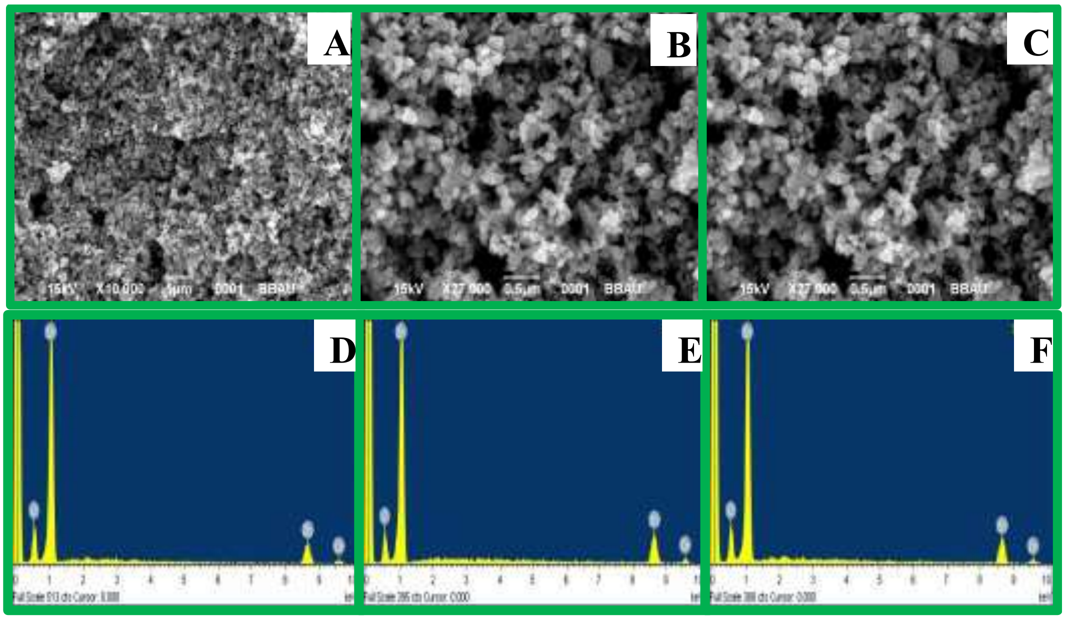

Figure 3.3: SEM results of ZnO nanomaterials at different calcinated temperatures and Room temperature.

3.3.3 ZnO Nanomaterials for Window Layer in Photovoltaic Applications

On the basis of above characterisations results of XRD, SEM, EDS, ZnO nanomaterials are suitable for window layer applications. The schematic representation of window layer in hetero-junction photovoltaic device is shown in **Fig. 3.4**. The hetero-junction photovoltaic device has the different multilayers of different functional materials such as ITO/CZTS/CdS/i-ZnO/Al:ZnO/ARC/Ag, where ITO is used as conducting substrate, CZTS is used as absorber layer, CdS is taken as buffer layer, intrinsic ZnO (i-ZnO) and Aluminum doped ZnO (Al:ZnO) are used as window layers, ARC is used as anti-reflection coating and silver past (Ag) is used as electrode.

As we know that the window layer is used to reduce the recombination of the charge carriers below the antireflection layer in the photovoltaic cell because window layers with high band gaps have passed the photons to the absorber layer either CZTS layer or SnS layer material. In hetero-junction thin-film solar cells, the window layer is mainly used to form *pn*-junctions with the absorber layer. The window layer is desired to achieve a high bandgap, small thickness and low series resistance for high optical throughput. The high electrical conductivity must be combined with a low value of the optical absorption constant (α) in the visible range. The absorber layers should have high optical absorption coefficient with high mobility, good carrier lifetime, and advanced crystallographic properties [**24**].

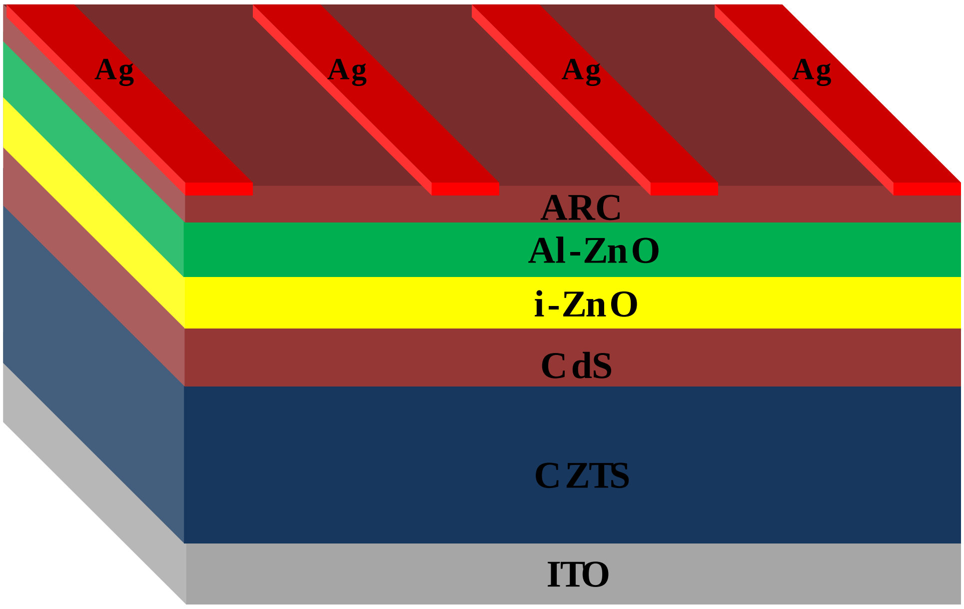

Figure 3.4: Representation of window layer (i-ZnO) in the hetero-junction Kesterite solar cell.

The several metal oxides are used as the window layer, because they are transparent and suitable for band alignment in the Kesterite PV devices. The Sn, In, Zn, and Cd metals oxide have wide bandgap larger than 2.6eV, which can be used as the window layer. The window layers of the ZnO and Al: ZnO materials are frequently used in the photovoltaic cells due to high bandgap **[20].** The large band gap window layer materials is absorbed the negative charge carriers from the buffer layer and reduced the recombination at the interface in kesterite PV devices. This window layer should have a small thickness (60-80nm) comparison to the thickness of convemsional absorber layer. Such thickness of the absorber layer is used to reduce series resistance in the thin film PV devices. The ZnO window layer, as a specific structure, can be considered to use in PV devices having some major purposes: (i) to form the *n*-type half of the *p*-*n* junction, (ii) to minimize to conduct recombination near the absorber/window interface, and (iii) current to metal grid. It is also obvious that the window layers should be transparent to incident light such that incoming light reaches easily at the absorber layer.The thin film ZnO nanomaterials can be fabricated by simple SPM without any surfactant and this method is best option for mass production of ZnO in industry.

The **Fig. 3.5** shows the schematic illustration of the conventional thin-film layer stack used in chalcopyrite solar cell and its associated energy band diagram in short-circuit and dark conditions **[26].**

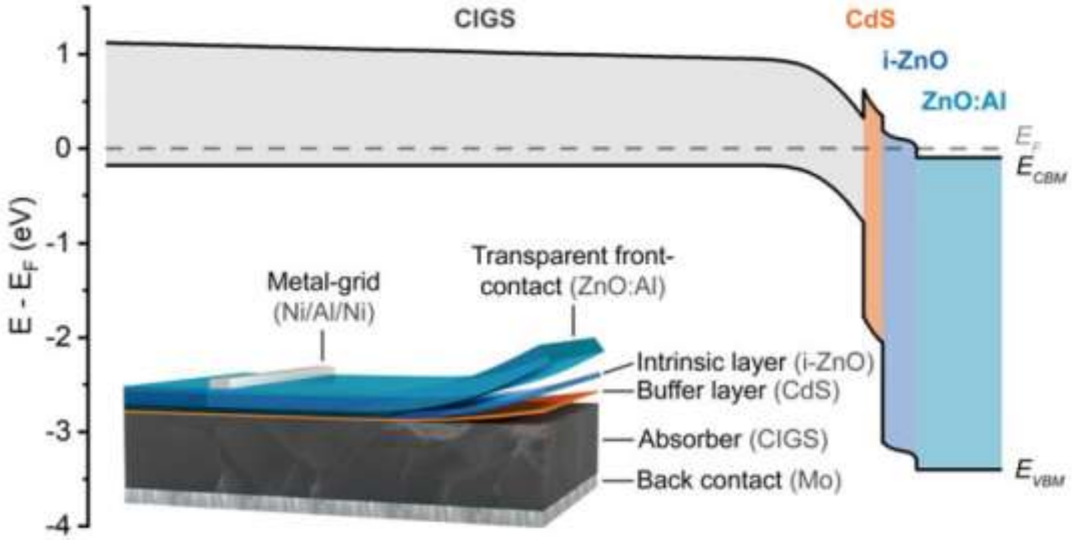

Figure 3.5: Schematic illustration of the conventional thin-film layer stack used in chalcopyrite solar cell and associated energy band diagram in short-circuitand dark conditions, ref. **[*26*].**

The chalcopyrite solar cell consists of a back contact with a substrate (not shown), a p-type material (CIGS), *n*-type material (CdS), and a metal grid. In between the buffer layer and metal-grid, the intrinsic and transparent contact layer are used for transport of charge carriers and ARC respectively. Now the electron-hole pairs are generated in the p-type material (CIGS), when high density of low energy photons reach into the CIGS. It is only possible when high density photons passes through all these layers (buffer, intrinsic, transparent and metal grid) without loss of energy then a large number of electron-hole pairs are generated after absorption of the high density of low energy photons.

Based on the synthesis and characterization analysis, elemental compositions, shapes, sizes and surface mophology the pure ZnO nanomaterials are found suiable for photocatalytic activity, which may be used for the removal of arsenic ingredient from water **[27]**.

3.4 Conclusion

In this chapter, we have concluded that the zinc oxide nanoparticles were synthesized by the low-cost and ecofriendly Coprecipitation method without any surfactant and this method is the best option to industrial production of ZnO nanomaterial without any surfactant. As-synrthesized material without any surfactant is crystalline similar results to synrthesized material with surfactant. It means that the synthesis of ZnO nanomaterials without any surfactant reduce the cost of the material production in their potential applications. The hexagonal wurtzite and polycrystalline nature of ZnO was confirmed by XRD patterns with lattice parameters a= 0.3248nm, c=0.5205nm. The crystalline nature of as synthesized ZnO material increases with calcinating temperature. As synthesized powdery ZnO nanomaterial has versatile applications including photovoltaic devices as a window layer and third-generation solar cell. Besides this, ZnO nanomaterial is also beneficial for the commercial use of other applications like water treatment in the photocatalytics process i.e. the as-synthesized ZnO material may be useful for the removal of arsenic ingredient from water.

References:

[1] Q. Zhang, C. S. Dandeneau, X. Zhou and G. Cao, ZnO Nanostructures for Dye-Sensitized Solar Cells, *Adv. Mater.*, 21, 4087– 4108, 2009.

[2] T. Dhakal, A. S. Nandur, R. Christian, P. Vasekar, S. Desu, C. Westgate, D. I. Koukis, D. J. Arenas and D. B. Tanner, Transmittance from visible to mid infra-red in AZO films grown by atomic layer deposition system, *Sol. Energ.*, 86 (5), 1306-1312, 2012.

[3] J. Huang, Z. Yin and Q. Zheng, Applications of ZnO in organic and hybrid solar cells, *Energy Environ. Sci*., 4, 3861–3877, 2011.

[4] S. Brintha and M. Ajitha, Synthesis and characterization of ZnO nanoparticles via aqueous solution, sol-gel and hydrothermal methods, *IOSR Journal of Applied Chemistry* 8, 66-72, 2015.

[5] A. Janotti and C. G. V. Walle, Fundamentals of zinc oxide as a semiconductor, *Rep. Prog. Phys*., 72, 1-29, 2009.

[6] D. M. Bagnall, Y. F. Chen, Z. Zhu, T. Yao, S. Koyama, M. Y. Shen and T. Goto, Optically pumped lasing of ZnO at room temperature, *Appl. Phys. Lett.*,70, 2230-2232, 1997.

[7] Z. M. Khoshhesab, M. Sarfaraz and M. A. Asadabad, Preparation of ZnO Nanostructures by Chemical Precipitation Method, *Synthesis and Reactivity in Inorganic, Metal-Organic, and Nano-Metal Chemistry*, 41(7), 814–819, 2011.

[8] S. Kumar and F. Singh, A. Kapoor, Synthesis and Characterization of Nano-Crystalline ZnO Quantum Dots via Sol–Gel Route for Dye-Sensitized Solar Cells, *Int. J. Recent Trends Elect. & Electr. Engg.*, 4(1), 25-29, 2014.

[9] A. J. Ahamed and P. V. Kumar, Synthesis and characterization of ZnO nanoparticles by Coprecipitation method at room temperature, *J. Chem. Pharm. Res*., 8(5), 624-628, 2016.

[10] Y. Yang, H. Chen, B. Zhao and X. Bao, Synthesis and characterization of lanthanum doped zinc oxide nanoparticles, *J. Cryst. Growth*., 263(1–4), 447-453, 2004.

[11] R. Suntako, Effect of zinc oxide nanoparticles synthesized by a precipitation method on mechanical and morphological properties of the CR foam, *Bull. Mater. Sci.* 38, 1033–1038, 2015.

[12] M. F. Romadhan, N. E. Suyatma and F. M. Taqi, Synthesis of ZnO Nanoparticles by Precipitation Method with Their Antibacterial Effect, *J. Chem. Indonesia*, 16 (2), 117-123, 2016.

[13] D. C. Reynolds, D. C. Look and B. Jogai, Optically pumped ultraviolet lasing from ZnO, *Solid State Commun*., 99, 873-875, 1996.

[14] M. A. Halim, Harnessing Sun's Energy with Quantum Dots Based Next Generation Solar Cell, *Nanomaterials*, 3, 22-47, 2013.

[15] A. Wibowo, M. A. Marsudi, M. I. Amal, M. B. Ananda, R. Stephanie, H. Ardy, L. J. Diguna, ZnO nanostructured materials for emerging solar cell applications, *RSC Adv.*, 10, 42838, 2020.

[16] S. Sharma and A. Bhattacharya, Drinking water contamination and treatment techniques, *Appl Water Sci*., 7:1043–1067, 2017.

[17] J. W. Moore, Inorganic Contaminants of Surface Water: Research and Monitoring Priorities, *Springer, New York*., (2012).

[18] M. Halim, P. Conte and A. Piccolo, Potential availability of heavy metals to phytoextraction from contaminated soils induced by exogenous humic substances. Chemosphere, *National centre for Biotechnology information, 52,* 265-275, 2003.

[19] P. Prachi, D. Gautam, Modatil and A. N. B. Nair, Nanotechnology in waste water treatment: A Review, *Int. J. Chem. Tech. Res.*, 5(5), 2303-2308, 2010.

[20] Q. F. Zhang, T. R. Chou, B. Russo, S. A. Jenekhe, Cao amd G. Z. Angew., Aggregation of ZnO Nanocrystallites for High Conversion Efficiency in Dye-Sensitized Solar Cells, *Chem. Int. Ed.*,47, 2402-2406, 2008.

[21] M. Shohel, M. S. Miran, M. A. B. H. Susan, M. Yousuf and A. Mollah, Calcination temperature-dependent morphology of photocatalytic ZnO nanoparticles prepared by an electrochemical–thermal method, *Research on Chemical Intermediates,* 42(6), 5281–5297, 2016.

[22] M. H. Rashid, M. Raula, R. R. Bhattacharjee and T. K. Mandal, Low-temperature polymer-assisted synthesis of shape-tunable zinc oxide nanostructures dispersible in both aqueous and non-aqueous media, *J. Colloid. Interf. Sci.* 339(1), 249-258, 2009.

[23] S. D. Lee, S.-H. Nam, M.-H. Kim, J.-H. Boo, Synthesis and Photocatalytic Property of ZnO nanoparticles Prepared by Spray-Pyrolysis Method, *Phys. Proced.*, 32, 320-326, 2012.

[24] K. L. Chopra, P. D. Paulson, and V. Dutta, Thin-film solar cells: An overview, *Prog. Photovol.*, 12, 69–92, 2004.

[25] E. R. Rwenyagila, B. A. Tuffour, M. G. Z. Kana, O. A. Ojo, W. O. Soboyejo, Optical properties of ZnO/Al/ZnO multilayer films for large-area transparent electrodes, *J. of Mat. Research*, 29(24), 2912-2920, 2014.

[26] F. Larsson, Window Layer Structures for Chalcopyrite Thin-Film Solar Cells, *Digital Comprehensive Summaries of Uppsala Dissertations from the Faculty of Science and Technology,* ISSN 1651-6214, 110, Uppsala: Acta Universitatis Upsaliensis, 1951.

[27] V. Gautam, thesis desert., Synthesis and characterization of doped ZnO nano-material for removing hazardous impurity of Arsenic in water, *BBA university, lucknow*, India, 2019.

CHAPTER 4

Functional Material (I_2-II-IV-VI_4) Cu_2ZnSnS_4 Synthesis without Vacuum Annealing for Photovoltaic Applications

Chapter 4

Functional Material (I_2-II-IV-VI_4) Cu_2ZnSnS_4 Synthesis without Vacuum Annealing for Photovoltaic Applications

4.1 Introduction

The functional material of I_2-II-IV-VI_4 group i.e. Cu_2ZnSnS_4 (CZTS or CZSS) has attracted enormous attention in promising development of solar energy conversion, hydrogen production, light emitting diode (LED), etc. The reason behind the emerging advancement of CZTS material is it's high absorbent (>10^4cm^{-1}), and contains the sustainable earth-abundant elements like Cu, Zn, Sn, S that makes it low cost, non-toxic, environment-friendly device **[1-3].** CZTS has tunability bandgap from 1.0 to 1.8 eV, which is an advanced feature to promote application as an absorber layer in PV devices. More discussion about this material for solar energy conversion applications has already been discussed in the **chapter-1.** From the "Introduction" chapter, we concluded that binary and ternary phases are the major problems in the CZTS, which are removed by the sulfurization process **[4].** Some researchers have also been tried to resolve these major issues from I_2-II-IV-VI_4 material by an effort of either sulfurization process or inert annealing process, which has a lot of hurdles in synthesis processes **[5].** The sulfurization/annealing process makes it costly and time taking process. Hence, CZTS synthesis methods have gained much attention for the exploration of novel methods across the globe.

To overwhelm the problems of the sulphurization/inert annealing process, lots of researchers have been used various methods for synthesizing CZTS nanomaterials (NMs) for wide photovoltaic applications **[6].** The various methods like Coprecipitation **[5]**, Sol-Gel **[7],** Solvothermal **[8],** Hot-injection **[9],** One-pot synthesis **[10]** and Microwave-assisted synthesis **[11]** are used to synthesis of CZTS NMs for photovoltaic materials applications. In the photovoltaic device, the CZTS is used as an absorber layer. The active area efficiency of CZTS solar cell was 6.77% by the fabrication of sputtering method **[2]**, and 8.4% by the co-evaporation deposition method **[12].** The high vacuum system in the thin film deposition process is the costly method for of CZTS solar cell, and non-vacuum system can provide low cost synthesis of CZTS solar cells. The most useful non-vacuum approaches include spray pyrolysis, electro-deposition/electrolysis deposition, Coprecipitation and ink approaches **[13-16].** Among the above non-vacuum methods, the CZTS nanomaterials are synthesized in the form of powder, ink and thin-film. In these forms of nanomaterials, they have been found stability for the large scale production of CZTS materials **[17].** The CZTS based solar cells were reported 5.1% efficiency by the solution ink methods **[18].** However, by replacing the Zn atom with the Cd atom, the efficiency of $Cu_2Zn_{1-x}Cd_xSnS_4$ was found 9.24% **[19].** The efficiency of powdery CZTS (CZTS,Se) nanocrystals fabricated device reported 7.2%, which was stable for powder form CZTS NMs **[20].** The dry nanocrystals based approaches draw more and more attention to the peoples because the solution ink method can control the stability and phases during the film deposition.

In the ***Mo/Absorber layer/buffer layer/nanostructured metal oxide/metal grids*** device, Pal et al. **[21]** found the drawbacks of thermal instability in the absorber layer**.** There is another limitation of photovoltaic that is the erosion reaction due to which surface instability of CZTS increasing at back contact of Mo layer **[22].** The metallic oxide layers between the CZTS and Mo contact prevents the direct contact of CZTS and conducting substrate, can overcome this type of problems. According to Yan et al. **[23]** offered a thin layer of TiO_2 in CZTS PV device with a conversion efficiency of 2.15**%.** Hamady et al. **[24]** observed theoretically to make a novel approach of InGaN Schottky based solar cell device, which can enhance the efficiency 22%**.** In this device, they also proposed that GaN could be replaced by the CZTS absorber *p*-type layer.

In this chapter, we have synthesized CZTS nanomaterials (NMs) by facile and low-cost Coprecipitation method without vacuum and without inert annealing/sulfurization, where the ethanol and water mixture were used as a solvent. This synthesis method is easy and simple synthesis and ecofriendly technique at room temperature (R_t ~35^0C). In this synthesis, we have not used any surfactants and vacuum/noble gases, which made it low-cost, and cheap, economically in comparison to other methods. The ethanol-solvent plays an important role in the formation of tetragonal structural CZTS phase in spherical NMs. The novelty in this work is that CZTS NMs (spherical) has synthesized without any sulphurization/vacuum/inert annealing, which impart the huge sulfur to save the atmosphere. Hence, the surface-to-volume ratio of CZTS NMs materials enhances the materials properties and appropriate characteristics of the materials, and the CZTS NMs may use as the photovoltaic absorber layer for solar energy conversion.

4.2 Experimental Method

Precursors Cupric (II) chloride ($CuCl_2.2H_2O$, 98.5%), Zinc (II) acetate ($Zn(CH_3COOH)_2.2H_2O$, 98.5%), Tin (II) Chloride ($SnCl_2$, 97%), were taken for metallic cations "Cu, Zn, and Sn", which was collected from Thermo Fisher Scientific Pvt. Ltd., India, and thiourea (NH_2CSNH_2 (reagent grade with 98%) was taken for "S" anion, which was collected from Sarabhai Chemicals Pvt. Ltd., India. The ethanol was taken from analytical reagent grade and De-ionized (DI) water from De-ionized water unit from Department of Chemistry, Babasaheb Bhimrao Ambedkar University, Lucknow, India.

4.2.1 Synthesis of CZTS Powder

To synthesize the CZTS NMs, we have taken the above precursors in certain stoichiometric ratio. First of all, metal precursors Cupric (II) chloride (8mmol, 0.5455gm.), Zinc (II) acetate (4mmol, 0.3512gm.), Tin (II) Chloride (4mmol, 0.3034gm.) were dissolved in ethanol and water in a beaker. After the stirring vigorously for 10 minutes, the thiourea (20mmol, 0.6090gm.) solution with ethanol and water was added quickly and stirred continuously. After the 3-4hours, we found the transparent homogeneous solution. Then mixture was transferred into a simple oven at 210^oC for 3hours and cooled down to the room temperature and got the black color precipitate (ppt). This ppt was centrifuged with alcohol and water three times at 7000 round per minute (r.p.m.) for 15 minutes and washed several times. After this process, the precipitate (ppt) was dried at 80^0C in the simple oven and crushed into a fine powder by using a mortar pestle and named as sample-A. In a similar process, sample-B and sample-C were prepared with the Sulphur salts variation of 18mmol (0.5480gm.) and 16mmol (0.4871gm.), respectively. The whole synthesis of ZnO NMs powder is shown by a schematic diagram in **Fig. 4.1**.

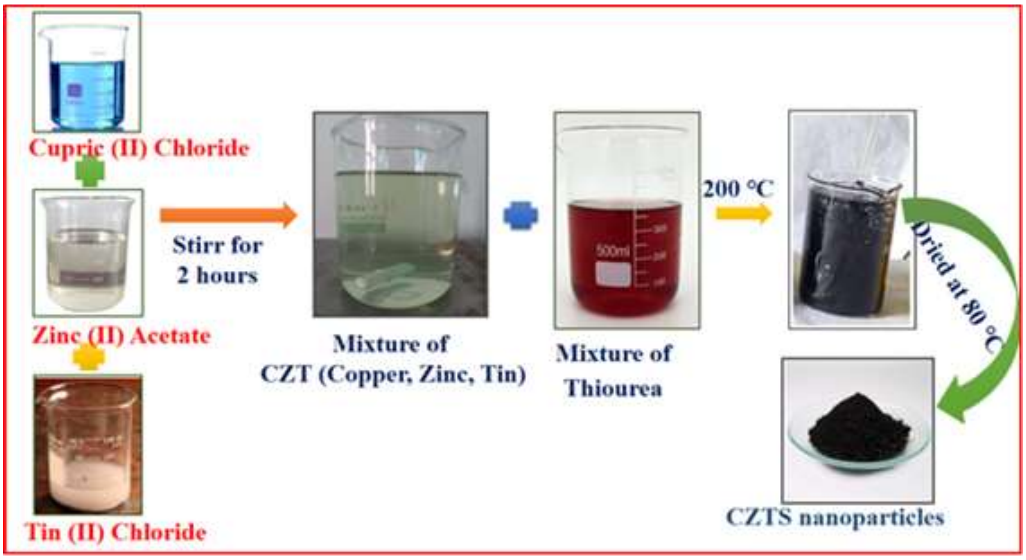

Figure 4.1: Schematic diagram for synthesis process of CZTS NCs by a chemical route.

4.2.2 Reaction Mechanism

During the synthesis process, metallic precursors react with organic solvent ethanol and form the metal alkoxide $[M(Tu)m]-OR$. At this step, thiourea reacts with metallic cations (Cu^{2+}, Zn^{2+}, Sn^{2+}) and forms the metal thiourea complexes. This metal alkoxide reacts with $[M(Tu)m]-X$ and forms the ester group complex $[M(Tu)m]-O-[M(Tu)m]$. The complex $[M(Tu)m]-O-[M(Tu)m]$ breaks into the binary sulfides e.g. Cu_xS, ZnS, Sn_xS, SnO_2 and volatile matter. At this stage, nucleation and growth of the nanomaterials are started and formed the polycondensation reactions. The $[M(Tu)m]-O-[M(Tu)m]$complexes are subjected to alcoholysis, and condensation reactions at 210°C and formed the CZSS spherical NMs. All steps of probable reactions are shown from eqn. (4.1) to eqn. (4.6) and given below:

$$metal(M)-anion+Thiourea(Tu)\rightarrow[M(Tu)m]-anion \tag{4.1}$$

$$[M(Tu)m]-anion+ROH\rightarrow[M(Tu)m]-OR+H-anion \tag{4.2}$$

$$[M(Tu)m]-anion+[M(Tu)m]-OR\rightarrow[M(Tu)m]-O-[M(Tu)m]+R-anion \tag{4.3}$$

$$[M(Tu)m]-O-[M(Tu)m]+R-X\rightarrow Cu_xS+ZnS+Sn_xS+SnO_2+Volatile(matter) \tag{4.4}$$

$$Cu_xS+ZnS+Sn_xS\rightarrow Cu_2ZnSnS_4 \tag{4.5}$$

$$Cu_xS + ZnS + SnO_2 + S \rightarrow Cu_2ZnSnS_4 \tag{4.6}$$

The symbols used in these equations are M, X, Tu, and R, *x* which means M=metal ions (Cu^{2+}, Zn^{2+}, Sn^{2+}), X=anions (CH_3COO^- or Cl^-), Tu= thiourea and R=organic molecular chains of ethanol, *x*= quantity of elements. The volatile mixture CS_2, CO_2, NO_2, SO_2, H_2O, and NH_4Cl are evaporated during the synthesis in oven at 210° C. The organic solvent such as ethanol easily formed the [M(Tu)m]–X from metallic cations & anions **[25, 26].** Generally, NMs synthesis in traditional non-aqueous solutions, O is formed the metal–oxygen–metal bond by the precursors **[27].** Actually, M–O bonds, M–S bonds, and O–M–S bonds of the thiourea–metal complex [M(Tu)m]–O–[M(Tu)m] system is coexisted in the precursors Gel formation step **[25].**

4.2.3 Thin Film Deposition

For the film fabrication of CZTS, soda lime glass (SLG) was used as substrate to deposit the CZTS film by spin coater, Systronics (HSC-8000) Pvt. Ltd. India. Before the deposition, the SLG substrate was cleaned by an ultrasonic bath in distilled water and ethanol and was dried at 80^0C in an oven. For the deposition, the CZTS solution was prepared in ethylene glycol (EG) and found a homogeneous solution after ultra-sonication. The film was deposited at 1000 r.p.m. for 30 seconds and repeated it 3-5 times to get the best thickness. This film was used to the characterization to observe the surface morphology by appropriate characterization techniques.

4.3 Results and Discussion

For phase purity and structural analysis, the CZTS NCs were characterized by Bruker D8 Advance X-ray diffractometer with 0.154056nm wavelength of X-Ray (Cu K-alpha radiation). The angle range was fixed 20^o-70^o and scanning rate of the sample was slow. For the optical analysis (such as absorption & bandgap evolution) of the sample, UV-visible absorption using a UV-Visible spectrophotometer (Evolution 201), Thermo Scientific Pvt. Ltd., U.S.A., was used in Nanoscience and sensors laboratory, Department of Physics, Babasaheb Bhimrao Ambedkar University, Lucknow, India-226025. The vibrational molecular study of the CZTS was done by the Raman spectrometer model (HORIBA Scientific, Jobin-Yvon Lab RAMHR 800UV) Pvt. Ltd., France, with laser light source wavelength 514 nm. The surface morphology of spin coated CZTS NMs was analyzed by SEM-JEOL Scanning electron microscope (JEOL Ltd. Tokyo Japan, JSEM-6490LV).

4.3.1 X-Ray Diffraction Analysis

The X-Ray diffraction patterns of CZTS NCs is shown in **Fig. 4.2** in which diffraction angle was taken 20^{o} C to 70^{o} C with slow scanning rate. The XRD patterns reveal that the signature of projecting peaks at angles (2θ) 28.5^{o}, 47.3^{o}, and 56.2^{o} corresponds to the planes (112), (200), and (312), respectively. This result is well matched with JCPDS card no. 26-0575 and found that CZTS is a tetragonal structure with Kesterite phase. This result reveals that low peak intensity of the plane (312) presence in sample-C are justified the minor impurities or deformations. In the XRD patterns, samples-A and B have high intensity peaks in comparison to sample-C that means A and B samples are less impure comparison sample C, and found the probability to pure the phase of Kesterite. Here, the peak positions and intensities are slightly decreased from sample-A to sample-C and it means the crystallinity decreases with sulphure ratio increases. The average crystalline size 15nm, 17nm, and 17nm was analyzed of sample A, B, C, respectively by Debye-Scherer's formula.

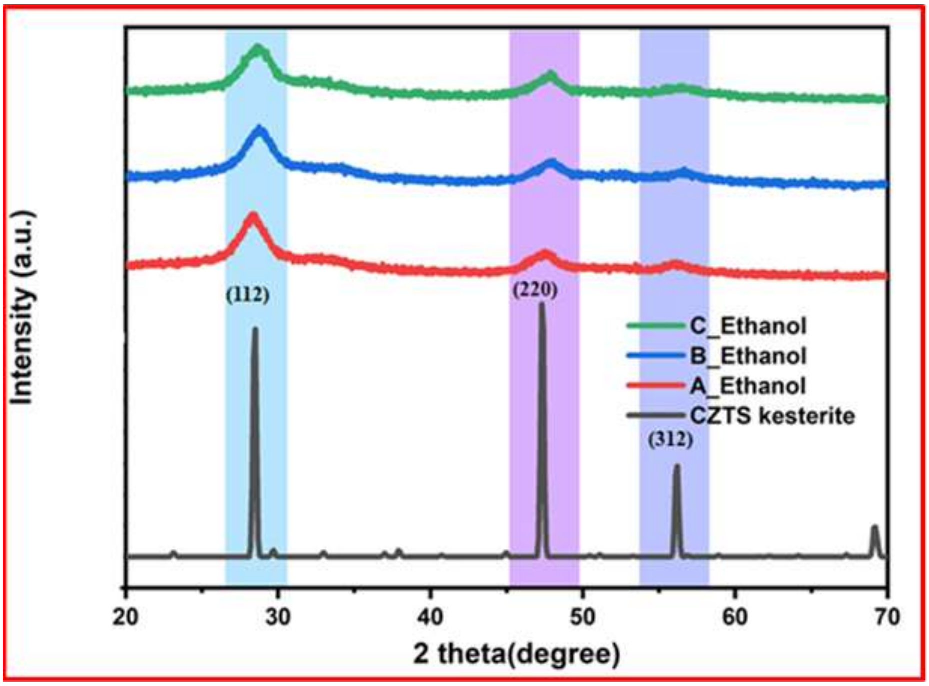

Figure 4.2: XRD patterns of CZTS samples A, B, C with the variation of concentration of Sulphur, comparative with standard CZTS Kesterite.

Cheng et al. **[26]** showed the XRD patterns of CZTS where Cu_3SnS_4, Cu_4SnS_4, CuS, Cu_2S, SnS, SnS_2 plane peaks were absent. This prediction reveals the purity in CZTS material, which is similar to our XRD results**.** Hence, CZTS NMs are to be found in the pure quaternary phase in nature, but XRD patterns of CZTS, CTS, and ZnS are indistinguishable, because the peak (220) in the CTS and ZnS has the same as the peak positions of plane (220) in the CZSS. For the suitable phase identifications in CZTS, further analysis is required e.g. Raman spectroscopy. Therefore, Raman Spectroscopy of the A, B, and C samples was done to distinguish the phases of CZTS, CTS, and ZnS materials.

4.3.2 Raman Spectroscope Analysis

The presence of spatial distinguishable phases can be distinguished through the Raman spectra. Minute differences in the phonon densities of states between the different chalcogenide phases can be distinguished from the shifting peaks in the Raman scattering of the samples. Himmrich and Haeuseler **[27]** announced that CZTS phases with its family of phases can be distinguished by the study of Raman spectroscopic characterization. They found one strong peak and two weak peaks of wavenumber at 336 cm^{-1} and 285 cm^{-1}, 365 cm^{-1}, respectively**.** The review literature of CZTS in Raman spectroscopy confirms that strong and weak intense peaks positions are found at wavenumber regions 332-339 cm^{-1} and 251-288 cm^{-1} and 368-374 cm^{-1} **[28, 29].**

Fig. 4.3 shows the Raman spectrum of CZTS NMs for sample-A, B, C, which were synthesized through Coprecipitation method without any surfactants. In this figure, Raman spectra are compatible with the XRD results, because XRD data were confirmed that the prepared CZTS NMs are tetragonal Kesterite phase structure. In this Raman spectrum, high intensity (major) peaks at 328 cm^{-1}, 332 cm^{-1}, 333 cm^{-1} with two shoulder peaks at 288 cm^{-1} and 351 cm^{-1}, 288 cm^{-1} and 352 cm^{-1}, 288 cm^{-1} and 355 cm^{-1} were found for prepared sample-A, B, C, respectively. These results are good in the case of announcement of samples. The reason behind this is the high amount of sulfur, that was taken for the optimization conditions of the stoichiometric ratio. In this synthesis method, the excess sulfur supply evaporates and supplies the sulfur atmosphere to maintain the stoichiometric ratio. In **Fig. 4.3,** some minor peaks are observed with less intensity at 475 cm^{-1} and 575 cm^{-1}, which confirms that there may be the phases of Cu_2SnS_3 and ZnO **[30].** But XRD characteristics have verified already that such compounds (Cu_2SnS_3 and ZnO) do not exist in CZTS material in Coprecipitation method.

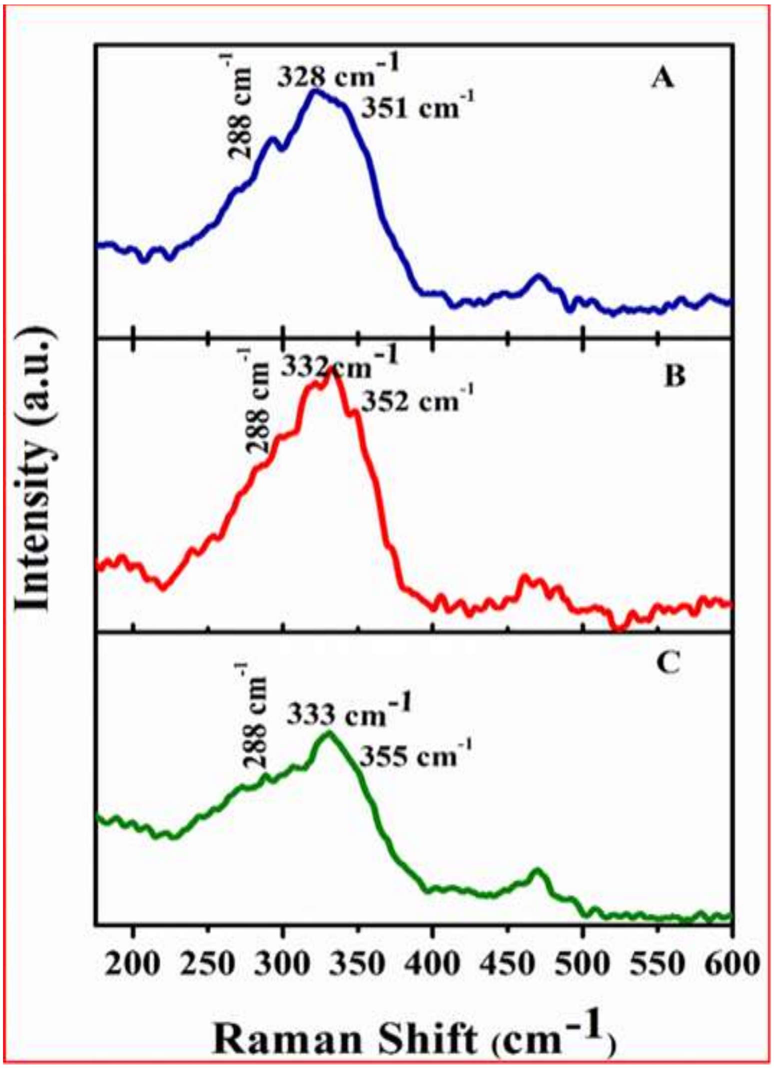

Figure 4.3: Raman spectra of CZSS Kesterite (NCs) synthesized from Cu^{2+}, and Sn^{2+} at 210°C while varying the S: M ratio. The sulfur source thiourea was varied from 16, 18, 20mmol i.e. sample A, B, and C, respectively.

The peak intensities of Raman Spectroscopy are shown lower and broader as confirmed by **Fig. 4.3**. The reason behind the broadening of peaks intensity is due to the phonon confinement in the CZTS NMs. It leads to break up the selection rule and it means that the non-zone-center phonons will participate in scattering **[27].** However, this observation confirms that peaks are shifted towards the higher wavenumbers (e.g., 332 to 333 cm^{-1}). Sample-A has the wave number 328 cm^{-1}, which is out of Kesterite wavenumber range 331-339 cm^{-1}, which was also confirmed by Wang et al. **[28, 31].** So, these results confirm that sample-A has not pure stoichiometric ratio and not fruitful for photovoltaic applications. The inhomogeneity in the structure is detected by peak shifting towards the higher angle side due to the disordered cations within the sub lattice. The secondary phases of Cu_2S, SnS, SnS_2, ZnS, Cu_2SnS_3, and Cu_3SnS_4 were not detected in these Raman spectra. After analyzing the XRD and Raman characterizations, we have concluded that Sample-B has given the best results for photovoltaic applications due to the proper stoichiometric ratio for a stable CZTS compound. The morphology of the samples is studied by scanning electron microscopy.

4.3.3 Scanning Electron Microscope Analysis

Surface analysis of the spin coated CZTS thin film was done by scanning electron microscope (SEM). To characterize the film, we have mounted the sample with platinum (Pt) coated on mounting stand. The surface morphology of CZTS NMs thin film with “S” element variations is shown in **Fig. 4.4 (a), (b) and (c).** The roughly distributed spherical type CZTS NMs on SLG substrate is shown in sample-A and it was found the cracked and clustered film, which is not useful for photovoltaic applications. However, the SEM analysis of the sample-B & C shows the changed size and shape of CZTS NMs. These samples have less cracked and clustered in comparison to sample-A, which is useful for photovoltaic applications.

The reason behind the cracking of the CZTS film is high rate of the solvent evaporation. This type of cracking problem may be removed by reducing the evaporation rate. The agglomeration is another problem, which is generated due to the anisotropic growth of NMs during fabrication process. The reason behind the anisotropic growth is the selective binding nature of ligands. If S element precursor thiourea increases, then the CZTS crystal growths of sample-A to sample-C are also increased. This effect is already discussed in XRD and supported the results. In the morphology analysis, reason behind the different resolutions of characterization images are that image of the surface was not clear. The size distribution with the fraction percentage of the CZTS NMs on the substrate (sample-B) is shown in **Fig. 4.4 (d).** Having a good phase and morphology in sample-B, the optical bandgap was analyzed only to see the suitability for the application of the photovoltaic cells.

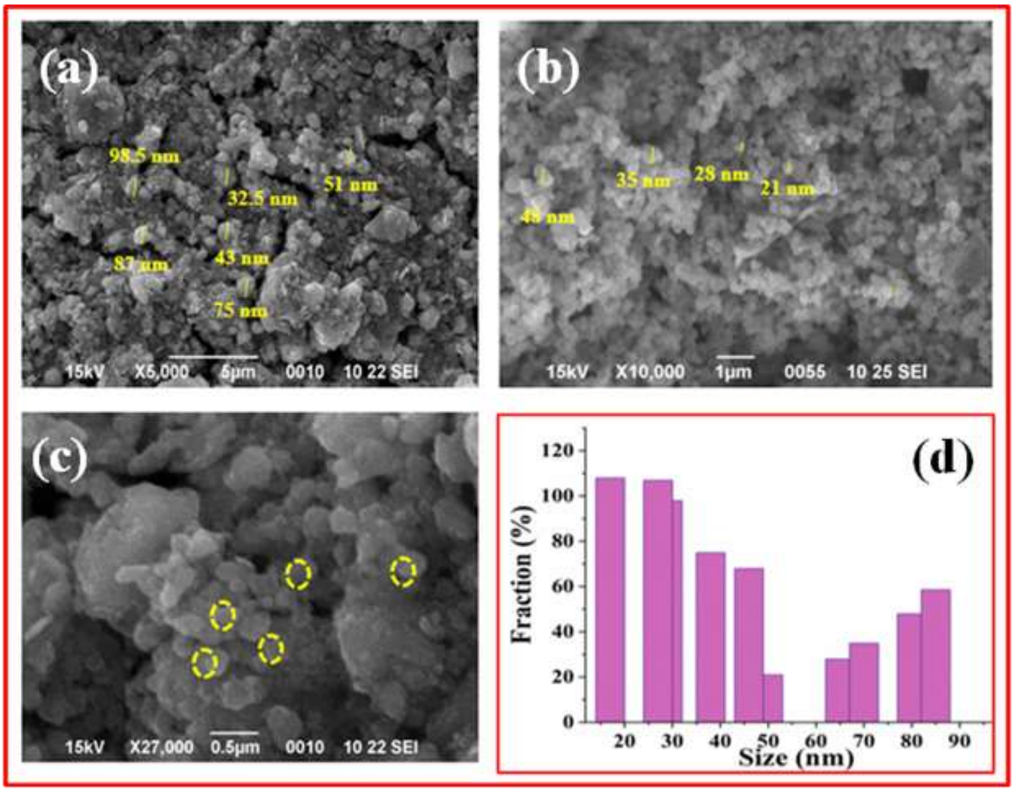

Figure 4.4: SEM images of CZTS powder thin film with Samples A, B, and C, respectively, and (d) size distribution with fraction percentage.

4.3.4 Optical Analysis

By the XRD and Raman characterization analysis, the sample-B was found to be a good material for photovoltaic applications. The optical analysis of sample B was done by UV-Visible spectrometer to characterize the band gap, which is shown in **Fig. 4.5**. The optical bandgap energy of the sample B was analyzed by using the Debye-Scherer's formula $\alpha=A(h\nu-E_g)^{1/2}/h\nu$ for direct bandgap and it was found 1.33 eV. This band gap is suitable for photovoltaic cell application, which was already theoretically predicted by Shockley and Queisser and is called Shockley and Queisser limit for PV cells. Besides this, the XRD analysis has been also shown that the Cu_2SnS_3 and ZnO phases do not exist. It means, CZTS is free from the Cu_2SnS_3 and ZnO. So, in the absence of sulphurization and salinization processes, the CZTS NMs impart less toxicity of the unusual materials in the synthesis and it is useful for the environment.

The nanomaterials of CZTS enhances the surface to volume ratio properties of the synthesized material and it reduces the size of the material. In this order, quantum confinements phenomenon is occurred in many electronic levels of CZTS NMs. In the deposition of CZTS thin film process, one dimension of the material is reduced to nano size and occured the *quantum well* due to restriction of the freely motion of electrons in 2D.

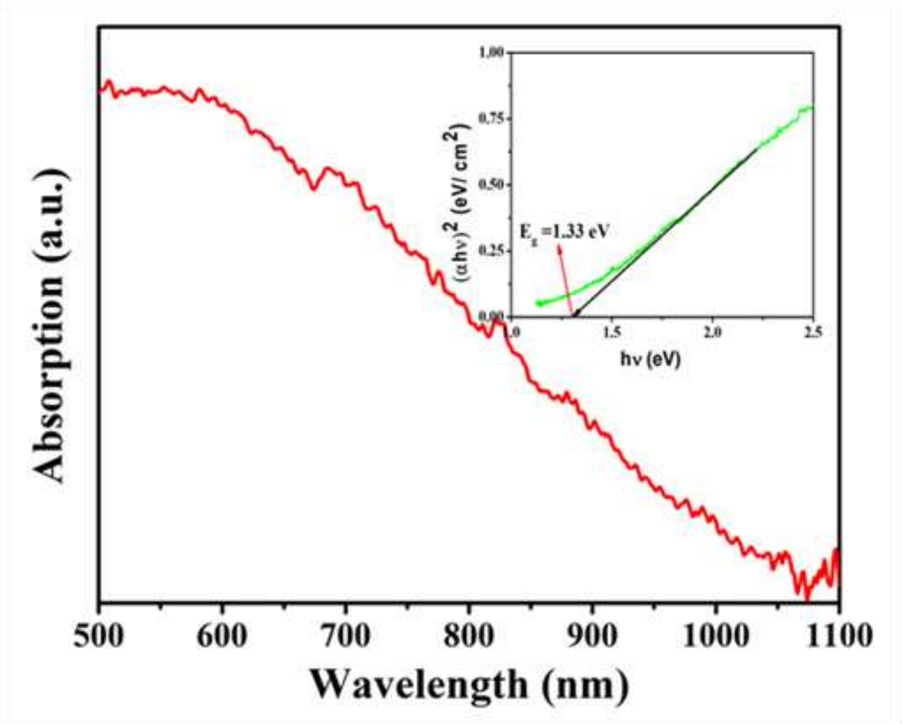

Figure 4.5: UV-visible absorption spectrum of the CZSS NCs. Inset shows the plot of $(\alpha h\nu)^2$ vs. $h\nu$.

The single quaternary phase, good surface morphology, suitable optical bandgap was found in the sample-B that means CZTS nanocrystals may be very useful material for photovoltaic cell applications.

4.4 Conclusion

In this chapter, we were synthesized the CZTS NMs with varying “S” the 16, 18, and 20mmol of precursor thiourea by the cost effective Coprecipitation method. For the fabrication the film, spin coater was used and dried it in a simple oven. The as-synthesized materials were done characterization analysis by XRD, Raman, and SEM techniques. The characterizations were confirmed that the sample-B with 18mmol thiourea concentration was found to be the best optimization result having the good morphology of the polycrystalline Kesterite phase. The average crystalline size of sample-B was analyzed and found about 17 nm. The optical band of CZTS NMs was found to be 1.33eV, which indicates that CZTS NMs suitable for photovoltaic cells. These exciting results for sample-B demonstrate that the synthesized CZTS NMs by

Coprecipitation method without sulphurization may be fulfilled the promise of a low-cost thin film for photovoltaic cell application. The novelty of this work is in the synthesis part where the CZTS is synthesized by Coprecipitation method without any sulphurization and solemnization processes. Such way of synthesis of the materials has less toxic as well as low hazardous for the environment. From this, we have revealed that the synthesis of the CZTS NMs by the Coprecipitation method without sulphurization may be the economically cheapest and low hazardous for the environment. The thin film of as-synthesized CZTS NMs may be used for Kesterite PV cells applications and best composition for mass production of solar cells based on Kesterite CZTS nanomaterials.

References:

[1] H. Katagiri, Proceedings of Symposium on Thin Film Chalcogenide Photovoltaic Materials, *Thin Solid Films,* 480:481, 426−432, 2005.

[2] H. Katagiri, K. Jimbo, S. Yamada, T. Kamimura, W. S. Maw, T. Fukano, T. Ito and T. Motohiro, Enhanced Conversion Efficiencies of Cu_2ZnSnS_4 Based Thin Film Solar Cells by Using Preferential Etching Technique. *Appl. Phys. Exp.*, 1, 041201-041202, 2008.

[3] Y. L. Zhou, W. H. Zhou, M. Li, Y. F. Du and S. X. Wu, Hierarchical Cu_2ZnSnS_4 Particles for a Low-Cost Solar Cell: Morphology Control and Growth Mechanism. *J. Phys. Chem. C.*, 115, 19632−19639, 2011.

[4] A. D. Collord, and H. W. Hillhouse, Composition Control and Formation Pathway of CZTS and CZTGS Nanocrystal Inks for Kesterite Solar Cells, *Chem. Mater.*, 27, 5, 1855-1862, 2015.

[5] Y. Sun, H. Zheng, X. Li, K. Zong, H. Wang and J. Liu, Reaction routes for the formation of a Cu_2ZnSnS_4 absorber material from homogenous ethanol-based solution, *RSC Adv.*, 3, 22095-22101, 2013.

[6] X. Bai, F. P. Milton, and Y. K. Gunko, Optical Properties, Synthesis, and Potential Applications of Cu-based Ternary or Quaternary Anisotropic Quantum Dots, Polytypic Nanocrystals, and Core/Shell Heterostructures. *Nanomaterials*, 9, 85-121, 2019.

[7] Z. Su, K. Sun, Z. Han, H. Cui, F. Liu, Y. Lai, J. Li, X. Hao, Y. Liu. and M. A. Green, Fabrication of Cu_2ZnSnS_4 solar cells with 5.1% efficiency via thermal decomposition and reaction using a non-toxic sol-gel route. *J. Mater. Chem. A*, 2, 500-509, 2014.

[8] W. C. Liu, B. L. Guo, X. S. Wu, F. M. Zhang, C. L. Mak, and K. H. Wong, Facile hydrothermal synthesis of hydrotropic Cu_2ZnSnS_4 nanocrystal quantum dots: band-gap engineering and phonon confinement effect. *J. Mater. Chem.* 1, 3182–3186, 2013.

[9] Q. Guo, H. W. Hillhouse, and R. Agrawal, Synthesis of Cu_2ZnSnS_4 Nanocrystal Ink and Its use for Solar Cells. *J. Am. Chem. Soc.*, 131, 11672–11673, 2009.

[10] M. Li, W. H. Zhou, J. Guo, Y. Zhou, Z. L. Hou, J. Jiao, Z. J. Zhou, Z. L. Du and S. X. Wu, Synthesis of pure metastable wurtzite CZTS nanocrystals by facile one-pot method. *J. Phys. Chem. C.*, 116, 26507−26516, 2012.

[11] A. M. Diamond, L. Corbellini, K. R. Balasubramaniam, S. Chen, S. Wang, T. S., Matthews, L. W. Wang, R. Ramesh, J. W. Ager, Copper-alloyed ZnS as a *p*-type transparent conducting material, *Phys. Status Solidi A.*, 209, 2186–2194, 2012.

[12] B. Shin, O. Gunawan, Y. Zhu, N. A. Bojarczuk, S. J. Chey and S. Guha, Thin film solar cell with 8.4% power conversion efficiency using an earth-abundant Cu_2ZnSnS_4 absorber, *Prog. Photovolt. Res. Appl.*, 21, 72–76, 2013.

[13] X. Lu, Z. Zhuang, Q. Peng and Y. Li, Wurtzite Cu2ZnSnS4 nanocrystals: a novel quaternary semiconductor, *Chem. Commun*., 47, 3141-3143, 2011.

[14] P. Jackson, D. Hariskos, R. Wuerz, O. Kiowski, A. Bauer, T.M. Friedlmeier, M. Powalla Properties of Cu(In,Ga)Se_2 solar cells with new record efficiencies up to 21.7%, *Phys. Status Solidi*, 2015, 928-31, 2015.

[15] S. A. Vanalakar, G. L. Agawane, S. W. Shin, M. P. Suryawanshi, K. V. Gurav, K. S. Jeong, P. S. Patil, C. W. Jeong, J. Y. Kim, J. H. Kim, A review pulsed laser deposited CZTS thin films for solar cell applications, *Journal of Alloys and Compounds*, 619, 109-121, 2015.

[16] Y. Shimamune, K. Jimbo, G. Nishida, M. Murayama, A. Takeuchi and H. Katagiri, Cu_2ZnSnS_4 formation by co-evaporation and subsequent annealing in S-flux using molecular beam epitaxy system, *Thin Solid Films*, 638, 312-317, 2017.

[17] D. K. Kaushik, T. N. Rao and A. Subrahmanyam, Studies on the disorder in DC magnetron sputtered Cu2ZnSnS4 (CZTS) thin films grown in sulfide plasma Surf. *Coat. Tech*., 314, 85-91, 2017.

[18] C. Sripan, R. Ganesan, E. M. Vinod and A. K. Wiswanath, The effect of sülfür on the phase formation of Cu_2ZnSnS_4 solar cell material, *Mater. Lett.*, 180, 295-297, 2016.

[19] E. A. Ramirez, A. Ramirez and G. Gordillo, Cu_2ZnSnS_4 thin films grown in one-step process by spray pyrolysis with improved properties, *Mater. Sci. Semicond. Process.*, 67, 110-117, 2017.

[20] Q. Guo, G. M Ford, W. Chang, D. Yang, B. C Walker, E. A. Stach, H. W. Hillhouse and Rakesh Agrawal, Fabrication of 7.2% Efficient CZTSSe solar cells using CZTS nanocrystals, *J. Am. Chem. Society*, 132, 17384-17386, 2010.

[21] K. Pal, P.Singh, , A. Bhaduri, and K. B. Thapa, Current challenges and future prospects for a highly efficient (> 20%) kesterite CZTS solar cell: A review. *Sol. Energy Mat. Sol. Cells*, 196, 138–156, 2019.

[22] J. J. Scragg, T. Kubart, J. T. Watjen, T. Ericson, M. K. Linnarsson, and C. P. Bjorkman, Effects of back contact instability on Cu_2ZnSnS_4 devices and processes. *Chem. Mater.*, 25, 3162-3171, 2013.

[23] R. Yan, L. Kang, Y. Sun and J. Zhang, Solution-processed Cu_2ZnSnS_4 thin film with mixed solvent and its application in superstrate structure solar cells, *RSC Adv.*, 8, 11469-11477, 2018.

[24] S. O. S. Hamady, N. Fressengeas, C. Chevallier, Q. Kieffer, Z. Hassan, M. A. Anas W. Lim and S. Ng, Development of novel thin film solar cells: design and numerical optimisation, *J. Phys. Sci.*, 30 (2), 199–205, 2019.

[25] K. Smolander, M. Ahlgren, M. Melnik, J. Skorsepa and K. Gyoryova, Bis (2-aminopyridine-*N*) bis(benzoato-*O*) zinc. *Acta Crystallogr., Sect. C: Cryst. Struct. Commun.*,50, 1900–1902, 1994.

[26] A. J. Cheng, M. Manno, A. Khare, C. Leighton, S. A. Campbell, and E. S. Aydil, Imaging and phase identification of Cu_2ZnSnS_4 thin films using confocal Raman Spectroscopy, *J. Vac. Sci. Technol. A*, 29 (5), 051203-051214, 2011.

[27] M. Himmrich and H. Haeuseler, Far infrared studies on stannite and wurtz stannite type compounds. *Spect. Chim. Acta Part A: Mol. Spect.*, 47 (7) 933-942, 1991.

[28] K. Wang, O. Gunawan, T. Todorove, B. Shin, S. J. Chey, N. A. Bozarezuk, D. Mitzi, *and* S. Guha, Thermally evaporated Cu_2ZnSnS_4 solar cells. *Appl. Phys. Lett.*, 97, 143508-143511, 2010.

[29] K. Woo, Y. Kim, and J. Moon, A non-toxic, solution-processed, earth-abundant absorbing layer for thin-film solar cells, *Energy Environ. Sci.*, 5, 5340-5345, 2012.

[30] A. E. Rakhshani, Sn-rich CZTS films spin-coated from methanol-based sol-gel solution: annealing effect on microstructure and optoelectronic properties. *J. Sol Gel Sci. Tech.*, 94, 270–278, 2020.

[31] K. Woo, Y. Kim and J. Moon, A non-toxic, solution-processed, earth-abundant absorbing layer for thin-film solar cells, *Energy Environ. Sci.*, 5, 5340-5345, 2012**.**

CHAPTER 5

Synthesis and Characterization of Functional Material (IV-VI) SnS for Energy Applications

Chapter 5

Synthesis and Characterization of Functional Material (IV-VI) SnS for Energy Applications

5.1 Introduction

In recent years, various 2-D layered materials have been attracted much more attention to researchers to fulfil the demand of the current challenges of optoelectronic devices. Most probable various layered materials are transition metal binary-chalcogenides **[1-3],** Graphene and MXenes **[4, 5]**, CNTs **[6, 7],** etc. Based on spectral regions for photodetection, optoelectronic photodetector devices are categorised into three types of photodetectors: Ultra Violet (UV, 10-380nm), Visible (VIS, 380-740nm), and Infra-Red (IR, 740nm-1mm). Lots of UV radiations (10-380nm) are insolated on the earth's surface, but they are restricted by the ozone layer, atmospheric dust, and moisture. The photodetectors in UV radiation (10-380nm) are known as "Solar Blind Photodetectors (SBPs)", and the photodetectors in the visible range (380-740nm) are known as "UV Blind Photodetectors (UBPs)". The UBP or visible photodetectors are widely used in spectroscopy, astronomy, imaging, medical diagnosis, and visible light communication applications. The photodetectors devices are fabricated by the multifunctional nanomaterials. The drawbacks of these photodetectors are low performance, short stability and use of hazardous elements. The fabrication of eco-friendly FMs by low-cost processing techniques is the solution of such problems **[8]**. Therefore, the low cost photodetectors are developed using the nanostructure materials. This impressive progress has been made in 2-D layer chalcogenide-based photodetectors because they have good absorption and optoelectronic properties of materials with high performance. [**9, 10].**

In semiconductor devices, IV–VI functional groups of compound PbS, $PbS_xSe_{(1-x)}$, SnTe, SnSe etc. have more attention due to their probable applications in optoelectronic devices such as solar cells, photo diodes, and LEDs traffic light, hydrogen generation devices etc. There are various 2-D layered semiconducting materials such as Si **[11],** GaN

[12], CdS,Se **[13]**, TiO$_2$ **[14]**, ZnS [**15**], SnO$_2$ **[16]**, SnS$_2$ [**17**], MoS$_2$ **[18]**,WS$_2$ [**19**]**,** SnS [**20**], SnSe **[21]**, have been great vigority in optical and optoelectronic properties for photo detective behavior. Recently, earth abundant constituents elements based detector, SnS, has much attention to make optoelectronic devices because SnS has high absorption constant (~10^5 cm^{-2}), low cost, ecofriendly and easily fabricated device **[22]**. The SnS is a p-type semiconductor (2-D layered) with indirect band gap (1.0-1.2 eV) and direct band (1.3-1.9 eV) [**23-25].** In general, the indirect band gap is found in thin film SnS layer, and the direct band gap is found for thick SnS layer **[26]**. **Fig. 5.1 (a)** shows the 2-D layered SnS materials with orthorhombic structure of double layers and **Fig. 5.1 (b)** shows the single molecule of SnS which was produced by BURAI software 1.3.2. In the **Fig. 5.1(a**), Sn and S are connected to each other by covalent bond in zigzag form. In bulk form, the SnS layers are connected by van-der-waal force. Sn and S has oxidation valancy +2 and -2, and has the orthorhombic unit cell with lattice parameters a=3.98 Å, b=4.33 Å and 11.18 Å **[27].** The 2D layered SnS thin films have been deposited by different techniques such as magnetron sputtering [**28**], thermal evaporation **[29]**, chemical bath deposition **[30]**, chemical vapor deposition **[31]**, and spray pyrolysis method [**32**].

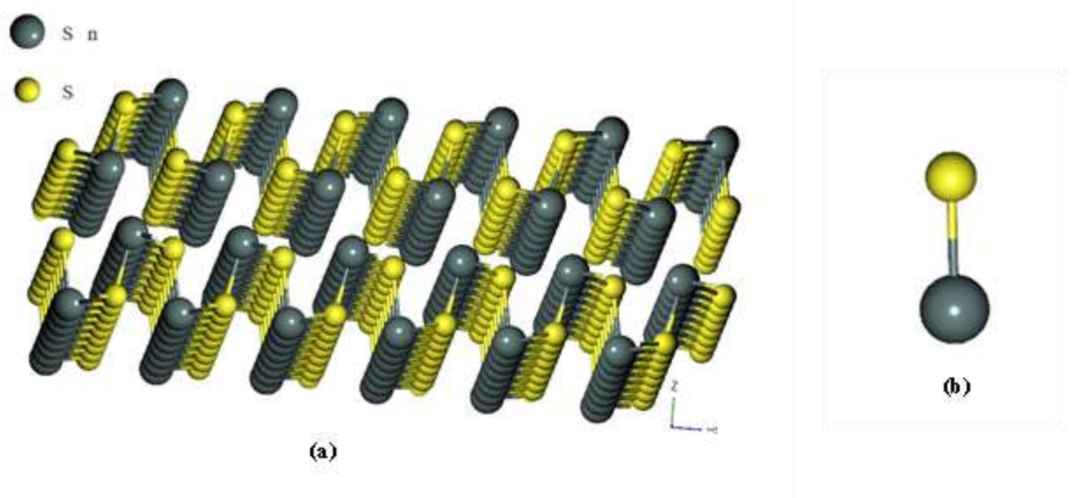

(a)

(b)

Figure 5.1: (a) Double zigzag layer of SnS molecules, (b) Single molecule of SnS.

The film deposition type methods are used to fabricate the optoelectronic devices by different group of researchers. In above mentioned fabrication method, Spray pyrolysis is the modest, less-time consuming, ecofriendly method and easy to scale up for commercial production among them. First time, Reddy et al. **[33]** synthesized the SnS nano-flake by spray pyrolysis for photovoltaic. Liu et al. **[34]** and Zheng et al. **[35]** reported the fastest response time 5.1ms and 15.1ms for SnS nano-flakes and nanowires respectively, which was synthesized by chemical vapour deposition (CVD) method. The CVD synthesis method needs vacuum with inert atmosphere that makes it costly and non-ecofriendly. Fast photo response and recovery time at room temperature are key points for this investigation. Some Researchers have been achieved significant success in important parameters of photoresponse and recovery times. The main issues in the CVD method are still remaining such as use of toxic, costly elements, and vacuum, inert atmosphere. Other issues like adhesion with substrate and hydrophilic surface are also important points being considered in fabrication of the devices.

SnS is a binary compound of the same groups, which is easy to synthesize and directly may be used as an absorber material for photovoltaic application. First time, Cho et al. **[36]** reported the hetero-junction SnS/CdS solar cell efficiency 4% in which SnS used as an absorber layer**.** The binary nano-flakes of SnS were synthesized by cost effective method like spray pyrolysis method (SPM). Due to non-peel off property, roughness film surface and indirect band gap nature, SnS may used as a junction-absorber (JABS) layer in Ag/ARC/Al-ZnO/i-ZnO/CdS/SnS/CZTS/ITO hetero-junction PV device**.** Because CdS/CZTS interface has cliff type band structure, That's why different types of recombination: thermionic and diffusion losses, interface recombination, Shockley Read Hall (SRH) recombination **[37]**. Due to these major problems of charge carriers loss, the efficiency of CZTS based solar cells couldn't touch the efficiency of CIGS till date, while the maximum properties of the both materials are same **[38]**. These problems can be resolved by using a new type arrengment of layers in solar cells. In this approach, the JABS layer may be used in the middle of absorber (CZTS) and buffer (CdS) layer in Ag/ARC/Al-ZnO/i-ZnO/CdS/SnS/CZTS/ITO. This approach will give an innovative idea to enhance the efficiency of photovoltaic devices because the thin film hetero-junction, JABS layer in the PV devices, makes it cheaper and ecofriendly in comparison to the Graphenes, MXenes, CNTs. In our view, it is adoptable in photovoltaic industry and it will replace in coming solar devices. Besides this, the layer will give stability and long durability to device, due to non-peel off property.

In this chapter, hydrophobic and scratch proof SnS nano flakes are synthesized by SPT method. The photodetector properties of SnS by SP method were competitively better than the photodetector properties of SnS by the CVD method **[39].** Such thin film of SnS nano flakes can be used as a JABS layer in Ag/ARC/Al-ZnO/i-ZnO/CdS/**SnS**/CZTS/ITO hetero-junction PV device to resolve the thermionic loss, diffusion loss and recombination problem in photovoltaic cell. The hydrophobicity and adhesion property of the sprayed SnS thin film gives advanced feature to photodetector device. This feature may be better option in atmospheric dusty area to autoclean the device. Hence, hydrophobic property resolves the problem of accumulated dust from optoelectronic devices. This cost effective and ecofriendly route of spray pyrolysis synthesis method may be industrialized. In this way, the SPM route can be superior over the CVD route for synthesis of SnS thin film photodetector. The stability of the SnS photodetector is also analyzed after one and half year and result reveals the stable of the device.

5.2 Experimental Method

All chemicals were purchased from Fisher scientific, India. Tin (II) chloride ($SnCl_2.2H_2O$) and thiourea ($CS(NH_2)_2$), ethanol and de-ionized (DI) water were the analytical reagent grade. The soda lime glass (SLG) substrates were purchased from HIMEDIA, India. All reagents and solvents were used without any further purification process. The SLG substrates were used by well manner purification.

5.2.1 Preparation of SnS Solution

In this synthesis, all chemicals are used of analytical grade and without any purification. The spraying precursor of SnS was prepared without any surfactant. In this process, tin chloride ($SnCl_2.2H_2O$, 0.1M) and thiourea ($CS(NH_2)_2$, 0.1M) were mixed in a solvent mixture of Deionized (DI) water and ethanol. The molar concentrations of Sn and S ions are fixed as [Sn]/[S]=1. After stirring at room temperature, we get the light milkish white homogeneous solution in which Sn (II) and S ions presented as shown in **Fig. 5.2.**

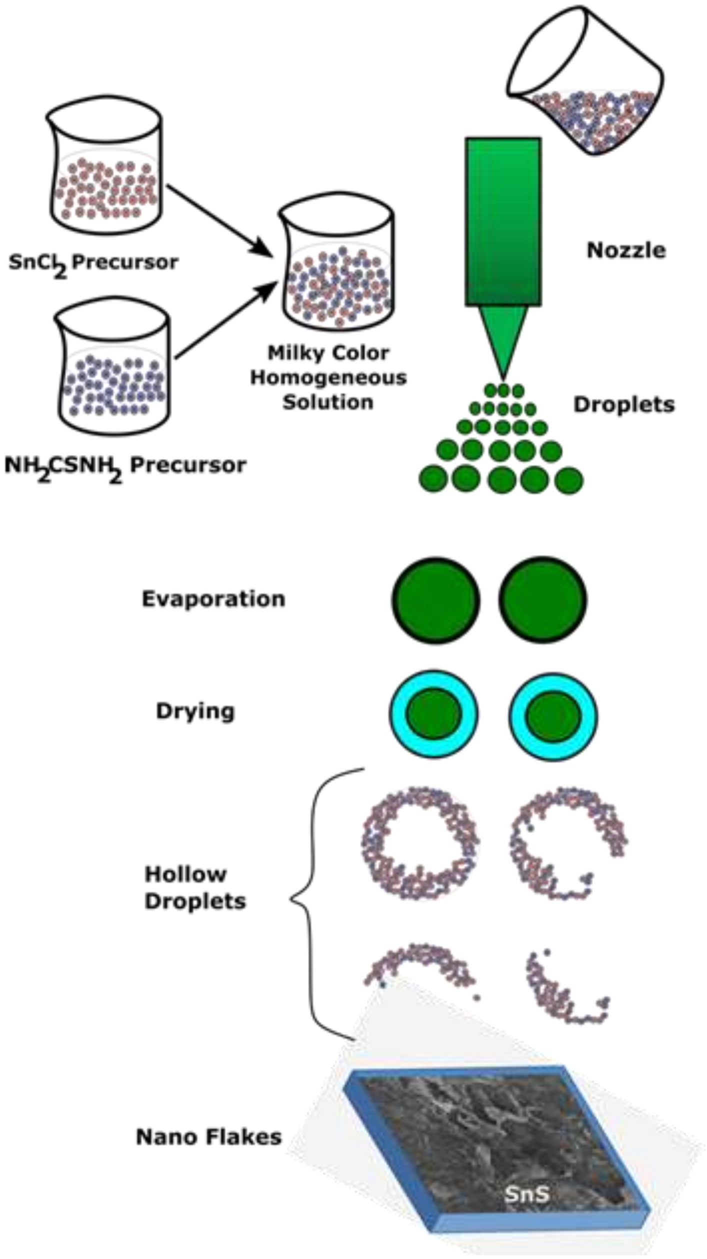

Figure 5.2: The Schematic diagram of synthesis SnS nanoflakes on SLG by SPM.

5.2.2 Synthesis Method

The spray pyrolysis method is self-assembled in our laboratory and this spray pyrolysis set-up is cost effective method for low-cost device fabrication. For the sample preparation, soda lime glass substrate (SiO_2) was cleaned by ultrasonic bath in DI water and methanol, respectively. By this process, the adsorption property of the film is enhanced and the film contact become strong. The precursor solution was prepared for spraying with the mixed solution of DI water and ethanol in ratio 3:1. Here, the ethanol is used to reduce the surface tension of water. Above precursor solution was sprayed by glass spray nozzle onto the sodalime substrate at 350°C. The distance between nozzle to substrate was 30cm. This distance plays key role to make the hollow shape droplets, which helps to synthesis the nano flakes structure. In spraying process of precursors, the spray rate (5-8ml/minute) was controlled by an air compressor. To balance the temperature of substrate, spray process was repeated randomly for 4-5 times. After that hot plate was cool down to room temperature normally, and SnS nano-flakes are formed on substrate, which is shown in **Fig. 5.3.** For reducing the possible contamination of Sn_2S_3 and SnS_2 phases, we have selected the Sn(II) salt rather than Sn(IV) salt. The molar concentration of tin chloride and thiourea were fixed at 0.1M and the [Sn]/[S] ratio was 1. The ratio Sn/S was maintained for 1 till synthesized the film. After stirring one hour at room temperature (R_t) 40°C, a homogeneous whitish solution was achieved. Hence, the prepared solution of SnS Chalcogenide was sprayed on the soda lime glass (SLG) substrate.

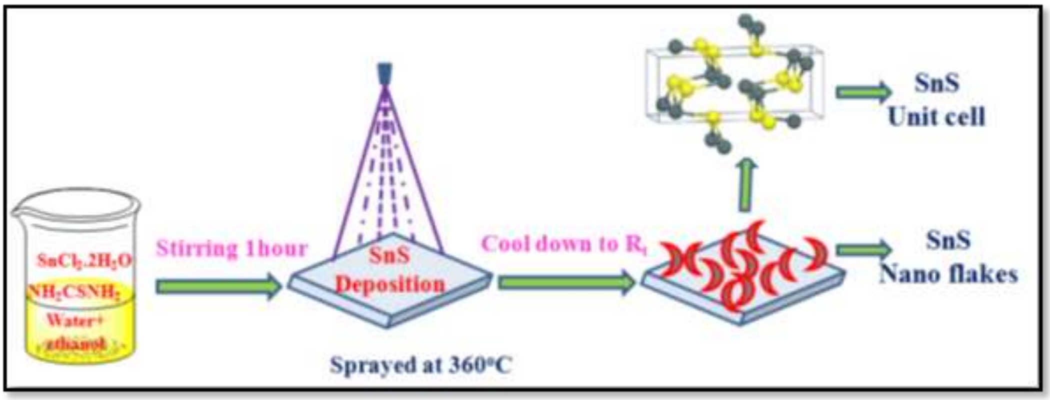

Figure 5.3: Schematic diagram of the formation of synthesis SnS nano flakes.

In the SPM, the precursor solution was sprayed on the glass substrate with keeping constant substrate temperature 360°C for the JABS layer. The compressed air by compressor (2.5HP) was used as a carrier gas. The pressure of carrier gas was 1.5bars and the spray rate was 5ml/minute. The distance between nozzle to substrate was constant at 30cm during spraying process. In the thin-film growth process of SnS material, the nano flakes of SnS are formed on the surface of SLG substrate, which is shown in **Fig. 5.3.**

5.2.3 Chemical Reaction during Synthesis of SnS Nanoflakes

SnS nano flakes based chalcogenide layered thin film was deposited by spray pyrolysis method (SPM). The thin film of chalcogenide SnS material was formed by following possible mechanism of chemical reaction **[40]**:

$$SnCl_2.2H_2O + H_2O + 2C_2H_5OH \longrightarrow Sn(OC_2H_5)_2 + 2HCl + 3H_2O \quad (5.1)$$

$$Sn(OC_2H_5)_2 \longrightarrow Sn^{++} + 2C_2H_5O^{-} \quad (5.2)$$

$$NH_2CSNH_2 + 2H_2O + 2C_2H_5OH \longrightarrow 2NH_3 + CO_2 + H_2S + 2C_2H_5OH \quad (5.3)$$

The overall ionic reaction is;

$$2NH_3 + CO_2 + H_2S + 2C_2H_5OH \longrightarrow 2NH_4^{+} + S^{--} + CO_2 + 2C_2H_5O^{-} + 2H^{+} \quad (5.4)$$

$$Sn^{++} + S^{--} \longrightarrow SnS \quad (5.5)$$

Hence, finally the metal ions, thiourea complex, ethanol and DI water were makes the precursor solution, inwhich the metal ion Sn is interacting with S ion.

Thus, the SnS and SnO_2 phase formation are given by the equation;

$$SnCl_2.2H_2O + NH_2CSNH_2 + H_2O + 2C_2H_5OH \longrightarrow SnS + 2HCl + H_2O + 2NH_4^{+} + CO_2 + 2C_2H_5O^{-} + SnO_2 \quad (5.6)$$

The sprayed thin-layered material of chalcogenide SnS is shown in **Fig. 5.4**. The **Fig. 5.4** clears that the nano-flakes are formed on the substrate. In the starting point of spray, fumes from the nozzle transported the SnS, SnO_2, HCl, H_2O, and C_2H_5OH compounds with carrier solvent into a form of tiny droplets.

5.2.4 Device Fabrication for Photodetector

For the device fabrication, sprayed thin-film SnS is used without any treatment. The silver paste was used to prepare the both electrodes of metal and mde a device SiO_2/SnS/Ag. This device is dried at 80^{o} C temperature on heating plate for 8-10 minutes. After the cooling it, the photodetector is ready to characterize.

To measure the photoelectric measurements, Keithley unit model 6517 B was used as a device analyzer. In this measurement, a white light source lamp (AM 1.5) of 550 nm wavelength is used on the film and illumination is deposited directly. After that, we have applied the voltage in the electrodes and measured the current in the same electrodes. A self-made drive circuit is used to measure the dark-current and photo-current. The Keithley unit Model 6517 B source meter has used to measure I-V characteristics of the device. To confirm the stability of the device, we have repeatedly measured the photoresponce characteristics after six months to one year. The results were repeated same as similar to the initial results.

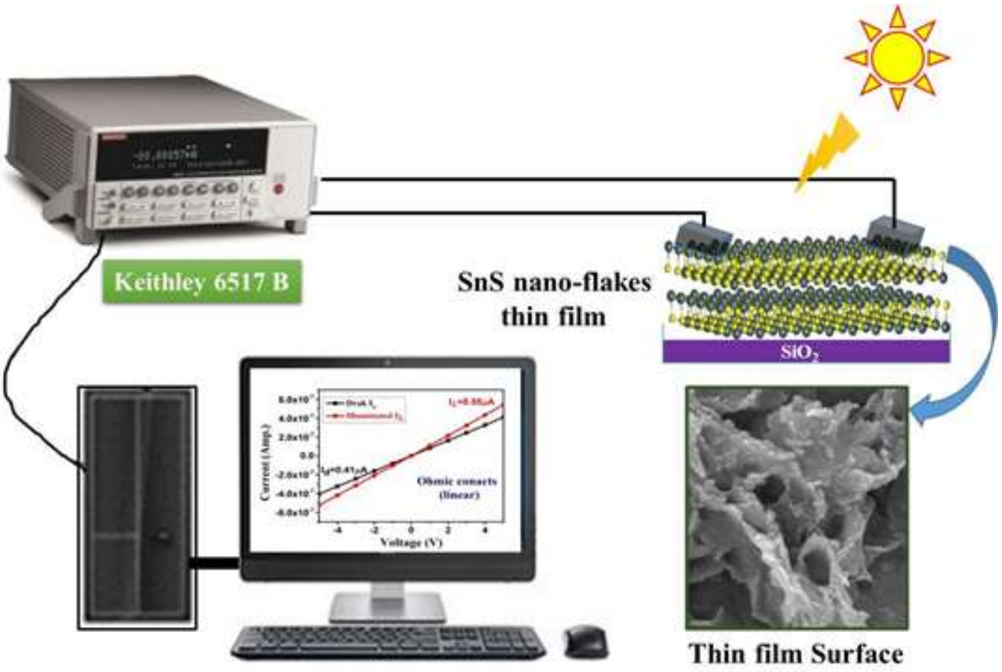

Figure 5.4: The photodetector set-up of SnS thin film nano-flakes for photoresponse measurements.

5.3 Results and Discussion

The structural properties of sprayed chalcogenide SnS thin film were analyzed by X-ray diffractometer system XPERT-PRO in the diffraction ranges of angle $20^o \leq 2\theta \leq 80^o$ with monochromatic source rays CuKα radiation (λ=1.54180A^o). SEM analysis was carried out through the JEOL/EO. The optical properties of the chalcogenide layered material SnS thin film were studied in the UV-Vis-IR range using a UV-Visible spectrophotometer 201. The probe contacts were developed on both ends of thin film using a silver paste with an average electrode separation of ~1cm. Thus, synthesized binary nano flakes thin film was employed to measure the I-V characteristics by homemade Keithley unit (model 6517 B). The set up of the photodetector is shown in **Fig. 5.4.**

5.3.1 SnS Layer for Visible Photodetector

In this chapter, we have synthesized the SnS layer with slightly variation of temperature of substrate and found SnS nanoflakes type structure. These structures are used in photodetectors and photovoltaic cells applications. The description of both applications are described in two parts in 5.3.1 and 5.3.2.

5.3.1.1 X-Ray Diffraction Analysis: SnS is a type of layered structure of semiconductor material. It has zig-zag structure that is shown in **Fig. 5.1 (a)**. This zig-zag structure supports to the bend shape crystals (nano flakes) during the spray process. The XRD characterization of SiO_2/SnS film was done for phase identification. The phase structure and phase purity of the SnS materials was studied and the phase patterns are shown in **Fig. 5.5 (a).**

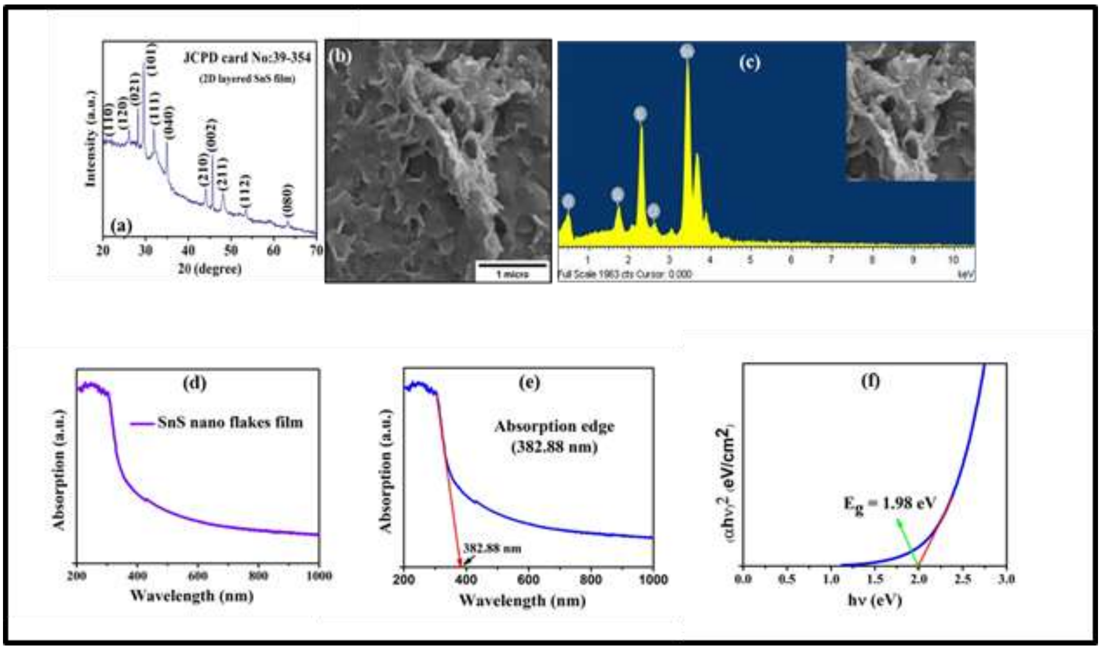

Figure 5.5: (a) XRD patterns of SnS and matched with JCPDS card no. 39-0354, (b) SEM Image, (c) EDX Image shows the presence of Sn, S, Si, O and Cl elements, (d) Absorption plot of SnS flakes at wavelength 200nm to 1000nm, (e) Absorption edge plot identified 382.88nm, (f) Tough-plot of SnS with analyzed result of band gap 1.98eV.

All peaks are indexed to orthorhombic structure of SnS phase of *P6nm* space group. The JCPDS card no 39-0354 is supported to our indexing results [**41]**. There are no other crystalline impurities peaks detected in the indexing and revealed that SnS is in pure form. In **Fig. 5.5 (a**) shows that slope is identified in the base line from higher to lower angles. The reason behind it, is soda lime glass (SiO_2) substrate because presence of peak (210) plane justify it **[42, 43]**.

5.3.1.2 Scanning Electron Microscope Analysis: Electron microscopy analysis of silica substrate justify that the amorphous nature and supported to the presence of element Si and O by EDX analysis, because SnS film was deposited on the silica (SiO_2) substrate. **Fig. 5.5 (b)** shows the typical FESEM image of layered polycrystallite SnS nano flakes thin film and represents that they have uniform flakes deposition in randomly oriented; and rough surface morphology onto the substrate without any cracks. These irregular interconnected flakes trap the light and increase the absorption of thin-film and supports to the optical characteristics results. The nanoflake type shapes are also helpful for strong absorption phenomenon and wettability characteristics **[44, 45]**. **Fig. 5.5 (c)** shows the EDX analysis of SnS film by Energy dispersive X-Ray electron microscopy. The selected area of the film from SEM result analysis is identified that elements Sn, S, Si, O, Cl are present there. Herein, the presence of Si and O are justify that film was deposited on soda lime glass substrate. Here, presence of Cl with very low intensity is due to precursor salts of cloride, thats why we can ignore it. So, we can say that SnS is in pure form and supported to the XRD pure phase results.

5.3.1.3 Optical Analysis: The **Fig. 5.4 (d-f)** shows the spectroscopic analysis of sprayed SnS thin film absorption, absorption-edge, tauc plot. In this analysis, **Fig. 5.4 (d)** shows the absorption of UV-Visible light of range 200-1000nm but the strong absorption peaks were identified at 200-700nm. In **Fig. 5.5 (d) and (e),** noise is identified at lower wavelength, which may be the instrumental error distortion. The absorption edge was extrapolated 383nm as shown in **Fig. 5.5 (e).** It confirms that the minimum 383nm wavelength range energy photons are started to excite the exciton for the generations of charge carriers. That’s why; we can say that this is better result at minimum lower wavelength for photocurrent generation purpose. The energy band gap is analyzed by absorption spectra of SnS film using the following relation [**46**]:

$$\alpha h\nu = B(h\nu - E_g)^n \qquad (5.7)$$

where B is the constant which is directly dependent on transition probability, h, ν, α and n symbolize the planks constant, frequency, absorption coefficient and transmission type parameter respectively. **Fig. 5.5 (f)** shows the tauc plot of $(\alpha h\nu)^2$ verses $h\nu$ graph for energy gap analysis. The band gap energy (E_g) was identified by extrapolating a line of $(\alpha h\nu)^2$ to intercepts the $h\nu$ axis and obtained the 1.98 eV band gap. The wavelength (623 nm) was identified by the formula, $\lambda = \frac{hc}{E_g} = 623$nm for the band energy gap. Hence, it confirms that SnS layer works strongly to enhance the electron-hole exchange when visible wavelength range 383-623 nm interacts due to excitonic effects **[47]**. This result suggests to make a Visible light photodetector.

5.3.1.4 Hydrophobicity Analysis: The wettability characteristic is an important property of optoelectronic devices for dusty area in the open atmosphere. This characteristic directly affects the device efficiency because muddy layer of the dust particles covers the device's active surface by hydrophilic nature of the film [**48].** So, hydrophobic surface of the device is required to gain the efficiency. By this hydrophobic nature of the SnS film, the surface removes the dust particle automatically by droplet of air moister that is the mechanism similar to lotus leaves cleaning of dew drops. Lotus leave surface is superhydrophobic as shown in **Fig. 5.6 (a) and (b) [49]**. **Fig. 5.6 (c)** shows the contact of water droplet with leave's micro structured surface. The schematic diagram of superhydrophobic phenomenon is clearly shown in **Fig. 5.6 (d**). A lot of researchers have extremely interested to develop superhydrophobic surface as it has anti-contaminating nature and self-cleaning ability of surface by moister dew. These characteristics can be controlled by composition variation materials and surface morphological structure shapes. Herein, **Fig. 5.6** (**e)** shows the front view of water droplet onto sprayed SnS thin film. **Fig. 5.6 (f)** shows the surface morphology of SnS thin film, which is micro-structured pyramids of nano orders flakes at the top view as 313x306x255nm^3 scale. This nano scale order measurement of surface leads to the lotus leave surface as ref. [**49]**, and edge-vise view of SnS film's surface morphology is shown in **Fig. 5.6 (j).** The **Fig. 5.6 (j)** confirms how the edges are embedded on the top view of SnS film. The micro structured pyramids of nano orders flakes shape in nanometer scales. On comparing to surface morphology of the SnS film to lotus leave SEM results, it confirms that layered SnS film have more nano order edges and roughness on the top view similar to lotus leave at particular area.

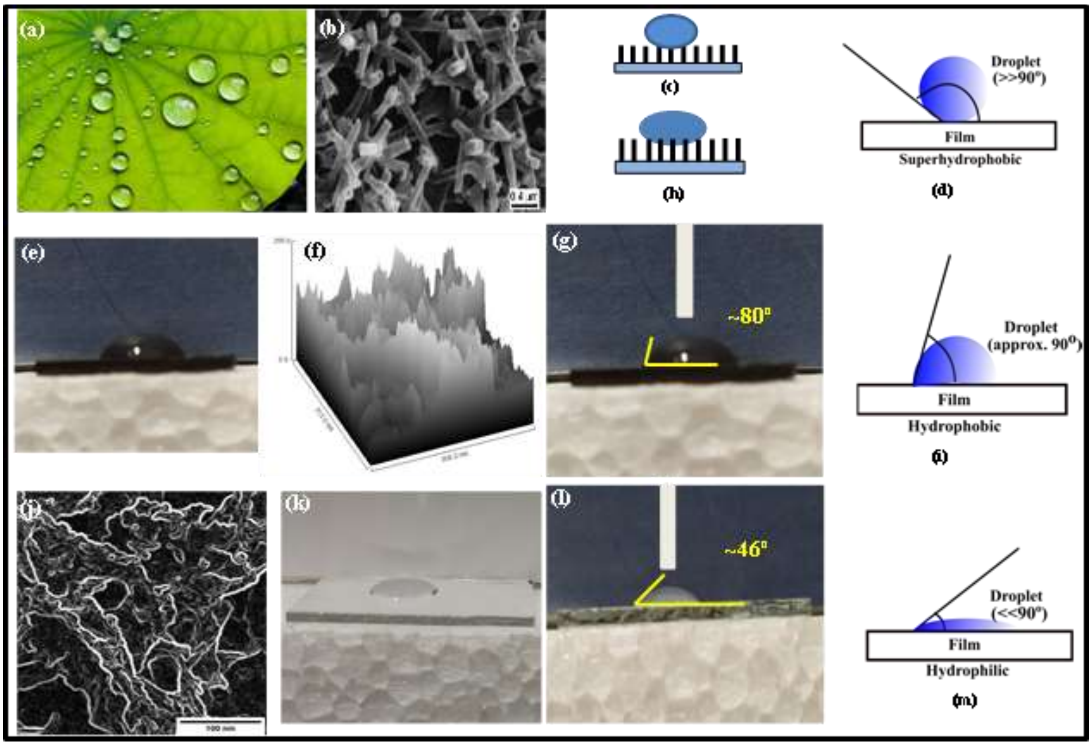

Figure 5.6: (a) Top view of water droplet on lotus plant's leave, (b) SEM morphology of lotus leave *[Koch at al. Soft Matter, 2009, 5, 1386-1393, copyright permission* ***[49]]***, (c) Water droplet contact with nanostructured surface of leave, (d) Schematic diagram of superhydrophobic nature of lotus leave (>>90^{o}), (e) Front view of water droplet on sprayed nanostructured SnS thin film, (f) Surface morphology of SnS at the top view from the SEM image, (g) Contact angle measurement of water droplet tangent with sprayed SnS thin film surface (~$80^{o} \leq 90^{o}$ angle), (i) Schematic diagram of hydrophobic nature of SnS nanostructured (approx. 90^{o}), (j) Edge view of SnS film surface SEM result, (k) Front view of droplet on bare glass substrate, (l) Angle measurement of droplet tangent with bare glass substrate (46^{o}<<90^{o}), (m) Schematic diagram of water droplet on bare glass substrate (<<90^{o}).

Fig. 5.6 (g) shows the contact angle measurement of water droplet tangent with sprayed SnS thin film surface is ~80^{o} which is equivalent to approximate 90^{o} ($80^{o} \leq 90^{o}$). The 80^{o} angle shows the hydrophobic nature with poor wettability and goes to near about super hydrophobic (≥ 90) nature **[50]**. **Fig. 5.5 (c) and (h)** illustrate the contact area of the water droplet on the protrusions layers surface i.e. Cassie Baxter (CB) state and wenzel-wenzel (W-W) state. These two states are contact angle measurements related to the wetting property of the film. **Fig. 5.6 (i)** show the schematic diagram of hydrophobic nature of SnS nanostructured i.e. approximately 90^{o}. The **Fig. 5.6 (i)** clearly reveals that deposited SnS films by spray pyrolysis method are hydrophobic in nature and also have to super hydrophobic due to protrusions layered surface. The water droplet makes an angle nearly 46° with bare glass substrate, which is hydrophilic (46°<<90°). This type of surface is harmful for optoelectronic devices due to adhesive property of the film. This hydrophobic characteristic supports to make the device with auto-clean surface, which is helpful to save the manpower.

5.3.1.5 Band Structure at Interface in the Device Ag/SnS/Ag: Spray deposited film SnS is best absorber and suitable for optoelectronic devices purpose because it exhibits the photo parameters. **Fig. 5.7 (a)** presents the schematic of the visible photodetector device of SnS layered with Ag contact of electrode. The equivalent circuit diagram of fabricated photodetector is shown in **Fig. 5.7 (c)** in which photo parameters are shown like applied input voltage=$\pm$5V, illumination current =I_λ, dark current = I_d, junction capacitance =C_j, junction resistance =R_j, series resistance =R_s, photo current =I_{ph}. The photo parameters are analyzed in the next section of I-V characteristics. For metallic electrode fabrication, Silver (Ag) is used. The reasons behind the choosing of material (Ag) as a electrode are: (a) the difference between the work functions of metal (ϕ_m) and semiconductor (ϕ_s) should be minimum, (b) ϕ_m should be greater than the electron affinity of semiconductor (χ_s). To fulfill these conditions, we have fabricated Ag electrode on SnS thin film for photo response testing. The contact of metal-semiconductor-metal (Ag/SnS/Ag) is represented by bricks as shown in **Fig. 5.7 (b).** Devika et al. [**51]** studied the ϕ_m, ϕ_s, χ_s parameters for different metal contacts with SnS i.e. Al/SnS, In/SnS, Ag/SnS and Sn/SnS. Here, we have estimated the barrier height (ϕ_B) for Ag/SnS junction using the formula ϕ_B =E_g- ($\phi_m - \chi_s$). The ϕ_m, χ_s values are taken from Ref. [**51]** and estimated the barrier height 0.82eV. This barrier height is an important feature for quick response in energy band diagram at Ag/SnS interface as shown in **Fig. 5.7 (d) and (e)** in dark and illumination for forward bias. According to Bueno et al. **[52]**, Ag/SnS structure is exhibited tunneling and field emission (ohmic) behavior below the <6V and thermionic emission (Schottky) behavior at higher (>6V) voltage. Here, the I-V characteristic of Ag/SnS structure shows the linear curve on applying voltage $\pm$5V and it shows the ohmic contact behavior. The barrier height ϕ_B is reduced in the illumination region (shown in dotted red line in **Fig. 5.6 (e)**) comparison to dark region. The linear I-V characteristics for dark and illumination confirms and supports the ohmic behavior as presented in **Fig. 5.9.** Ohmic contact is significantly gradable for device performance, and it can pass the required current with a voltage drop **[53]**. This junction is more suitable for the device efficiency compare to rectifier junction because ohmic contact has negligible junction resistance ($R_j \approx 0$). At the Ag/SnS junction, the bands are bending downward to align the Fermi levels (as shown in **Fig. 5.7 (b) and (c))** because work function of Ag and SnS are very closer to each other. In the dark region, depletion layer is formed at Ag/SnS junction with barrier thickness (δ). In this junction, the opposite charge is collected as +ve in Ag and –ve in SnS sides. In this state, charge carrier concentrations in SnS are very low in the dark region, due to which barrier thickness (δ) is high and the hopping probability is reduced. This thickness hinders the carriers flow of a very few holes or electrons cross the barrier due to which very less dark current is detected as shown in **Fig. 5.7 (e)**.

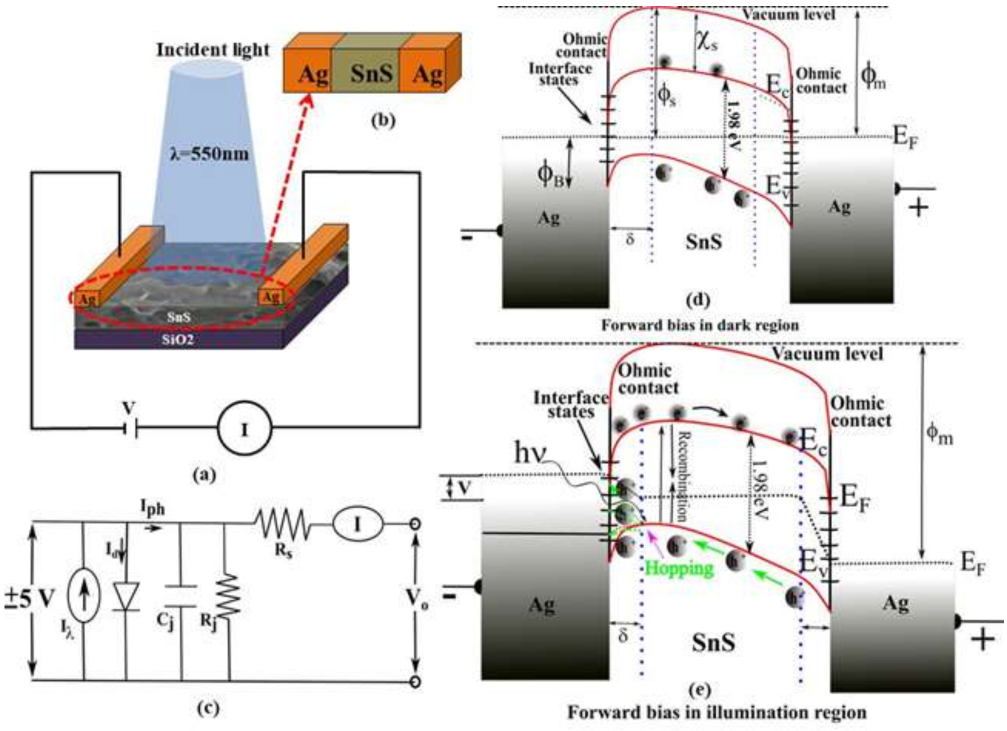

Figure 5.7: Schematic diagram representation: (a) Photodetector device with average wavelength 550nm light source for photo response measurement, (b) Photodetector contacts with metal (Ag)/Semiconductor (SnS)/metal (Ag) bricks, (c) Equivalent circuit diagram of photodetector (Input voltage=±5V, illumination current =I_λ, dark current = I_d, Junction capacitance =C_j, Junction resistance =R_j, Series resistance =R_s, photo current

$=I_{ph}$) (d) The electronic band structure for forward bias in dark region, (e) Electronic band structure for forward bias in illumination region at -5V to +5V.

In the illumination region, electron-hole pairs are generated in SnS and increased the holes into majority charge carriers. As a result, barrier thickness (δ) is decreased on increasing the concentration of charge carriers in SnS material. This makes probability to hopping of holes to barrier height. In this mechanism, junction resistance is reduced. For forward bias, holes are attracted towards –ve end of Ag and electrons are attracted towards the +ve end of Ag. As holes are moving towards the -ve end of Ag, Fermi level raises up to voltage V in Ag to balance Fermi energy. In this process, valance band energy is shifted to voltage V as shown dotted red line in **Fig. 5.6 (e)** and this voltage is known as photo voltage (V). This phenomenon reduces the recombination probability in SnS and increases the lifetime of charge carriers **[54]**. In the illumination state, the barrier thickness (δ) is reducing, the holes will be hopping or tunneling to the –ve end electrode easily compere to dark region and increasing the photo voltage (V). That's why the response time of the film is directly affected with hopping phenomenon of holes and it helps to make the high response device of photodetector [**55, 56].**

5.3.1.6 Photoparametrs in Photodetector Device: Fig. 5.8 (a-d) show the typical photo response output characteristics of sprayed SnS thin film for two terminal device (diode) characteristics, in dark and illuminated white light source with average wavelength 550nm, at room temperature. To measure the photo resistance of the film, the light source was turned ON/OFF periodically in 30seconds. The decreasing in the photoresistence of the device was analyzed by the formula $\Delta R = \frac{l}{tdq\mu\Delta n}$, where l is length, d is width and t is thickness of the SnS thin film and q is electronic charge and μ is the mobility, and Δn is change in the concentration of charge carriers thats are generated in illuminated light [**57].** The electrical resistance of the device is decreased from 0.7883 MΩ to 0.0103 MΩ (i.e. ΔR=0.7780 MΩ) within 30seconds loop for dark and illumination light (100mW/cm^2) and this change in the resistance is supported to the photo resistive behavior **[58].** This result is shown in **Fig. 5.8 (a**) and reported very low resistance, which is suitable for photodetector purposes. The Ag metal has less resistance in comparison to SnS semiconductor. So, the whole resistance of the device (Ag/SnS/Ag) is included the junction resistance (R_j) and series resistance (R_s) of the device. The variation in the electrical resistance can be explained by the photo excited/generated charge carriers (as shown in **Fig. 5.7 (e)**).

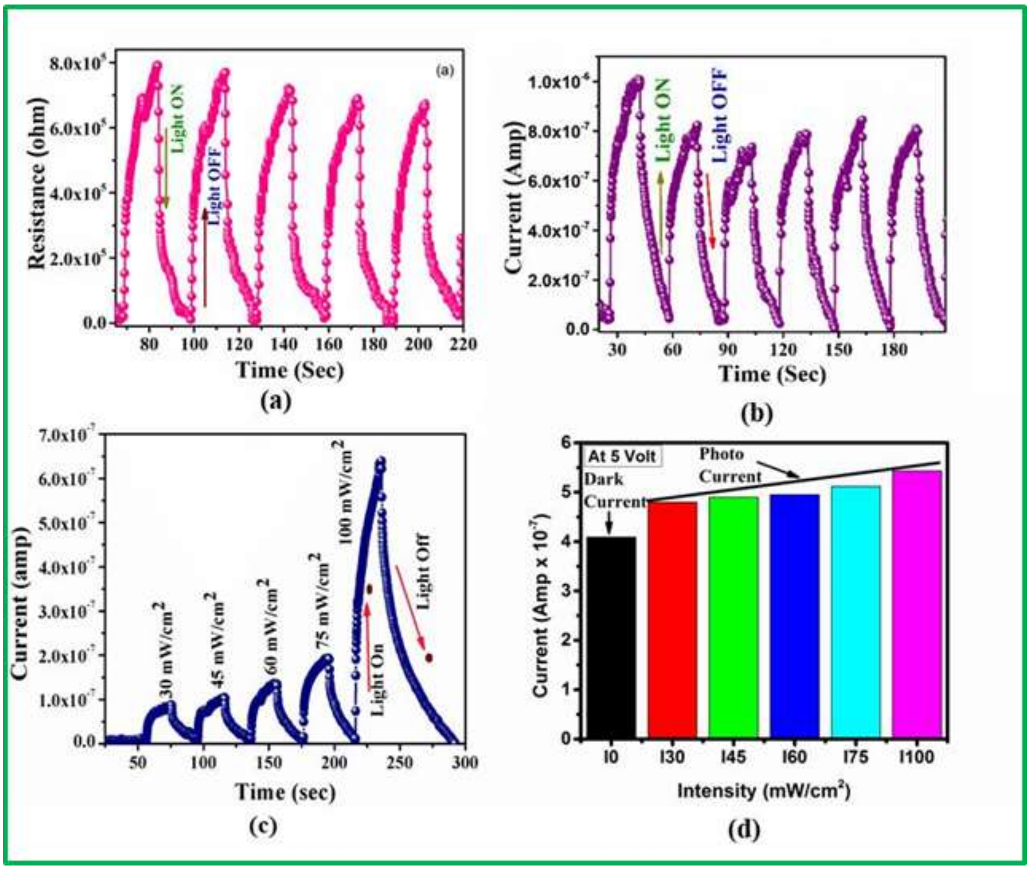

Figure 5.8: Photo-resistance of sprayed SnS thin film: (a) Resistance vs. time graph, (b) Current vs. time graph, (c) Current vs. time graph at different illumination intensities for illumination, (d) response vs. recovery graph at 100mW/cm^2.

In the forward biasing, holes are hopping to the interfacial state of the band and collecting by –ve (Ag) electrode. As a result, junction resistance is reduced to negligible value. This junction resistance is negligible in illumination comparison to dark region. This photoresistence value of the device is repeated the same results after one year or six months, which strongly supports to make the stable device for long period. The dynamic resistance of thin-film for illuminated and dark light can be attributed by following relations **[59]:**

$$R_l = R_0\left[1 + exp\left(\frac{t}{\tau_{responce}}\right)\right] \tag{5.8}$$

$$R_d = R_0\left[1 - exp\left(\frac{t}{\tau_{recovery}}\right)\right] \tag{5.9}$$

where R_0 is the steady state resistance and R_l, R_d are the dynamic resistances with illuminated light for response and without illumination (dark) for recovery, respectively.

The time response and recovery are represented by $\tau_{response}$ and $\tau_{recovery}$, and evaluated by the dynamic resistance graph from **Fig. 5.8 (c).** The evaluated response time and recovery time for the sprayed SnS thin film are found 1.69seconds and 1.56seconds, respectively. These results are full satisfactory for the fabrication of stable, ecofriendly, non-toxic, low cost and less time-consuming device. In current some results of the photodetector show the fast response and recovery time, but they have toxic constituents and unstable for long time. The fast response material's synthesis methods are not affordable for common people. More about the photo response and recovery time is studied in latest literature survey as given below **Tab. 5.1**. From the table, we have analyzed that sprayed SnS thin film has the high response as well as high recovery time in comparison to previously reported results for the same. Hence, SnS thin film may be used for low cost and nontoxic, and less-time consuming ecofriendly purposes. In this table, refs. [**60-62**] show the high response results but toxicity, cost, time consuming, and stability, non-ecofriendly synthesis parameters are the main issue still now. That's why; these devices with different methods are not practically feasible for commercial applications. The sprayed SnS thin film resolves these problems with satisfactory response results. Our results may attract to the industrial community to explore more practically feasible devices with stable results and may use to advance auto-clean surface property for commercial applications.

Table 5.1: Comparative chart of response and recovery time of Chalcogenide materials with earlier reported results:

Material	**Synthesis methods**	**Atmospheric effects**	**Cheap/ Costly**	**Resistivity(MΩ)**	**Response time**	**Recovery time**	**Year**	**Ref.**
SnSe	Solvothermal	Toxic	Costly	100.00	3	3	2016	**[63]**
SnS	CVD/Vacuume method	Hazaedious	Costly	-	5.1ms	8.8ms	2018	**[64]**
SnX (X=S, Se)	CVD/Vacuume method	Hazaedious	Costly	-	1.2ms	15.1 ms	2018	**[65]**
CuSe	Pallet method	Toxic	Low cost	-	15.7s	16.5s	2019	**[66]**

SnSe/SiO$_2$/Si	sputtering method	Toxic	High cost	-	73.1s	23.7s	2021	**[67]**
SnS	CBD	Highly toxic	Low cost	-	0.18s	0.16s	2020	**[68]**
SnS	Spray pyrolysis	Non toxic	Cheap	0.7780	1.69s	1.56s	Present work	

The sensitivity measurement for the SnS film was found that this film mainly responds to photons. The photosensitivity is the one of the significant parameter which proves the quality of the photodetector devise. The photosensitivity of the film is identified 34.14%, which was done at room temperature by simple light source. If we analyze this with laser light source, it will definitely enhance the photosensitivity of the film. Generally, photosensitivity parameter can be calculated by the change in the electrical resistance of the thin film as [**69, 70]:**

$$Photosensitivity = \frac{I_\lambda - I_d}{I_d} X100 \qquad (5.10)$$

Here, the photocurrent, $I_{ph}=I_\lambda - I_d=0.14\mu A$, was identified in illumination of light intensity 100mW/cm^2 as shown in **Fig. 5.9.** The contact area of electrodes is not proper touched on flakes surface, due to which carrier's collection on electrode is low. That's why; this identified current is very low in the device. If we increase the area contact of the electrode to flakes, in a systematic way, then the charge carrier's concentration increases and current increases definitely. Another reason to lower current may be the lower crystallinity of the SnS nanoflakes thin film. From **Fig. 5.8 (b),** it is justify that current is decreasing, as light is in off state, because exciton generation is stopped and generated exciton with in the last 30 seconds helps to flow the currents after that the current decreases slowly. Hence, we can say that it is highly time dependent photocurrent of the device. Here, we consider the 30seconds time laps is taken to rise the 90% of the photocurrent in the illumination of 100mW/Cm^2. The fast response express that generation of exciton by the visible light (382.88-623.23nm) and fall of current confirms the electron hole pair recombination process in the film on OFF state of light. **Fig. 5.9** shows that the current increments linearly as the illumination intensity from I=0 to I=100MW/cm^2 increases. Hence, it will work in the solar radiation of AM1.5 and confirms that the current increments as intensity vary from 0 mW/cm^2 to 100mW/cm^2. These properties of the SnS thin film will helps to make the best visible photodetector and supports to the stable device.

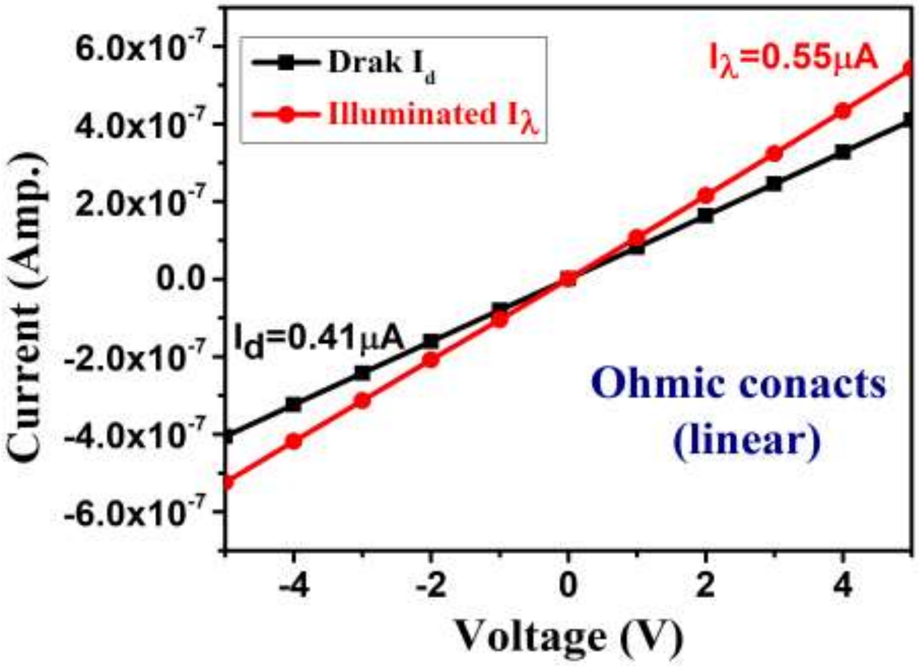

Figure 5.9: I-V measurement of sprayed SnS thin film and confirms that the ohmic contacts of metal (Ag) and SnS.

In this research work, we have synthesized the photodetector of the structure SiO_2/SnS/Ag with advanced hydrophobic surface and analyzed the photo response time, recovery time, photocurrent, photosensitivity and stability properties of the Visible light photodetector. The highest response and recovery time of the SnS photodetector using SPM were reported the first time in our best knowledge. Besides this, the SnS photodetector by SPM method has nontoxic, ecofriendly, less time consuming synthesis and low cost device, which may be practically feasible for commercial application devices.

5.3.2 SnS Nanoflakes Layer for Photovoltaic Cells

This is the another application part of this chapter, in which we have discussed importance of as synthesized JABS layer in Kesterite photovoltaic device. This layer may be helpful to remove the interfacial layers of CNTs, Graphene, MXenes, etc. More discussion about the SnS nanoflakes layer characteristics are analysed in this section.

5.3.2.1 X-Ray Diffraction Analysis: The crystallographic nature of the sprayed chalcogenide layered SnS nano flakes thin films was analyzed using X-ray diffraction, and the obtained diffraction patterns or planes were finally indexed (120), (021), (101), (111), (040), (210), (002), (211), (112) for angle 2θ=26.17°, 28.18°, 29.53°, 31.95°, 34.93°, 44.11°, 45.62°, 48.15°, and 53.51° as shown in the **Fig. 5.10**. The planes (120), (021), (101), (111), (040), (002), (211), (112) are out of the indexing planes were confirmed the orthorhombic. Crystalline SnS matched the JCPDS card number 39-0354, which is similar to already reported results in Ref. **[71, 72].** So, our obtained results are justified with reported results. The film prevents degradation of the films due to the tightly bound crystalline SnS structure **[73]**. It will give the rigidity to the JABS layer. The lattice constants of the crystal structure are a=0.4329 nm, b=1.1192 nm and c=0.3984 nm. The crystalline size of the material is calculated by Debye-Sherrer's formula which is given as:

$$D(nm) = \frac{K\lambda}{\beta\ cos\theta} \qquad (5.11)$$

where K = 0.9 (constant), λ =0.15474 nm, β= FWHM (radian) and θ= half of the diffraction angle.

Using this formula, we have calculated the average crystallite size as shown in **Tab. 5.2**. The average size of crystalline material of the synthesized SnS thin film was found about 28.53nm and the value of strain (i.e. slope of the line in **Fig. 5.10**) in SnS film was found about 0.1913x 10^{-5}.

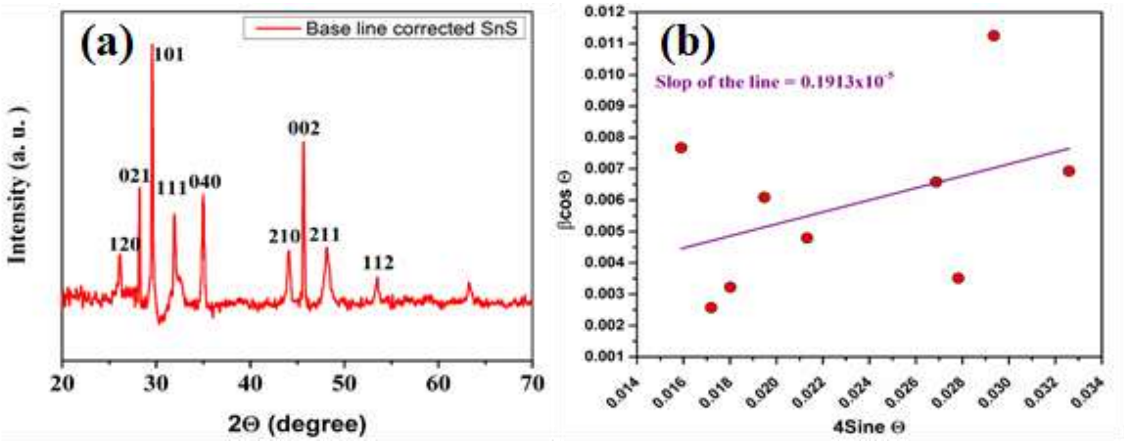

Figure 5.10: Characterization SnS JABS layer grown onto soda lime glass substrate: (a) XRD patterns and (b) W-H plot.

Table 5.2: Calculation of average crystallite size calculated by Debye sherrer's formula and William-Hall parameters:

Peaks	**2θ**	**θ**	**FWHM**	**Crystallite**	**FWHM x**	**4Sine θ**

No.	(degree)	(degree)	(degree)	size (D (ө))	Cosine ө	
1	26.10217	13.05110	0.45105	17.62196	0.0076719	0.0159084
2	28.21133	14.10566	0.14716	53.97197	0.0025694	0.0171939
3	29.57074	14.78537	0.18439	42.42529	0.00321944	0.0180224
4	31.96572	15.98286	0.34857	22.44247	0.00608596	0.0194820
5	34.98973	17.49487	0.27451	28.49733	0.00479287	0.0213251
6	44.09692	22.04846	0.37705	20.91190	0.00658314	0.0268755
7	45.66221	22.83110	0.20095	38.92946	0.0035085	0.0278294
8	48.16509	24.08255	0.64392	12.14835	0.011243	0.029355
9	53.47912	26.73956	0.39687	19.70934	0.006929	0.0325935
	Avg. size=			**28.52756**		

5.3.2.2 Field Effect Scanning Electron Microscope Analysis: Fig. 5.11 shows the FESEM, SEM and EDS results of sprayed SnS layer. This **Fig. 5.11** justify that SnS material has sprayed surface with nano flakes and found that the material uniformly distribution over the soda lime glass substrate. Further, FESEM and SEM analysis were done at different scales to clear view of the nano flakes. SnS material is formed the tightly bonded nano flakes on the glass substrate in the thin film grow process by spray pyrolysis method without any surfactant. These flakes are found interconnecting to each other in irregular forms, which is confirmed by FESEM in the **Fig. 5.11 (a)** and **(c)**. These figures confirms that JABS layer has very high rough surface. The roughness of the SnS layer will give to the junction rigidity and durability. SnS nano flakes will be helpful to increase the absorption of solar cell because pores of the film are less than 100nm order [**74**]. As a resultant, high rough surfaces and different shapes and sizes of the particles on the films are enhanced the photo activity of the film.

According to Sun et al. **[75]** the pore size and surface roughness directly are affected the diffusion barrier in the film. This will be another reason to enhance the photovoltaic property of the solar cell by the JABS layer. This layer camouflages to illuminated photons and reduces the refraction. The photon energy forwards to the CZTS absorber layer, which will affects directly to the efficiency. The study of the **Fig. 5.11** shows that FESEM and SEM results are very similar surface morphology.

Energy Dispersive X-ray Spectroscopy (EDS) is an instrument that is similar to Electron Probe Micro Analyzer (EPMA), which is used to analyze the characteristic X-ray that is generated onto the substance surface by irradiating electron beam. **Fig. 5.11 (d)** shows EDS results of SnS JABS layer, which was sprayed on soda lime glass substrate and identified constituents content in the SnS thin film in the form of the peak's percentage of Tin (Sn), Sulphur (S), Silicon (Si), Oxide (O) and Chloride (Cl). The constituent elements Sn and S are also presented as shown in **Tab. 5.3**. The presence of O and Si elements in this result justify that there is probability of impurity in the sample. But this probability is reduced because soda lime glass substrate has the same elements present. Another reason to presence of the oxygen in the sample is that O is absorbed by soda lime glass substrate at high temperature in the synthesis process. Here, Cl element is also minutely presented which may be impurity of the material and can be neglected.

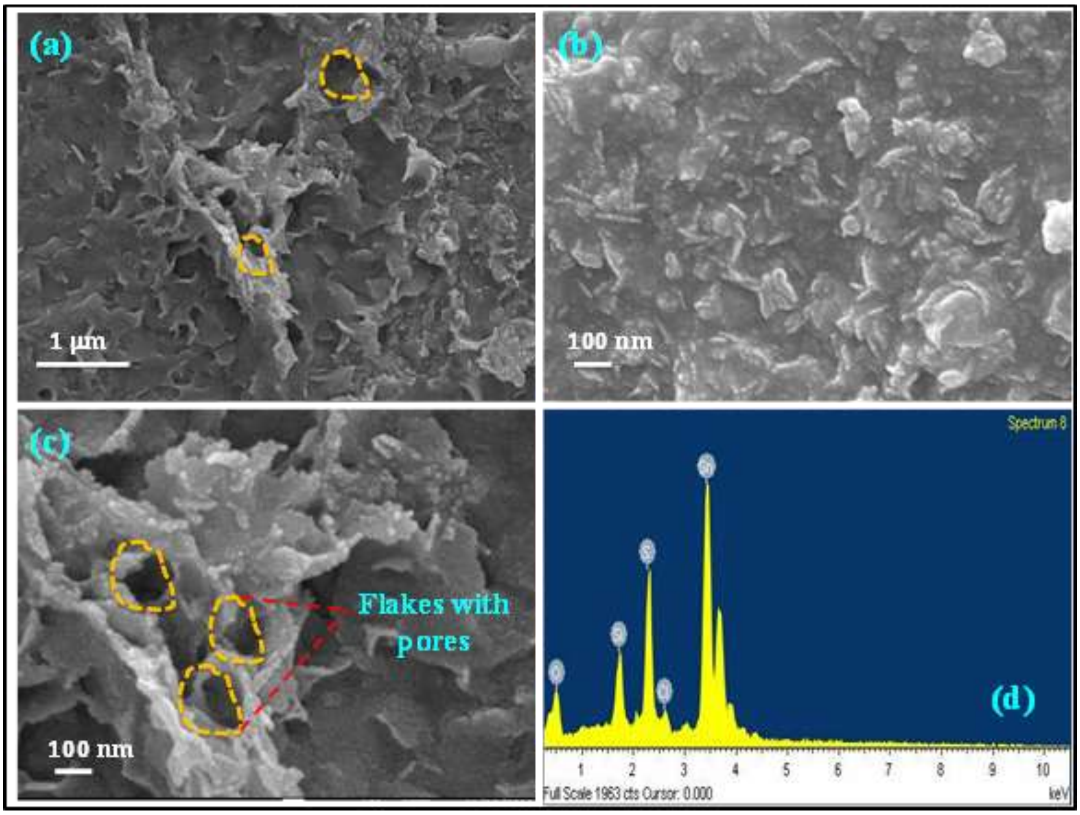

Figure 5.11: Surface morphology of sprayed SnS thin film: (a) and (c) FESEM (at different scale) and (b) SEM (d) EDS.

Table 5.3: Constituent of SnS thin film with weight ratio is given from SEM characterization:

Elements	Weight (%)	Atomic weight
O_2	29.87	65.89
Si	4.50	5.65
S	9.80	10.78
Cl	1.54	1.53
Sn	54.30	16.15
Total=	**100**	

5.3.2.3 Electron Probe Micro Analysis: Electron Probe Micro Analyzer (EPMA) is a tool that is used to analyze elements composition, by irradiating electron beams onto the substance surface. **Fig. 5.12** shows the EPMA results of SnS JABS thin film, in which Sn (red colour) and S (Blue) elements are observed in uniform distribution and confirmed that SPM have uniform distribution of the elements during spray system. The images were measured at 1mm scale. The results of EPMA justify that Sn and S are presented at substrate during spray pyrolysis process, which is supported the results of the XRD; and SnS is presented in thin film.

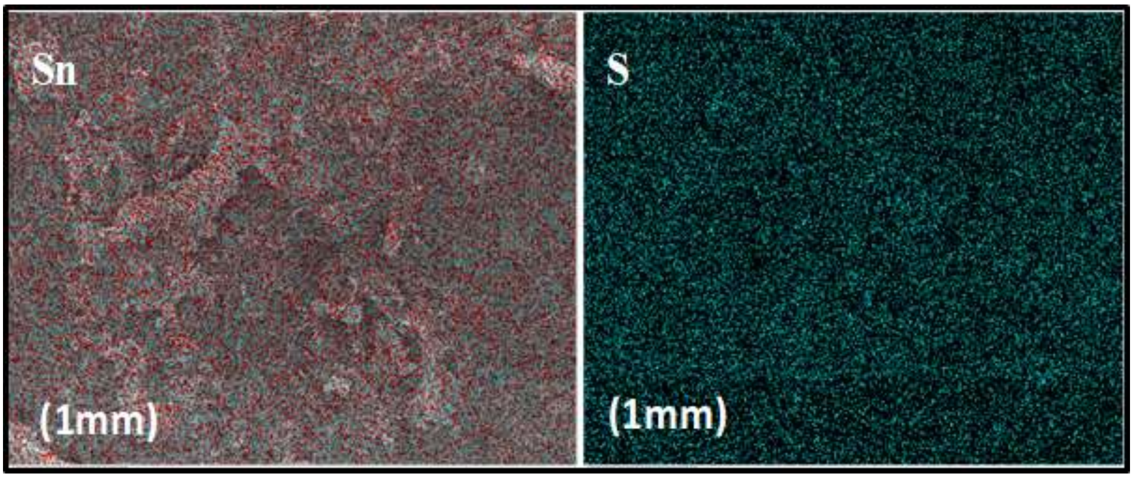

Figure 5.12: Elemental analysis of sprayed SnS thin film shown Sn and S elements by red and blue colors, respectively.

5.3.2.4 Non-Peel off Analysis: For testing non-peel off property, we have taken a safety pin to scratch on the pre-synthesized thin film. The scratched was done on the film in open environment and a picture of scratched film was taken by a normal 48 Mega Pixel mobile camera. Hence, a simple scratch test on spray deposited SnS film was carried out. It shows that the film was very well adhesive on substrate and films was non-peel off. The proper nucleation and growth in SnS nanoflakes films make the improved adhesion by the low cost spray pyrolysis method [**73]**. **Fig. 5.13** shows that SnS nano flakes films materials are strongly structured and bonded on SLG substrate. On performing scratch test on the films, it shows that SnS thin films are very difficult to scratch from substrate and such property may be useful as the application in scratch-less devices.

The layer of nano flakes may be layered-off from the substrate by the KEPTON tape. This tape is more adhesive, which is generally used to layer-up the film from the substrate. This layer may be used as per requirement such as JABS layer in the hetero-junction solar cells.

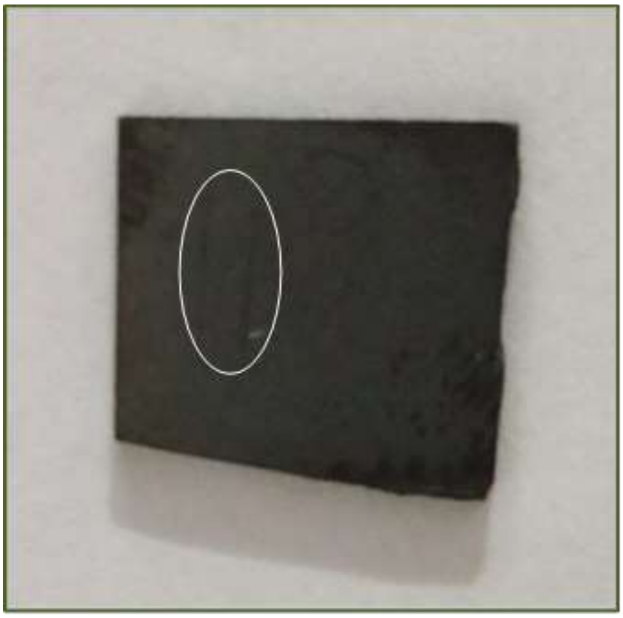

Figure 5.13: Dotted circle covering two scratched lines on SnS sprayed thin film.

5.3.2.5 Optical Analysis: Fig. 5.14 shows the absorbance spectra and tauc plot of as synthesized SnS nanoflakes thin-film in the range of 400-1000nm. The absorption results significantly shows that the absorption is decreased as increase the wavelength of Visible light. In the UV Visible absorption spectra graph plot, x-axis in nm (wavelength) in the range of 400-1000nm and y-axis for absorption in atomic unit (a. u.). The absorption peak is sharp in the visible range as shown in **Fig. 5.14**. The sharp absorption peaks materials have shown more than 30% efficient photovoltaic property **[76]**. The optical band gap of thin film was analyzed from tauc formula [**77]**;

$$(\alpha h\nu)^2 = A(h\nu - E_g) \tag{5.12}$$

where α = absorption coefficient, A= constant (independent on photon energy) and h= Planck's constant.

The sub-plot of $(\alpha h\nu)^2$ vs. $(h\nu)$ of the SnS thin film is shown in **Fig. 5.14**. The indirect inter-band transitions were assisted by phonons in the SnS thin-film. The band gap (E_g) was calculated and obtained about 1.98eV. According to the ref**. [78]**, the sprayed SnS thin films have band gap 1.74eV and such SnS thin films can be used in photovoltaic application. Hence, the band gap of the nanoflakes thin-film is found to be 1.98eV and the result is supported for photovoltaic cell.

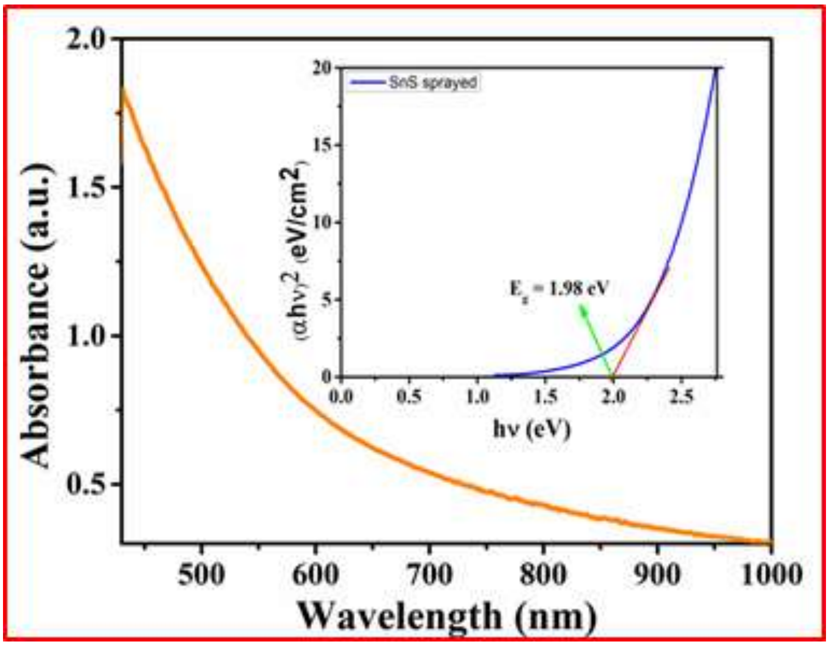

Figure 5.14: UV-Visible absorbance of binary nano flakes layered SnS thin film and tauc plot in the inset figure.

5.3.2.6 I-V Characteristics of SnS Nano-Flakes Layer

At the constant room temperature (32°C) with the dark condition of the light, the electronic states with the Fermi level of SnS thin film are in equilibrium. As illuminated photons on the sample, the temperature is increased due to which the thermal equilibrium is disturbed, and attained a latest equilibrium.

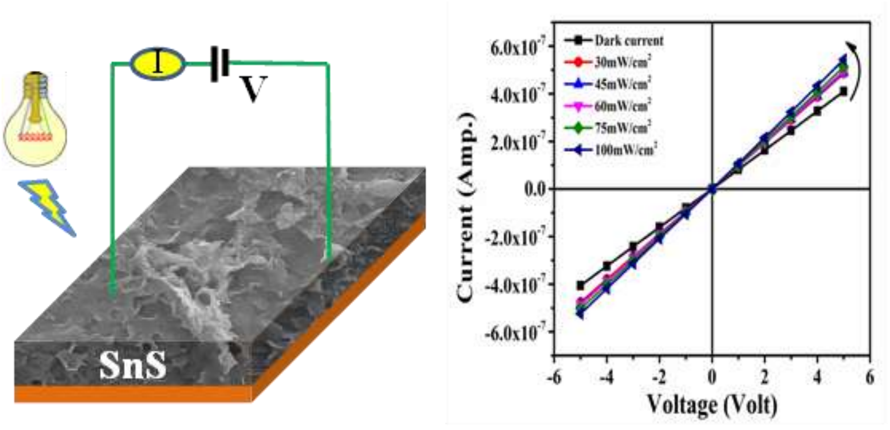

(a) (b)

Figure 5.15: I-V characteristics of nano flakes layer: (a) schematic diagram of set-up, (b) at dark illumination and different illumination intensities like 30 mW/cm^2, 45 mW/cm^2, 60 mW/cm^2, 75 mW/cm^2 and, 100 mW/cm^2.

In presence of electric field, electronic states of electronic equilibrium are perturbed and converted it into new set of charge carriers in the film. The charge carriers make a dark current in without illumination of thin film. When illuminated photon is interacted with SnS molecules and generated the pairs of holes and electrons:

$$h\nu = e^{-1} + h^{+1} \tag{5.13}$$

In the pairs of holes and electrons, some electrons have sufficient energy to make the transitions from valance band (V.B.) to conduction band (C.B.) **[79, 80]**. The electrical resistance is decreased when the time of illumination is increased, because electron hole pairs increase as time of exposer increase. As soon as light illumination is off, all electronic states in the band regain their original states. Nano flakes type structure of the SnS thin film sample provide a large surface area, and active sites generate the electron-hole pairs during the interaction of photon phonon.

From **Fig. 5.15**, it is clear that the I-V characteristics measurement of sprayed binary nano flakes from without illumination (dark current) to with different illumination intensities (30mW/cm^2, 45mW/cm^2, 60mW/cm^2, 75mW/cm^2 and 100mW/cm^2). From the **Fig.5.15**, it clears that the current is increased linearly as the intensity of illumination is increased, and found the maximum current for 100mW/cm^2 illumination. **Fig. 5.15 (b)** shows that slope of I-V curve for 100mW/cm^2 is maximum, however, the slope of dark current I-V curve is minimum.

The increasing slope reveals that the presence of excess photo generated carriers and is contributed to increase in current. Intensity versus photocurrent concept has been already discussed in photoelectric effect of light **[81]** and the results are supported our results. Thus, we can say that the sprayed SnS thin film with less toxic nature may be a potential candidate for single junction solar cell applications.

5.3.2.7 JABS Layer Approach in the Device Ag/ARC/Al-ZnO/i-ZnO/CdS/SnS/CZTS/ITO

On the basis of above characterizations, we can say that these binary nano flakes are suitable for photovoltaic purpose and have excellent electronic behavior for supporting the new approach of JABS layer. This approach is helpful to resolve the challenging problem of recombination in the Kesterite solar cells. Kesterite structures have the similar crystal structure that is associated optoelectronic properties to CIGS. The Kesterite photovoltaic is already competing to the CIGS with 22% efficiency **[82]**. The CIGS contains rare earth and toxic element of Indium. The Indium (In) can be replaced by zinc (Zn) and tin (Sn) elements, because the Zn and Sn both have a complete similar to the octet of In **[83]** . According to Wang et al. [**84]**, the CZTSSe device has the highest record efficiency 12.6% with the Ni-Al Contact/MgF_2/ITO/i-ZnO/CdS/CZTSSe/Mo/SLG, and without Se based CZTS device has the maximum record efficiency 10% **[85]**. The CZTS based photovoltaic device has some drawbacks on junction recombination such as: interface recombination, Shockley Read Hall (SRH) recombination, and thermionic diffusion losses [**37]**. The CZTS is a quaternary compound which is a hurdle to control the stoichiometric ratio. Therefore, the presence of the thermionic and diffusion emission loss, CdS/CZTSSe Interface recombination and SRH recombination losses, radiative and non-radiative recombination in the CZTS based photovoltaic cells are the main reasons behind it for not fulfill the Shockley and Queisser limit ~32.2% efficiency. Thermionic and diffusion emission loss, interface recombination of CdS/CZTSSe and SRH recombination losses are the junction problems in the conduction band offset (CBO) and Valance band offset (VBO). However, the SnS based single junction solar cell has theoretically predicted with the efficiency 32% [**86, 87]** .

Keeping in mind to these problems, we have resolved both issues and proposed a new approach of a SnS junction absorption (JABS) layer that insert into the hetero-junction device (as shown in schematic **Fig. 5.16**). The beauty of this layer, we have already discussed in characterization parts. Here, we reveal the importance of nano flakes JABS layer in the device Ag/ARC/Al-ZnO/i-ZnO/CdS/SnS/CZTS/ITO, which was already found in the literature survey. Here, we are proposing this hetero structure device with the following fabrication methods similar to Wang et al. **[88]**.

The CBO and VBO in the Kesterite PV devices structure have some challenging problems because “cliff” and “spike” are formation in the band structure, which is called type I, and type II formations. The “spike” is validated to the efficiency of kesterite solar cell and the “cliff” is reason for recombination. The CdS buffer layer (*n*-type) has slightly higher energy at junction as compere to the CZTS absorber as shown in **Fig. 5.18 (a)** “cliff”. According to Niemegeers et al. **[89]** and Minemoto et al**. [90]**, the CBO spike was minimized by the three types of recombinations as discuss above. The spike directly affects the efficiency parameters like open circuit voltage (V_{oc}), current density (J_{sc}) and fill factor (FF). The spike type band alignment in CdS/CIGS is generally observed and the CBO has less than $\Delta E = 0.40eV$ is valid reason for 22% efficiency.

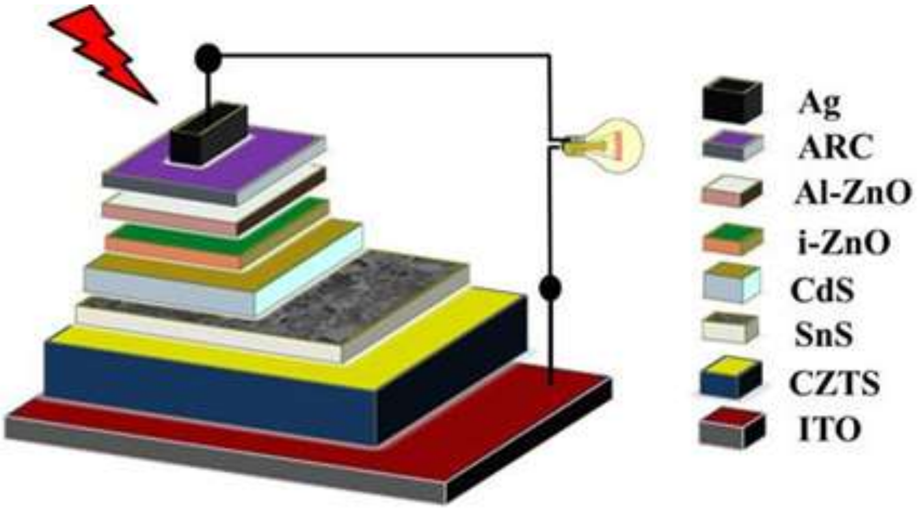

Figure 5.16: Schematic diagram of hetero-junction solar cell Ag/ARC/Al-ZnO/i-ZnO/CdS/SnS/CZTS/ITO using the binary chalcogenide nanoflakes layer.

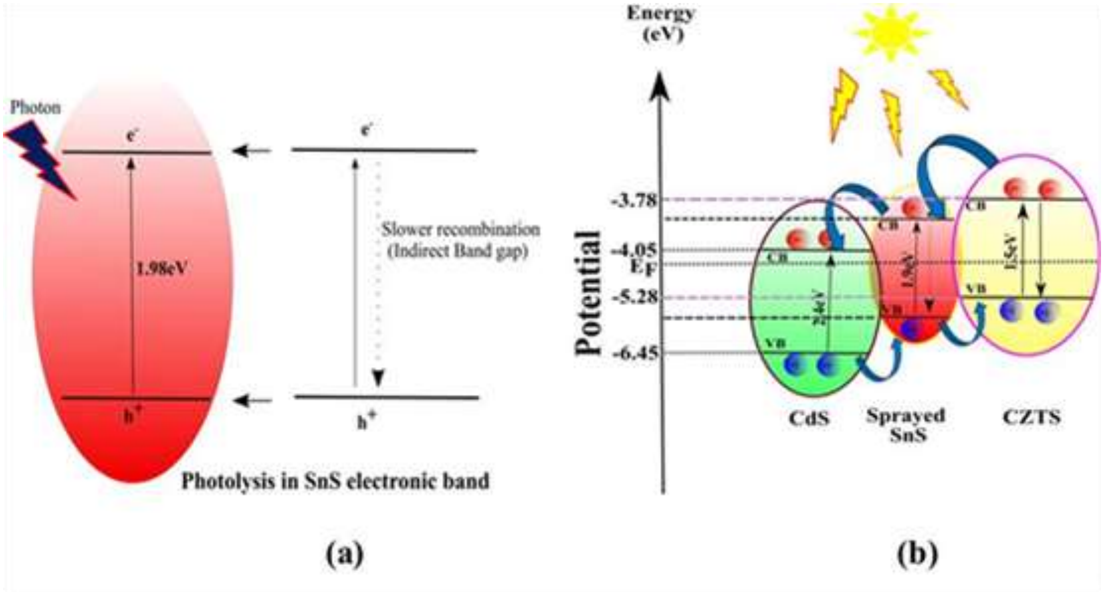

(a)

(b)

Figure 5.17: Photolysis in (a) SnS semiconductor, and (b) electron-hole transport phenomenon at the junction of buffer and absorber layer.

According to Ramya et al. **[91],** CBO energy (ΔE) of the CdS/SnS junction was found ~0.36eV, which is more beneficial to reduce the recombinations. A schematic representation of the photolysis in SnS and CdS/SnS/CZTS layer is shown in **Fig. 5.17 (a) and (b)**. The CBO energy of SnS has slightly above as compered to the CBO energy of CdS that is slightly lower as compered to the CBO energy of CZTS. In this mechanism, thermionic and diffusion emission loss is reduced, CdS/CZTSSe interface recombination and SRH recombination, the electron transportation in the devices may be easy to enhance the efficiency where the holes are bubble-up in CB and VB.

On the basis of all of above discussions, we purpose a new innovative approach by inserting the JABS layer into the CZTS devices where the spike band alignments are formed as shown in **Fig. 5.18 (b).** The spike type alignment may be resolved the problem of junction recombinations, which is the main problem in the field of kesterite photovoltaic cells.

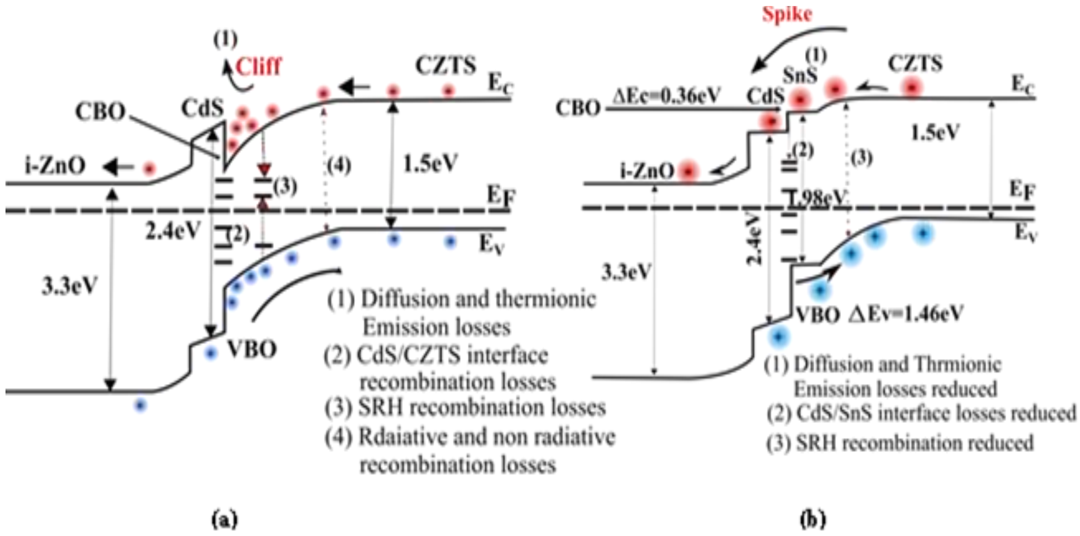

Figure 5.18: Effect of SnS Buffer layer in hetro-junction solar cell band diagram (a) without SnS, and (b) with SnS.

5.3.4 Importance of JABS Layer in Photovoltaic Solar Cell

Using the JABS layer, optoelectronic mechanism of the device can be changed. After all_discussions, we can say that the JABS layer can enhance the efficeiency of kesterite photovoltaic cells and may be useful in kesterite solar industries. Some others materials such as Graphene, CNTs, etc. may be also used at junction for reducing recombinations **[37].** These layers are not used as the absorptive layers that layers are not more effective for the kesterite solar devices. The reason behind to use of the JABS in the kesterite photovoltaic cells are given below:

- JABS layer is easy to synthesis with low cost and homemade spray pyrolysis without any surfactants.
- Nanoflake type shapes are helpful to chemoflauge the light and increased the absorption of absorptive layer (SnS+CZTS) on layer.
- The I-V characteristics of SnS nano flake layer are analysed that as increasing the illumination intensity, the more numbers of electron-holes pairs are generated and photocurrent is increased. This mechanism confirms that this layer is supported the *pn*-junction mechanism.
- SnS layer is non-peel off film, which is helpful to give the rigidity to the junction for long durability.

- SnS layer has a sharp absorption peak and band gap 1.98eV, which is helpful to enhance efficiency in the photovoltaic field.
- After using this approach, the spike type structure in the SnS has formed in the electronic band structure, which is similar to CdS/CIGS junction. The SnS layer has resolved to reduce the cliff type problem of kesterite PV cells.
- The CBO and VBO energy levels of the SnS layer has a order 0.36eV and 1.46eV with CdS Buffer layer, which is helpful to transport the charge carriers easily comparison to without using JABS layer.
- JABS layer is made by binary chalcogenide materials. The binary-binary chalcogenide_materials make a junction, which are more suitable similar to the CdS/CdTe because this type of junctions has less dangling bonds and low free energy. In our case JABS layer, it has less dangling bonds and low free energy comparison to quaternary the CZTS.

5.4 Conclusion

The SnS thin film was successfully synthesized on soda lime glass substrate at 350^{o}C temperature by the modest spray pyrolysis method. The hydrophobic characteristic was enhanced the advanced features in the application of photodetector device for using the open atmosphere. The XRD patterns of the films were revealed the orthorhombic polycrystalline in nature. The SEM and FESEM analysis have confirmed that the SnS thin film has good morphology with nano-flakes and this morphology has validated the high surface to volume ratio. The optical band gap of the SnS thin film was calculated from the Tauc plot and found the 1.98eV energy band gap. The Energy band gap result is suitable for photodetector. Hence, the response time and the recovery times were calculated for photodetector to analyze the photo response of chalcogenide SnS thin film, and found to be 1.69sec and 1.56sec, respectively. The photosensitivity and photocurrent of the film were found to be 34% and 0.14μA respectively. The changed resistance (ΔR) of the film was analyzed and found about 0.7780MΩ for 30seconds. The SnS thin film photodetector is feasible for commercial application devices, because it is grown by nontoxic, ecofriendly and cheap materials; less time consuming and low cost of SPM technique.

The synthesized binary nano flake thin film are the orthorhombic crystalline in nature, which was conformed by the XRD characterization. The average size of crystalline material was found to be 27.68nm. UV-Visible characterization has confirmed that the SnS layer has found the sharp peaks in the absorption with 1.98 eV band gap. The I-V characteristic has confirmed that current is increased as the illumination intensity is increased. EPMA ananlysis confirmed that Sn and S elements are distributed is uniform on surface area. The nanoflakes layer is found the non-peel off film, which may give to the junction's rigidity. The nano flakes type shapes of SnS trap the light to increase the absorption as shown in optoelectronic and I-V characteristics, which is helpful in photovoltaic industry. In the new approach, the the SnS layer may be used as a JABS layer in the CZTS based photovoltaic devices i.e. junction–absorption layer in the hetro junction solar cell. The JABS layer can resolve the charge carriers recombination problems in Ni-Al Contact/MgF_2/ITO/i-ZnO/CdS/CZTS/Mo/SLG type of devices. The SnS nano flake is suitable for JABS layer because it has positive band offset ($\Delta E=0.36eV$), which is helpful to enhance the efficiency of Kesterite type solar cell Ag/ARC/Al-ZnO/i-ZnO/CdS/SnS/CZTS/ITO device and may be capable to break the highest record efficiency of solar cell. The JABS layer may be used in other hetero-junction devices such as absorber layers of CIGS, CdTe, CZTSSe and Cu_2InSe_3 etc.

References:

[1] Q. H. Wang, K. K. Zadeh, A. Kis, J. N. Coleman and M. S. Strano, Electronics and optoelectronics of two-dimensional transition metal dichalcogenides, *Nat. Nanotechnol*., 7(11), 699-712, 2012.

[2] Y. Cui, B. Li, J. Li and Z. M. Wei, Chemical vapor deposition growth of two-dimensional hetero-junctions, *Sci. China: Phys., Mech. Astron*., 61, 016801, 2018.

[3] R. Cheng, Y. Wen, L. Yin, F. Wang, F. Wang, K. Liu, T. A. Shifa, J. Li, C. Jiang, Z. Wang and J. He, Ultrathin single-crystalline CdTe nanosheets realized via van der Waals epitaxy, *Adv. Mater.*, 29, 1703122, 2017.

[4] Y. Gogotsi, and B. Anasori, The Rise of MXenes, *ACS Nano*, 13, 8, 8491–8494, 2019.

[5] X. Jiang, S. Liu, W. Liang, S. Luo, Z. He, Y. Ge, H. Wang, R. Cao, F. Zhang, Q. Wen, J. Li, Q. Bao, D. Fan, and H. Zhang, Broadband Nonlinear Photonics in Few-Layer MXene $Ti_3C_2T_x$ (T = F, O, or OH), *Laser Photonics Rev.*, 12(2), 1700229, 2017.

[6] P. Avouris, J. Appenzeller, R. Martel and S. J. Wind, Carbon Nanotube Electronics, *Proceedings of the IEEE*, 91, 11, 2003.

[7] L. M. Peng, Z. Zhang, S.Wang, Carbon nanotube electronics: recent advances, *Mat. today*, 17(9), 433-442, 2014.

[8] W. Tian, D. Liu, F. Cao and L. Li, Hybrid Nanostructures for Photodetectors, *Adv. Optical Mater*., 5(4), 1600468, 2016.

[9] W. S. Yun, S. W. Han, S. C. Hong, I. G. Kim, J. D. Lee, Thickness and strain effects on electronic structures of transition metal dichalcogenides: 2H-MX_2 semiconductors (M = Mo, W; X = S, Se, Te), *Phys. Rev. B*, 85, 033305, 2012.

[10] A. Kuc, N. Zibouche and T. Heine, Influence of quantum confinement on the electronic structure of the transition metal sulfide TS_2, *Phys. Rev. B*, 83, 245213, 2011.

[11] C. Yang, C. J. Barrelet, F. Capasso and C. M. Lieber, Single *p*-type/intrinsic/*n*-type silicon nanowires as nanoscale avalanche photodetectors, *Nano Lett.*, 6, 2929–2934, 2006.

[12] H. Wu, Y. Sun, D. Lin, R. Zhang, C. Zhang and W. Pan, GaN Nanofibers based on Electrospinning: Facile Synthesis, Controlled Assembly, Precise Doping, and Application as High Performance UV Photodetector, *Adv. Mater.*, 21, 227-231, 2009.

[13] Y. Jiang, W. J. Zhang, J. S. Jie, X. M. Meng, X. Fan and S. T. Lee, Photoresponse properties of CdSe single-nanoribbon photodetectors, *Adv. Funct. Mater.*, 17, 1795-1800, 2007.

[14] Y. Xie, L. Wei, Q. Li, Y. Chen, S. Yan, J. Jiao, G. Liu and L. Mei, High-performance self-powered UV photodetectors based on TiO2 nano-branched arrays, *Nanotechn.*, 2014, 25, 075202.

[15] X. Wang, Z. Xie, H. Huang, Z. Liu, D. Chen and G. Shen, Gas sensors, thermistor and photodetector based on ZnS nanowires, *J. Mater. Chem.*, 22, 6845–6850, 2012.

[16] L. Hu, J. Yan, M. Liao, L. Wu and X. Fang, Ultrahigh External Quantum Efficiency from Thin SnO_2 Nanowire Ultraviolet Photodetectors, *Small*, 7, 1012–1017, 2011.

[17] G. Su, V. G. Hadjiev, P. E. Loya, J. Zhang, S. Lei, S. Maharjan, P. Dong, M. A. P, J. Lou and H. Peng, Chemical Vapor Deposition of Thin Crystals of Layered Semiconductor SnS_2 for Fast Photodetection Application, *Nano Lett.* 15, 506-513, 2015.

[18] B. Pal, A. Singh, G. Sharada, P. Mahale, A. Kumar, S. Thirupathaiah, H. Sezen, M. Amati, L. Gregoratti, U. V. Waghmare and D. D. Sarma, Chemically exfoliated MoS_2 layers: Spectroscopic evidence for the semiconducting nature of the dominant trigonal metastable phase, *Phys. Rev. B*, 96, 195426, 2017.

[19] K. Vasu, H. S. S. R. Matte, S. N. Shirodkar, V. Jayaram, K. P. J. Reddy, U. V. Waghmare, C. N. R. Rao, Effect of high-temperature shock-wave compression on few-layer MoS_2, WS_2 and $MoSe_2$, *Chem. Phys. Lett.*, 582, 105–109, 2013.

[20] F. Lu, J. Yang, R. Li, N. Huo, Y. Li, Z. Wei, J. Li, Gas Dependent Photoresponce of SnS Nanoparticles-Based Photodetectors. *J. Mater. Chem. C*, 3, 1397-1402, 2015.

[21] X. Liu, Y. Li, B. Zhou, X. Wang, A. N. Cartwright, M. T. Swihart, Shape-Controlled Synthesis of SnE (E=S,Se) Semiconductor Nanocrystals for Optoelectronics, *Chem. Mater*, 26, 3515−3521, 2014.

[22] X. Zhou, Q. Zhang, L. Gan, H. Li, J. Xiong and T. Zhai, Booming Development of Group IV-VI Semiconductors: Fresh Blood of 2D Family, *Adv. Sci. (Weinh)*, 2016, 3, 1600177.

[23] J. H. Ahn, M. J. Lee, H. Heo, J. H. Sung, K. Kim, H. Hwang and M. H. Jo, Deterministic Two-Dimensional Polymorphism Growth of Hexagonal *n*-Type SnS_2 and Orthorhombic *p*-Type SnS Crystals, *Nano Lett.*, 15, 3703-08, 2015.

[24] Z. Mutlu, R. J. Wu, D. Wickramaratne, S. Shahrezaei, C. Liu, S. Temiz, A. Patalano, M. Ozkan, R. K. Lake, K. A. Mkhoyan and C. S. Ozkan, *Small*, 2016, 12, 2998-3004.

[25] W. Wang, K. K. Leung, W. K. Fong, S. F. Wang, Y. Y. Hui, S. P. Lau, Z. Chen, L. J. Shi, C. B. Cao and C. Surya, *J. Appl. Phys.*, 2012, 111, 093520.

[26] G. A. Tritsaris, B. D. Malone, and E. Kaxiras, Optoelectronic properties of single-layer, double-layer, and bulk tin sulfide: A theoretical study, *J. Appl. Phys.*, 113, 233507, 2013.

[27] S. Del Bucchia, J. C. Jumas and M. Maurin, Acta Crystallogr., *Sect. B: Struct. Crystallogr.Cryst. Chem.*, 37, 1903-05, 1981.

[28] K. Hartman, J. L. Johnson, M. I. Bertoni, D. Recht, M. J. Aziz, M. A. Scarpulla and T. Buonassisi, SnS thin-films by RF sputtering at room temperature, Thin Solid Films, 519, 7421, 2011.

[29] R. W. Miles, O. E. Ogah, G. Zoppi and I. Forbes, Thermally evaporated thin films of SnS for application in solar cell devices, *Thin Solid Films*, 2009, 517, 4702.

[30] F. Gode, E. Guneri and O. Baglayan, Effect of tri-sodium citrate concentration on structural, optical and electrical properties of chemically deposited tin sulfide films, *Appl. Surf. Sci.*, 318, 227, 2014.

[31] D. Zheng, H. Feng, M. Long, F. Wu, P. Wang, F. Gong, X. Wu, J. C. Ho, L. Liao, W. Hu, High performance infra-red Photodetectors based on *p*-type, SnX(X=S, Se) Nano wires grown via Chemical vapour deposition, *ACS Nano,* 12(7), 7239-7245, 2018.

[32] N. K. Reddy and K. T. R. Reddy, Growth of polycrystalline SnS films by spray pyrolysis, *Thin Solid Films,* 4, 325, 1998.

[33] N. K. Reddy, K. T. R. Reddy, Growth of polycrystalline SnS films by spray pyrolysis, Thin Solid Films 325 (1998) 4–6.]

[34] X. Liu, Y. Li, B. Zhou, X. Wang, A. N. Cartwright, M. T. Swihart, Shape-Controlled Synthesis of SnE (E = S, Se) Semiconductor Nanocrystals for Optoelectronics, *Chem. Mater.,* 26, 3515−3521, 2014.

[35] D. Zheng, H. Fang, M. Long, F. Wu, P. Wang, F. Gong, X. Wu, J. C. Ho, L. Liao and W. Hu, High-Performance Near-Infrared Photodetectors Based on *p*-Type SnX (X = S, Se) Nanowires Grown via Chemical Vapor Deposition, *ACS Nano*, 12, 7239−7245, 2018.

[36] J. Y. Cho, S. Y. Kim, R. Nandi, J. Jang, H. S. Yun, E. Enkhbayar, J. H. Kim, D. K. Lee, C. H. Chung, J. H. Kim and J. Heoa, Achieving Over 4% Efficiency for SnS/CdS Thin-Film Solar Cells by Improving Heterojunction Interface Quality, *J. Mater. Chem. A,* 8**,** 20658-20665, 2020.

[37] K. Pal, P. Singh, A. Bhaduri, K. B. Thapa, Current challenges and future prospects for a highly efficient (>20%) kesterite CZTS solar cell: A review, Sol. Energy Mater. Sol. Cells, 196, 138-156, 2019.

[38] S. Siebentritt, Why are kesterite solar cells not 20% efficient?, May 2013, *Thin Solid Films*, 535(1), 1-4, 2013.

[39] G. Liu, Y. Li, B. Li, H. Tian, C. Fan, Y. Zhang, Z. Hua, M. Wang, H. Zhenga and E. Li, High-performance photodetector based on two-dimensional Tin (II) sulfide (SnS) nano flakes, *J. Mate. Chem. C,* 00, 1-3, 2018.

[40] J. S. Morrison, Some reactions of tin (ii) chloride in non-aqueous solution, *University of New Hampshire,* Doctoral Dissertations, 808, 1965, https://scholars.unh.edu/dissertation/808?utm_source=scholars.unh.edu%2Fdissertation%2F808&utm_medium=PDF&utm_campaign=PDFCoverPages.

[41] C. H. An, K. B. Tang, G. H. Shen, C. R.Wang, Q. Yang, B. Hai and Y. T. Qian, Growth of belt-like SnS crystals from ethylenediamine solution, *J. Cryst. Growth,* 244, 333, 2002.

[42] P. Nayar and A. Khanna, Formation of crystalline aluminum silicate hydroxide layer during deposition of amorphous alumina coatings by electron beam evaporation, *Vacuum*, 89, 17-20, 2013.

[43] I. Battisha and A. E. Nahrawy, Physical Properties of Nano-Composite Silica-Phosphate Thin Film Prepared by Sol Gel Technique, *New Journal of Glass and Ceramics*, 2, 17-22, 2012.

[44] J. Krč and M. Topič, O*ptical modeling and simulation of janezkrčmarkotopič thin-film photovoltaic devices, CRC Press Taylor & Francis Group*, 6000 Broken Sound Parkway NW, Suite 300, 2013.

[45] J. Fengab, Z. Guo, Wettability of graphene: from influencing factors and reversible conversions to potential applications, *Nanoscale Horiz.*, 4, 339-364, 2019.

[46] A. Akkari, C. Guasch, N. K. Turki and J. Tauu, Chemically deposited tin sulphide, *J. Alloys Compound.*, 490, 180, 2010.

[47] S. Wu, L. Cheng and Q. Wang, Excitonic effects and related properties in semiconductor nanostructures: roles of size and dimensionality, *Mater. Res. Express*, 4, 085017, 2017.

[48] W. H. Ng, Y. Lu, H. L., C. J. Carmalt, I. P. Parkin and A. J. Kenyon, Controlling and modelling the wetting properties of III-V semiconductor surfaces using re-entrant nanostructures, *Sci. Rep.*, 8, 3544, 2018.

[49] K. Koch, B. Bhushan, Y. C. Jung, W. Barthlott, Fabrication of artificial Lotus leaves and significance of hierarchical structure for superhydrophobicity and lowadhesion, *Soft Matter.Soft Matter,* 5, 1386-139, 2009.

[50] N. Gao and Y. Yan, Characterisation of surface wettability based on nanoparticles, *Nanoscale*, 4, 2202, 2012,.

[51] M. Devika, N. K. Reddy, F. Patolsky, and K. R. Gunasekhar, Ohmic contacts to SnS films: Selection and estimation of thermal stability, *J. Appl. Phys.*, 104, 124503, 2008.

[52] P. R. Bueno, J. A. Varela, and E. Longo, SnO_2, ZnO and related polycrystalline compound semiconductors: An overview and review on the voltage-dependent resistance (non-ohmic) feature, *J. Eur. Ceram. Soc.*, 28, 505, 2008.],

[53] S. M. Sze, M. K. Lee, Semiconductor Devices Physics And Technology, *John Wiley & Sons,Inc.*, 3rd Edition, USA, ISBN 978-0-470-53794-7, 2002.

[54] C. H. Kuo, J. M. Wu, S. J. Lin and W. C. Chang, High sensitivity of middle wavelength infrared photodetector based on an individual InSb nanowire, *Nanoscale Res. Let.*, 8, 327, 2013.

[55] X. Liu, F. Li, M. Xu and J. Qi, Self-powered, high response and fast response speed metal–insulator–semiconductor structured photodetector based on 2D MoS_2, *RSC Adv.*, 8, 28041-28047, 2018.

[56] W. Ouyang, F. Teng, J. H. He and X. Fang, Enhancing the Photoelectric Performance of Photodetectors Based on Metal Oxide Semiconductors by Charge-Carrier Engineering, *Adv. Funct. Mater.*, 29(9), 1807672, 2019.

[57] N. Kurra, V. S. Bhadram, C. Narayana, and G. U. Kulkarni, Few layer graphene to graphitic films: infrared photoconductive *versus* bolometric response, *Nanoscale,* 5, 381-389, 2013.

[58] B. Haraoubia, 1 - Nonlinear Two-terminal Devices, *Nonlinear Electronics 1 Nonlinear Dipoles, Harmonic Oscillators and Switching Circuits*, 1-81, 2018, https://doi.org/10.1016/B978-1-78548-300-4.50001-4.

[59] R. K. Tripathi, O. S. Panwar, I. Rawal, B. P. Singh, B. C., Yadav, Study on nanocrystalline silicon thin films grown by the filtered cathodic vacuum arc technique using boron doped solid silicon for fast photo detectors, *Taiwan Inst. Chem. Eng.,* 86, 185-191, 2018.

[60] G. Liu, Y. Li, B. Li, H. Tian, C. Fan, Y. Zhang, Z. Hua, Mengjun Wang, H. Zhenga and E. Li, High-performance photodetector based on two-dimensional Tin (II) sulfide (SnS) nanoflakes, *J. Mate. Chem. C,* 00, 1-3, 2018.

[61] D. Zheng, H. Feng, M. Long, F. Wu, P. Wang, F. Gong, X. Wu, J. C. Ho, L. Liao, W. Hu, High performance infra-red Photodetectors based on *p*-type, SnX(X=S, Se) Nano wires grown via Chemical vapour deposition, *ACS Nano,* 12, 7, 7239–7245, 2018.

[62] M. S. Mahdi, H. S. Al-Arab, H. S. Al-Salman, K. Ibrahim, N. M. Ahmed, A. Hmood and M. Bououdina, A high-performance near-infrared photodetector based on *p*-SnS phase, *Mater. Lett.*, 273, 127910, 2020.

[63] A. S. Pawbake, S. R. Jadkar and D. Late, High performance humidity sensor and photo detector based on SnSenanorods, *Mater. Res. Exp.*, 3(10), 105038, 2016.

[64] G. Liu, Y. Li, B. Li, H. Tian, C. Fan, Y. Zhang, Z. Hua, M. Wang, H. Zhenga and E. Li, High-performance photodetector based on two-dimensional Tin (II) sulfide (SnS) nanoflakes, *J. Mate. Chem. C,* 00, 1-3, 2018.

[65] D. Zheng, H. Feng, M. Long, F. Wu, P. Wang, F. Gong, X. Wu, J.C. Ho, L. Liao and W. Hu, High performance infra-red Photodetectors based on p-type, SnX(X=S, Se) Nano wires grown via Chemical vapour deposition, *ACS Nano,* 12, 7, 7239–7245, 2018.

[66] S. C. Singh, Y. Peng, J. Rutledge, and C. Guo, Photothermal and Joule-Heating-Induced Negative-Photoconductivity-Based Ultraresponsive and Near-Zero-Biased Copper Selenide Photodetectors, *ACS Appl. Electron. Mater.*, 1, 1169-1178, 2019.

[67] H. Xu, Y. Liu, H. Liu, S. Dong, Y. Wu, Z. Wang, Y. Wang, M. Wu, Z. Han and L. Hao, Pd-decorated 2D SnSe ultrathin film on SiO_2/Si for room-temperature hydrogen detection with ultrahigh response, *J. Alloys & Comp.*, 851, 156844, 2021.

[68] M. S. Mahdi, H. S. A.-Arab, H. S. A.-Salman, K. Ibrahim, N. M. Ahmed, A. Hmood, M. Bououdina, A high-performance near-infrared photodetector based on p-SnS phase, *Mater. Lett.*, 273, 127910, 2020.

[69] K. M. Chahrour, N. M. Ahmad, M. R. Hashim, N. G. Elfadill and M. Bououdina, *Sens. Actuators A*, 239, 209, 2016.

[70] M. S. Mahdi, K. Ibrahim, A. Hmood, N. M. Ahmed, S. A. Azzez and F. I. Mustafa, A highly sensitive flexible SnS thin film photodetector in the ultraviolet to near infrared prepared by chemical bath deposition, *RSC Adv.*, 6, 114980-114988, 2016.

[71] B. Ghosh, R. Roy, S. Chowdhury, P. Banerjee, S. Das, Synthesis of SnS thin films via galvano static electro deposition and fabrication of CdS/SnS hetero structure for photovoltaic applications, *Appl. Surf. Sci.*, 256, 4328-4333, 2010.

[72] J. Chao, J. Wang, X. Xu, Q. Xiang, W. Song, G. Chen, J. Hu and D. Chen, Tin sulfidenanoribbons as high performance photoelectron chemical cells, flexible photodetectors and visible-light-driven Photocatalysts, *RSC Advances,* 3, 2746-2753, 2013.

[73] E. Veena, K. V. Bangera, G. K. Shivakumar, Effect of annealing on the properties of spray-pyrolysed lead sulphide thin films for solar cell application, *Appl. Phys. A: Mater. Science & Process.*, 123(5), 1-12, 2017.

[74] D. L. Domtau, J. Simiyu, E. O. Ayieta, G. M. Asiimwe and J. M. Mwabora, Influence of Pore Size on the Optical and Electrical Properties of Screen Printed TiO_2 Thin Films, *Hindawai*, Article ID 7515802, 2016.

[75] J. N. Sun, Y. Hu, W. E. Frieze, W. Chen, and D. W. Gidley, How Pore Size and Surface Roughness Affect Diffusion Barrier Continuity on Porous Low-k Films, *J. The Electrochem. Society*, 150 (5), 2003.

[76] Y. Kato, S. Fujimoto, M. Kozawa, and H. Fujiwara, Maximum Efficiencies and Performance-Limiting Factors of Inorganic and Hybrid Perovskite Solar Cells, Phys. Rev. A., 12, 024039, 2019.

[77] C. D. Lokhande, A chemical method for tin disulphide thin film deposition, *J. Phys. D.* 23, 1703, 1990.

[78] T. Sall, B. M. Soucase, M. Mollar, J. A. Sans, SnS Thin Films Prepared by Chemical Spray Pyrolysis at Different Substrate Temperatures for Photovoltaic Applications, *J. Elect. Mater. 46*, 1714-1719, 2017.

[79] I. Rawal, R. Tripathi, O. S. Panwar, Easy Synthesis of Organic-Inorganic Hybrid Nanomaterials: Study of DC Conduction Mechanism for Light Dependent Resistors, *RSC Adv.*, 6, 31540, 2016.

[80] Y. Matsuoka, A. Fujiwara, N. Ogawa, K. Miyano, H. Kataura, Y. Maniwa, S. Suzuki and Y. Achiba, Temperature dependence of photoconductivity at 0.7 eV in single-wall carbon nanotube films, *Sci. Technol. Adv. Mater.* 4, 47, 2003.

[81] D. A. Neamen, 4th ed., *Semiconductor Physics and Devices: Basic Principles, Published by McGraw-Hill Inc.*, 1221 Avenue of the Americas, New York, NY 10020, 2003.

[82] M. Powalla, S. Paetel, E. Ahlswede, R. Wuerz, C. D. Wessendorf, and T. M. Friedlmeier, hin-film solar cells exceeding 22% solar cell efficiency: An overview on CdTe-, Cu(In,Ga)Se2-, and perovskite-based materials, *App. Phys. Rev.*, 5, 041602, 2018.

[83] A. Walsh, S. Chen, S. H. Wei and X.G. Gong, Kesterite thin-film solar cells: advances in materials modeling of Cu_2ZnSnS_4, *Adv. Energy Mater.*, 2, 400-409, 2012.

[84] W. Wang, M. T. Winkler, O. Gunawan, T. Gokme, T. K. Todorov, Y. Zhu and D. B. Mitzi, Device Characteristics of CZTSSe Thin-Film Solar Cells with 12.6% Efficiency, *Adv. Energy Mater.*, 4(7),1301465, 2014.

[85] C. Yan, J. Huang, K. Sun, S. Johnston, Y. Zhang, H. Sun, A. Pu, M. He, F. Liu, K. Eder, L. Yang, J. M. Cairney, N. J. Ekins-Daukes, Z. Hameiri, J. A. Stride, S. Chen, M. A. Green and X. Hao, Cu_2ZnSnS_4 solar cells with over 10% power conversion efficiency enabled by hetero-junction heat treatment, *Nature Energy*, 3, 764-772, 2018.

[86] L. Sun, , R. Haight, P. Sinsermsuksakul, S. B. Kim, H. H. Park and R. G. Gordon., Band alignment of SnS/Zn(O,S) heterojunctions in SnS thin film solar cells. *Appl. Phys.Lett.*, 103(18), 181904, 2013.

[87] T. Ikuno , R. Suzuki , K. Kitazumi , N. Takahashi , N. Kato , K. Higuchi, SnS thin film solar cells with $Zn_{1-x}Mg_xO$ buffer layers, *Appl. Phys. Lett., 102*, 193901, 2013.

[88] W. Wang, M. T. Winkler, O. Gunawan, T. Gokme, T. K. Todorov, Y. Zhu, and D. B. Mitzi, Device Characteristics of CZTSSe Thin-Film Solar Cells with 12.6% Efficiency, *Adv. Energy Mater.* 4, 1301465, 2014.

[89] A. Niemegeers, M. Burgelman, A. Devos, On the CdS/$CuInSe_2$ conduction band discontinuity, *Appl. Phys. Lett., 67*, 843, 1995.

[90] T. Minemoto , T. Matsui , H. Takakura , Y. Hamakawa , T. Negami, Y. Hashimoto , T. Uenoyama , M. Kitagawa, Theoretical Analysis of the Effect of

Conduction Band Offset of Window/CIS Layers on Performance of CIS Solar Cells using Device Simulation, *Sol. Energy Mater. Sol.Cells*, 67, 83, 2001.

[91] K. Ramya, K.T. R. Ramakrishna, Investigations on the parameters limiting the performance of CdS/SnS solar cell, *Int J Energy Res.*, 1–7, 2017.

CHAPTER 6

Conclusions and Future Prospects

Chapter 6

Conclusions and Future Prospects

The 21st century is the era of technological development of functional and smart materials for sustainable energy applications. The researchers of materials science and engineering under the STEM (Science, Technology, Engineering and Mathematics) are looking towards the functional materials of the metals and alloys, polymers, ceramics, and composite materials as the energy materials, and have developed the nanostructured functional materials, called energy materials, which are considered the best materials for fabricating the sustainable energy devices. The energy materials and their novel technologies are needed to be developed for fulfilling the demand of low cost and eco-friendly sustainable energy. Today, the researchers across the globe are focussed on developing efficient and utilization energy devices, and targeting to meet the challenges of increasing demand of energy and their high prices. The fabricated devices should be in such a way that they have affiliated with the low environmental impact. In this direction, the new approaches are searching to convert photon energy density into electron energy density by photovoltaic (PV) solar cell, it is the best way to get sustainable and plentiful energy. The design and manufacture of PV solar cells can be used for reduced cost and eco-sustainable devices. For developing novel approaches, researchers are trying to engineer low cost, abundant materials with bearable and high efficient devices. Therefore, we have also tried to study how the functional ZnO, SnS, CZTS materials are synthesized using abundant materials and low-cost synthesis processes.

6.1 Conclusion

In nature, various materials have their different crystal structures and they are found with different sizes and shapes. The different sizes and shapes of materials show distinct characteristics depending on their atomic compositions and volumetric parameters. Apart from the microsized materials having dimension at nanometers (~10^{-9} m or nm) exhibiting novel properties, the technological applications of such nano dimensional materials is called as nanotechnology, which deals with different electrical, optical and electronic as well as opto-electronic devices. The materials at nano scale reveal various novel phenemona that can be used in the fabrication of cost effective and highly efficient energy devices. With different fields of sciences, nanotechnology is one of the most popular area of sciences for current research and development in all technical disciplines, while the study of nanomaterials and their properties for nanotechnology is known as nanoscience. In nanoscience, researchers are working to develop functional materials with high value of the ratio of performance to cost for energy applications. The functional materials (FMs) of ceramics, metals, polymers, and composite have specific or native properties of the materials, such as ferroelectricity, piezoelectricity, magnetism, electron-transport property, and energy storage functions. Semiconductors have the intermediate characteristics property between the conductors and insulators, also they have energy band gaps lower than insulators but higher than conductors. Furthermore, if we increase the concentration of impurity in the semiconductor/generally known as extrinsic semiconductor, the electrical and optical properties of the semiconductors becomes sensitive than the parent semiconductor/generally known as intrinsic semiconductor. The Si, Ge, GaAs, Al, $BaTiO_3$, CdS, Cu_2InS_3, and Cu_2ZnSnS/Se are the popular energy materials and the functional elements like In, Se, Cd, etc. are frequently doped in pure materials. The composition of functional materialsis with rare-earth elements are costly than the composition of functional materialsis with abundant earth elements. This is the main drawbacks of such energy efficient materials use in the solar cells.

Nowadays, the inorganic transition metal chalcogenides have generated a great interest among researchers to investigate the low-cost efficient materials. Using these materials, the cost-effective energy devices can be fabricated in electronic chips, energy conversions, and energy storage devices. The transition metal chalcogenides are emerging chalcogenide nanocomposites, which mainly include binary, ternary, quaternary metal chalcogenides, etc. Ternary and quaternary compounds have Perovskite-type structures, which are significant materials for both fundamental and scientific research. Besides this, SnS (binary chalcogenide) is also quite interesting owing to its excellent properties of hydrophobic and absorption that ensures its applicability in photodetector application.

In top down approach of the field of nanoscience and nanotechnology, spray-coated chalcogenide materials are the best for versatile applications in materials science and engineering. In the last few years, the optical and electronic properties of chalcogenide semiconductor nanostructures have been of great interest, both theoretically and experimentally. As we know that the continuous energy levels at the macro meter scale changes into the discrete energy levels at the nanometer scale due to the phenomenon of quantum confinement. Quantum confinement effects occur in many electronic levels e.g. quantum wells (QWs), quantum wires (QWRs), and quantum dots (QDs). The level of electron density depends on the dimensionality of a semiconductor. Two dimensional semiconductors are realized as ***quantum well*** due to the restriction of free motion in one direction. In quantum dots, the density of states shows discrete energy levels due to the trapping in 3-D confinement. The energy levels can be monitored with different values by controlling the shapes and sizes of the material, and the confinement potential. The electronic transitions in discrete energy levels can be used to model the optical properties of quantum well. Quantum wells are very tiny particles (size 2nm to 10nm) that can be fabricated into a sheet form. They have unique optical and electronic properties due to their two-dimensional quantum confinement regime.

In our research work, we have discussed the present issues of photovoltaic devices. We come to know that, photovoltaic cell efficiency and other parameters related to the cell as well as their cost, are the main issues. The study shows that inorganic functional materials at the nanometer scales can resolve all these issues. For instant, CZTS materials have a high absorption coefficient, suitable bandgap, low cost and eco-friendly photovoltaic properties. Hence, the inorganic chalcogenide materials may be excellent materials for energy conversion devices. Therefore, the researchers strive towards the synthesis of such materials from different methods to achieve various photovoltaic applications including solar cells.

In first chapter, we have identified some problems of photovoltaic efficiency in Kesterite solar cells and described the CZTS phases, electronic band structures, and important parameters to enhance the photovoltaic efficiency. The CZTS is an I_2-II-IV-VI_4 group functional material. The photovoltaic properties of CZTS solar cells have been found with the high efficiency, when CZTS is found in a single phase, recombination losses (effective parameters) at the interface of buffer and absorber layers. The effective parameters in the photovoltaic Kesterite solar cells are discussed briefly. On the other hand, the big challenge of the low-cost Kesterite photovoltaic devices is to enhance the conversion efficiency more than 20% using the different layers. The main reason for the low efficiency of Kesterite solar cells is the high loss of charge carriers by the recombination losses (diffusion and thermionic losses) during charge transportation and the charge collection at the electrodes. The recombination losses are affected directly by the interfacial layer between the absorber layer and the buffer layer as well as the absorber layer and the metallic contact. Generally, CdS is the best interfacial layer between buffer and absorber of the CIGS solar cell, but it is not perfect for the CZTS,Se solar cell as the recombination timing of the CZTS, Se solar cell at the interface is very low as compared to the CIGS solar cell. The main reason for low recombination in the CdS/CZTS interface is due to Cd diffusion in the absorber layer at the time of solar cell fabrication. The interface of CdS/CZTS has a spike-type band offset**.** Hence, it is required to develop a suitable buffer layer for replacing the CdS layer, i.e. appropriate function interfacial layer between the buffer and the absorber. The researchers have been using carbon nanotubes (CNTs) as an interfacial layer to remove the recombination. The CNT may be the perfect buffer layer to reduce the recombination between the absorber and the buffer layers, due to breathing mode of the cylindrical type molecules of the CNTs. Some researchers have been also used the Graphenes/MXenes nanolayers in place of CNTs, which is also the best solution for such problems of loss. The Mo(S_2/Se_2) layer between absorber and metallic contact is another hurdle to enhance the efficiency of the Kesterite solar cell. The Mo interface plays a vital role in the reduced efficiency of Kesterite solar cell because it has maximum series resistance. The Mo(S_2/Se_2) layer forms oftenly in the Kesterite solar cell during the annealing process and concludes two points: (i) we should not anneal the solar cell after the complete fabrication of the device, and (ii) we should remove Mo metal with high work function metals such as Ni (5.22), NiO (>5.2), Pd (5.22), Pt (5.64). To obtain the single phase of CZTS, we can use the certain stoichiometry ratio of precursor elements during the synthesis of CZTS materials. Copper, Zinc, Tin and Sulphur in the CZTS composite make it non-toxic and environment friendly. The synthesis of the CZTS composite resolves the problems of time taking and low-cost synthesis by the co-precipitation method. In second chapter, we have discussed the synthesis methods and characterization techniques for chalcogenide materials. The issues of phase problem of composition, toxic elements to environment, time taking and cost-effective methods are identified. Keeping these issues in mind, we have decided to work on the synthesis methods especially the Co-precipitation and Spray Pyrolysis methods. These methods are the cheapest, nontoxic, less-time consuming and eco-friendly device fabrication of chalcogenide materials. The synthesized materials have characterized by XRD, EDS, SEM, FESEM, UV-Visible, Raman spectroscopy, XPS, I-V characteristics measurement Keithley tools.

Chapter three includes the synthesis of ZnO nanomaterials by a cost-effective co-precipitation method without any surfactant and structural analysises for better PV device, because ZnO nanomaterials are considered as the efficient material for solar energy devices. The XRD, EDS, SEM characterizations of synthesized ZnO nanomaterials show the crystalline nature of nanomaterials. The crystalline results of the nanomaterials are similar to that of pre-synthesized ZnO with surfactant. The study concludes that we can save expenditure cost of surfactant and time of synthesis. The properties of synthesized ZnO may be tuned with calcinated temperature related crystallinity. Based on the study of characterizations, we can say that ZnO may be used as a window layer in hetero-junction Kesterite PV device applications.

In fourth chapter, CZTS nanocrystals have synthesized with S variation by the Co-precipitation method without any type of annealing. In the synthesis of nanocrystals, no any surfactant be used in the precursor solution. The synthesized Sample-B (18mmol quantity of Sulphur in precursor solution) is characterized by XRD, EDS, SEM, Raman, UV-Visible techniques and investigated that CZTS is polycrystalline and stoichiometric. The observed polycrystalline results are similar to the results found by vacuum annealing/sulphurization method. The surface electron microscope (SEM) reveals that the polycrystalline CZTS phase has good morphology for better electronic and optical characteristics. The obtained exciting results demonstrate that the nanocrystals are systhesised by proper route may fulfill the promise of low-cost thin film for photovoltaic cell applications. The novelty of this work is the synthesis of CZTS nanocrystals by co-precipitation method without any sulphurization and selenisation processes. This route of synthesis supports low cost, less time-consuming, and nontoxic synthesis and suitable use for absorber layer in Kesterite photovoltaic application.

Chapter five includes the optical and electronic studies of binary nanoflakes layered SnS thin film synthesized by the Spray Pyrolysis method (SPM), which is a cheap, less time consuming, non-toxic and ecofriendly method. The nanoflake shapes of SnS trap the light and increase the absorption as shown in optoelectronic and I-V characteristics, which is helpful in the photovoltaic industry. A layer of SnS nano flake is suitable for the JABS layer or interfacial layer because it has a positive band offset, which removes the thermionic loss and diffusion loss of charge carriers at the interface. In this JABS mechanism, the efficiency of Kesterite type PV device of structure, Ag/ARC/Al-ZnO/i-ZnO/CdS/***SnS***/CZTS/ITO, is helpful to enhance the conversion efficiency. Such an arrangement may be capable to achieve the highest record efficiency of a solar cell. On the other hand, the photo parameter of the SnS nano-flakes layer has been analyzed and investigated the photo response, photosensitivity, photocurrent and photo resistance. These photo parameters justify the application of photo-detector with low cost. The thin-film SnS photodetector is feasible for commercial application devices because it is grown by nontoxic, eco-friendly, less time consuming and low cost SPM method, and cheap abundant materials. This layer has one advanced feature of hydrophobicity which provides to the automated dust-free devices that is similar to the dew-drops in the water lotus leaves. This synthesis work is suitable for commercial application with saving and eco-friendly devices.

Table 6.1: The chapter wise conclusion of the thesis:

<table>
<tr><th>Chapter No.</th><th>Photovoltaic Materials</th><th>Size (nm)</th><th>Energy Band-gap (eV)</th><th>Applications</th><th>Recovery Time (s)</th><th>Response Time (s)</th><th>Toxicity Nature</th><th>References</th></tr>
<tr><td>Ch. 1</td><td colspan="7">Introduction</td><td>[1, 2]</td></tr>
<tr><td>Ch. 2</td><td colspan="7">Synthesis Methods and Characterization Techniques</td><td></td></tr>
<tr><td>Ch. 3</td><td>ZnO without surfactant</td><td>22-28</td><td>3.2</td><td colspan="3">Window layer</td><td>Non-toxic</td><td>[3]</td></tr>
<tr><td>Ch. 4</td><td>Cu_2ZnSnS_4</td><td>15-17</td><td>1.33</td><td colspan="3">Absorber layer</td><td>Non-toxic</td><td>[4]</td></tr>
<tr><td rowspan="2">Ch. 5</td><td rowspan="2">SnS flakes</td><td rowspan="2">27.68</td><td rowspan="2">1.98</td><td>Photodetector</td><td>1.56</td><td>1.69</td><td rowspan="2">Non-toxic</td><td>[5]</td></tr>
<tr><td colspan="3">JABS layer in Photovoltaic Cells</td><td>[6]</td></tr>
</table>

Ch. 6	Conclusion and Future Prospects

The overall outline of this thesis concludes that the synthesis of the nanomaterials with suitable methods may decrease the cost of the photovoltaic devices. The crystallite size, strain, energy band-gap, composition of salts, photo-sensitivity; response and recovery time of photocell, are some valuable characterizations of the nanomaterials for photovoltaic devices. The main aim of the thesis is to investigate the effective parameters of photovoltaic devices. Hence, we concentrated to study how to get a photovoltaic device with high efficiency and low cost, eco-friendly, less-time consuming and non-toxic synthesis methods using the functional materials. The spray pyrolysis technique coated SnS is the best functional material for energy application with the advanced hydrophobic nature of SnS film for photodetector at room temperature. The coated SnS thin film exhibits the highest response and recovery time and such materials can be commercialized with better photo resonance. We have also introduced a JABS layer for heterojunction Kesterite photovoltaic devices to remove the different types of losses at the interface junction. The chapter wise conclusion of the thesis is tabulated in **Tab. 6.1**.

6.2 Scope of Further Research

Demand of global energy has been growing exponentially in this information of technology age. The coal, oil, and gas resources are contributed expressively to generate the electricity energy. Although, these traditional energy have also contributed to an increase pollution in the world and human health deterioration. The global renewable energy especially solar energy is the best solution to fulfill the energy demand. The solar energy is converted into the electricity energy by the photovoltaic devices. The cost of the convetional photovoltaic device is very high and the constituents of the device is hazardous for environment. In future, the high efficient photovoltaic devices with low cost, non-toxic and eco-friend materials need to fulfill the demand of energy. Indeed, the development of functional nanomaterials can be best option for photovoltaic cells. The composition of functional nanomaterials controls the cost of devices, and synthesis processing of the compositions controls the structure of the materials. Both compositions and structures of the namomaterials are related to the performance as well as the cost of materials. In materials science and engineering, we study that the ratio of the performance and the cost of the materials always must be high for the commercial devices.

In this research work, we have tried to find out the low cost, non-toxic and eco-friendly functional nanomaterials and tried to choose the feasible methods for synthesis the composition at room temperature. For this, we have synthesized ZnO, CZTS and SnS functional materials by coprecipitation method (CPM) and spray pyrolysis method (SPM) because Zn, Cu, Sn, Zn and S are abundant earth elements and CPT/SPT are cost-effective and eco-friendly synthesis methods. Using CPT, we have synthesized the II-IV group (ZnO) functional material without any surfactants. The characterizations of ZnO nanomaterials have been justified that ZnO nanomaterials may be used as window layer of the hetero-junction Kesterite solar cell. By taking balanced stoichiometric ratio of the precursor of Zn, Cu, Sn and S elements, the stable quaternary compound of CZTS can be synthesized in the open environment. The characterizations of CZTS nanomaterials have been valided that CZTS compound may be suitable for absorber layer in photovoltaic solar cells. Using SPM, a thin film of SnS functional nanomaterials has synthesized and the SnS thin film has hydrophobic characterstic property that may use as the hydrophobic photodetectors. The I-V characterizations of SnS functional nanomaterials have been justified for hydrophobic photodetector with better photo response and recovery time in comparison to the traditional photodetector.

Our studies reveal that the CPT and SPT are the best synthesis methods for the low-cost, high efficient and eco-friendly functional nanomaterials (ZnO, CZTS and SnS) for optical and electronic devices. The photovoltaic solar cells and the hydrophobic photodetectors may be fabricated with the abundant elements and appropriate synthesis methods. By adopting the abundant elements and appropriate synthesis methods, the ZnO, CZTS and SnS functional nanomaterials may be implemented to industry for mass production of the photovoltaic solar cells and hydrophobic photodetectors. The ratio of the performance to the cost of the material may be high by choosing the low cost, non-toxic and eco-friendly elements, and ecofriendly synthesis processes for structural modification.

References:

[1] K. Pal, K. B. Thapa, and A. Bhaduri, A Review on the Current and Future Possibilities of Copper-Zinc Tin Sulfur Thin Film Solar Cell to Increase More Than 20% Efficiency, ***Adv. Sci. Eng. Med***., 10, 1-7, 2018.

[2] K. Pal, P. Singh, A. Bhaduri and K. B. Thapa, Current challenges and future prospects for a highly efficient (> 20%) kesterite CZTS solar cell: A review, ***Sol. Energy Mater. & Sol. Cells.,*** 196, 138–156, 2019.

[3] Shweta, K. Pal and K. B. Thapa, Synthesis and characterization of ZnO nano-particles for solar cell application by the cost effective co-precipitation method without any surfactants, ***AIP Conf. Proc.,*** 2142, 030008-1–030008-4, 2019.

[4] K. Pal, D. K. Maurya, P. Chaudhary, K. B. Thapa, and B. C. Yadav, Co-precipitation Synthesis with a Variation of the Sulphur Composition of Kesterite Phase Cu_2ZnSnS_4 (CZSS) without Annealing, ***Process, J. Phys. Sci.,*** 32(2), 27–39, 2021.

[5] K. Pal, P. Chaudhary, R. K. Tripathi, S. Tiwari, and K. B. Thapa, B. C. Yadav, Non-toxic, low cost, stable, and auto-cleaned visible photodetector of Tin (II) Sulphide (SnS) nanoflakes for commercial application, ***Mater. Chem. & Phys***., August 2021(*Communicated-JESTCH-S-21-05227*).

[6] K. Pal, R. K. Tripathi, K. B. Thapa, Non-peel-off and recombination reducing JABS layer into the hetero-junction Cu_2ZnSnS_4 solar cell: A new approach, ***Asia-Pacific Journal of Science and Technology***, August 2021(*Communicated-APST-S-21-01397*).

Solar Energy Materials and Solar Cells 196 (2019) 138–156

Contents lists available at ScienceDirect

Solar Energy Materials and Solar Cells

journal homepage: www.elsevier.com/locate/solmat

Current challenges and future prospects for a highly efficient (> 20%) kesterite CZTS solar cell: A review

Krishan Pal, Pawan Singh, Abhishikta Bhaduri, Khem B. Thapa*

Department of Physics, School of Physical and Decision Sciences, Babasaheb Bhimrao Ambedkar University (A Central University), Lucknow-226025 (UP), India

ARTICLE INFO

Keywords:
Kesterite
Recombination
Band offset
Defect
Interface layer
CZTS solar cell

ABSTRACT

CZTS has kesterite structure and the composition's formula is $Cu_2ZnSn(S/Se)_4$. The efficiency of CZTS-Se (Copper—Zinc—Tin-Sulphur-Selenium) solar cell, ~12.6%, is much lower than the efficiency of CIGS (Copper—Indium—Gallium—Selenium) solar cell, ~22.6%. But the CZTS-Se may be the counterpart of the CIGS and the efficiency may be increased up to 32.2% as theoretically predicted by the Shockley-Queisser (SQ) limit. In solar cell technology, it has been depicted that the efficiency of the solar are affected by the two parameters: (i) variation of the solar insolation and (ii) quality of the materials. Besides this, the narrow phase stability of quaternary phases, unfavorable band alignments, mid-gap states and band tails are main reasons of deficit in the efficiency of kesterite due to the coexistence of the secondary and ternary phases, carrier recombination at the interfaces, defects and series resistances. As a result, the kesterite solar cell has the fluctuated open circuit voltage and the loss of energy. In addition to this, the champion CZTS-Se solar cell is not so environmental friendly because Se is the toxic and the rare earth element. This review provides the vital approaches by discussing the proper materials processing and the appropriate solution to enhance the efficiency of kesterite (CZTS, CZTSe and CZTS/Se) solar cells. Due to the large area quality, high absorption and low-cost materials of the kesterite, it may be used directly in harvesting the solar energy. We have also discussed how to reduce the recombination of the electron-hole pairs by using the interfacial layer so that the efficiency of the kesterite solar cells can be improved.

1. Introduction

The energy crisis is a fascinating problem in this world for twenty-first century. The current energy consumption of the world is 16 TW (16×10^{12} Watt) and it will become 30 TW in 2050 [1]. The 80% energy is generated from the sustainable energy sources e.g. oil, gas, coal etc. and remaining 20% energy from renewable energy sources e.g. water, solar, wind etc. [2]. The solar, wind and water energy sources are abundant on the earth and are to be free of cost if we are able to develop low cost devices, that is, solar cell that converts solar energy to electric energy. The sustainable energy is used at mankind's demand and may affect the climate change for the long-term by producing outcome harmful products. On the other hand, the renewable energy is an alternative source of energy, which is environment friendly for the earth and the best for health security purpose.

The solar energy is easily available, directly accessible and free source of energy on the earth and it is free of cost. The solar insolation on the earth is incident directly about 1.2×10^5 TW (1 TW = 10^{12} Watt) on the earth surface in which 3.6×10^4 TW on land only [1]. The change in the amount of radiation emitted by the Sun at a particular location increases dramatically due to local effects such as clouds and seasonal variations, as well as other effects such as “the length of the sunny day” at the particular latitude. But the solar radiation in desert regions tends to have lower variations due to local atmospheric phenomena such as clouds [3]. The solar radiant energy spectrum with percentage distribution intensity versus wavelength of the incident photons is shown in Fig. 1.1 [4]. This figure predicts that the maximum intensity of the radiation is to have in the visible wavelength range.

The high-energy conversion devices like solar cells are dependent upon the material's property. The materials quality modifies the photovoltaic property and enhances efficiency of the solar cells. So, researchers are working to enhance the materials quality by manipulating the “material compositions”. The efficiency of the solar cell can be enhanced up to Shockley-Queisser limit by manipulating the material with the help of the material processing. The solar cell is the best source to fulfill the large energy requirements globally without any harmful effect to the atmosphere and environment.

The development of the solar cell is categorized into three

---

* Corresponding author.
E-mail address: khem.bhu@gmail.com (K.B. Thapa).

https://doi.org/10.1016/j.solmat.2019.03.001
Received 2 July 2018; Received in revised form 23 February 2019; Accepted 2 March 2019
0927-0248/

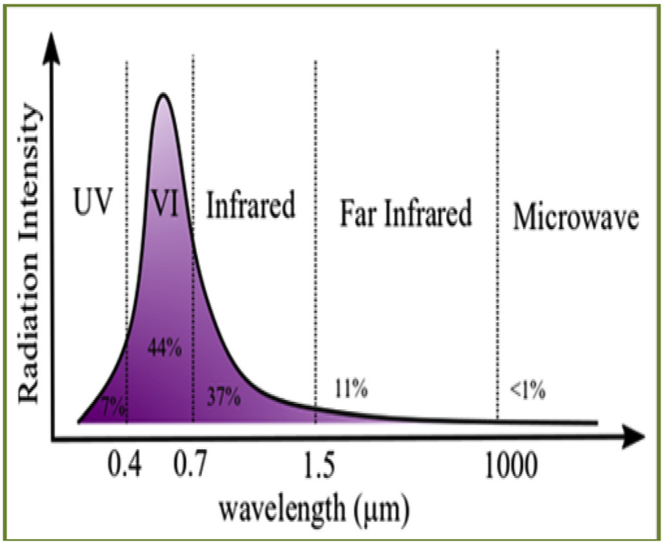

Fig. 1.1. Radiant energy over the solar spectrum radiation intensity versus wavelength, permission taken.

generations on the basis of physical properties and their production costs:

(i) First generation solar cells: These cells are made by p-n homojunction devices and thickness of film used is more than 180 µm. Si and Ge materials are considered for a solar cell in this generation with the defect free and the indirect band gap semiconductors.
(ii) Second generation solar cells: These are the hetero-junction devices made by the direct transition semiconductor materials (CdTe, CIGS) polycrystalline thin film ($> 2\,\mu m$) to absorb the visible wavelength part of the electromagnetic spectrum. In such cells, there are some challenges related to the recombination time, the homogeneous composition and the earth-abundant element composite. The production cost of these cells is approximately US$1.00 per watt.
(iii) Third generation solar cells: These are made by the semiconducting organic macromolecules, inorganic nanoparticles or hybrids materials e.g. polymer and bio-mimetic. The quantum dot, multi-junction/tandem solar cell, intermediate solar cell, hot carrier solar cell, photon up conversion, down conversion and solar thermal technology are devices in this field. The production cost of these cells is less than US$0.50 per watt.

All generations of the solar cell work on the generation of the electron-hole-pairs. But the electron-hole pairs are dependent upon the property of the materials. The materials of the solar cells have following processes for conversion of the solar energy into the electricity:

(i) The effective absorption of the incident photons having the energy 1.1–2.0 eV.
(ii) The generation of the electron hole-pairs.
(iii) The separation of the electron-hole pairs before the recombination.
(iv) The collection of the photo-generated charges by the metallic contacts or electrode.

The high priority of the solar cell in emerging technology is the cost-effective production with high efficiency and long durability. The first-generation silicon-based solar cell is owned the maximum number of photovoltaic cells in the market because of its eco-rich material resource, having non-toxic nature and durability. But there is no more probability to increase the photovoltaic efficiency due to less the absorption of silicon. So a lot of materials of the high absorption coefficient have been searched out in place of the silicon, having the effectiveness in photovoltaic property e.g., Cadmium Telluride (CdTe), Copper Indium Sulfide (CIS), Copper Indium Gallium Selenide (CIGS) and Copper Zinc Tin Sulphur (CZTS). However, CdTe, CIS, CIGS are already industrialized but the CZTS is emerging as a photovoltaic due to large area quality, high absorption and low-cost. The CdTe, CIGS and CIS have to face some snag due to Indium and Telluride that are the rare elements and their prices are now already increasing rapidly as they are highly used in the liquid crystal display industries [5]. Besides this, Iron Sulfide (FeS_2), Copper Sulphide (Cu_2S), Copper Oxide (Cu_2O) and Tin Sulphide (SnS) are also considered as the photovoltaic materials.

The researchers are synthesizing the CIS and CZTS based solar cells with the composition of Cu, Zn, Sn, In and S elements. These elements are available in the earth's crust as ~50, 75, 2.2 and 260 ppm (parts per million), respectively, but on the other hand, the availability of Indium is ~0.049 ppm only [6]. Due to toxicity of Cd and Se and availability issues of In and Te, the production of the photovoltaic devices based on these absorber layer is limited. Therefore it is required to replace by Zn and Sn, which have emerged the quaternary compound I-II-IV-VI group elements: $Cu_2ZnSn(S/Se)_4$ as shown Fig. 1.2 [9]. The CZTS has mind attention to the researchers due to the photovoltaic properties. The champion fficiency of the CZTS-Se is 12.6%, but the Shockley Queisser (SQ) limit predicted that the efficiency of photovoltaic materials would be ~32.2% [7,8]. Hence, the probability of research in the quaternary compound I-II-IV-VI group elements is remained to be carried out in the field of the solar cells.

The kesterite (CZTS) has the classic photovoltaic properties like

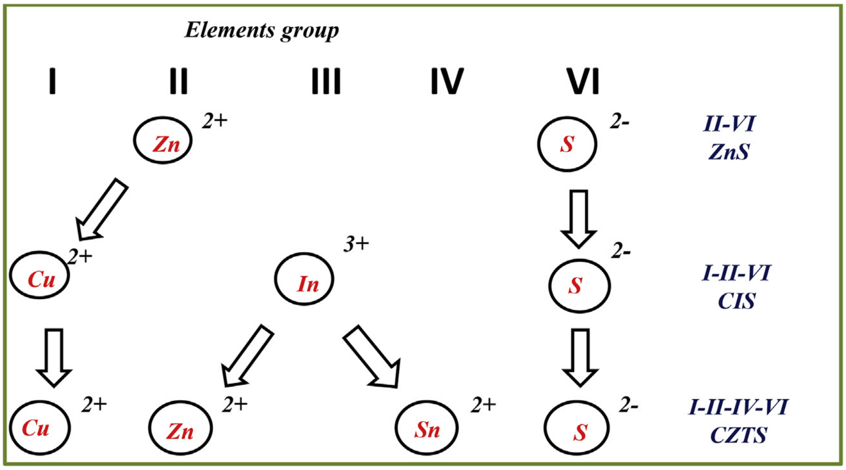

Fig. 1.2. The relationship between binary, ternary, and quaternary semiconductors to produce CZTS starting from II-VI compound, permission taken.

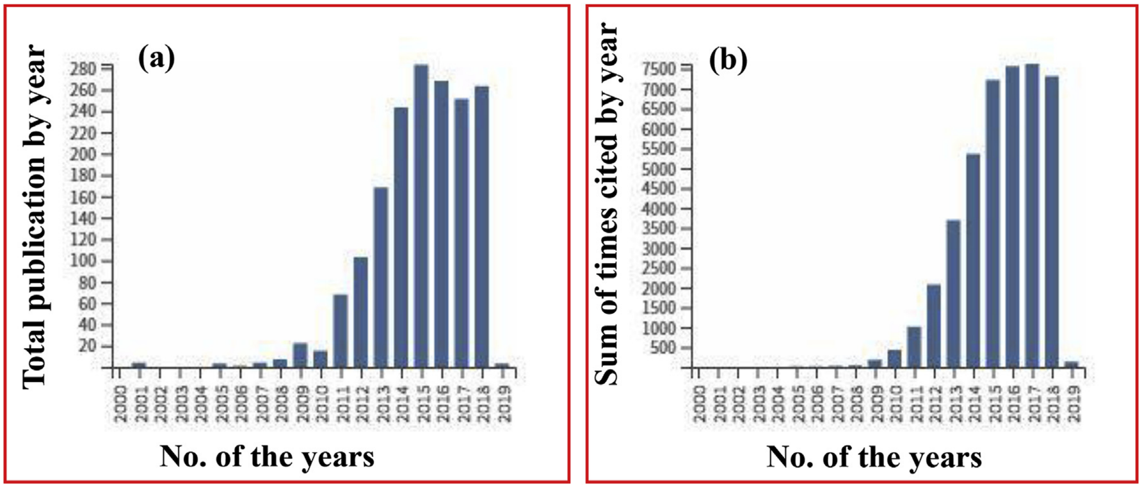

Fig. 1.3. Up gradation of Kesterite CZTS publication year wise shown in chart-flow in solar cell context: (a) Number of the publication versus Years, (b) Number of the citation versus Years. (Source: the web of the science).

direct-band gap, high absorption coefficient and optical band gap energy of the range 1.4–1.5 eV which is highly desired for the photovoltaic materials [10-23]. The Copper Zinc Tin Sulphide/Selenide shows two types of the equilibrium states. First one is the kesterite ($I\bar{4}$) and second one is the stannite (I42 m), which can be explained by crystallographically studies. The kesterite provides more stable equilibrium than the stannite. These structures are similar to each other, but they expected in different positions of the Cu and Zn. It is well known that the kesterite (CZTS) compound appears more thermo-dynamically stable in comparison to stannite compound [24]. The constituents of CZTS are easily available in the earth crust that is non-toxic and low cost.

The literature survey shows a large number of the publications and their citations in this field. It predicts that a lot of works are going on the kesterite phase for the photovoltaic applications as shown in Fig. 1.3. Due to the high absorbance and the direct band gap of the CZTS, there is another application of the CZTS such as photoluminescence [10-23]. The kesterite absorbers demonstrate the high absorption coefficient of > 10^4 cm^{-1} and the direct tunable band gap in the range of 1.0–1.5 eV, which allows for the effective absorption of incident photons in the absorbers with thicknesses of a few micron [25].

Owing to the optimal characteristics of the CZTS, the CZTS enables generation up to 32.2% power conversion efficiency with photons of energy 1.1–1.6 eV. According to the Shockley–Queisser theory, in the maximum probability of conversion of the solar energy to the electricity is more suitable for the overall working materials due to having the large area quality, high absorption and low-cost [7]. Fig. 1.4 shows the salient features of the CZTS/Se that are highly absorbed, earth-abundant and tunable direct band gap materials. These are the valuable parameters for the fabrication of the modern CZTS kesterite solar cell to generate power conversion efficiency up to 32.2%.

1.1. Fundamental properties

To investigate the physical and the chemical properties of the kesterite material, we study the properties of material, such as equilibrium of the kesterite, phase of the kesterite, energy band of the kesterite, etc.

1.1.1. Equilibrium of the kesterite

A lot of controversies are presented to explain the structure of Cu_2ZnSnS_4. By the first principle of study, it is proved that the kesterite is the more stable compound as compared to mono-crystalline Cu_2ZnSnS/Se_4 stannite structure in an I_2-II-IV-VI_4 group, as the stannite phase has slightly higher energy than the kesterite [26]. The copper and the zinc atoms are in an alternate position or d-wick-off position of the space group; where there is equal probability to take alternate statistically occupied positions [27]. The partial disordering of the Cu—Zn atomic layer is made in the kesterite and the stannite. The difference between the atomic numbers of the Cu and the Zn is minor. The molecule growth's temperature is high because these elements have high melting point.

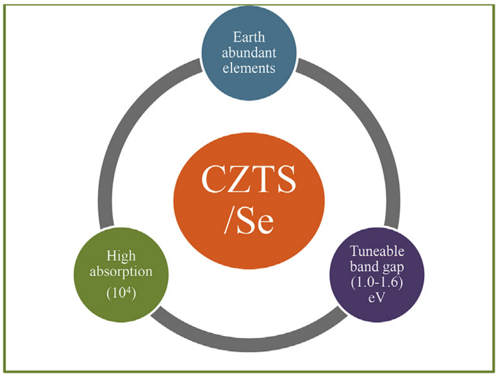

Fig. 1.4. The salient features of CZTS/Se which are highly absorbent, rare earth metal and tunable direct band gap.

Mostly, the thin film deposition of the CZTS as an absorber layer has been produced at 500^0–600 °C temperature. This temperature supplies the sufficient energy for the solid-state chemical reaction and the grains growth, the defects free grain boundary; and inserts the volatile specy from the gas phase to the solid phase. At the elevated temperature, CZTS is formed as the equilibrium phase with two volatile phases SnS_2 and S. To control these phases, the Le-Chatelier principle on post-deposition high-temperature annealing of the CZTS film is followed [28].

In the chemical equilibrium of CZTS, the forward and the backward reactions are occurred at the same rate at the atomic and molecular levels. Hence, there is no net change in the concentration of products and reactants; as shown in equations in two steps given below [29];

$$Cu_2S(s) + ZnS(s) + SnS(s) + \frac{1}{2}S_2 \Leftrightarrow CZTS(s) \tag{1.1}$$

$$SnS(s) \Leftrightarrow SnS(g) \tag{1.2}$$

In the equilibrium state of CZTS, the kesterite has to be the standards value of lattice a = 0.5435 nm, c = 1.0843 nm. The lattice constants are varying with the element ratio of sulphur and selenium. In

Table 1a
The lattice constant and the band gap of CZTS and CZTSe in the tetragonal unit cell of the kesterite structure.

Compound	Conductivity	a (A^0)	c (A^0)	Band gap (eV)	Reference
Sulphide	p-type	5.427	10.840	1.5	[30]
Selenide	p-type	5.40	10.846	1.0	[31]

the study of variation of sulphur and selenium quantities, the lattice constants of sulphide are less than that of selenide in the kesterite as shown in Table 1a.

From Table 1a, it is clear that the CZTS is better than the CZTSe because sulphide have more accurate values of lattice constants and band gap. On the basis of these properties, we can say that the CZTS is the counter-part of the CIGS. Some more physical, chemical and structural properties of the CZTS are compared with the CIGS. The composition of CIGSe, CZTSe and CZTSSe are also compared with these CZTS and CIGS. This comparison is explained in Table 1b, which helps to explain the photovoltaic aspects of the CZTS.

From the above Table 1b, it has been cleared that the maximum properties of the kesterite are similar to the CIGS. The charge carriers concentration and current density of the kesterite are slightly better than the CIGS. Due to which, we can say that the CZTS is best substitute for the CIGS for photovoltaic application. And it is well known that only charge carriers' lifetime (250 ns) is the main factor of the CIGS for high efficiency. But the CZTS has very low charge carriers lifetime (2.5/15 ns). Hence, the major problem is that the kesterite CZTS has very high recombination rate and it is a typical task to synthesize the pure CZTS materials. On synthesizing the CZTS, the secondary phases are also formed and those will be explained in the next section. Though there is no appropriate characterization technique to identify the exact phase of kesterite, but nevertheless the research work is going under the progress.

1.1.2. Phase of the kesterite

Synthesizing the quaternary compound (I_2-II-IV-VI_4) is more complex in the comparison to ternary, binary and unary phase because it is difficult to control morphology, phase structure and stoichiometry. On synthesizing the quaternary compound Cu_2ZnSnS_4, the quaternary (Cu_2ZnSnS_4), ternary (Cu_2SnS_3), binary compounds (CuS, ZnS, SnS, Cu_2S, SnS_2) phases are found. The properties of the secondary phases are described in Table 1c. These secondary and ternary phases influence the histrionics of the kesterite solar cell.

From Table 1c, it is cleared that binary phase ZnS is the main hurdle because it generally created during synthesis and insulator type phase. In X-ray diffraction (XRD) in characterization of the CZTS, the peaks are overlapped of ZnS and CZTS at (112) plane due to which it is typical task to analyse the XRD data of CZTS. So, this phenomenon is identified by Raman spectroscopy characterization. This ZnS phase can be removed by etching the HCl. And the other phases (CuS, Cu_2S, SnS and SnS_2) can be removed by etching the KCN. The formation of these phases is disturbed the phase equilibrium. The phase equilibrium can be controlled by the variation of composition of element ratio, temperature and pressure. To optimize the suitable phase, it is compulsory to take one parameter and other parameters variable [41]. Several research works have been done on the kesterite with the variation of the composition of element, temperature and pressure, which are explained in section 3.0. The variation of these parameters affects the solar cell performance. Hence, the limitations of elements composition ratio: Cu/(Zn + Sn) and Zn/Sn, controlling phases and defects for growth of single-phase the kesterite are required. The photovoltaic performance is affected on the composition ratio variation. For better performance of the solar cell, the research works have done by considering two ways (i) either Cu poor or (ii) Cu rich.

The single phase kesterite formation is found in the narrow range of chemical energy, $-0.4 < \mu_{Cu} < 0$, where phase space is studied by the first principle study [42-44]. For the stability, the kesterite must have the formation energy -4.21 eV and the secondary phase ZnS has formation energy -1.75 eV. Mostly, high-efficiency devices are associated with the Cu-poor and Zn-rich condition because it preferences the copper vacancy defect, which helps to increase the efficiency which is described in the next section. Mitzi et al. [45] recommended the conditions of Cu-poor and Zn-rich for the growth of world record highly efficient CZTSSe device under the equilibrium conditions. Kategri et al. [46] investigated the pseudo-ternary phase diagram of the Cu_2ZnSnS_4 system to grow the formation of kesterite family and proposed CZTS having high dependency on composition and temperature as shown in Fig. 1.5.

1.2. Energy band of the kesterite

The total energy of the band and the band structure of the kesterite can be identified by the first principle study, the density functional theory (DFT). There is one electronic parameter like the band gap, which is obtained by the semi-local functional, PW91 [47]. To obtain the quantitative estimation of the changed band gap, the hybrid functional theory is used such as the Hartree-Folk, the HSE (Heyd-Scuseria-Ernzerhof) and the screening constant□(= 0.11 bohr^{-1}) and the energy exchange-correlation is given as [47,48];

$$E_{xc}^{HSE}(\omega) = \frac{1}{4}E_x^{Fock,SR} + \frac{3}{4}E_x^{PBE,SR} + E_x^{PBE,LR} + E_C^{PBE} \tag{1.3}$$

where first term represents the exchange component of electron-electron interaction that is separated in short range or Fock exchange energy in short range and second, third, fourth terms are the exchange energies calculated by the generalized gradient approximation (GGA) density functional in short range, long range and direct exchange energy, respectively. By equation (1.1), the energy band gaps of CZTS and

Table 1b
The comparative study of chalcoginide CZTS, CZTSe, CZTSSe, CIGS and CIGSe with different properties.

Properties	CZTS	CZTSe	CZTSSe	CIGS	CIGSe	Ref.
Lattice constants (a, c) A^0	a = 5.427, b = 10.840	a = 5.40, b = 10.846	a = 5.40 b = 10.846	a = 5.6–5.8, c = 11.0–11.5	a = 5.6–5.8, c = 11.0–11.5	[30,31]
Space group	$I\bar{4}$/I42 m	$I\bar{4}$/I42 m	$I\bar{4}$/I42 m	$I\bar{4}2d$	$I\bar{4}2d$	
Crystal structure	Tetragonal	Tetragonal	Tetragonal	Tetragonal	Tetragonal	[32,33]
Density (gm/cm^3)	4.56	4.56	4.56	5.7	5.7	[32]
Band gap (eV)	1.4–1.5	1.0	1.4–1.5	1.0–1.7	1.0–1.7	[33,34]
Crystal energy (meV/atom)	2.86	2.86	2.86	–	–	[35]
Absorption coeff. (cm^{-1})	10^4	10^4–10^5	10^4–10^5	10^4–10^5	10^4–10^5	[34]
Carrier concentrations (cm^{-1})	10^{15}–10^{20}	10^{15}–10^{20}	10^{15}–10^{20}	$10^{17–18}$	$10^{17–18}$	[29]
Carriers lifetime majority/minority (ns)	15/2.5	15/2.5	15/2.5	250	–	[36]
Current density (mA/cm^2)	10^{-6}-10^{-3}	10^{-6}-10^{-3}	10^{-6}-10^{-3}	10^{-8}	–	[37]
Melting point (^{0}C)	990	990	990	1070-990	1070-990	[38,40]
Efficiency (%)	8.4	10.1	12.6	22.6	–	[8,39,69]

Table 1c
The characteristics of the secondary phases in the Kesterite are given below.

Properties	CZTS	ZnS	CuS	Cu_2S	SnS_2	Cu_2SnS_3
Band gap (eV)	1.4–1.5	3.54–3.68	1.55	1.21	2.2	0.98–1.35
Structural properties	Kesterite type $I\bar{4}$	Sphalerite & Wurtzite $I\bar{4}3m$	Hexagonal crystal	Chalcocite	Rhombohedral	Cubic and Tetragonal
Electrical properties	Semi-conductor, p-type	Insulator, p-type	p-type	metal like, highly defective	n-type	p-type
Effect on solar cell	Absorbing material	Active area/photocurrent reduce	Positive response	Short the solar cell	n-type, forms diode and barrier for carrier collection	Affect carrier Collection at electrode/V_{oc}
Removal of Secondary phases		ZnS:HCl, ZnSe: $(KMnO_4+H_2SO_4)/Na_2S$ Etching	KCN	KCN	KCN Etching	KCN Etching

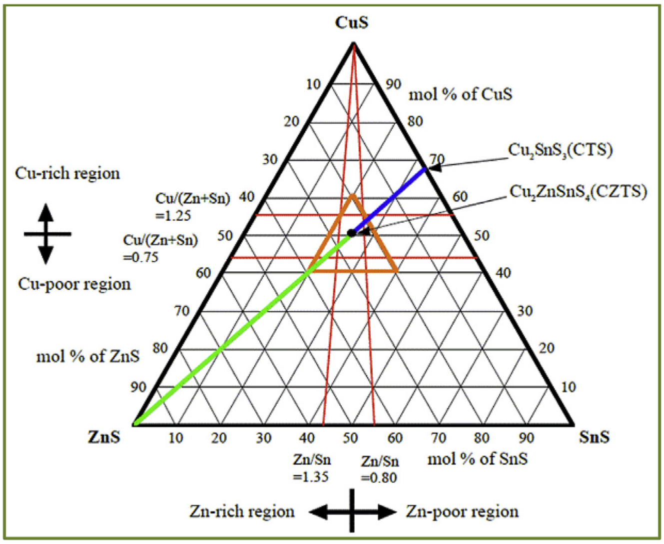

Fig. 1.5. Phase diagram of the CZTS pseudo-ternary system is consist of CuS, ZnS, SnS with ratio 50:25:25 respectively. Reproduced with the permission.

CZTSe are calculated and the values have been matched with the experimental results [49-51].

The energy stability in the band gaps is explained by Chen et al. [47] which are followed as;

(i) The kesterite has lower energy than the stannite and the Wurtzite (WZ) kesterite has also lower energy than the Wurtzite stannite.
(ii) The kesterite structure is more stable than the stannite (Cu_2Cd-IV-S_4 series exception case in the Stannite).
(iii) The energy difference between kesterite and Stannite becomes smaller monotonically as IV-group cations changes from Si to Sn element.
(iv) All the above facts are common for sulphide and selenide compounds.

The electrostatic Madelung energy is correlated with the stability of the Wurtzite (WZ) structure versus the Zinc Blende (ZB) structure that is identified by the binary WZ and ZB structures. The total energy of the kesterite depends on the sum of both the Madelung energy and the strain energy. The strain and the Madelung energy of kesterite are lower compare to stannite. Due to the low strain and low Madelung energies, the kesterite is found in the ground state. Hence, the kesterite is more stable than the stannite.

1.3. Band structure

The group I_2-II-IV-VI_4 compound has a tetrahedral geometry which is similar to group-IV, III-V, II-VI semiconductors. This compound contains eight electrons around each anion and forms the four bonds with a closed valence shell. The electronic band structure of the quaternary compound CZTS and CZTSe is shown clearly in Fig. 1.6 and the density of states are calculated by the first principle method [29]. The figure shows the four symmetry directions comparable to the band structure of CIGS,Se. The energy refers to the valence band maximum (dashed lines). The spin-orbit interaction is also included, but the index of the bands (j = v_1, v_2, v_3 and c_1) refers to spin-independent bands, where c_1 represents the lowest conduction band or conduction band minimum (CBM) and v_1 represents the topmost valance band or valance band maximum (VBM).

In the chain of band structure explanation, Chen et al. [47] have found the following results:

(i) The I_2-II-IV-VI_4 compound semiconductors have the direct band gap at the Γ-point (the calculated band gap energy shown in Table 1d).
(ii) The top valence band (VBM) has the anti-bonding component of the p-d orbital hybridization between the VI-group anion and the I-group cation.
(iii) The bottom conduction band (CBM) has the anti-bonding component of s-s and s-p orbital hybridization between the IV-group cation and VI-group anion.

As the group-IV cations change from Si to Ge and Sn, the band gaps are decreased in the order identified by GGA, GGA + HSE, HSE functional method as shown in Fig. 1.7.

In Table 1d, the kesterite structure has E_g = 1.56 eV in CZTS and E_g = 1.05 eV in CZTSe as calculated by the GGA + QP density functional theory. These calculated results agree well with band-gap determination by the various measurement techniques [52–63]. (see Fig. 1.7).

2. The progress of conversion efficiencies of kesterite solar cells

In 1988, Ito and Nakazawa [64] had reported the photovoltaic effect of CZTS material for first time and they found open-circuit voltage of 165 mV with such device. After that Friedlander and Kategri [41,65] also reported and modified results of conversion efficiencies with 2.3% and 2.63%. In 2008, Kategri group [68] had reported the increased efficiency of the solar cells by 6.3% through the optimization by sulfurization. In same year, more than thousands of papers have been published on the CZTS synthesis and some of the papers were reported the good results of the photovoltaic application. The current world record efficiency of the kesterite CZTS Se based thin film solar cells is 12.6% [8]. In 2010, Todorov et al. [67] had already reported that CZTSSe based solar cells had obtained 9.6%. The total progress of highest conversion efficiencies of CZTS, CZTSe, CZTS,Se in lustrum timing is shown in Fig. 2.1(a&b). The latest world record efficiency is achieved in joint research with the IBM and the Tokyo Ohka Kogyo (TOK) and has also been independently verified by Newport

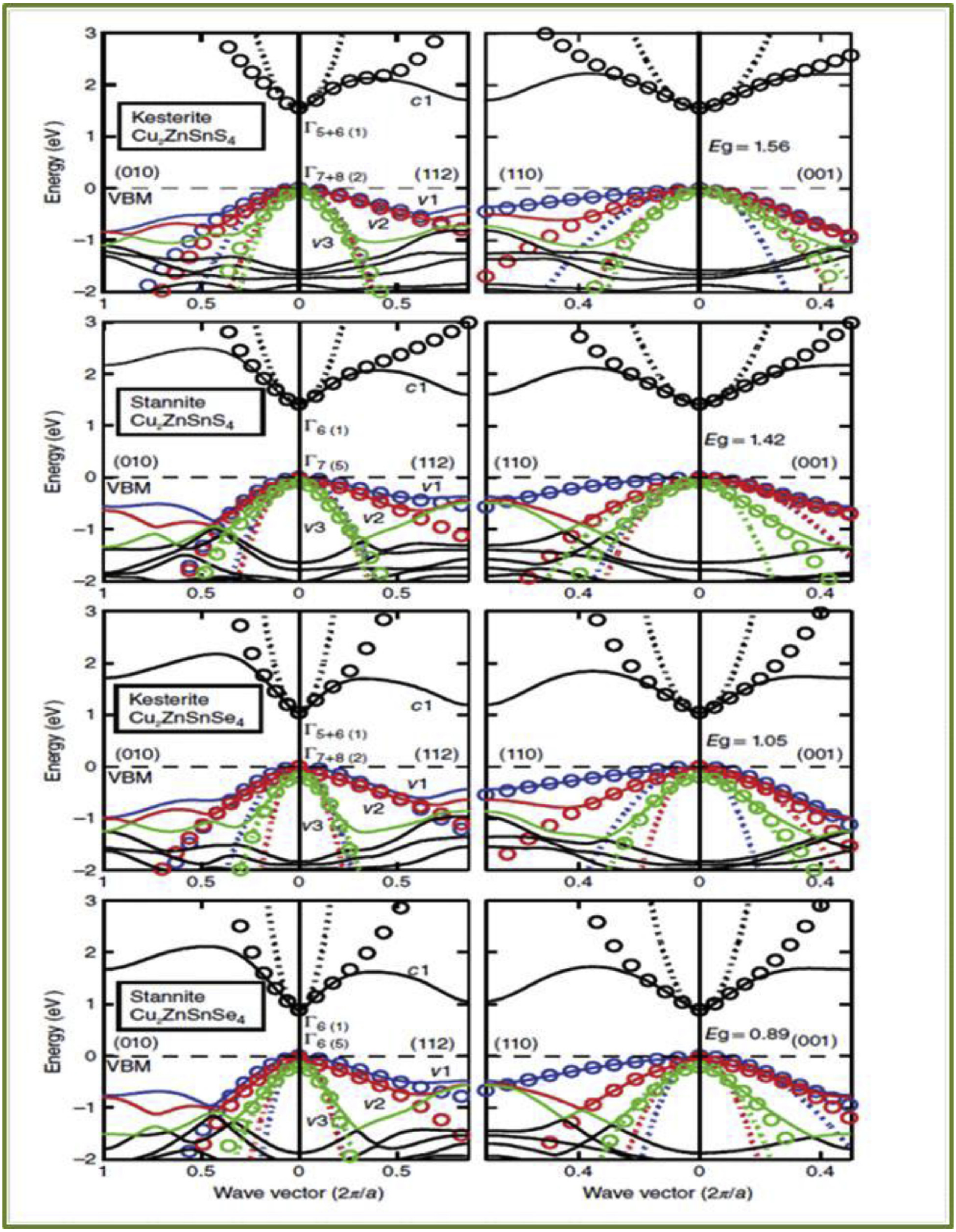

Fig. 1.6. The electronic band structure $E_j(k)$ of the kesterite and Stannite structures of CZTS and CZTSe along four symmetry directions. Reproduced with the permission.

Table 1d
The calculated Γ-point band-gap energy (E_g) of kesterite and Stannite.

Methods	CZTS kesterite (eV)	CZTS stannite (eV)	CZTSe kesterite (eV)	CZTSe stannite (eV)
GGA + QP	1.56	1.42	1.05	0.89
HSE06	1.47	1.27	0.90	0.70
GW_0	1.57	1.40	0.72	0.85

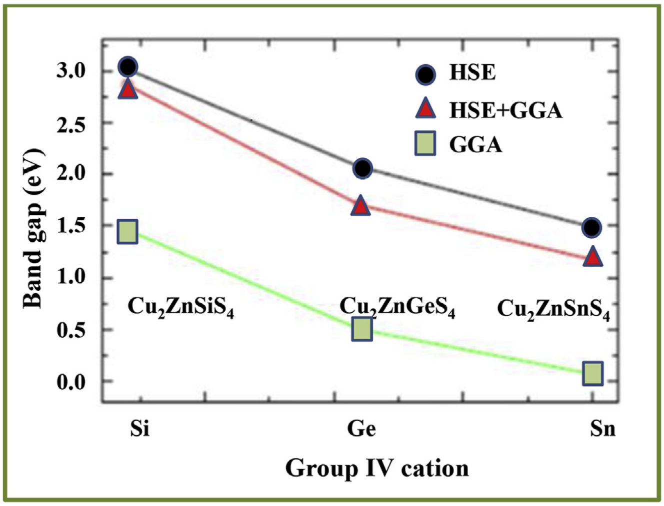

Fig. 1.7. Calculated band gap of kesterite $Cu_2Zn\text{-}IV\text{-}S_4$ which decreases as the group-IV cations change from Si to Ge to Sn, using the methods: (i) GGA functional (green), (ii) GGA + HSE functional (red), (iii) HSE functional (blue). Reproduced with the permission.

Corporation[72-76]. The current highest reported conversion efficiencies of the kesterite are shown in below Table 2a by different synthesis methods.

2.1. Sprayed kesterite

The vacuum and the non-vacuum based techniques are used to synthesize the kesterite CZTS. In the non-vacuum, the spray pyrolysis is mostly used to synthesize the sulphide and the oxide because this method is very cheap, easily available, having high roughness surface film and easy to grow the multilayers in the controlled thickness. The highest record conversion efficiency of pure sulphur based on the sprayed kesterite is shown in Table 2b. Some important parameters in sprayed kesterite are carrier gas, spray atmosphere, substrate temperature and annealing condition.

Larramona et al. [77] had reported more than 5.0% efficient for spray coated CZTS solar cell. To fabricate the solar cell, they deposited the CZTS film in two parts and fabricated the solar cell. In the first part, Cu—Zn—Sn—S colloidal dispersion in the ethanol and water solvent were used in the spray-pyrolysis method. They used XY-axis robotic spray pyrolysis set-up and N_2 carrier gas in N_2 glove box. In the second part, two-steps for annealing process: (i) annealed 15 min at 525 °C with the pure N_2 atmosphere (ii) annealed 60 min at 525 °C with H_2S (3% N_2) atmosphere and after that they got finally 2 μm thick film. They deposited the buffer layer of cadmium sulphide (CdS, 60 nm) by chemical bath deposition (CBD) and etching by HCl (8%). and sample was finalized with the deposition of intrinsic zinc oxide (i-ZnO, 60 nm) and Indium Tin Oxide (ITO, 250 nm) as a window layer by using magnetron sputtering.

3. Parameters to affect the performance of solar cell efficiency and photoluminescence performance

There is a lot of works have been done on the CZTS for solar cell application but nevertheless is not commercialized and because the CdS/CZTS solar cell efficiency depends on open circuit voltage (V_{oc}), current density (J_{sc}) and fill factor (FF). The solar cell efficiency parameters are shown in Fig. 3.1. The open circuit voltage (V_{oc}) is urged by carrier generation and recombination near the charge-separating junction in solar cell and plays a dominant role. Thus, the CdS/CZTSSe solar cell has the conversion efficiency approximately 12.6% [8]. Hence, the fault of the deficit in the efficiency of the solar cell have been deliberated by the researchers to understand the junction characteristics, current collection and recombination mechanisms in the current generation of devices.

In the CdS/CZTS solar cell, the junction characteristics, the current collection and the recombination mechanisms are modified by the variation in parameters, such as the composition of element (defects and graineries are created), the substrate temperature, the annealing, the sulpherisation, the concentration, the pH of salt's solution and the interface carrier recombination centre. The absorber composite CZTS has direct band gap with 1.4–1.6 eV, radiative and non-radiative recombination having the high absorption coefficient in visible energy range. Thus, these properties are suitable for photoluminescence as well as for solar cell. Most of the cases, the CZTS shows a broad peak of 1.3 eV in photoluminescence spectroscopy [83-87]. Grossberg et al. [88] detected two peaks of photoluminescence due to the random distribution of defects, potential fluctuates in CZTS. Thus, the perturbation of the band structure is created and the photoluminescence peaks are shifted to the lower energies [89] and vice-versa in the

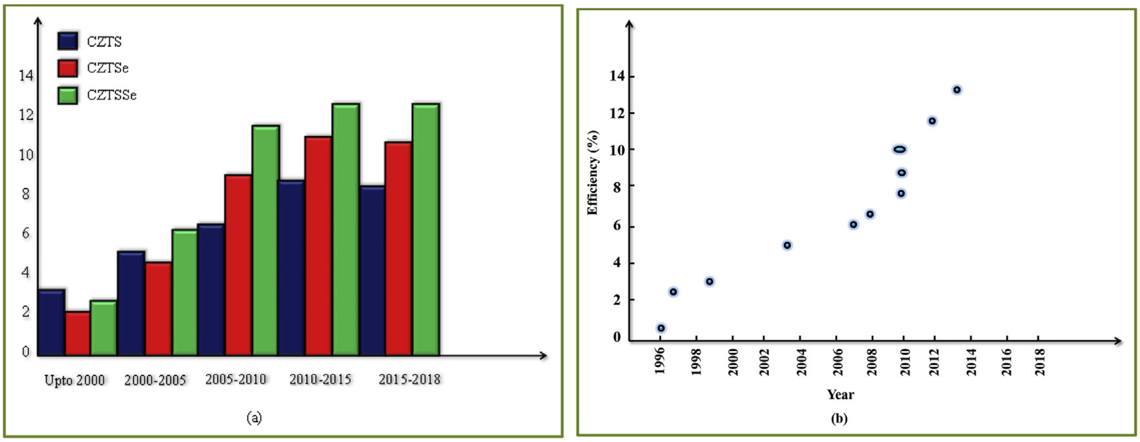

Fig. 2.1. (a&b) The highest efficiency development chart of CZTS, CZTSe, CZTSSe. The total progress in the best conversion efficiency of Kesterite solar cell is in lustrum timing. Development of conversion efficiency of kesterite thin film solar cells in biennium timing. Self-designed (a) and (b) reproduced with the permission.

Table 2a
The current highest reported conversion efficiency of kesterite solar cell is shown with V_{oc} open circuit voltage, J_{sc} current densities and fill factor (FF).

Methods	Materials	Voc (mV)	J_{sc} (mA/cm^2)	FF	Conv. effi. (%)	Time	Ref.
CBD method (non-vacuum)	CZTS	610	17.9	62.0	6.67	2008	[66]
Thermal evaporation (vacuum)	CZTS	661	19.5	65.8	8.84	2011	[69]
Spin coating (Vacuum)	CZTSe	422.8	38.7	61.9	10.1	2012	[48]
Electro-deposition (Non-vacuum)	CZTSe	390.0	35.3	58.0	8.0	2014	[70]
Hydrazine- slurry method (vacuum)	CZTSSe	513.4	35.2	69.8	12.6	2014	[8]
Spray Pyrolysis method (non-vacuum)	CZTSSe	–	–	–	5.1	2014	[71]

Table 2b
The highest conversion efficiency of pure Sulphur based sprayed kesterite

Spray type/key	Precursors/solvent/carrier gas	Substrate temperature [^{0}C]/ etching	Annealing condition	J_{sc} (mA/ cm^2)	Voc (mV)	FF (%) Area (cm^2)	Eff. [%]	R_s/R_{sh} (Ω cm^2)	Ref.
Pneumatic XY robotics	$CuCl_2$,$ZnCl_2$, $SnCl_4$, NaHS/water + ethanol/N_2 (glove box)	300 °C/HCl (8%)	N_2; 525 °C, 15min + H_2S; 525 °C, 60 min	19	630	50 0.25	5	4/300	[77]
Pneumatic/(8 nm)	$CuCl_2$, $ZnCH_3COOH$, $SnCl_4$, NH_3CSNH_3/ water/air (air)	331	331, 30 min	8.3	430	52	1.8	9.7/252	[78]
Pneumatic/	$CuCl_2$, $ZnCH_3COOH$, $SnCl_4$, NH_3CSNH_3/ water/Ar (Ar box)	360/KCN (1%)	Ar, S + Sn + 580 °C, 30 min	9.8	421	34.3 0.09	1.4	18/89	[79]
Pneumatic/Ar and Ar + H_2 carrier gas	$CuCl_2$, $ZnCH_3COOH$, $SnCl_4$, $NH3CSNH_3$/ water/Ar (Ar)	220 KCN (1%)	Ar, S + Sn + 580 °C, 30 min	10.7	407	33 0.09	1.4	17/70.8	[80]
Pneumatic/	$CuCl_2$, $ZnCH_3COOH$, $SnCl_4$, NH_3CSNH_3/ water/Ar (Ar)	350 KCN (1%)	Ar, S + Sn + 580 °C, 30 min	10.3	356	32.5 0.09	1.2	16/61	[36]
Pneumatic/	$CuCl_2$, $ZnCH_3COOH$, $SnCl_4$, $NH3CSNH_3$/ water/Ar (Ar)	450 KCN (1%)	Ar, S + Sn + 580 °C, 30 min	7.5	361	37.1 0.09	1	15	[81]
Pneumatic/	$CuCl_2$, $ZnCH_3COOH$, $SnCl_4$, NH_3CSNH_3/water/Ar + H_2 (Air)	220 KCN (1%)	Ar, S + Sn + 580 °C 30 min	10.7	407	33	1.4	17.3/ 70.8	[82]

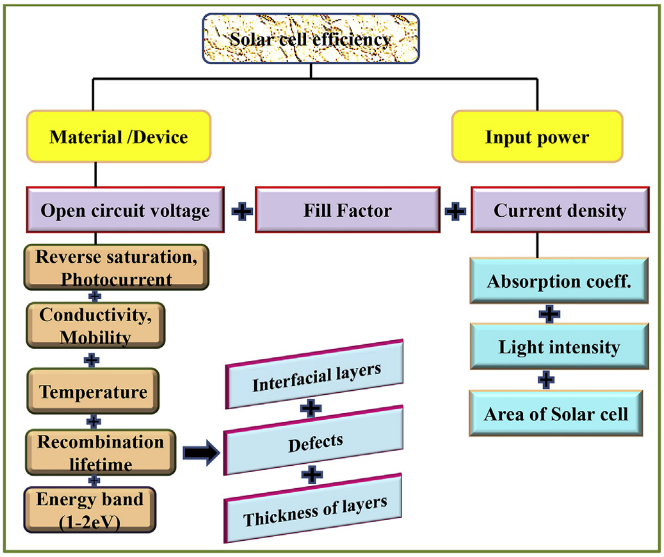

Fig. 3.1. The block diagram of the solar cell efficiency parameters is shown.

excitation power [90-93].

3.1. Effect of composition of elements ratio

The effect of the variation of constituent elements of the CZTS results as the variation of characteristic of the composite with surface morphology and microstructure, i.e., graineries and defects, photoluminescence (PL) properties. These parameters affect the solar cell performance directly. The variation of constituent elements quantitatively influenced the kesterite properties such as Cu poor and Zn rich ratio having better photovoltaic properties [94]. The composition ratio versus efficiency is shown in Fig. 3.2. From this figure, it is concluded that the highest efficiency region would be changed by Cu/(Zn + Sn) and Zn/Sn. The values of the Cu/(Zn + Sn) and Zn/Sn could be laid in between 0.80-0.90 and 1.2–1.3, respectively. The particle size increases with increasing the Cu/(Zn + Sn) ratio as reported by Sahayraja et al. [182]. The particle size is obtained up to 1 μm for 0.80–0.90 for Cu/(Zn + Sn) and 1.2–1.3 for Zn/Sn [182]. The high efficiency of the CZTS device was reported at this size of the particle. Ref. [95-98] were also reported the photovoltaic properties of CIS and CIGS that are dependent on the ratio of Cu/In and Cu/(In + Ga) and investigated the effect of Cu/(Zn + Sn) and Zn/Sn in CZTS,Se. This is randomly created bulk defects and affected the grain sizes. The variation of Cu/Zn + Sn and Zn/Sn ratio in the CZTS solar cell is shown in Table 3a. On study the review literature of the kesterite, the suitable composition ratio Cu-poor and Zn-rich would be laid 0.80–0.90 for Cu/(Zn + Sn), 1.1–1.3 for Zn/Sn and 1.6 for Cu/Sn to get the high-efficiency solar cell as shown in

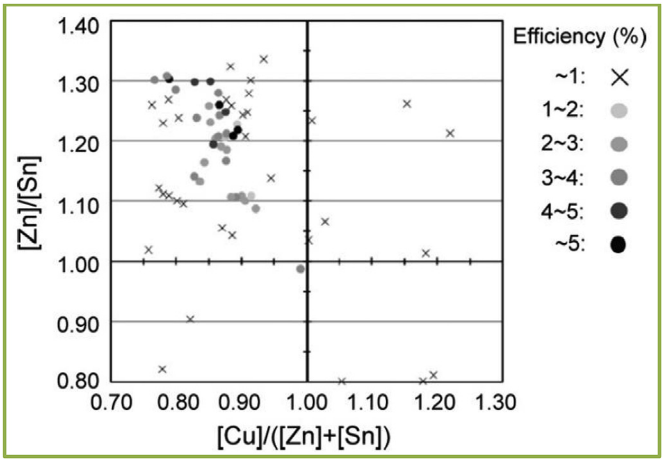

Fig. 3.2. The composition ratio of Cu/(Zn + Sn) and Zn/Sn with the efficiency. Reproduced with permission.

Table 3a
The role of composition ratio in the Kesterite characterization analyzed

Methods/Material	Precursor Salts/Solvents/Temperature	Ratio Cu/(Zn + Sn) or Zn/Sn	Characterization	Applications	Ref.
Co-evaporation/CZTSe	Cu, ZnSe, Sn, Se/$T_{sub.} = 623^0$ K, $T_{an.} = 723^0$ K	0.85–1.15	● 0.90–1.10 ● Single phase ● Polycrystalline ● Kesterite ● The intensity of (1 1 2) increased ● FWHM decrease ● Band gap, and resistivity (23–0.02 Ohm-cm) decreased with ratio increases ● Grain size decreases with ratio decreases ● Grains densely packed and roughness 3–5 nm in Cu-poor ● a = 0.568 nm, c = 1.138 nm	–	[100]
Multilayer of precursors by e-evaporation/CZTS	ZnS, Sn, Cu/T_{sulf} = 550 °C with Nitrogen (1 h)	0.813–0.659	● a = 5.432 and c = 10.835 Å. ● Anti-sites Zn_{Sn} or Cu_{Sn}, Sn_{Zn} and V_{Sn} vacancy defects ● Intensities tell Stannite phase absent ● Average grain size ● The energy gap (1.47–1.63 eV) increases with the ratio of Tin ● The density of acceptor defects V_{Sn}, Cu_{Sn}, and Zn_{Sn} anti-sites reduced Tin content	–	[101]
RF co-sputtering/CZTS	Cu, ZnS, Sn, SnS/flow rate: 50 sccm, Ar gas: pressure = 0.5 Pa, Sub. Rotation = 20 rpm, Pre-sputter time = 3 min, T_{an} = 580 °C (5 °C/mnt)	0.75–1.25, 0.80–1.35	● Optimum band gap = 1.5 eV ● Abs. Coef. = 10^{-4} cm^{-1} ● Pseudo-ternary CuS−ZnS−SnS phase diagram	Solar cell	[102]
Spray Pyrolysis/CZTS	Cupric Chloride, Zinc Acetate, Stannic Chloride, Thiourea/pH: 3.0, 4.5, 5.5/T_{sub} = 643 K, Spray Rate 12 ml/min,	0.90–1.32	● Polycrystalline ● Non-stoichiometric (pH = 3) ● Band gap = 1.45 eV ● a = 0.542 nm, c = 1.085 nm ● Resistivity = 0.1 Ω cm-2.9 Ω cm	–	[103]
Vacuum evaporation/CZTS	Cu, Zn, Sn, S salts, T_{sub} = 550 °C,	0.82–1.06,1.1	● Grain size ≥1 µm increased, Resistivity decreased (2.5 × 10 − 1 Ω cm-7.0 × 10 − 3 Ω cm) ● Better crystallinity with increasing ratio	Solar cell	[104]
Sol-Gel/CZTS	Copper acetate monohydrate, Zinc acetate di-hydrate, Tin chloride die-hydrate, DW, ammonium acetate, N_2 and H_2S (5%) at 500 °C for 1 h	0.73–1.0, 1.15	● Amount of Zn or Sn decreased with increasing Cu ratio ● The grain size increased as the ratio of decreased ● Band gap (1.62–1.40 eV) ● Cu/(Zn + Sn) = 0.80 exhibited The highest efficiency due to the large grains	A solar cell (2.03%)	[105]
Spray pyrolysis/CZTS	$CuCl_2$, $Zn(CH_3CO_2)_2$ $SnCl_4$, $SC(NH_2)_2$/T_{sub} = 450 °C, air Pressure = 20,000 Pa, Spray deposition rate = 3 ml/min (20 min time)	0.73–1.0	● Increasing temperature (°C) helps grain size growth (550 °C - 580 °C) ● CTS, CZTS phases ● Low-frequency band presented ● Low resistivity with high ZnS binary phase concentration	A solar cell (0.49%)	[106]
Multilayer precursors by e-beam evaporation/CZTS	ZnS, Sn, Cu, T_{sub} = 150, multiple layers structure: ZnS/Cu/Sn/ZnS/Cu/Sn/ZnS	0.92–0.75	● Transmittance wavelength range (250–2500 nm) ● Spurious phases ($Cu_{(2-x)}S$, $Cu_xSn_yS_z$, Sn_xS_y) ● Band gap 1.48–1.62 eV ● Band gap shrinkage with the increase of the [Cu]/[Sn] ratio defect-induced on band gap ● Shrinkage acceptor defects (V_{Sn}, Cu_{Sn}, and Zn_{Sn} anti-sites) created by reduced Tin content ● Density and the energy gap is not influenced by the Zn content but influenced [Sn]/[Cu] ratio		[107]

(*continued on next page*)

Table 3a (*continued*)

Methods/Material	Precursor Salts/Solvents/Temperature	Ratio Cu/(Zn + Sn) or Zn/Sn	Characterization	Applications	Ref.
Co-evaporation/AZTSe	Ag, Zn, Sn, Se/T_{sub} = 150 °C, T_{anml} = 500 °C, Thickness-2μm, Etching by KCN (1 M) for 3 min/pressure = 10^{-9} Torr	Ag/Sn = 1.50–1.85, Zn/Sn = 1.03–1.15	● Ag-poor (smaller grains) ● ZnSe, Ag_2Se, Ag_8SnSe_6 secondary phases ● Carrier density (~1012/cm^3) and electron mobility (~100 cm^2/V.s) ● The PL intensity reduced on increasing Sn (decreasing the Ag/Sn ratio) increase average grain size ● Minimize non radiative recombination ● Prevent band gap ● Narrowing or the formation of deep defects on high Ag/Sn ratio	Solar cell	[108]

Fig. 3.2.

3.2. Role of defect in the device efficiency

The secondary phases play a major role in the device as discussed in Table 1c. The lattice defects also play crucial role to the recombination of electron-hole pairs, the generation and separation in the application of semiconductors for the photovoltaic devices. The defects have identified in the form of the vacancies, anti-sites, interstitials and defect complexes. Table 3b is indicated the defects, defect ionizations level and impact on the solar cell. The defects also created the shallow donor and acceptor levels and mid-gap and deep trap state between the band gaps of the kesterite [99].

The $V_{Cu,}$ Cu_{Zn} and Cu_{Zn} + Zn_{Cu} defects are favorable to improve the solar cell efficiency but other defects such as V_{Zn}, V_{Sn}, V_S, V_{Se} are unfavorable because V_{Cu} is the vacancy of Cu atom that creates the displacement of the atom in the unit cell of the CZTS. Similarly, other vacancies also create the displacement of the related atoms. When Cu atom displaces by Zn atom in the CZTS unit cell, then the anti-site defect Cu_{Zn} is created and similarly other anti-site defects are also created. However, when two anti-site defects combine then they make defect complexes [109–111]. These defects have a special ionization levels due to which the number of charge carrier or conductivity (p-type) and recombination are affected as V_S and V_{Se} form the mid-gap states while the V_{Zn} and V_{Sn} form the deep levels and mid gap states within the band gap range and Cu_{Zn} and Zn_{Cu} form the shallow acceptor and donor levels, respectively [112]. The anti-site Sn_{Zn} forms the two mid gap states and interstitials Cu_i, Zn_i form the shallow donor level and mid gap states in Cu rich/stoichiometric conditions. The non-stoichiometric condition/Cu poor Zn rich condition is beneficial for high efficiency of the solar cell, but also forms the undesirable defects [113]. The defect complexes Cu_{Zn} + Zn_{Cu}, Cu_{Sn} + Sn_{Cu}, Zn_{Sn} + $Sn_{Zn,}$ V_{Cu} + Zn_{Cu}, V_{Zn} + Sn_{Zn}, Zn_{Sn}+2Zn_{Cu}, 2Cu_{Zn} + Sn_{Sn} are formed by the vacancies, interstitials, anti-site defects in the CZTS because the formation energy is lower than the individual defect. Till date, no more works have been done on defects; it is not easy to observe the defects by any advanced instrument. The density of the defects in the CZTS is found 10^{18} cm^{-3} which has impact on the efficiency of the solar cell [112].

The ratio Cu/(Zn + Sn) and Zn/Sn impacts the solar cell efficiency due to carrier collection at the electrode because V_{Cu} and Cu_{Zn} antisite defects affect the p-type conductivity of CZTS [114]. The shallow donor Zn_{Cu} defect ionize to positive charge and behave as an electron sink and hole barrier. In CZTSSe solar cell, this defect creates inhomogeneity and increases the electron recombination as well as the open circuit voltage. The limited V_{oc} is controlled by deep level recombination centers in the bulk interface and grain boundary [115,116]. The defect (V_{Cu} + Zn_{Cu}) helps in the transportation of charge in CZTS,Se because this defect repels the majority charge carriers (holes) and collects the electrons to the n-type buffer layer. These can be created by the Cu poor and Zn rich condition [117]. But V_{oc} reduces in CZTSSe devices due to defects by the recombination centers at interfaces and grain boundaries in the bulk material. The point defect creates the band gap fluctuations due to non-uniform chemical stoichiometry [118]. Some defects like Zn_{Sn}, O_{Se}, Na_i, at the grain boundaries create the barrier for holes and helps to transport the electrons through the grain boundaries [119120].

3.3. Substrate temperatures/annealing/sulpherisation

The substrate temperature and the annealing or sulpherisation are other parameters that affect the physics of solar cell. The secondary phases, defects, lattice mismatch and diffusion of elements across the interface are created. The effect of substrate temperature investigated at room temperature (R_t) to 450 °C, the crystalline structure of the Kesterite is identified at 370 °C [66]. The grain size is increased with increasing temperature as shown inFig. 3.3.

Table 3b
The defect, ionization level and impacts on solar cell description given below

Type of defects	Ionization level of Defects	Formation Energy (eV)	Impact on CZTS solar cell
V_{Cu}	1 Acceptor (−)	0.02	Ionized from (0/0) to −1 state and transition level ε(-/0) forms the shallow state (favorable)
V_{Zn}	2 Acceptor (2-)	–	Deep levels (unfavorable)
V_{Sn}	4 Acceptor (4-)	–	Deep levels (unfavorable)
$V_{S/Se}$	1 Donor (−)	–	Mid-gap state (unfavorable)
Cu_{Zn}	1 Acceptor (−)	≥ 0.02	Deeper than V_{Cu} (favorable)
Zn_{Cu}	1 Donor (−)	–	Shallow level near the conduction band (unfavorable)
Cu_{Sn}	1 Acceptor (1-)	–	Deep and multi-levels (unfavorable)
Sn_{Cu}	2 Donor (2+)	–	Deep level and mid-gap state (unfavorable)
Zn_{Sn}	2 Acceptor (2-)	–	Deep levels (unfavorable)
Sn_{Zn}	2 Donor (2+)	–	Mid-gap states (unfavorable)
Cu_i	1 Donor (2+)	–	Shallow states near conduction band (unfavorable)
Zn_i	2 Donor (2+)	–	Mid-gap states (unfavorable)
Stoichiometry defect: $Cu_{Zn}+Zn_{Cu}$, $Cu_{Sn}+Sn_{Cu}$, $Zn_{Sn}+Sn_{Zn}$	–	≥ 2	$Cu_{Zn}+Zn_{Cu}$ low impact on optoelectronic properties and other decrease the band gap 0.3 eV
Non-stoichiometry defect: (V_{Cu} + Zn_{Cu}), (V_{Zn} + Sn_{Zn}), ($Zn_{Sn}+2Zn_{Cu}$), ($2Cu_{Zn}$ + Sn_{Sn})	–	~ 0.3–0.6	Significant impact and responsible for local variation in chemical potential

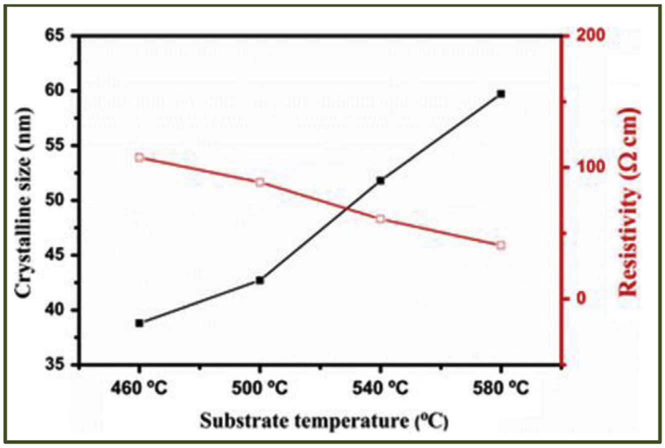

Fig. 3.3. Crystallinity and resistivity of the CZTS thin film with annealing temperature 460 °C–580 °C.

We studied in the literature review the substrate temperature and annealing or sulpherisation as given in Table 3c. From above study, we concluded that the suitable synthesized temperature (spray pyrolysis) for the Kesterite is 340^0–410 °C and the annealing temperature is 460^0–580 °C. These ranges are proposed for better results to improve the qualities of the absorber layer of the CZTS. But the secondary phases, defects and $Mo(S/Se)_2$ layers are created between the absorber and Mo metallic layer. The Sn and S elements are evaporated at high temperature and so these elements create non-stoichiometric CZTS film at high temperature. Hence, the balanced stoichiometry is obtained by controlling the temperature and the ratio of the constituent elements like Cu, Zn, Sn, S, Se.

Mkawi et al. [133] studied the chemical composition of the CZTS thin film misbalanced of increasing the annealing temperature 460^0–580 °C, where the resultant phase of the CZTS is misbehaved. Zhou et al. [130] proposed that the absorption coefficient vary with temperature and photon energy.

Hence, the oxide type impurities of the CZTS thin film can be removed by annealing at high temperature and the molecules have the sufficient energy to form the proper structure. But in this process, the sulphur is also evaporated. To diagnose this problem, we pass the inert atmosphere (Argon or Nitrogen) and hydrogen sulphide (H_2S) with CZTS sample during the annealing.

4. Interfaces in CZTS solar cell

The phase impurity and the poor interface quality mainly affect the performance of the solar cell efficiency in the device. So, the interface quality can be improved using the Buffer layer. As we know that the solar cell efficiency is dependent on the parameters: (i) open circuit voltage (V_{oc}), (ii) short circuit current density (J_{sc}), (iii) fill factor (FF). The open circuit voltage (V_{oc}) is reduced by the interface recombination of the device. To elucidate the open circuit voltage deficit, the mechanism of the carrier recombination is analysed by equation (4.1);

$$V_{oc} = \frac{E_A}{q} - \frac{AkT}{q}\ln\frac{J_{00}}{J_L} \tag{4.1}$$

where E_A = activation energy for recombination, A = ideality factor, q = electronic charge, k = Boltzman constant, J_{00} = reverse saturation current density and J_L = photocurrent density [134].

The device structure of the CZTS solar cell is shown in Fig. 4.1. The secondary phases and defects are created at the interfaces by the inter-diffusion of the materials. The inter-diffusion is done by the annealing and the secondary phases created like Cu_2S at CdS/CZTS and ZnS& SnS_2 at CZTS/Mo interfaces [135–137]. However, the Cd is diffused into CZTS and Zn &S are diffused into CdS layer. As a result, the band alignment is switched at CdS and CZTS interfaces and the carrier transport is disrupted [138].

During the sulfurization process, MoS_2 or $MoSe_2$ layer is created at the CZTS and Mo interfaces and this process is very arduous to the efficiency of the solar cell [139–141]. But some papers have explained that these layers affect the open circuit voltage due to the shifting band alignment between CZTS and Mo interfaces [112,132,134,142].

4.1. CdS and CZTS interfaces

The CdS (n-type) and the CZTS (p-type) layers form a p-n junction in the metal grids in the form of Al−ZnO/i-ZnO/CdS/CZTS/Mo/SLG as a device, where Al−ZnO is the aluminium doped zinc oxide. The p-n junction of the CdS and CZTS interface is an interesting area of the research work because the maximum charge carrier's loss near the interface is due to the recombination and the band offset on transportation of charge carriers. There are two types of recombination/band offset that are formed: spike and cliff. It can be determined by X-ray photoelectron spectroscopy which is shown in Fig. 4.2.

Scheer et al. [143] explained that the spike barrier is the trammel. This trammel restricts to flow of electrons from CZTS to CdS and as a

Table 3c
The role of the substrate temperature and annealing in the Kesterite characteristics to affect the solar cell parameters.

Methodology	Precursor salts/Solvents	Temperature/Annealing (^{0}C)	Characterization	Ref.
Spray Pyrolysis/CZTS	Copper chloride, Zinc chloride, Tin chloride, Thiourea/DW	273–360	● Best crystalline at 340 °C ● Average roughness value, Grain size increases as T_{subs} increases ● Energy band gap = 1.5 eV	[121]
Co-evaporation Technique/CZTSe	Cu, ZnSe, Sn	250–400	● The grain morphology and size improvement. ● Optical direct band gap = 1.48 eV ● Fundamental absorption region ~10^5 cm^{-1}	[122]
Co-sputtering Binary Sulphides/ Annealing/CZTS	Cu_2S, ZnS, and SnS_2	125/500-650	● Grain size 0.5 µm–1 µm due to which less recombination.	[123]
Spray pyrolysis/CZTS	Copper chloride, Zinc chloride, Tin chloride, Thiourea/2-Methoxyethanol, Monoethanolamine(MEA),	170/500	● Planes (112), (200), (220), and (312) indicating that the kesterite structure	[124]
Co-evaporation/CZTS	Cu, Zn, Sn, S	125, 325, 118, 130/575	● Rapid thermal annealing enhances the grain growth of the CZTS absorber And the efficiency is boosted from 1.12 to 2.56% ● Increased secondary phases, air voids and reflection drags	[125]
Spray pyrolysis/CZTS	Copper acetate, Zinc acetate, Tin chloride, Thiourea/Spray rate = 5 cc/min,/Nozzle to Substrate distance 33 cm, Nozzle diameter 0.05	400	● a = 5.422 A, c = 10.842 A ● Small particle size 200–400 nm ● Optical band gap- 1.5 eV ● A large shift of bandwidth from the absorption edge	[126]
Spray pyrolysis/CZTS	Copper chloride, Zinc chloride, Tin chloride, Thiourea/DW	200–500	● Energy band gap- 1.47 eV sprayed at 500 °C ● J_{SC} = 7.31 mA/cm^2, V_{OC} = 0.39 V, *FF* = 0.30, ● Power conversion efficiency of 0.86%.	[127]
Spray pyrolysis/CZTS	Copper chloride, Zinc chloride, Tin chloride and Thiourea/DW/Spray rate 5 ml/min, Time 60 s, distance substrate to spray nozzle 40 cm	200–400	● Planes (112), (220) and (116) attributed to kesterite ● a = 0.5435 nm, c = 1.0843 nm ● Crystallite sizes are 21.16 nm, 26.51 nm, 30.27 nm,35.12 nm for 250 °C, 300 °C, 350 °C and 400 °C respectively ● The roughness and the grain size increase with temperature increases ● Optical band gap- .45 eV, 1.55 eV, at 250 °C, 350 °C respectively	[128]
Spray pyrolysis/CZTS	Copper chloride, Zinc chloride, Tin chloride, Thiourea/DW/Nozzle to substrate distance 30 cm, Spray time 10 s, Spray interval 2 min, Pressure 1.5 bar	200–450	● Planes (112), (200), (220), (312) peaks attributed and 112 peaks shifts to higher value ● Crystallite size increases as temperature increases ● Absorption coefficient increases with increasing $T_{subs.}$	[129]
Ultrasonic Spray pyrolysis system/ CZTSe	Copper chloride, Zinc chloride, Tin chloride, Penta-hydrate, Indium Chloride, Thiourea, Elemental Selenium powder	450	● Conversion efficiency 5.74% ● Defects at 19 meV (V_{Cu}), 58 meV, and 118 meV (CuZn) with integrated defect densities.	[130]
Spray pyrolysis/CZTS	Copper chloride, Zinc chloride, Tin chloride Thiourea/DW	325	● Energy band gap = 2.00–2.25 eV	[131]

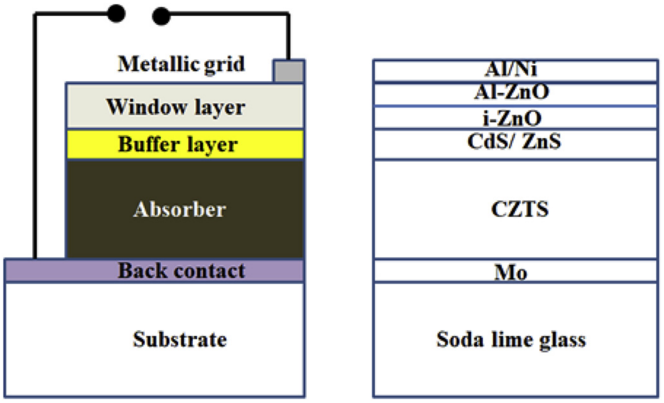

Fig. 4.1. Basic structure of CZTS solar cell with back contact, an absorber layer, Buffer layer, window layer, and grids.

result the V_{oc} is increased. And the cliff barrier or negative band offset helps to flow of electrons from CZTS to CdS and as result the Jsc, V_{oc} and the fill factor (FF) are enhanced [144,145]. The mechanism of the charge carriers transport across the potential barrier can be explained as shown in Fig. 4.2(c) and (d). The studies of effective of variation of S/(S + Se) ratio and band alignment are given below in Table 4a [146].

The CdS/CZTS interface has shown the cliff type structure and CdS/CZTS,Se has shown the spike type structure [147,148]. Tajima et al. [149] estimated the conduction band offset (CBO) at the CdS/CZTS interface by the valance band offset (VBO). The band gap of the materials can be measured by hard X-ray photoelectron spectroscopy. They also reported the flat band conduction band minimum (CBM) as shown in Fig. 4.3. This condition helps to charge transportation smoothly at the junction CdS/CZTS interface.

4.2. ZnO/CdS interface

To enhance the efficiency of the kesterite solar cell, i-ZnO/Al—ZnO, In_2O_3, ZnSnO, GaP materials are used as the window layer. Such materials are highly conductive having wide optimal band gap and are highly transparent in desired spectrum [150,151]. These layers are used in the CZTS and CIGS solar cells. Janotti et al. [152] analysed that i-ZnO/Al—ZnO is the best window layer and shown the positive response such as improved V_{oc} for the solar cell application [153].

The band alignment of the ZnO and CdS interface is investigated for CIGS absorber [154]. The band alignment explained the charge carrier's transportation as shown in Fig. 4.4. But another investigation has showed the flat band offset as $CBO = 0.1 \pm 0.15\,eV$ and $VBO = -0.96 \pm 0.15\,eV$ which support the charge transportation at the interface [155].

4.3. CZTS and Mo interface

The charge collection point/electrode is the parameter at which there is the charge carriers loss in the device of solar cell. This is the deleterious effect to enhance the efficiency of solar cell because V_{oc} is affected. So, a lot of metallic coated substrates are used to collect the charges. The metals like W, Mo, ITO, FTO, Cr, V, Ti, Mn, Au, Ni, Ag, Pt, Nb, etc. are used to collect the charge carriers as the electrode [156]. Mostly Mo is used in the high-efficiency solar cell such as CIS, CIGS because it has ohmic contact, good adhesion and formed the diffusion barrier layer $(MoS/Se)_2$ [157,158]. Hence, the Mo metal is used in the kesterite solar cell that may increase the open circuit voltage (V_{oc}). But some researchers reported its negative impact on the solar cell device [159,160]. There are more requirements to do the research work in this field.

Scragg et al. [161] observed that if the electrodeposited CZTS/Mo/SLG film is annealed/sulfurized/selenized at 550 °C, then the thickness of the film is increased with the increasing time and the decreasing temperature, where grain size also reduces the film thickness [162].

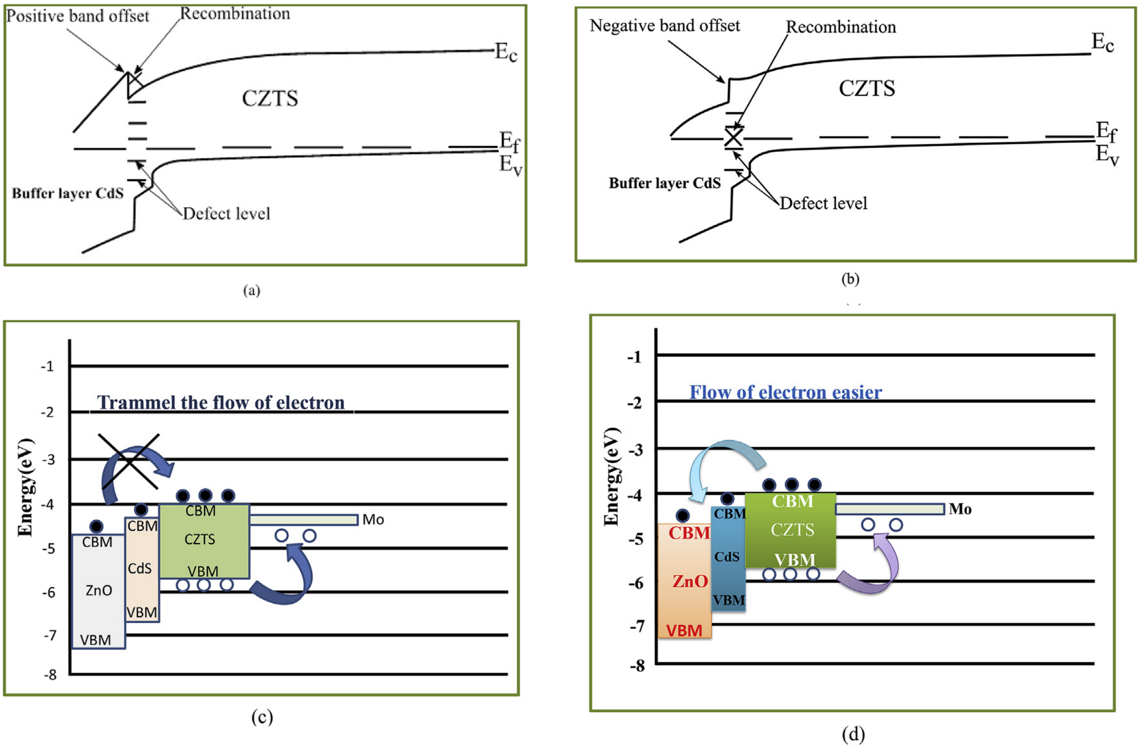

(a) (b) (c) (d)

Fig. 4.2. (a and b)The structure of the band offset are (a) spike type, (b) cliff type barriers.(c) No carriers transport at the interface.(d) carriers transport at the interface for photo-generated electrons and inject electrons.

Table 4a
Comparison effect of variation of S and Se on band alignment is given below

Increasing parameter	Effective parameter	Effect on band alignment
Sulphur	The band gap of CZT(S,Se) increases	● Valance band edge shifts towards the higher binding energy, ● Reducing the VBO and CB edge [146]
Selenium	The band gap of CZTS reduces	● Conduction Band edge shifts downwards [146]

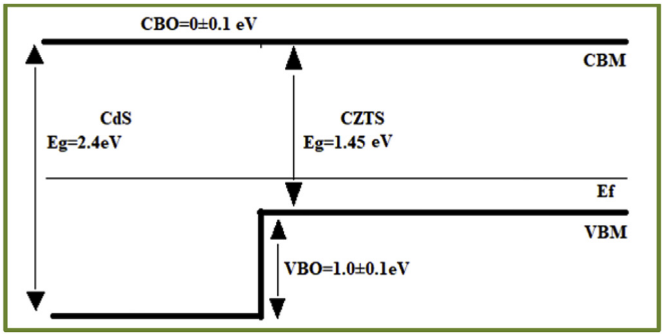

Fig. 4.3. The CdS/CZTS interface band alignment shown the flat CBM.

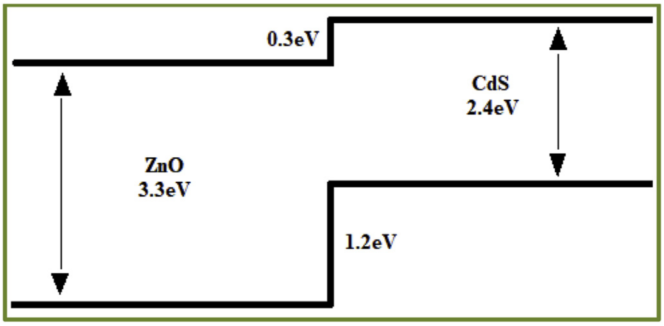

Fig. 4.4. The band diagram of ZnO/CdS interface showed the band offset 0.3 eV Conduction Band Minimum (CBM) and 1.2eV Valance Band Maximum (VBM).

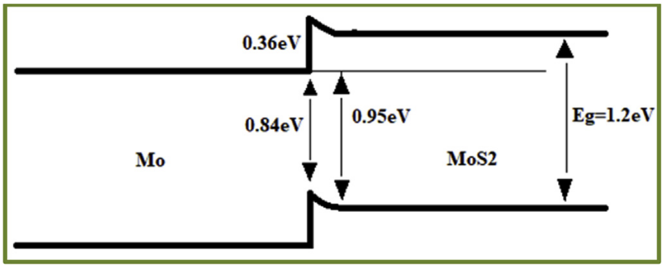

Fig. 4.5. Band diagram of Mo/MoS_2 interface in which CBO is 0.36 eV.

The thickness of the MoS_2 layer was helpful in the device performance, if TiN layer is used [163,164]. The band offset CBO is 0.36 eV at the Mo/MoS_2 interface as shown in Fig. 4.5 [165].

Currently, there are some intermediate layers used to improve the back contact of the CZTS solar cell. These intermediate layers are TiN, Silver, Bismuth, Carbon, ZnO, Al_2O_3, TiB_2 at the CZTS and Mo interface. The coating of these materials is applied on the substrate in the nanometer range. The CZTS solar cell was reported with the efficiency 5.5% with 621 mV open circuit voltage, 18.71 mA/cm^2 current density and fill factor 47.1% when intermediate layer TiN was deposited by sputtering process [166]. The CZTSe with TiN layer was also reported the efficiency 8.9% with 385 mV open circuit voltage, 42.60 mA/cm^2 current density and fill factor 54.2% [167].

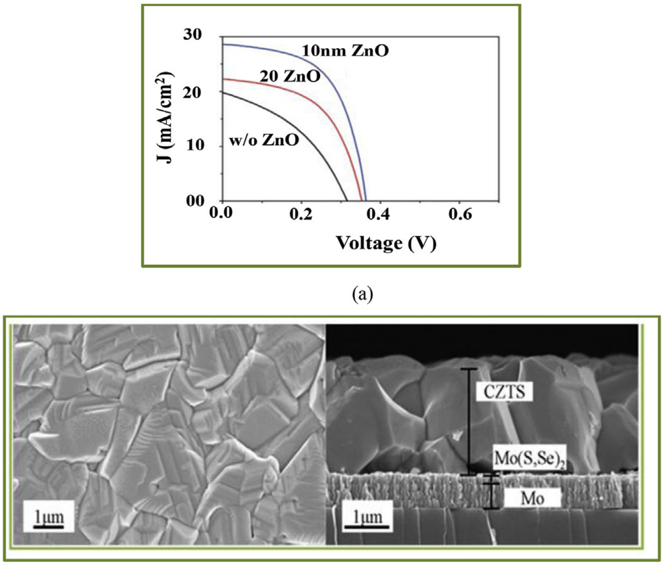

(a)

(b)

Fig. 4.6. (a) The J-V Characteristics of the CZTSe with efficiency, open circuit voltage and fill factor in 1.5AM illumination and quantum efficiency shown in the inset. Permission granted for the image.(b) Top and cross-section view of the CZTS absorber layer and MSe_2 and Mo layer. Reproduced with the permission.

Table 4b
Using the different layers between the Mo and CZTS, Se absorber layers to enhance the solar cell efficiency.

Absorber layer	Intermediate layer	V_{oc} (mV)	J_{sc} (mA/cm^2)	FF (%)	Eff. (%)	R_{sc} (ohm cm^2)	Ref.
CZTS	TiN	621	18.70	47.10	5.5	6.90	[170]
CZTSe	TiN	385	42.60	54.20	8.9	1.80	[167]
CZTS	C	560	16.96	56.00	5.5	2.00	[171]
CZTSSe	C	439	27.90	59.20	7.2	0.53	[172]
CZTS	ZnO	364	28.60	57.50	6.0	0.50	[167]
CZTSe	ZnO	641	15.97	42.00	4.3	15.10	[168]
CZTS	Ag	597	15.05	49.20	4.4	12.80	[173]
CZTS	TiB_2	598	13.21	56.00	4.4	10.30	[174]
CZTS	Bi	590	15.70	51.00	4.8	5.67	[175]
CZTS	Al_2O_3	657.8	19.76	65.91	8.57	1.97	[176]

If the 10 nm thickness of ZnO layer is used in between Mo and CZTS layers, the efficiency is enhanced from 2.5% to 6% with reducing the series resistance (R_s) [168]. Liu et al. [169] reported the enhancement of the efficiency of the solar cell from 1.13% to 4.3% with decreasing the voids and the thickness of the MoS_2. Fig. 4.6(a)shows the J-V characteristics of the CZTSe solar cell under AM 1.5G illumination with or without the ZnO layer and the quantum efficiency of devices is shown in the inset. Fig. 4.6 (b) shows the top view and the cross-section of the CZTS, Se absorber layer, $MoSe_2$ layer and Mo layer on the substrate. The figure shows that the crystalline size becomes the order of micro size in which the recombination is reduced due to micro crystalline [8]. The results of the enhanced solar cell efficiency are modified as shown in Table 4b.

A lot of investigations are required to remove the charge carriers (holes) collection problems at the CZTS,Se and Mo interfaces. The low

Table 5
Champion solar cells efficiency of CIGS and CZTSSe are given below.

Absorber material	V_{oc} (mV)	J_{sc} (mA/cm^2)	Fill Factor (%)	η (%)	Ref.
CIGS	746	36.6	79.3	22.6	[181]
CZTS,Se	513.4	35.2	69.8	12.6	[8]

resistive, the highly conductive and the suitable band alignment materials will have a good transportation of the holes.

5. Role of the thickness of the layers in the solar cell

The thickness of the solar cell layer is another main parameter of the solar cell which mostly affects cost and open circuit voltage in the second generation solar cell. The best-reported absorber layer thickness is ≥ 100 nm which balances the R_s and absorption coefficient [181]. The best thickness of the window layer was reported 60 nm-1μm and interfacial layers were reported 5–20 nm as discussed earlier.

6. Future possibilities of kesterite in solar cell application

There is a big challenge for researchers to enhance the conversion efficiency of the kesterite (CZTS/CZTSe/CZTS,Se) solar cell with the low-cost methodology. The efficiency of CZTS, Se has low results as compared to the efficiency of CIGS as shown in Table 5 The efficiency of CZTS,Se is tending to rise up to 22.6% by manipulating the materials. The main reason of low efficiency of kesterite solar cell is that the high loss of charge carriers by the recombination during charge transportation and the charge collection at the electrode. These parameters are affected directly by the interfacial layer between the absorber and the buffer/window layers and the absorber and the metallic contacts. The best buffer layer is CdS for the CIGS solar cell but it is not perfect for the CZTS,Se solar cell because the recombination timing of the CZTS,Se solar cell at the interface is very low as compared to the CIGS solar cell as discussed earlier in the introductory section. The main reason of low recombination in CdS/CZTS interface is Cd diffusion in absorber layer at the time of solar cell fabrication. The interface of CdS/CZTS has spike type band offset with 0.4 eV energy [177]. As a result, the mismatched lattice problems have been created [177]. Hence, it is required to develop the suitable buffer layer in place of the CdS, i.e. appropriate function interfacial layer between the buffer and the absorber.

The best solution of the above discussed problem is the carbon nanotube (CNT). The CNTs are the cylindrical type molecule and having valuable applications for electronic, optic, nanotechnology and other field of the materials science. The CNTs have a unique feature breathing mode of cylindrical type molecules. The feature of the nanotube structure is to make fine tuning through the narrow selectivity of the wavelength of emission and can be detected by the light. Due to the breathing mode of the cylindrical type molecules of the carbon nanotubes (CNT), the CNT may be the perfect buffer layer to reduce the recombination between the absorber and the buffer layers. Similarly, Graphene nano layer may also be the best solution of this problem.

The Mo(S_2/Se_2) layer is another hurdle in the efficiency enhancement of the kesterite solar cell. The Mo interface plays vital role to the enhancement of the kesterite solar cell because it has maximum series resistance. The Mo(S_2/Se_2) layer is formed often in the kesterite solar cell during the annealing process. Hence, we have concluded two points clearly that (i) we should not have annealed the solar cell after the complete fabrication and (ii) we should remove the Mo metal by the high work function metal such as Ni (5.22), NiO (> 5.2), Pd (5.22), Pt (5.64) [178–180]. Here, fabrication of the solar cell without annealing may be the wonderful task because this idea avoids the formation of MoS_2/Se_2 layer and diffusion of the metallic salts layers across the interfaces having the high work function for metal. In the presence of the high work function layer, all charge carriers (holes) may be collected in the right manner to enhance the efficiency of the solar cell. During the charge collection of the electrode, will not be the energy loss for high work function electrode. This will form the ohmic contact with the kesterite solar cell and have more probability to extract the charge carriers.

7. Summary

In this review, we have discussed all the issues related to the efficiency of the kesterite solar cell particularly the CZTS. The CZTS may become the counterpart of the CIGS for the advanced solar technology, if we are able to remove challenging issues of the composition like the secondary phases, the defects, the interfacial recombination and the annealing temperatures, etc. In this regards, we have diagnosed all the problems one by one and given some appropriate solution for each issue. The technical issues are also raised as the prime way to restrict the CZTS solar cell efficiency more than~ 20%. Although there are significant progresses have been made to achieve the enhanced efficiency of the CZTS solar cell, further the new process is required to improve the efficiency of the CZTS solar cells experimentally up to 32.2% as predicted theoretically by the Shockley-Queisser (SQ) limit. The efficiency of the CZTS solar cell may be achieved > 20% by removing all the issues and it will became the future solar cell device having the high absorption coefficient and the low cost as discussed in this review. Moreover, we have also observed some important facts which are as follows:

(i) The secondary phases of CuS, Cu_2S, SnS, SnS_2 and Cu_2SnS_3 can be removed by the KCN etching. However, the secondary phase of ZnS can be removed by the HCl etching. Further, we can get the pure phase for the CZTS thin film.
(ii) The defects in the CZTS are needed to be suppressed for the band tailing and the band edge potential fluctuations by the post annealing the sample at low temperature and as a result there will be the reduced concentrations of Cu_{Zn} and Zn_{Cu} defects and the E_g will be increased.
(iii) The composition ratio of the Cu and Zn elements of the CZTS is to be controlled for the narrow phase stability with Cu-poor and Zn-rich condition. In the annealing process, S element may be used to suppress the decomposition of the CZTS/Mo interfaces.
(iv) Finally, the kesterite CZTS solar cell is to be reduced for the interface recombination at the buffer layer. The absorber interfaces having spike like structure of conduction band offset is an ideal condition. This spike like structure can be achieved by adjusting the band structure of the buffer layer by the creating/coating the inversion layer in the middle of the buffer and the absorber layers.

Acknowledgement

Mr. Krishan Pal likes to thank to UGC, New Delhi for the financial support through RGNF National fellowship (F1-17.1/2015-16/RGNF-2015-17-SC-UTT-25302). We are also thankful to Prof. B.C. Yadav, Dr. A. K. Yadav and Mr. Diptarka Roy, Department of Physics, School of Physical and Decision Sciences, Babasaheb Bhimrao Ambedkar University (A Central University), Lucknow, India; for their kind support and consistent help. Specially, we would like thank to Dr. Satendra Pal Singh, Research Professor, Sejong University, Seoul, South Korea for providing the data of CZTS from Web of Science and Dr. Narendra Kumar, Department of Physics, Mody University of Science and Technology, India, for the critical reading and incorporating corrections in the manuscript.

References

[1] A. Muratoglu, M.I. Yuce, World energy outlook and place of renewable resources, Int. J. Sci. and Tech. Rech. 1 (2015) 10–17 https://www.researchgate.net/

publication/282974763.
[2] J.J. Scragg, D. Berg, P.J. Dale, A 3.2% efficient kesterite device from electrodeposited stacked elemental layers, J. Electroanal. Chem. 646 (2010) 52–59 https://doi.org/10.1016/j.jelechem.2010.01.008.
[3] K. Wang, R.E. Dickinson, Contribution of solar radiation to decadal temperature variability over land, Proc. Natl. Acad. Sci. U.S.A. 110 (2013) 14877–14882 https://doi.org/10.1073/pnas.1311433110.
[4] H.W. Wua, A. Emadia, G. de Graafa, J. Leijtensb, R.F. Wolffenbuttel, Design and fabrication of an albedo insensitive analog sun sensor, Procedia Eng 25 (2011) 527–530 https://doi.org/10.1016/j.proeng.2011.12.131.
[5] S.I. Swati, R. Matin, S. Bashar, Z.H. Mahmood, Experimental study of the optical properties of Cu_2ZnSnS_4 thin film absorber layer for solar cell application, IOP Conf. Series J. Phys. 4567 (2018) 012010–012016 https://doi.org/10.1088/1742-6596/1086/1/012010.
[6] H. Kategori, N. Sasaguchi, S. Hando, S. Hoshino, J. Ohashi, T. Yokota, Preparation and evaluation of CZTS thin films by sulfurization of E-B evaporated Precursors, Sol. Energy Mater. Sol. Cell. 49 (1997) 407–414 https://doi.org/10.1016/S0927-0248(97)00119-0.
[7] W. Shockley, H.J. Queisser, Detailed balance limit of efficiency of *p-n* junction solar cells, Jpn. J. Appl. Phys. 32 (1961) 510–519 https://doi.org/10.1063/1.1736034.
[8] W. Wang, M.T. Winkler, O. Gunawan, T. Gokmen, T.K. Todorov, Y. Zhu, D.B. Mitzi, Device characteristics of CZTSSe thin-film solar cells with 12.6% efficiency, Adv. Energy Mater 4 (2014) 1301465–1301470 https://doi.org/10.1002/aenm.201301465.
[9] A. Walsh, S. Chen, S.H. Wei, X.G. Gong, Kesterite thin-film solar cells: advances in materials modeling of Cu_2ZnSnS_4, Adv. Energy Mater. 2 (2012) 400–409 https://doi.org/10.1002/aenm.201100630.
[10] H. Wang, Progress in thin film solar cells based on Cu_2ZnSnS_4, Int. J. Photoenergy 201 (2011) 1–10 https://doi.org/10.1155/2011/801292.
[11] S. Delbos, Kesterite thin films for photovoltaics: a Review, EPJ Photovoltaics 3 (2012) 1–13 https://doi.org/10.1051/epjpv/2012008.
[12] K. Ramasamy, Mohammad A. Malika, P. O Brien, Routes to copper zinc tin sulfide Cu_2ZnSnS_4 a potential material for solar cells, Chem. Commun. (J. Chem. Soc. Sect. D) 48 (2012) 5703–5714 https://doi.org/10.1039/C2CC30792H.
[13] M.I. Hossain, Prospects of CZTS solar cells from the perspective of material properties fabrication methods and current research challenges, Chalcoginide Lett 9 (2012) 231–242 https://www.researchgate.net/publication/288703672.
[14] S. Abermann, Non-vacuum processed next-generation thin film photovoltaic: towards marketable efficiency and production of CZTS based solar cells, Sol. Energy 94 (2013) 37–70 https://doi.org/10.1016/j.solener.2013.04.017.
[15] M.P. Suryawanshi, G.L. Agawane, S.M. Bhosale, S.W. Shin, P.S. Patil, J.H. Kim, A.V. Moholkar, CZTS based thin film solar cells: a status review, Materials Technology, Adv. Perform. Mater. 28 (2013) 98–109 https://doi.org/10.1179/1753555712Y.0000000038.
[16] H. Azimi, Y. Hou, C.J. Brabec, Towards low-cost, environmentally friendly printed chalcopyrite and kesterite solar cells, Energy Environ. Sci. 7 (2014) 1829–1849 https://doi.org/10.1039/C3EE43865A.
[17] X. Song, X. Ji, M. Li, W. Lin, X. Luo, H. Zhang, A review on development prospect of CZTS based thin film solar cells, Int. J. Photoenergy (2014) 1–11 2014 https://doi.org/10.1155/2014/613173.
[18] L.M. Peter, Electrochemical routes to earth-abundant photovoltaic: a mini-review, Electrochem. Commun. 50 (2015) 88–92 https://doi.org/10.1016/j.elecom.2014.11.012.
[19] S.A. Vanalakar, G.L. Agawane, S.W. Shin, M.P. Suryawanshi, K.V. Gurav, K.S. Jeon, P.S. Patil, C.W. Jeong, J.Y. Kim, J.H. Kim, A review on pulsed laser deposited CZTS thin films for solar cell applications, J. Alloy. Comp. 619 (2015) 109–121 https://doi.org/10.1016/j.jallcom.2014.09.018.
[20] S. Siebentritt, S. Schorr, Kesterites a challenging material for solar cells, Prog. Photovoltaics 20 (2012) 512–519 https://doi.org/10.1002/pip.2156.
[21] C.M. Fella, Yaroslav E. Romanyuk, Ayodhya N. Tiwari, Technological status of $Cu_2ZnSn(S, Se)_4$ thin film solar cells, Sol. Energy Mater. Sol. Cell. 119 (2013) 276–277 https://doi.org/10.1016/j.solmat.2013.08.027.
[22] D.B. Mitzi, Oki Gunawan, Teodor K. Todorov, D. Aaron R. Barkhouse, Prospects and performance limitations for Cu–Zn–Sn–S–Se photovoltaic technology, Philos Trans A Math Phys Eng Sci 371 (2013) 20110432–20110455 https://doi.org/10.1098/rsta.2011.0432.
[23] T.J. Huang, X. Yin, G. Qi, H. Gong, CZTS-based materials and interfaces and their effects on the performance of thin film solar cells, Phys. Status Solidi R. 08 (2014) 735–762 https://doi.org/10.1002/pssr.201409219.
[24] S. Schorr, Structural aspects of adamantine like multinary chalcogenides, Thin Solid Films 515 (2007) 5985–5991 https://doi.org/10.1016/j.tsf.2006.12.100.
[25] D.B. Mitzi, O. Gunawan, T.K. Todorov, K. Wang, S. Guha, The path towards a high-performance solution-processed kesterite solar cell, Sol. Energy Mater. Sol. Cell. 95 (2011) 1421–1436 https://doi.org/10.1016/j.solmat.2010.11.028.
[26] I.D. Olekseyuk, L.D. Gulay, I.V. Dydchak, L.V. Piskach, O.V. Parasyuk, O.V. Marchuka, Single crystal preparation and crystal structure of the Cu_2Zn/Cd, $Hg/SnSe_4$ compounds, J. Alloy. Comp. 340 (2002) 141–145 https://doi.org/10.1016/S0925-8388(02)00006-3.
[27] A. Nateprov, V.C. Kravtsov, G. Gurieva, S. Schorr, Single-crystal X-ray structure investigation of $Cu_2ZnSnSe_4$, Surf. Eng. Appl. Electrochem. 49 (2013) 423–426 https://doi.org/10.3103/S1068375513050098.
[28] P. Atkince, J. de Paula, Elements of Physical Chemistry, fifth ed., Oxford University press, Oxford, Great Britain, 2009.
[29] K. Ito, Copper Zinc Tin Sulfide-Based Thin Film Solar Cells, first ed., John Wiley and Sons Ltd., Chichester, West Sussex, United Kingdom, 2015.
[30] JCPDS Card: 26-0575.
[31] H. Wang, Progress in thin film solar cells based on Cu_2ZnSnS_4, Int. J. Photoenergy 2011 (2011) 801292–801302 https://doi.org/10.1155/2011/801292.
[32] L. Guen, W.S. Glaunsinger, Electrical, Magnetic and EPR studies of the quaternary chalcogenide $Cu_2A^{II}B^{IV}X_4$ prepared by iodine transport, J. Solid State Chem. 35 (1980) 10–21 https://doi.org/10.1016/0022-4596(80)90457-0.
[33] T. Tinoco, C. Rincon, M. Quintero, G. Sanchez Perez, Phase diagram and optical energy gaps for $CuIn_yGa_{1-y}Se_2$ alloys, Phys. Status Solidi 124 (1991) 427–434 https://doi.org/10.1002/pssa.2211240206.
[34] X. Zhang, G. Guo, C. Ji, K. Huang, C. Zha, Y. Wang, L. Shen, A. Gupta, N. Bao, Efficient thermolysis route to monodisperse Cu_2ZnSnS_4 nanocrystal with controlled shape and structure, Sci. Rep. 4 (2014) 5086–5093 https://doi.org/10.1038/srep05086.
[35] S. Chen, X.G. Gong, A. Walsh, S.H. Wei, Crystal and electronic band structure of Cu_2ZnSnX_4 (X = S and Se) photovoltaic absorbers: first-principles insights, Appl. Phys. Lett. 94 (2009) 041903–041907 https://doi.org/10.1063/1.3074499.
[36] O.V. Galan, J.A. Andrade-Arvizu, Y. Sanchez, M.E. Rodriguez, E. Saucedo, D. Seuret-Jimenez, M. Titsworth, Route towards low cost-high efficiency second generation solar cells: current status and perspectives, J. Mater. Sci. Mater. Electron. 26 (2014) 5562–5572 https://doi.org/10.1007/s10854-14-2196-4.
[37] A. Fairbrother, E. Saucedo, X. Fontane, V. Izquierdo-Roca, D. Sylla, M. Espindola Rodriguez, F.A. Pulgarin Agudela, O. Vigil Galan, A. Perez Rodriguez, Preparation of 4.8% Efficiency CZTS Based Solar Cell by a Two-step Process, Photovoltaic Specialists Conference (PVSC), 2012 (2012), pp. 002679–002684 38th IEE https://doi.org/10.1109/PVSC.2012.6318146.
[38] H. Matsushita, T. Ichikawa, A. Katsui, Structural, thermodynamical and optical properties of Cu_2-II-IV-VI_4 quaternary compounds, J. Mater. Sci. 40 (2005) 2003–2005 https://doi.org/10.1007/s10853-005-1223-5.
[39] P. Jackson, R. Wuerz, D. Hariskos, E. Lotter, W. Witte, M. Powalla, Cover Picture: effects of heavy alkali elements in $Cu(In,Ga)Se_2$ solar cells with efficiencies up to 22.6%, Phys. Status Solidi R 10 (2016) 583–586 https://doi.org/10.1002/pssr.201600199.
[40] R.M. Jones, Mechanics of Composite Materials, second ed., Taylor and Francis, Philadelphia, PA, 1999.
[41] T.M. Friedlmeier, N. Wieser, T. Walter, H. Dittrich, H.W. Schock, Heterojunctions based on Cu_2ZnSnS_4 and $Cu_2ZnSnSe_4$ thin films, Proceedings of the 14th European Photovoltaic Specialists Conference, Barcelona, 1997, pp. 1242–1245 https://doi.org/10.1557/opl.2011.844.
[42] S. Chen, X.G. Gong, A. Walsh, S.H. Wei, Defect physics of the kesterite thin-film solar cell absorber Cu_2ZnSnS_4, Appl. Phys. Lett. 96 (2010) 021902–021906 https://doi.org/10.1063/1.3275796.
[43] A. Walsh, S. Chen, S.H. Wei, X.G. Gong, Kesterite of the thin film solar cell: advances of materials modeling Cu_2ZnSnS_4, Adv. Energy Mater. 2 (2012) 400–409 https://doi.org/10.1002/aenm.201100630.
[44] A. Nagoya, R. Asahi, R. Wahl, G. Kresse, Defect formation and phase stability of Cu_2ZnSnS_4 photovoltaic material, Phys. Rev. B 81 (2010) 113202–113206 https://doi.org/10.1103/PhysRevB.81.113202.
[45] D. Mitzi, O. Gunawan, T. Todorov, K. Wang, S. Guha, The path towards a high-performance solution-processed kesterite solar cell, Sol. Energy Mater. Sol. Cell. 95 (2011) 1421 https://doi.org/10.1016/j.solmat.2010.11.028.
[46] H. Katagiri, K. Jimbo, M. Tahara, H. Araki, K. Oishi, The influence of the composition ratio on CZTS-based thin film solar cells, Mater. Res. Soc. Symp. Proc. 1165 (2009), https://doi.org/10.1557/PROC-1165-M04-01.
[47] S. Chen, A. Walsh, Y. Luo, J.H. Yang, X.G. Gong, S.H. Wei, Wurtzite derived polytypes of kesterite and Stannite quaternary chalcogenide semiconductors, Phys. Rev. B 82 (2010) 195203–195211 https://doi.org/10.1103/PhysRevB.82.195203.
[48] J. Paier, M. Marshman, K. Hummer, G. Kresse, I.C. Gerber, J.G. Angyan, Screened hybrid density functionals applied to solids, J. Chem. Phys. 124 (2006) 154709–154723 https://doi.org/10.1063/1.2187006.
[49] S. Ahn, S. Jung, J. Gwak, A. Cho, K. Shin, K. Yoon, D. Park, H. Cheong, J.H. Yun, Determination of band gap energy Eg of $Cu_2ZnSnSe_4$ thin films: on the discrepancies of reported band gap values, Appl. Phys. Lett. 97 (2010) 021905–021909 https://doi.org/10.1063/1.3457172.
[50] S. Chen, X.G. Gong, A. Walsh, S.H. Wei, Crystal and electronic band structure of Cu_2ZnSnX_4 (X = S and Se) photovoltaic absorbers: first-principles insights, Appl. Phys. Lett. 94 (2009) 041903–041907 https://doi.org/10.1063/1.3074499.
[51] J. Paier, R. Asahi, A. Nagoya, G. Kresse, Cu_2ZnSnS_4 as a potential photovoltaic material: a hybrid Hartree-Fock density functional theory study, Phys. Rev. B 79 (2009) 115126–115134 https://doi.org/10.1103/PhysRevB.79.115126.
[52] J.O. Jeon, K.D. Lee, L.S. Oh, S.W. Seo, D.K. Lee, H. Kim, J. Jeong, M.J. Ko, B.S. Kim, H.J. Son, J.Y. Kim, Highly efficient copper–zinc–tin–selenide (CZTSe) solar cells by electro deposition, Chem. Sus. Chem. 7 (2014) 1073–1077 https://doi.org/10.1002/cssc.201301347.
[53] N. Nakayama, K. Ito, Sprayed films of stannite Cu_2ZnSnS_4, Appl. Surf. Sci. 92 (1996) 171–175 https://doi.org/10.1016/0169-4332(95)00225-1.
[54] N. Kamoun, H. Bouzouita, B. Rezig, Fabrication and characterization of Cu_2ZnSnS_4 thin films deposited by spray pyrolysis technique, Thin Solid Films 515 (2007) 5949–5952 https://doi.org/10.1016/j.tsf.2006.12.144.
[55] F. Gao, S. Yamazoe, T. Maeda, K. Nakanishi, T. Wada, Structural and optical properties of In-free $Cu_2ZnSn(S,Se)_4$ solar cell materials, Jpn. J. Appl. Phys. 51 (2012) 1–5 10NC29 https://doi.org/10.1143/JJAP.51.10NC29.
[56] K. Tanaka, Y. Fukui, N. Moritake, H. Uchiki, Chemical composition dependence of morphological and optical properties of Cu_2ZnSnS_4 thin films deposited by sol-gel sulfurization and Cu_2ZnSnS_4 thin film solar cell efficiency, Sol. Energy Mater. Sol. Cell. 95 (2011) 838–842 https://doi.org/10.1016/j.solmat.2010.10.031.
[57] M. Patel, I. Mukhopadhyay, A. Ray, Structural, optical and electrical properties of

spray-deposited CZTS thin films under a non-equilibrium growth condition, J. Phys. D Appl. Phys. 45 (2012) 445103–445110 https://doi.org/10.1088/0022-3727/45/44/445103.

[58] S. Ahn, S.H. Jung, J.Y. Gwak, A. Cho, K. Shin, K. Yoon, D.Y. Park, H. Cheong, J.H. Yun, Determination of band gap energy (Eg) of $Cu_2ZnSnSe_4$ thin films: on the discrepancies of reported band gap values, Appl. Phys. Lett. 97 (2010) 1–3 021905 https://doi.org/10.1063/1.3457172.

[59] R. Haight, A. Barkhouse, O. Gunawan, B. Shin, M. Copel, M. Hopstaken, D.B. Mitzi, Band alignment at the $Cu_2ZnSn(S_xSe_{1-x})_4$/CdS interface, Appl. Phys. Lett. 98 (2011) 253502–253506 https://doi.org/10.1063/1.3600776.

[60] J. He, L. Sun, S. Chen, Y. Chen, P. Yang, J. Chu, Composition dependence of structure and optical properties of $Cu_2ZnSn(S,Se)_4$ solid solutions: an experimental study, J. Alloy. Comp. 511 (2012) 129–132 https://doi.org/10.1016/j.jallcom.2011.08.099.

[61] I. Repins, C. Beall, N. Vora, C. De Hart, D. Kuciauskas, P. Dippo, B. To, J. Mann, W.C. Hsu, A. Goodrich, R. Noufi, Co-evaporated $Cu_2ZnSnSe_4$ films and devices, Sol. Energy Mater. Sol. Cells 101 (2012) 154–159 https://doi.org//10.1016/j.solmat.2012.01.008.

[62] K. Jimbo, R. Kimura, T. Kamimura, S. Yamada, W.S. Maw, H. Araki, K. Oishi, H. Katagiri, Cu_2ZnSnS_4-type thin film solar cells using abundant materials, Thin Solid Films 515 (2007) 5997–5999 https://doi.org/10.1016/j.tsf.2006.12.103.

[63] A. Ennaoui, M. Lux-Steiner, A. Weber, D. Abou-Ras, I. Kotschau, H.W. Schock, R. Schurr, A. Holzing, S. Jost, R. Hock, T. Vos, J. Schulze, A. Kirbs, Cu_2ZnSnS_4 thin-film solar cells from electroplated precursors: novel low-cost perspective, Thin Solid Films 517 (2009) 2511–2514 https://doi.org/10.1016/j.tsf.2008.11.061.

[64] K. Ito, T. Nakazawa, Electrical and optical properties of Stannite-type quaternary semiconductor thin films, Jpn. J. Appl. Phys. 27 (1988) 2094–2097 https://doi.org/10.1143/JJAP.27.2094.

[65] H. Katagiri, Kotoe Saitoh, Tsukasa Washio, Hiroyuki Shinohara, Tomomi Kurumadani, Shinsuke Miyajima, Development of thin film solar cell-based on Cu_2ZnSnS_4 thin films, Sol. Energy Mater. Sol. Cells 65 (2001) 141–148, https://doi.org/10.1016/S0927-0248(00)00088-X.

[66] S.A. Nadi, P. Chelvanathan, Z. Zakaria, M.M. Alam, Z.A. Alothman, K. Sopian, N. Amin, Post-deposition annealing effect on Cu_2ZnSnS_4 thin films grown at different substrate temperature, Int. J. Photoenergy (2014) 589027–589034 2014 https://doi.org/10.1155/2014/589027.

[67] T.K. Todorove, K.B. Reuter, D.B. Mitzi, High-efficiency solar cell with earth-abundant liquid-processed absorber, Adv. Energy Mater. 22 (2010) E156–E157 https://doi.org/10.1002/adma.200904155.

[68] H. Kategori, Kazuo jimbo, satoru yamada, tsuyoshi kamimura, win shwe maw, tatsuo fukano, tadashi Ito, tomoyoshi motohiro, enhanced conversion efficiencies of Cu_2ZnSnS_4-based thin film solar cells by using preferential etching technique, APEX 1 (2008) 041201–041202 https://doi.org/10.1143/APEX.1.041201.

[69] B. Shin, O. Gunawan, Y. Zhu, N.A. Bojarczuk, S.J. Chey, S. Guha, Thin film solar cell with 8.4% power conversion efficiency using an earth-abundant Cu_2ZnSnS_4 absorber, Prog. Photovolt. 21 (2011) 72–76 https://doi.org/10.1002/pip.1174.

[70] J.O. Jeon, K.D. Lee, L.S. Oh, S.W. Seo, D.K. Lee, H. Kim, J.H. Jeong, M.J. Ko, B.S. Kim, H.J. Son, J.Y. Kim, Highly efficient copper–zinc–tin–selenide (CZTSe) solar cells by electro deposition, Chem. Sus. Chem. 7 (2014) 1073–1077 https://doi.org/10.1002/cssc.201301347.

[71] X. Zeng, K.F. Tai, T. Zhang, C.W. JohnHoa, X. Chen, A. Huan, T.C. Sum, L.H. Wong, $Cu_2ZnSn(S,Se)_4$ kesterite solar cell with 5.1% efficiency using spray pyrolysis of aqueous precursor solution followed by selenization, Sol. Energy Mater. Sol. Cells 124 (2014) 55–60 https://doi.org/10.1016/j.solmat.2014.01.029.

[72] L. Yao, J. Ao, M.J. Jeng, J. Bi, S. Gao, G. Sun, Q. He, Z. Zhou, Y. Sun, L.B. Chang, A CZTSe solar cell with 8.2% power conversion efficiency fabricated using electrodeposited Cu/Sn/Zn precursor and a three-step selenization process at low Se pressure, Sol. Energy Mater. Sol. Cells 159 (2017) 318–324 https://doi.org/10.1016/j.solmat.2016.09.028.

[73] S. Giraldo, T. Thersleff, G. Larramona, M. Neuschitzer, P. Pistor, K. Leifer, A. Perez-Rodriguez, C. Moisan, G. Dennler, E. Saucedo, $Cu_2ZnSnSe_4$ solar cells with 10.6% efficiency through innovative absorber engineering with Ge superficial nanolayer, Prog. Photovoltaics 24 (2016) 1359–1367 https://doi.org/10.1002/pip.2797.

[74] G. Zoppi, I. Forbes, R.W. Miles, P.J. Dale, J.J. Scragg, L.M. Peter, $Cu_2ZnSnSe_4$ Thin film solar cells produced by selenisation of magnetron sputtered precursors, Prog. Photovoltaics 17 (2009) 315–319 https://doi.org/10.1002/pip.886.

[75] S. Bag, O. Gunawan, T. Gokmen, Y. Zhu, D.B. Mitzi, Hydrazine-Processed Ge-substituted CZTSe solar cells, Chem. Mater. 24 (2012) 4588–4593 https://doi.org/10.1021/cm302881g.

[76] S.A. Kissin, A Reinvestigation of the Stannite (Cu_2FeSnS_4)-kesterite (Cu_2ZnSnS_4) pseudo-binary system, Can. Mineral. 27 (1989) 689–697 https://www.researchgate.net/publication/267400947.

[77] G. Larramona, S. Bourdais, A. Jacob, C. Chone, T. Muto, Y. Cuccaro, B. Delatouche, C. Moisan, D. Pere, G. Dennler, Efficient Cu_2ZnSnS_4 solar cells spray coated from a hydro-alcoholic colloid synthesized by instantaneous reaction, RSC Adv. 4 (2014) 14655–14662 https://doi.org/10.1039/C4RA01707B.

[78] V.G. Rajeshmon, N. Poornima, C.S. Kartha, K.P. Vijayakumar, Modification of optoelectronic properties of sprayed In_2S_3 thin film diffusion for application as a buffer layer in CZTS based solar cell, J. Alloy. Comp. 553 (2013) 239–244 https://doi.org/10.1016/j.jallcom.2012.11.106.

[79] O. Vigil Galan, M. Caurel, M. Espindola Rodriguez, D. Jimenez Olarte, M. Aguilar Frutis, E. Saucedo, Electrical properties of sprayed Cu_2ZnSnS_4 thin films and its relation with secondary phase formation and solar cell performance, Sol. Energy Mater. Sol. Cells 132 (2013) 557–562 https://doi.org/10.1016/j.solmat.2014.10.009.

[80] M. Espindola Rodriguez, D. Sylla, Y. Sanchez, S. L. opez-Marino, X. Fontane, J. Lopez-Garcıa, M. Placidi, A. Perez-Rodrıguez, O. Vigil-Galan and E. Saucedo, Pneumatically sprayed Cu_2ZnSnS_4 films under Ar and Ar–H_2 atmosphere, J. Phys. D Appl. Phys., 47 245101-245108. http://iopscience.iop.org/0022-3727/47/24/245101.

[81] O. Vigil-Galan, Maykel Courel, M. Espindola-Rodriguez, V. Izquierdo Roca, E. Saucedo, A. Fairbrother, Toward a high Cu_2ZnSnS_4 solar cell efficiency processed by spray pyrolysis method, J. Renew. Sustain. Energy 5 (2013) 053137–053152 https://doi.org/10.1063/1.4825253.

[82] M. Espindola Rodriguez, D. Sylla, Y. Sanchez, S. Lopez-Marino, X. Fontane, J. Lopez-Garca1, M. Placidi, A. Perez-Rodrıguez, O. Vigil-Galan, E. Saucedo, Pneumatically sprayed Cu_2ZnSnS_4 films under Ar and Ar–H_2 atmosphere, J. Phys. D Appl. Phys. 47 (2014) 245101–245109 https://doi.org/10.1088/0022-3727/47/24/245101.

[83] M.A.M. Khan, S. Kumar, M. Alhoshan, A.S. Al Dwayyan, Spray pyrolyzed Cu_2ZnSnS_4 absorbing layer: a potential candidate for photovoltaic applications, Optic Laser. Technol. 49 (2013) 196 https://doi.org/10.1016/j.optlastec.2012.12.012.

[84] Y. Miyamoto, K. Tanaka, L. Oonuki, N. Moritake, H. Uchiki, Optical properties of Cu_2ZnSnS_4 thin films prepared by sol-gel and sulfurization method, Jpn. J. Appl. Phys. 47 (2013) 596–597 https://doi.org/10.1143/JJAP.47.596.

[85] J.P. Leitao, N.M. Santos, P.A. Fernandes, P.M.P. Salome, A.F. da Cunha, J.C. Gonzalez, G.M. Ribeiro, F.M. Matinaga, Photoluminescence and electrical study of fluctuating potentials in Cu_2ZnSnS_4 based thin films, Phys. Rev. B 84 (2011) 024120–024128 https://doi.org/10.1103/PhysRevB.84.024120.

[86] K. Tanaka, Y. Miyamoto, H. Uchiki, K. Nakazawa, H. Araki, Donor-acceptor pair recombination luminescence from Cu_2ZnSnS_4 bulk single crystals, Phys. Status Solidi 203 (2006) 2891–2896 https://doi.org/10.1002/pssa.200669545.

[87] H. Yoo, J. Kim, L. Zhang, Sulfurization temperature effects on the growth of Cu_2ZnSnS_4 thin film, Curr. J. Appl. Phys. 12 (2012) 1052–1057 https://doi.org/10.1016/j.cap.2012.01.006.

[88] M. Grossberg, J. Krustok, J. Raudoja, T. Raadik, The role of structural properties on deep defect states in Cu_2ZnSnS_4 studied by photoluminescence spectroscopy, Appl. Phys. Lett. 101 (2012) 102102–102107 https://doi.org/10.1063/1.4750249.

[89] K. Hones, E. Zscherper, J. Scragg, S. Siebentritt, Shallow defects in Cu_2ZnSnS_4, Physica B 404 (2009) 4949–4952 https://doi.org/10.1016/j.physb.2009.08.206.

[90] S. Siebentritt, U. Rau, Wide-Gap Chalcopyrites, first ed., Springer Verlag Berlin Heidelberg, Berlin, 2006.

[91] S.A. Schumacher, J.R. Botha, Photoluminescence study of potential fluctuations in thin layers of Cu $(In_{0.75}Ga_{0.25})(S_ySe_{1\text{-}y})_2$, J. Appl. Phys. 99 (2006) 063508-8 https://doi.org/10.1063/1.2180429.

[92] P.W. Yu, Excitation-dependent emission in Mg-, Be-, Cd-, Zn-implanted GaAs, J. Appl. Phys. 48 (1977) 5043 https://doi.org/10.1063/1.323631.

[93] V.V. Osipov, T.I. Soboleva, M.G. Foigel, Impurity radiative recombination in heavily doped semiconductors, Sov. Phys. Semiconduct. 11 (1977) 752 http://www.jetp.ac.ru/cgi-bin/dn/e_048_03_0527.pdf.

[94] H. Katagiri, K. Jimbo, W.S. Maw, K. Oishi, M. Yamazaki, H. Araki, A. Takeuchi, Development of CZTS-based thin film solar cells, Thin Solid Films 517 (2009) 2455–2460 https://doi.org/10.1016/j.tsf.2008.11.002.

[95] J. Piekoszewski, J.J. Loferski, R. Beaulieu, J. Beall, B. Roessler, J. Shewchun, RF-sputtered $CuInSe_2$ thin films, Sol. Energy Mater. 2 (1980) 363–372 https://doi.org/10.1016/0165-1633(80)90012-X.

[96] R. Noufi, R. Axton, C. Herrington, S.K. Deb, Electronic properties versus composition of thin films of CuInSe2, Appl. Phys. Lett. 45 (1984) 668–670 https://doi.org/10.1063/1.95350.

[97] J. Tuttle, D. Albin, J. Goral, C. Kennedy, R. Noufi, Effects of composition and substrate temperature on the electro-optical properties of thin film $CuInSe_2$ and $CuGaSe_2$, Sol. Cell. 24 (1988) 67–79 https://doi.org/10.1016/0379-6787(88)90037-3.

[98] I. Repins, M.A. Contreras, B. Egaas, C. DeHart, J. Scharf, C.L. Perkins, Bobby to and Romenel Noufi, 19.9%-efficient ZnO/CdS/$CuInGaSe_2$ solar cell with 81.2% fill factor, Prog. Photovoltaic 16 (2008) 235–239 https://doi.org/10.1002/pip.822.

[99] S. Chen, J.H. Yang, X.G. Gong, A. Walsh, S.H. Wei, Intrinsic point defects and complexes in the quaternary kesterite semiconductor Cu_2ZnSnS_4, Phys. Rev. B 81 (2010) 245204 https://doi.org/10.1103/PhysRevB.81.245204.

[100] G. Suresh Babu, Y.B. Kishore Kumar, P.U. Bhaskar, V. Sundara Raja, Effect of Cu/(Zn + Sn) ratio on the properties of co-evaporated $Cu_2ZnSnSe_4$ thin films, Sol. Energy Mater. Sol. Cell. 94 (2010) 221–226 https://doi.org/10.1016/j.solmat.2009.09.005.

[101] Claudia Malerba, Cristy Leonor Azanza Ricardo, Matteo Valentini, Francesco Biccari, Melanie Muller, Luca Rebuffi, Emilia Esposito, Pietro Mangiapane, Paolo Scardi, Alberto Mittiga, Stoichiometry effect on Cu_2ZnSnS_4 thin films morphological and optical properties, J. Renew. Sustain. Energy 6 (2014) 011404-12 https://doi.org/10.1063/1.4866258.

[102] H. Katagiri, K. Jimbo, M. Tahara, H. Araki, K. Oishi, The influence of the composition ratio on CZTS-based thin film solar cells, Mater. Res. Soc. Symp. Proc. 1165 (2009) 01 https://doi.org/10.1557/PROC-1165-M04-01.

[103] Y.B. Kishore Kumar, G. Suresh Babu, P. Uday Bhaskar, S. Sundara Vanjari, Effect of starting-solution pH on the growth of Cu_2ZnSnS_4 thin films deposited by spray pyrolysis, Phys. Status Solidi 206 (2009) 1525–1530 https://doi.org/10.1002/pssa.200824424.

[104] T. Tanaka, A. Yoshida, D. Saiki, K. Saito, Q. Guo, M. Nishio, T. Yamaguchi, Influence of composition ratio on properties of Cu_2ZnSnS_4 thin films fabricated by

co-evaporation, Thin Solid Films 518 (2010) S29–S33 https://doi.org/10.1016/j.tsf.2010.03.026.

[105] K. Tanaka, Y. Fukui, N. Moritake, H. Uchiki, Chemical composition dependence of morphological and optical properties of Cu_2ZnSnS_4 thin films deposited by sol-gel sulfurization and Cu_2ZnSnS_4 thin film solar cell efficiency, Sol. Energy Mater. Sol. Cell. 95 (2011) 838–842 https://doi.org/10.1016/j.solmat.2010.10.031.

[106] M. Espindola-Rodriguez, M. Placidi, O. Vigil-Galan, V. Izquierdo-Roca, X. Fontane, A. Fairbrother, D. Sylla, E. Saucedo, A. Perez-Rodriguez, Compositional optimization of photovoltaic grade Cu_2ZnSnS_4 films grown by pneumatic spray pyrolysis, Thin Solid Films 535 (2013) 67–72 https://doi.org/10.1016/j.tsf.2012.12.082.

[107] C. Malerba, F. Biccari, C. Leonor, A. Ricardo, M. Valentini, R. Chierchia, M. Muller, A. Santoni, E. Esposito, P. Mangiapane, P. Scardi, A. Mittig, CZTS stoichiometry effects on the band gap energy, J. Alloy. Comp. 582 (2014) 528–534 https://doi.org/10.1016/j.jallcom.2013.07.199.

[108] T. Gershon, K. Sardashti, Y.S. Lee, O. Gunawan, S. Singh, D. Bishop, A.C. Kummel, R. Haight, Compositional effects in $Ag_2ZnSnSe_4$ thin films and photovoltaic devices, Acta Mater. 126 (2017) 383–388 https://doi.org/10.1016/j.actamat.2017.01.003.

[109] H. Katagiri, K. Saitoh, T. Washio, H. Shinohara, T. Kurumadani, S. Miyajima, Development of thin film solar cell based on Cu_2ZnSnS_4 thin films, Sol. Energy Mater. Sol. Cell. 65 (2001) 141–148 https://doi.org/10.1016/S0927-0248(00)00088-X.

[110] R.A. Wibowo, W.S. Kim, E.S. Lee, B. Munir, K.H. Kim, Single step preparation of quaternary $Cu_2ZnSnSe_4$ thin films by RF magnetron sputtering from binary chalcogenide targets, J. Phys. Chem. Solids 68 (2007) 1908–1913 https://doi.org/10.1016/j.jpcs.2007.05.022.

[111] T. Tanaka, T. Nagatomo, D. Kawasaki, M. Nishio, Q.X. Guo, A. Wakahara, A. Yoshida, H. Ogawa, Preparation of Cu_2ZnSnS_4 thin films by hybrid sputtering, J. Phys. Chem. Solids 66 (2005) 1978–1981 https://doi.org/10.1016/j.jpcs.2005.09.037.

[112] S. Chen, A. Walsh, X.G. Gong, S.H. Wei, Classification of lattice defects in the kesterite Cu_2ZnSnS_4 and $Cu_2ZnSnSe_4$ earth-abundant solar cell absorbers, Adv. Mater. 25 (2013) 1522–1539 https://doi.org/10.1002/adma.201203146.

[113] K. Tanaka, M. Oonuki, N. Moritake, H. Uchiki, Cu_2ZnSnS_4 thin film solar cells prepared by non-vacuum processing, Sol. Energy Mater. Sol. Cell. 93 (2009) 583–587 https://doi.org/10.1016/j.solmat.2008.12.009.

[114] M. Kumar, A. Dubey, N. Adhikari, S. Venkatesan, Q. Qiao, Strategic review of secondary phases, defects, defect-complexes in kesterite CZTS-Se solar cells, Energy Environ. Sci. 8 (2015) 3134–3159 https://doi.org/10.1039/C5EE02153G.

[115] T.K. Todorov, J. Tang, S. Bag, O. Gunawan, T. Gokmen, Y. Zhu, D.B. Mitzi, Beyond 11% efficiency: characteristics of state-of-the-art Cu2ZnSn(S,Se)4 solar cells, Adv. Energy Mater. 3 (2013) 34–38 https://doi.org/10.1002/aenm.201200348.

[116] A. Polizzotti, I.L. Repins, R. Noufi, S.H. Wei, D.B. Mitzi, The state and future prospects of kesterite photovoltaics, Energy Environ. Sci. 6 (2013) 3171–3182 https://doi.org/10.1039/C3EE41781F.

[117] S.Y. Chen, X.G. Gong, A. Walsh, S.H. Wei, Defect physics of the kesterite thin-film solar cell absorber Cu_2ZnSnS_4, Appl. Phys. Lett. 96 (2010) 021902-3 https://doi.org/10.1063/1.3275796.

[118] A. Polizzotti, I.L. Repins, R. Noufi, S.H. Wei, D.B. Mitzi, The state and future prospects of kesterite photovoltaics, Energy Environ. Sci. 6 (2013) 3171–3182 https://doi.org/10.1039/C3EE41781F.

[119] W.J. Yin, Y.L. Wu, S.H. Wei, R. Noufi, M.M. Al-Jassim, Y.F. Yan, Engineering grain boundaries in $Cu_2ZnSnSe_4$ for better cell performance: a first-principle study, Adv. Energy Mater. 4 (2014) 1300712–1300717 https://doi.org/10.1002/aenm.201300712.

[120] W.M. Haynes, D.R. Lide, Thomas J. Bruno, CRC Handbook of Chemistry and Physics: A Ready-Reference Book of Chemical and Physical Data, CRC press, New York, 1969.

[121] N. Kamoun, H. Bouzouita, B. Rezig, Fabrication and characterization of Cu_2ZnSnS_4 thin films deposited by spray pyrolysis technique, Thin Solid Films 515 (2007) 5949–5952 https://doi.org/10.1016/j.tsf.2006.12.144.

[122] G.S. Babu, Y.B. Kishore Kumar, P.U. Bhaskar, V. Sundara Raja, Growth and characterization of co-evaporated $Cu_2ZnSnSe_4$ thin films for photovoltaic applications, J. Phys. D Appl. Phys. 41 (2008) 205305 https://doi.org/10.1088/0022-3727/41/20/205305.

[123] W.M. Hlaing Oo, J.L. Johnson, A. Bhatia, E.A. Lund, M.M. Nowell, M.A. Scarpulla, Grain size and texture of Cu_2ZnSnS_4 thin films synthesized by cosputtering binary sulfides and annealing: effects of processing conditions and sodium, J. Electron. Mater. 40 (2011) 2214–2241 https://doi.org/10.1007/s11664-011-1729-3.

[124] H.T. Kim, D. Kim, C. Park, Temperature effects on Cu_2ZnSnS_4 (CZTS) films deposited by spraying method, Mol. Cryst. Liq. Cryst. 564 (2012) 155–161 https://doi.org/10.1080/15421406.2012.691733.

[125] D.B. Mitzi, O. Gunawan, T.K. Todorov, K. Wang, S. Guha, The path towards a high-performance solution-processed kesterite solar cell, Sol. Energy Mater. Sol. Cell. 95 (2011) 1421, https://doi.org/10.1016/j.solmat.2010.11.028.

[126] H. Cuin, X. Liu, N. Song, N. Li, F. Liu, X. Hao, Impact of rapid thermal annealing of Mo coated soda lime glass substrate on device performance of evaporated Cu_2ZnSnS_4 thin film solar cells, Mater. Lett. 125 (2014) 40–43, https://doi.org/10.1016/j.matlet.2014.03.122.

[127] R.J. Deokate, A.D. Adsool, N.S. Shinde, S.M. Pawar, C.D. Lokhande, Structural and Optical properties of spray deposited CZTS thin film, Energy Procedia 54 (2014) 627–633, https://doi.org/10.1016/j.egypro.2014.07.304.

[128] S.M. Bhosale, M.P. Suryawanshia, M.A. Gaikwad, P.N. Bhosale, J.H. Kim, A.V. Moholkar, Influence of growth temperatures on the properties of photoactive CZTS thin films using spray pyrolysis technique, Mater. Lett. 129 (2014) 153–155, https://doi.org/10.1016/j.matlet.2014.04.131.

[129] S. Thiruvenkadam, D. Jovina, A. Leo Rajesh, The influence of deposition temperature in the photovoltaic properties of spray deposited CZTS thin films, Sol. Energy 106 (2014) 166–170, https://doi.org/10.1016/j.solener.2014.02.041.

[130] S. Zhou, R. Tan, X. Jiang, X. Shen, W. Xu, W. Song, Growth of CZTS thin films by sulfurization of sputtered single layered Cu–Zn–Sn metallic precursors from an alloy target, J. Mater. Sci. Mater. Electron. 24 (2013) 4958–4963, https://doi.org/10.1007/s10854-013-1507-5.

[131] D.B. Khadka, S.Y. Kim, J.H. Kim, A non vacuum approach for fabrication of $Cu_2ZnSnSe_4/In_2S_3$ thin film solar cell and optoelectronic characterization, J. Phys. Chem. C 119 (2015) 12226–12235, https://doi.org/10.1021/acs.jpcc.5b03193.

[132] K. Diwatea, K. Mohiteb, M. Shindec, S. Rondiyaa, A. Pawbakea, A. Dated, H. Pathane, S. Jadkare, Synthesis and characterization of chemical spray pyrolyzed CZTS thin films for solar cell applications, Energy Procedia 110 (2017) 180–187, https://doi.org/10.1016/j.egypro.2017.03.125.

[133] E.M. Mkawi, K. Ibrahim, M.K.M. Ali, K.M.A. Saron, M.A. Farrukh, Nageh K. Allam, Influence of substrate temperature on the properties of electrodeposited kesterite Cu_2ZnSnS_4 (CZTS) thin films for photovoltaic applications, J. Mater. Sci. Mater. 26 (2015) 222–228, https://doi.org/10.1007/s10854-014-2387-z.

[134] O. Gunawan, T.K. Todorov, D.B. Mitzi, Loss mechanisms in hydrazine-processed $Cu_2ZnSn(Se,S)_4$ solar cells, Appl, Phys. Lett. 97 (2010) 233506-3 https://doi.org/10.1063/1.3522884.

[135] T. Kato, H. Hiroi, N. Sakai, S. Muraoka, H. Sugimoto, Characterization of Front and Back Interfaces on $Cu_2ZnSnS_{4,}$ Thin-Film Solar Cells, EU. PVSEC., 2012, pp. 2236–2239 https://www.researchgate.net/profile/Takuya_Kato3/publication/271814692.

[136] J.T. Watjen, J.J. Scragg, T. Ericson, M. Edoff, C. Platzer-Bjorkman, Secondary compound formation revealed by transmission electron microscopy at the Cu_2ZnSnS_4/Mo interface, Thin Solid Films 535 (2013) 31–34 https://doi.org/10.1016/j.tsf.2012.11.079.

[137] N. Muhunthan, O.P. Singh, M. Thakur, P. Karthikeyan, D. Singh, M. Saravanan, V. Singh, Interfacial properties of CZTS thin film solar cell, Sol. Energy (2014) 1–8 2014 https://doi.org/10.1155/2014/476123.

[138] T. Kato, H. Hiroi, N. Sakai, H. Sugimoto, Characterization of Front and Back Interfaces on Cu_2ZnSnS_4 Thin-Film Solar Cells, PSECE, 2013, pp. 2125–2127 https://www.researchgate.net/profile/Takuya_Kato3/publication/271814692.

[139] K.J. Yang, J.H. Sim, B. Jeon, D.H. Son, D.H. Kim, S.J. Sung, D.K. Hwang, S. Song, D.B. Khadka, J. Kim, Effects of Na and MoS_2 on Cu_2ZnSnS_4 thin-film solar cell, Prog. Photovoltaics 23 (2015) 862–873 https://doi.org/10.1002/pip.2500.

[140] B. Shin, Y. Zhu, N.A. Bojarczuk, S.J. Chey, S. Guha, Control of an interfacial $MoSe_2$ layer in $Cu_2ZnSnSe_4$ thin film solar cells: 8.9% power conversion efficiency with a TiN diffusion barrier, Appl. Phys. Lett. 101 (2012) 053903-4 https://doi.org/10.1063/1.4740276.

[141] J.J. Scragg, T. Kubart, J.T. Watjen, T. Ericson, M.K. Linnarsson, C. Platzer-Bjorkman, Effects of back contact instability on Cu_2ZnSnS_4 devices and processes, Chem. Mater. 25 (2013) 3162–3171, https://doi.org/10.1021/cm4015223.

[142] B. Shin, N.A. Bojarczuk, S. Guha, On the kinetics of $MoSe_2$ interfacial layer formation in chalcogen-based thin film solar cells with a molybdenum back contact, Appl. Phys. Lett. 102 (2013) 091907-3 https://doi.org/10.1063/1.4794422.

[143] R. Scheer, H.W. Schock, Chalcogenide Photovoltaics: Physics, Technologies, and Thin Film Devices, first ed., John Wiley and Sons, Halle (Saale), Germany, 2011.

[144] M. Gloeckler, J. Sites, Efficiency limitations for wide-band-gap chalcopyrite solar cells, Thin Solid Films 480–481 (2005) 241–245, https://doi.org/10.1016/j.tsf.2004.11.018.

[145] S. Sharbati, J.R. Sites, Impact of the band offset for n-Zn(O,S)/p-Cu(In,Ga)$Se_{[2]}$ solar cells, IEEE J. of Photovolt. 4 (2014) [697]–[702] https://ieeexplore.ieee.org/iel7/5503869/6744664/06722905.

[146] R. Haight, A. Barkhouse, O. Gunawan, B. Shin, M. Copel, M. Hopstaken, D.B. Mitzi, Band alignment at the $Cu2ZnSn(S_xSe_{1-x})_4/CdSCu_2ZnSn(S_xSe_{1-x})_4$/CdS interface, Appl. Phys. Lett. 98 (2011) 253502–253503 https://doi.org/10.1063/1.3600776.

[147] A. Santoni, F. Biccari, C. Malerba, M. Valentini, R. Chierchia, A. Mittiga, Valence band offset at the CdS/Cu_2ZnSnS_4 interface probed by x-ray photoelectron spectroscopy, J. Phys. D Appl. Phys. 46 (2013) 175101–175105 https://doi.org/10.1088/0022-3727/46/17/175101.

[148] R. Haight, A. Barkhouse, O. Gunawan, B. Shin, M. Copel, M. Hopstaken, D.B. Mitzi, Band alignment at the $Cu_2ZnSn(S_xSe_{1-x})_4$/CdS interface, Appl. Phys. Lett. 98 (2011) 253502–253503 https://doi.org/10.1063/1.3600776.

[149] S. Tajima, K. Kataoka, N. Takahashi, Y. Kimoto, T. Fukano, M. Hasegawa, H. Hazama, Direct measurement of band offset at the interface between CdS and Cu_2ZnSnS_4 using hard X-ray photoelectron spectroscopy, Appl. Phys. Lett. 103 (2013) 243906-4 https://doi.org/10.1063/1.4850235.

[150] J. Keller, J. Lindah, M. Edoff, L. Stolt, T. Torndahl, Potential gain in photocurrent generation for Cu (In, Ga) Se_2 solar cells by using In_2O_3 as a transparent conductive oxide layer, Prog. Photovoltics 24 (2016) 102–107, https://doi.org/10.1002/pip.2655.

[151] K.H. Huang, J.G. Yu, C.P. Kuo, R.M. Fletcher, T.D. Osentowski, L.J. Stinson, M.G. Craford, A.S.H. Liao, Twofold efficiency improvement in high-performance AlGaInP light-emitting diodes in the 555-620 nm spectral region using a thick GaP window layer, Appl. Phys. Lett. 61 (1992) 1045–1047 https://doi.org/10.1063/1.107711.

[152] A. Janotti, C.G. Van de Walle, Fundamentals of zinc oxide as a semiconductor, Rep. Prog. Phys. 72 (2009) 126501–126529, https://doi.org/10.1088/0034-4885/72/12/126501.

[153] U. Rau, M. Schmidt, Electronic properties of $ZnO/CdS/Cu(In,Ga)Se_2$ solar cells aspects of hetero-junction formation, Thin Solid Films 387 (2001) 141–146, https://doi.org/10.1016/S0040-6090(00)01737-5.

[154] M. Ruckh, D. Schmid, H.W. Schock, Photoemission studies of the ZnO/CdS

interface, J. Appl. Phys. 76 (1994) 5945–5948 https://doi.org/10.1063/1.358417.

[155] L. Weinhardt, C. Heske, E. Umbach, T. Niesen, S. Visbeck, F. Karg, Band alignment at the i-ZnO/CdSi-ZnO/CdS interface in Cu(In,Ga)(S,Se)$_2$Cu(In,Ga)(S,Se)$_2$ thin-film solar cells, Appl. Phys. Lett. 84 (2004) 3175–3177 https://doi.org/10.1063/1.1704877.

[156] K. Orgassa, H.W. Schock, J.H. Werner, Alternative back contact materials for thin film Cu(In, Ga)Se$_2$ solar cells, Thin Solid Films 431 (2003) 387–391, https://doi.org/10.1016/S0040-6090(03)00257-8.

[157] L. Assmann, J. Bernede, A. Drici, C. Amory, E. Halgand, M. Morsli, Study of the Mo thin films and Mo/CIGS interface properties, Appl. Surf. Sci. 246 (2005) 159–166 https://doi.org/10.1016/j.apsusc.2004.11.020.

[158] J.J. Scragg, J.T. Watjen, M. Edoff, T. Ericson, T. Kubart, C. Platzer-Bjorkman, A detrimental reaction at the molybdenum back contact in Cu$_2$ZnSn(S,Se)$_4$ thin-film solar cells, J. Am. Chem. Soc. 134 (2012) 19330–19333 https:/doi.org/10.1021/ja308862n.

[159] S. Nishiwaki, N. Kohara, T. Negami, T. Wada, MoSe $_2$ layer formation at Cu(In,Ga) Se $_2$/Mo interfaces in high efficiency Cu(In$_{1-x}$Ga $_x$)Se $_2$ solar cells, Jpn. J. Appl. Phys. 37 (1998) L71 https://doi.org/10.1143/JJAP.37.L71.

[160] T. Kato, H. Hiroi, N. Sakai, H. Sugimoto, Buffer/absorber interface study on Cu$_2$ZnSnS$_4$ and Cu$_2$ZnSnSe$_4$ based solar cells: band Alignment and its impact on the solar cell performance, PSECE, 2013, pp. 2125–2127, https://doi.org/10.4229/28thEUPVSEC2013-3AO.5.1.

[161] J.J. Scragg, J.T. Watjen, M. Edoff, T. Ericson, T. Kubart, C. Platzer-Bjorkman, A detrimental reaction at the molybdenum back contact in Cu$_2$ZnSn(S,Se)$_4$ thin-film solar cells, J. Am. Chem. Soc. 134 (2012) 19330–19333, https://doi.org/10.1021/ja308862n.

[162] Y. Feng, T.K. Lau, G. Cheng, L. Yin, Z. Li, H. Luo, Z. Liu, X. Lu, C. Yang, X. Xiao, A low-temperature formation path toward highly efficient Se-free Cu$_2$ZnSnS$_4$ solar cells fabricated through sputtering and sulfurization, CrystEngComm 18 (2016) 1070–1077, https://doi.org/10.1039/c5ce02279g.

[163] K.J. Yang, J.H. Sim, B. Jeon, D.H. Son, D.H. Kim, S.J. Sung, D.K. Hwang, S. Song, D.B. Khadka, J. Kim, Effects of Na and MoS2 on Cu2ZnSnS4thin-film solar cell, Prog. Photovoltaics 23 (2015) 862–873, https://doi.org/10.1002/pip.2500.

[164] B. Shin, Y. Zhu, N.A. Bojarczuk, S.J. Chey, S. Guha, Control of an interfacial MoSe2 layer in Cu2ZnSnSe4 thin film solar cells: 8.9% power conversion efficiency with a TiN diffusion barrier, Appl. Phys. Lett. 101 (2012) 053903-4 https://doi.org/10.1063/1.4740276.

[165] T.P. Dhakal, S. Harvel, M. van Hest, Glenn Teeter, Back Contact Band Offset Study of Mo-CZTS Based Solar Cell Structure by Using XPS/UPS Techniques, IEEE, 2015, https://doi.org/10.1109/PVSC.2015.7355623.

[166] J.J. Scragg, T. Kubart, J.T. Watjen, T. Ericson, M.K. Linnarsson, C. Platzer-Bjorkman, Effects of back contact instability on Cu$_2$ZnSnS$_4$ devices and processes, Chem. Mater. 25 (2013) 3162–3171, https://doi.org/10.1021/cm4015223.

[167] B. Shin, Y. Zhu, N.A. Bojarczuk, S.J. Chey, S. Guha, Control of an interfacial MoSe$_2$ layer in Cu$_2$ZnSnSe$_4$ thin film solar cells: 8.9% power conversion efficiency with a TiN diffusion barrier, Appl. Phys. Lett. 101 (2012) 053903-4 https://doi.org/10.1063/1.4740276.

[168] S. Lopez-Marino, M. Placidi, A. Perez-Tomas, J. Llobet, V. Izquierdo-Roca, X. Fontane, A. Fairbrother, M. Espindola-Rodriguez, D. Sylla, A. Perez-Rodriguez, Inhibiting the absorber/Mo-back contact decomposition reaction in Cu$_2$ZnSnSe$_4$ solar cells: the role of a ZnO intermediate nanolayer, J. Mater. Chem. 1 (2013) 8338–8343, https://doi.org/10.1039/C3TA11419H.

[169] X. Liu, H. Cui, W. Li, N. Song, F. Liu, G. Conibeer, X. Hao, Improving Cu$_2$ZnSnS$_4$ (CZTS) solar cell performance by an ultrathin ZnO intermediate layer between CZTS absorber and Mo back contact, Physica Status Solidi RRL 8 (2014) 966–970 https://doi.org/10.1002/pssr.201409052.

[170] J.J. Scragg, T. Kubart, J.T. Watjen, T. Ericson, M.K. Linnarsson, C. Platzer-Bjorkman, Effects of back contact instability on Cu$_2$ZnSnS$_4$ devices and processes, Chem. Mater. 25 (2013) 3162–3171, https://doi.org/10.1021/cm4015223.

[171] F. Zhou, F. Zeng, X. Liu, F. Liu, N. Song, C. Yan, A. Pu, J. Park, K. Sun, X. Hao, Improvement of J_{sc} in a Cu$_2$ZnSnS$_4$ solar cell by using a thin carbon intermediate layer at the Cu$_2$ZnSnS$_4$/Mo interface, ACS Appl. Mater. Interfaces 7 (2015) 22868–22873, https://doi.org/10.1021/acsami.5b05652.

[172] F. Zeng, K. Sun, L. Gong, L. Jiang, F. Liu, Y. Lai, J. Li, Back contact absorber interface modification by inserting carbon intermediate layer and conversion efficiency improvement in Cu$_2$ZnSn(S,Se)$_4$ solar, Phys. Status Solidi R. 9 (2015) 687–691, https://doi.org/10.1002/pssr.201510280.

[173] H. Cui, X. Liu, F. Liu, X. Hao, N. Song, C. Yan, Boosting Cu$_2$ZnSnS$_4$ solar cells efficiency by a thin Ag intermediate layer between absorber and back contact, Appl. Phys. Lett. 104 (2014) 041115-4 https://www.researchgate.net/publication/260598835.

[174] F. Liu, K. Sun, W. Li, C. Yan, H. Cui, L. Jiang, X. Hao, M.A. Green, Enhancing the Cu2ZnSnS4 solar cell efficiency by back contact modification: inserting a thin TiB2 intermediate layer at Cu$_2$ZnSnS$_4$/Mo interface, Appl. Phys. Lett. 104 (2014) 051105-5 https://doi.org/10.1063/1.4863736.

[175] Z. Tong, K. Zhang, K. Sun, C. Yan, F. Liu, L. Jiang, Y. Lai, X. Hao, J. Li, Modification of absorber quality and Mo-back contact by a thin Bi intermediate layer for kesterite Cu$_2$ZnSnS$_4$ solar cells, Sol. Energy Mater. Sol. Cell. 144 (2016) 537–543 https://doi.org/10.1016/j.solmat.2015.09.066.

[176] F. Liu, J. Huang, K. Sun, C. Yan, Y. Shen, J. Park, A. Pu, F. Zhou, X. Liu, J.A. Stride, M.A. Green, X. Hao, Beyond 8% ultrathin kesterite Cu2ZnSnS4 solar cells by interface reaction route controlling and self-organized nano pattern at the back contact, NPG Asia Mater. 9 (2017) e401, https://doi.org/10.1038/am.2017.103.

[177] T. Minemoto, T. Matsui, H. Takakura, Y. Hamakawa, T. Negami, Y. Hashimoto, T. Uenoyama, M. Kitagawa, Theoretical analysis of the effect of conduction band offset of window/CIS layers on performance of CIS solar cells using device simulation, Sol. Energy Mater. Sol. Cells 67 (2001) 83–88 https://doi.org/10.1016/S0927-0248(00)00266-X.

[178] J. Holzl, F.K. Schulte, H. Wagner, Solid Surface Physics, Springer Verleg, Berlin, Germany, 1979.

[179] J.C. Riviere, M. Green (Ed.), Solid State Surface Science, Marcel Dekker, New York, USA, 1969.

[180] H.B. Michaelson, The work function of the elements and its periodicity, J. Appl. Phys. 48 (1977) 4729–4733 https://doi.org/10.1063/1.323539.

[181] A.J. Moule, J.B. Bonekamp, K. Meerholz, The effect of active layer thickness and composition on the performance of bulk-hetero-junction solar cells, J. Appl. Phys. 100 (2006) 094503 https://doi.org/10.1063/1.2360780.

[182] S. Sahayaraj, G. Brammertz, M. Buffiere, M. Meuris, J. Vleugels, J. Poortmans, Effect of Cu content and temperature on the properties of Cu$_2$ZnSnSe$_4$ solar cells, EPJ Photovoltaics 7 (2016) 70304–70313 https://doi.org/10.1051/epjpv/2016004.

Article

Advanced Science, Engineering and Medicine
Vol. 10, 1–7, 2018
www.aspbs.com/asem

A Review on the Current and Future Possibilities of Copper-Zinc Tin Sulfur Thin Film Solar Cell to Increase More Than 20% Efficiency

Krishan Pal, Khem B. Thapa*, and Abhisikta Bhaduri

Department of Applied Physics, School for Physical Sciences, Babasaheb Bhimrao Ambedkar University
(A Central University), Lucknow (UP), India

The non-toxic and eco-friendly solar-cell of CZTS thin film could be produced as an absorber. CZTS has two structures which are known as stannite-type (space group I42m) and kesterite type (space group $I\bar{4}$). In recent years, Kasterite-based solar cells have attracted more attention for their significant reduced toxicity and greater abundance of ingredient elements. In this review, we shall discuss the current and future probabilities of this important thin film technology. In such thin film technology, we mainly focus on three features of the device: (i) Secondary phases of the absorber bulk defects and grain boundaries, (ii) The interface between the absorber (kesterite) and the buffer layer, (iii) The interface between the absorber (kesterite) and the Mo back contact. Due to non-toxic, eco-friendly and the silent features of the CZTS structure, the current and future possibilities of CZTS thin film solar cell is required to study. The potential research on CZTS may increase or improve efficiency of such cell more than 20%.

Keywords: Kesterite, Stannite, Secondary Phase, Grain Boundaries and the Buffer Layer.

1. INTRODUCTION

Three types of thin film materials have become industrially famous to produce solar energy and these solar cells are amorphous silicon (a-Si), Cadmium telluride (CdTe), Copper-Indium-Gallium Selenide/Sulfide (CIGS), where CIGS has reached the highest efficiencies ($\geq$20%) and can compete with poly-crystalline silicon. But CIGS will have to face some difficulties like Indium is a rare element and non-abundant within the next some years due to which the price is increasing rapidly.[1] As the availability of Cu, Zn, Sn and S are $\sim$50, 75, 2.2 and 260 ppm in the earth's crust respectively and the enforceable of Indium is only $\sim$0.049 ppm, indium can be replaced by Zinc and Tin and hence the quaternary compound copper zinc tin sulphide/selenide $Cu_2ZnSn(S/Se)_4$ (CZTS) has emerged.[2] CZTS is a quaternary compound that has a direct band gap, $E_g = (1.4–1.5)$ eV with 10^4 cm^{-1} absorption coefficient and *p*-type conductivity (Intrinsic point defects).[2]

According to crystallography studies, CZTS has two equilibrium structures called as (i) Kesterite type ($I\bar{4}$), (ii) Stannite type (I42m). However, due to thermo dynamical stability, mostly CZTS material appears in kesterite phase. Kasterite-based solar cells have attracted more attention for significant cells.

According to the Shockley–Queisser photon balance limit, theoretically, 32.2% conversion efficiency is estimated of the single-junction CZTS(Se) solar cells.[3] CZTS(Se) show extended behavior to be the ideal thin film solar cell material for low-cost, sustainable, high-efficiency, and environment-friendly photovoltaic technology.[4]

In 1997, Katagiri et al.[5] reported the first vacuum deposited CZTS solar cell and identified a power conversion efficiency of 0.66%. In 2013, the efficiency of the CZTSSe cell was reported to be 12.6% which was the current world record.[6] Since 2013, a lot of works has been done on CZTS for photovoltaic applications. A solution-based film deposition approach has been used since 2009. There is a contradiction that solution-deposited films are generally lower performing compared to vacuum-deposited analogous. The best kesterite solar cell have with a S/(S+Se) ratio of about 40%, band gap 1.15 eV, and

---

* Author to whom correspondence should be addressed.

an efficiency of 10.1% which is determined by quantum efficiency measurements.[8]

There is a lot of review papers have been published on kesterite solar cells[11–24] due to their non-toxic and eco-friendly behavior. Previously, a lot of researchers identified the key issues to determine the properties of kesterite absorbers, such as crystal structure, phase diagram, secondary phases, chemical composition, defect physics, electronic band structure, grain boundaries, optical properties, fabrication strategies and characterization methods, and two critical interfaces, i.e., the interfaces between the kesterite absorber and the molybdenum (Mo) back contact and between the kesterite absorber and the CdS buffer layer.[9] Although there are some best-quality review papers have been published to summarize the challenges and promises of kesterite devices.[9] In this work, our objective is to provide a brief description, including more recent selected studies, synthesis process and observations to identify new pathways to obtain highly efficient kesterite solar cells in future.

Besides this kesterite solar cell, people are also working on CNT based solar cells as it is experimentally seen that the efficiency of solar cell can be enhanced up to 16% when the carbon nanotubes are taken inside the cell.[40]

1.1. Copper Zinc Tin Sulfur Compound

Copper-Zinc Tin Sulfur (CZTS) is a quaternary compound of I–II–IV–VI group element. It has tremendous properties such as high absorbent, earth-abundant, non-toxic, direct band gap. Depending on the position of Cu and Zn, CZTS be classified as Kesterite and Stannite structure with different characteristics. The Kesterites have the specific characteristics for solar cell application at which research work is going on last ten years. The physical, chemical and optical properties of CZTS are controlled by synthesis process and stoichiometry.

1.2. Synthesis of Copper Zinc Tin Sulfur

Copper Zinc Tin Sulfur is produced by many methods such as Sol–Gel, spray pyrolysis, hot-injection, and CVD. In the growth of CZTS by spray pyrolysis involve the secondary and ternary phases which affect the electronic and optical properties. Sometimes CZTS are also prepared Physical Vapour Deposition method.[41] CVD results in CZTS is a good quality but toxic gases are reduced.

2. ELECTRICAL/OPTICAL PROPERTIES OF CZTS

Electrical properties of CZTS can be easily understood from the band structure of the compound. CZTS obey the Lewis octet rule with S or Se anion atom. The bonds of the anion atom formed a closed valance shell (CVS). CZTS constructs from ZnS by replacing the Zn atom to Cu and Sn. In this process, Valance electrons are preserved in number. CZTS has band geometry similar to the traditional semiconductors as Ge, ZnS, GaAs. CZTS have sp^3 hybridization and for anions, it includes Cu-d anion-p hybridized antibonding state and for cations, Cu has 1s-valence electron in CZTS or CZTSe. Since 2009, several works are going on DFT-based theoretical studies of CZTS, Se and identified crystalline and electronic structures, material properties, defect properties. We estimated the gap energy 1.5 eV for CZTS and 1.0 eV for CZTSe by the methods HSE06, GW$_0$ and GGA plus calculation.[25]

The optical properties of CZTS can be easily understood in complex dielectric functional term $\varepsilon(\omega) = \varepsilon_1(\omega) + i\varepsilon_2(\omega)$ and absorption coefficient $\alpha(\omega)$. The imaginary part of this function is calculated:[42]

$$\varepsilon_2^{\alpha\beta}(\omega) = \lim_{q\to 0} \frac{4\pi^2 e^2}{\Omega q^2} \sum_{c,v,k} 2\omega_k \delta(E_k(k) - E_v(k) - \omega) \times \left\langle \frac{u_c(k+e_\alpha q)}{u_v k} \right\rangle \langle u_c(k+e_\beta q)/u_v(k)\rangle$$

The real part of this function is calculated by the Kremers-Kroning transformation relation:

$$\varepsilon_1^{\alpha\beta}(\omega) = 1 + \frac{2}{\pi} P \int_0^\infty \frac{\omega' e_2^{\alpha\beta}(\omega')}{\omega'^2 - \omega^2 + i\eta}\, d\omega'$$

And the absorption coefficient is calculated from the complex dielectric function.

3. CHEMICAL PROPERTIES OF CZTS

Chemical properties of the CZTS, Se understood from the chemical composition, element behavior, and synthesis techniques. There is a typical task to synthesize a single-phase polycrystalline thin film due to the low thermal stability of compound and secondary phases are generated, in which Cu_2SnSe_3 restricts the open circuit voltage and ZnSe reduce the photocurrent.[43, 44] The stability of the material depends on the equilibrium constant K. The equilibrium constant directly depends on the Gibbs free energy and temperature.

4. CZTS AS A SOLAR CELLS

In this world, most of the energy generated from the fossil fuel. These Fossils fuel produces harmful gases as CO, CO_2 etc. with burning. The solar energy is the best substitute in the environmental and economical point of view. To use the solar energy, the solar cell is best option to convert the solar energy into electrical energy. Operation of a solar cell is explained by the following factors:

(a) Generation of electron–hole pairs after the light absorption.
(b) Dispersing of the charge carriers.
(c) Separating the electron and hole.
(d) Charge carriers collection.

According to the Yadav et al.,[57] there is compulsory appropriate band gap of 1.1 to 1.7 eV, direct band

Table I. The role of composition ratio in the solar cell efficiency.

Material	Methods	Composition ratio (Cu/Zn + Sn, Zn/Sn)	Characterisation	Efficiency	Reference
CZTSe	Box-type vacuum coating system	0.90–1.10	Single phase, electrical resistivity 0.02–23-Om-cm, polycrystalline	–	[5]
CZTS	RF cosputtering continued with sulfurization	0.75–1.25, 0.80–1.35	$V_{oc} = 623$ mV, $J_{sc} = 13.9$ mA/cm^2, FF = 0.6	Conversion efficiency = 5.19	[46]
CZTS	Co-evaporation	0.86 to 1.06	Crystallinity and grain size increased	–	[47]
CZTS	Vapor-phase sulfurization	0.82–0.94	$V_{oc} = 735$ mV	2.62%	[48]
CZTS	PLD	0.63–1.08, 0.67–0.86	$V_{oc} = 546$ mV, $I_{sc} = 6.78$ mA/cm^2, FF = 0.48	1.74%	[49]
CZTS	Co-sputtering technique	0.85, 1.25	$V_{oc} = 610$ mV, $J_{sc} = 17{:}9$ mA/cm^2, FF = 0:62, $R_s = 4{:}25$, and $R_{sh} = 370$	6.77%	[50]

Table II. Development of solar cells by various methods.

Materials	Deposition technique	Theoretical/Experimental efficiency	Band gap	Advantage	Disadvantage	References
CdS/CZTSSe	Spray pyrolysis, sputtering, PVD	32.2%, 12.6%	Direct band gap/1.4–1.5 eV	Abundant, cheap, green material	Mixed phases, difficult to synthesize	[10, 25]
CdTe/CdS	Evaporation sublimation, screen printing technique	32%, 16.5%	1.5 eV	Good stability, high module efficiency	Toxicity of Cd, availability of Te	[51, 52]
CuInGaS/Se	Evaporation, sputter deposition, electroplating, spray pyrolysis	28–32%, 22.6%	1.0–1.7 eV	Good stability	Multiple binary phases, cell to cell mismatch	[53]
CNT based	CVD, sputtering, electroplating	32%, 16%	Direct band gap/1.5 eV	Lighter flexible	Costly, toxic gas CO released on synthesis	[54]
Perovskite	Spray pyrolysis, PLD, PVD	32.2%, 23.6%	Graded band gap	Low cost, high efficiency	Low stability	[25, 55]

structure, easy availability, Non-toxic, Easy, reproducible deposition technique, suitable for large area production excellent photovoltaic conversion efficiency long-term stability. So, the CZTS have maximum characteristics as above given. On analyzing the solar cell overview, we have found that the efficiency is increased by the change in the ratio and synthesis technique of the CZTS compound. CZTS was used in cells as a *p*-type semiconductor and CdS is act as *n*-type material. The role of the composition ratio on the solar cell efficiency is shown in the Table I.

Thin film technology reduced the amount of solar cell material which affects the cost of the cell. There are some profits, to using this technology such as reduction in recombination losses, reduce the series resistance. In Table II, the efficiency of the synthesis technique with advantages and disadvantages of different types of solar cell is depicted. It can be seen that there is a big research gap between the theoretical and experimental efficiency of the solar cell which is shown the maximum probability of remaining experimental work.

5. CURRENT AND FUTURE POSSIBILITIES OF CZTS TO INCREASE THE EFFICIENCY

5.1. The CZTS Bulk Defect and Grain Boundaries

To improve the efficiency of a solar cell, it is very important to understand the thermodynamic stability of the quaternary compounds CZTS, CZTSe and the formation mechanism of the dominant intrinsic defects. The important material properties are lattice defects, which are important for the application of the semiconductors in photovoltaic devices since they directly influence the recombination of electron–hole pairs and the generation and separation. For CZTS, the formation energy of intrinsic point defects such as vacancies (V_{cu}, V_{zn}, V_{sn}), antisite (Cu_{zn}, Cu_{sn}, Zn_{cu}, Sn_{cu}, Zn_{sn}, Sn_{zn}), and interstitials (Cu_i, Zn_i, Sn_i, Se_i) at different chemical-potential points are shown in Table III. They can be classified as the formal valency of the elements electron acceptor and donors which as shown in Figure 1. Table III shows that the formation energy of Cu_{Zn} antisite is lower than those of other defects in copper poor condition and the acceptor defects (e.g., V_{Zn}, Zn_{Sn}, Cu_{Sn}) have higher formation energy.[26]

Table III. Calculated defect formation energies (eV) for intrinsic point defects in CZTS with different growth condition.[25]

Defect	Zn poor condition	Cu poor conditions
V_{Cu}	0.590	0.21–0.67
Zn_{Cu}	−0.064 to −0.318	2.43–2.60
Cu_{Zn}	0.378–0.632	−0.16 to 0.01
V_{Zn}	0.631–0.885	0.39–1.02
Sn_{Zn}	0.158–0.599	4.11–4.44
Sn_{Cu}	0.170–0.732	6.54–7.05

The intrinsic defect is common to both chalcopyrites and kesterites. The acceptor level is introduced by V_{Cu} and shown always shallow. This is uninfluenced by the replacement of Indium by Zn and Sn cations. The transition energy level of V_{Cu} which is ionized from neutral 0 to -1 charge is even 10 meV for Cu_2ZnSnS_4. The level of Cu_{Zn} is 0.11 eV for $Cu_2ZnSnSe_4$ and 0.15 eV for Cu_2ZnSnS_4 in 128-atoms super cell, which is deeper than V_{Cu}.[26] The upper valence band of kesterite CZTS composed of the anti-bonding states between Cu 3*d* and S 3*p* shells as shown in Figure 2. This is enhanced when one Zn and Cu atom is replaced by each other. It is weakened when one Cu is replaced by a vacancy. So the associated acceptor level of Cu_{Zn} is pushed up, and thus appears deeper than that of V_{Cu}.

The ionization of the effective Cu_{Zn} antisite with a high population can produce a significant amount of hole carriers. The high formation energy of other acceptor defects (Cu_{Sn}, Zn_{Sn}, V_{Zn} and V_{Sn}) has induced a valence change of more than two. The contribution to observe the *p*-type conductivity is negligible in the single-phase kesterite samples. However, they could contribute to luminescence and act as recombination centers.

The Grain boundaries are reported to exhibit advanced electronic properties in Cu-poor and Zn-rich CZTS and CZTSSe solar cells.[30] The grain boundaries may be used as electron flow channel nay than the effective recombination centers. The grain boundaries may act as an electrostatic potential barrier to increase charge separation near the grain boundaries due to potential spike formation. In 2013, Polizzotti have suggested in the Cu-poor and Zn-rich conditions, the defect clusters $[V_{Cu}+Zn_{Cu}]$ are thermodynamically favourable in ordered defect compound (ODC).[29] The ODC model decreases the valence band energies and conduction band edge energies of the kesterite. By which it leads to the potential barrier which attracts electrons and repels holes toward grain boundaries. Yin studied the properties of grain boundaries and proposed a different theory using the first-principles density functional theory (DFT).[30] After the theoretical calculation, they studied that the deep defects affected by the wrong bonds of Cu–Sn and Se–Se at grain boundaries are passivated by Zn_{Sn} and O_{Se} through breaking or weakening of these bonds, which reduces recombination of grain boundaries.

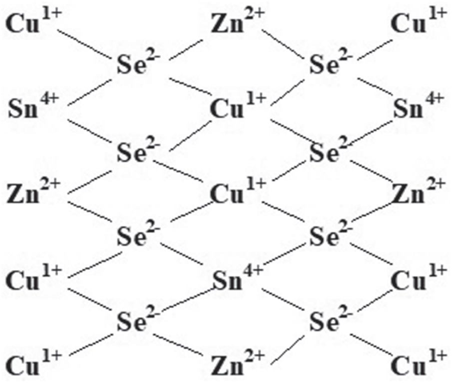

Figure 1. The crystal structure and the nominal valence of cations and anions of $Cu_2ZnSnSe_4$. The circles show that the Se anions are in the 8-electrons full shell state (solid and dashed circles mean the Se anions are in different layers parallel to the plane).[26]

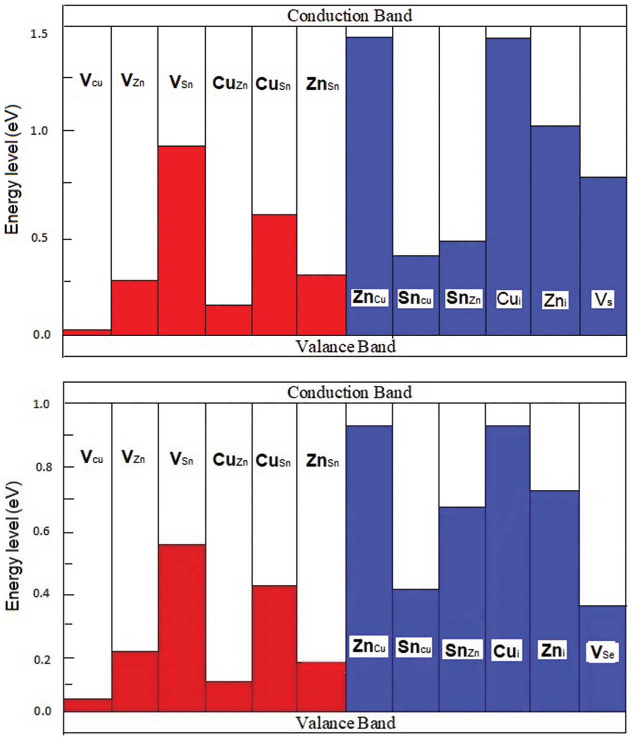

Figure 2. The ionization levels of intrinsic defects in the band gaps of Cu_2ZnSnS_4 (top) and $Cu_2ZnSnSe_4$ (bottom).[27]

The effect of Na has been investigated on the grain boundaries. On SLG substrate, Na is profitable for high-efficiency CIGS solar cells. During the high-temperature deposition/annealing process in CIGS solar cells, sodium can out-diffuse. Hence, the effect of Na on kesterite solar cells investigated, less. Na role plays a major, in grain growth mechanism.[33] The effect of Na on the grain growth of kesterite has been found to exhibit a threshold type behavior. For the growth of large grain size, there is compulsory required critical concentration of sodium. The concentration of sodium reduces the grain size due to the formation of a secondary phase of NaCl. There is a formation of low melting point compounds of Na which was proposed as the mechanism to explain the enhanced grain size.[34, 35] At the growth temperature, the liquid compounds of sodium remove ZnS in the copper-poor and zinc-rich growth conditions and increase the mobility of grain boundaries and cause large grain size. The formation of liquid compounds of sodium is not observed directly in experiments. Na was observed to passivation the grain boundaries and reduces the non-radiative recombination in vacuum-deposited CZTS, due to which V_{oc} is improved. Na was demonstrated to increase the hole concentrations in monocrystalline and polycrystalline crystals and to improve open circuit voltage.

Presence of sodium increases the concentration of both acceptors and compensating donors which were experimentally found by the temperature-dependent Hall measurements. The increase in acceptor concentration is more significant than the compensating donor concentration, by which net carrier concentration gets increased.

According to research on effect of sodium on chalcopyrites, there are four assumptions on CZTS crystals: (i) Increasing the carrier concentration and reducing the compensation are due to the antisite Na_{Cu} defect which inhibits the formation of the donor-type Zn_{Cu} defect, (ii) The increase of carrier concentration and removal of donor-type V_s defect are due to the correlation of sodium (Na) and oxygen (O_2), (iii) the acceptor-type Na_{Zn} antisite defect formed by Na increases carrier concentration, (iv) Na helps to increase the net carrier concentration without introducing defects. Still, further investigations are required to understand the mechanism of the effect of sodium on the carrier concentration.

5.2. The Interface Between the Kesterite Absorber and the Buffer Layer

One the most critical factors in achieving high-performance device is to offset the buffer layer the of conduction band/kesterite absorber. A spike confirms that the buffer layer has the conduction band minimum (CBM) higher than the kesterite absorber as shown in Figure 3(a). The negative value of conduction band offset (CBO) shows a cliff in which the CBM of the buffer layer is lower than that of the kesterite absorber as shown in Figure 3(b).

The cliff-like structure conformation acts as a barrier (0.4 eV) to stop the flow of injected electrons in the forward bias. The interfacial recombination is increased by the accumulation of injected electrons between the majority hole carriers in Copper Indium Gallium Sulfide (CIGS) and it results in reducing V_{oc}. The spike does not form a barrier for injected electrons and V_{oc} remains nearly constant. In the cliff conformation, fill factor decreases because of the reduced V_{oc}, and in the spike conformation, if CBO is over 0.4 eV then current is reduced. Hence, in devices, CIGS/CdS exhibits excellent performance in the spike conformation with a CBO of 0.0 eV to 0.4 eV.

There is considering alternative buffer layers which have been replacing the toxic CdS buffer layer and to achieve an optimal interface band alignment. There are works going on alternative buffer layers such as ZnS, ZnO, In_2S_3. At the interface of CZTSSe/ZnO, a small negative conduction band offset of −0.1 eV indicates the cliff formation. Due to which V_{oc} and FF may be reduced because of the increased interface recombination via interface defects. A large spike of 1.1eV at the CZTSSe/ZnS interface and power conversion efficiency of near zero was also observed.

After applying a hybrid buffer layer of In_2S_3/CdS on the CZTS, enhanced V_{oc} and boost efficiency was observed.[38] Tanaka reported the CdS buffer layer annealed in air at 200 °C for 30 min, but the device performance change was not discussed.[36] For the *n*-type window layer, CdS is used in high-efficiency CdTe solar cells.[39] On increased oxygen composition, the optical band gap energy of CdS:O increases, which reduces the short wavelength light absorption in the window layer and increased the J_{sc}. It is also seen the possibility that the increased band gap energy of CdS:O modifies the CBO at the CdTe/CdS interface which is reduced the interface recombination, leading to improved V_{oc} and FF at 6% oxygen composition.[9] For the high performance of kesterite solar cells, increased the transparency of the layer and adjusted the CBO at the interface, the CdS:O buffer layer can be well beneficial.

5.3. The Interface Between Kesterite Absorber and Mo Back Contact

Molybdenum (Mo) films mostly fulfil the requirements of a back contact which have been widely used in

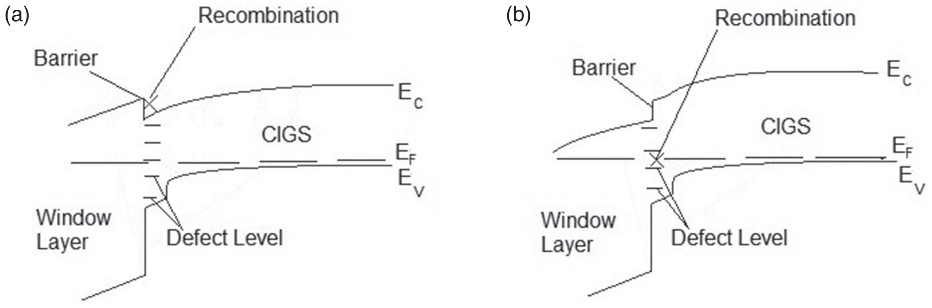

Figure 3. Schematic energy band diagram structures: (a) spike (b) cliff.[9]

photovoltaic solar cells, as they process at high temperature. There is a formation of the $MoSe_2$ layer by annealing 2 nm thick layer of sputtered Mo for 20 min at 500 °C in a low pressure of Se atmosphere.[40] The thin $MoSe_2$ layer was used to decrease the contact resistance and the back contact recombination, therefore improving V_{oc} and FF. The CZTS is non-stable, at the high processing temperature (500–600 °C) in Mo contact. The decomposition is given below as;

$$2Cu_2ZnSnSe_4 \rightarrow 2Cu_2Se + 2ZnSe + 2SnSe + 2Se(g) \quad (1)$$

$MoSe_2$ is generated by the following reaction at CZTS/Mo contact

$$Mo + 2Se \rightarrow MoSe_2 \quad (2)$$

The combination of two reactions (1) and (2), at contact CZTS/Mo is given;

$$\begin{aligned} 2Cu_2ZnSnSe_4 + Mo \rightarrow\ & 2Cu_2Se + 2ZnSe \\ & + 2SnSe + MoSe_2 \quad (3) \end{aligned}$$

The free energy change was calculated from the reaction (3) which was −100 kJ and −150 kJ for CZTSe, and CZTS respectively at 550 °C.[9] The negative sign of free energy changes indicates that the thermodynamically favorable reaction is decomposited and the unstable CZTS/Mo interface may occur. Due to the instability of the Mo back contact, it potentially causes loss of V_{oc}, J_{sc} and FF in CZTS device. Hence, there are two approaches to eliminate the detrimental effect: (i) Replace the Mo by more inert back contact and (ii) Use an intermediate layer between CZTS and Mo. However, Mo is the best choice material for a back contact and it has achieved the highest conversion efficiency in the quaternary photovoltaic.

Various intermediate layers have been fabricated to the decomposition of CZTS at the Mo back contact. A TiN barrier layer was deposited at the Mo/CZTS interface, keeping $MoSe_2$ thickness <300 nm and consequently, the efficiency (V_{oc}, J_{sc} and FF) increased significantly and obtained well grain structure at the high annealing temperature of 570 °C.

Lopez-Marino have used a ZnO barrier layer to decompose the CZTSe in the Mo back contact and found that this layer improved the interface morphology, reduced the density of voids, and decreased series resistance ($3.7\ \Omega cm^2$ to $<0.1\ \Omega cm^2$).[39] Consequently, the efficiency: FF and J_{sc} got improved and V_{oc} increased significantly.

6. CONCLUSION

The kesterite absorber of the CZTS thin film solar cell may be synthesized to develop the non-toxic and eco-friendly solar-cells. The efficiency of the CZTS thin film solar cells may enhance efficiency more than 20% by focusing on following features like secondary phases of the kesterite absorber bulk defects grain boundaries, the interface between the kesterite absorber and the buffer layer, and the interface between the kesterite absorber and the Mo back contact. Due to the reduced toxicity, greater abundance of the constituent elements and efficiency enhanced upto 20%; the kesterite CZTS based solar cells are attracting in the field of energy and considerable attention for research in recent years.

Acknowledgments: The author Krishan Pal would like to thank, National Fellowship (RGNF), UGC, New Delhi for financial support. I am also grateful for the consistent support and help from Dr. Bal Chandra Yadav and Dr. A. K. Yadav, Department of Applied Physics, Babasaheb Bhimrao Ambedkar University (A Central University) Lucknow.

References and Notes

1. H. Flammersberger, Experimental Study of Cu_2ZnSnS_4 Thin Films for Solar Cells [Thesis], Inst. for Teknikvetenskaper, Uppsala **(2010)**.
2. K. Diwate, K. Mohite, M. Shinde, S. Rondiya, A. Pawbake, A. Date, H. Pathan, and S. Jadkar, *Energy Procedia* 110, 180 **(2017)**.
3. W. Shockley and H. J. Queisser, *J. Appl. Phys.* 32, 510 **(1961)**.
4. S. Das, K. C. Mandal, and R. N. Bhattacharya, Springer Series in Material Science, edited by Springer Int. Publ., Switzerland **(2016)**, Vol. 218, pp. 25–74.
5. H. Kategori, N. Sasaguchi, S. Hando, S. Hoshino, J. Ohashi, and T. Yokota, *Sol. Energy Mater. Sol. Cells* 49, 407 **(1997)**.
6. W. Wang, M. Twinkler, O. Gunawan, T. Gokmen, T. K. Todorov, Y. Zhu, and D. B. Mitzi, *Advanced Energy Materials* 4, 1301465 **(2013)**.
7. M. A. Green, K. Emery, Y. Hishikawa, W. Warta, and E. D. Dunlop, *Progress in Photovoltaics: Research and Applications* 23, 805 **(2015)**.
8. S. Siebentritt, *Thin Solid Films* 535, 1 **(2013)**.
9. X. Liu, Y. Feng, H. Cui, F. Liu, X. Hao, G. Conibeer, D. B. Mitzi, and M. Green, *Progress in Photovoltaics: Research and Application* 24, 879 **(2016)**.
10. H. Katagiri, K. Jimbo, W. S. Maw, K. Oishi, M. Yamazaki, H. Araki, and A. Takeuchi, *Thin Solid Films* 517, 2455 **(2009)**.
11. H. Wang, *Int. Jorn. of Photoenergy* 201, 1 **(2011)**.
12. S. Delbos, *EPJ Photovoltaics* 3, 1 **(2012)**.
13. K. Ramasamy, M. A. Malik, and P. O'Brien, *Chemical Communications (Cambridge, England)* 48, 5703 **(2012)**.
14. M. I. Hossain, *Chalcogenide Letters* 9, 231 **(2012)**.
15. S. Abermann, *Solar Energy* 94, 37 **(2013)**.
16. M. P. Suryawanshi, M. P. Suryawanshi, G. L. Agawane, S. M. Bhosale, S. W. Shin, P. S. Patil, J. H. Kim, and A. V. Moholkar, *Advanced Performance Materials* 28, 98 **(2013)**.
17. H. Azimi, Y. Hou, and C. J. Brabec, *Energy and Environmental Science* 6, 1829 **(2014)**.
18. X. Song, X. Ji, M. Li, W. Lin, X. Luo, and H. Zhang, *International Journal of Photoenergy* 2014, 1 **(2014)**.
19. L. M. Peter, *Electrochem. Commun.* 50, 88 **(2015)**.
20. S. A. Vanalakar, G. L. Agawane, S. W. Shin, M. P. Suryawanshi, K. V. Gurav, K. S. Jeon, P. S. Patil, C. W. Jeong, J. Y. Kim, and J. H. Kim, *J. Alloys Compd.* 619, 109 **(2015)**.
21. S. Siebentritt and S. Schorr, *Progress in Photovoltaics: Research and Applications* 20, 512 **(2012)**.
22. C. M. Fella, Y. E. Romanyuk, and A. N. Tiwari, *Sol. Energy Mater. Sol. Cells* 119, 276 **(2013)**.
23. D. B. Mitzi, O. Gunawan, T. K. Todorov, and D. A. Barkhouse, *Philos. Trans. A Math. Phys. Eng. Sci.* 371, 20110432 **(2013)**.
24. T. J. Huang, X. Yin, G. Qi, and H. Gaung, *Physica Status Solidi—Rapid Research Letters* 8, 735 **(2014)**.

25. K. Ito, Copper Zinc Tin Sulfide-Based Thin Film Solar Cells, 1st edn., Wiley Publishing House, UK (**2015**).
26. S. Chen, A. Walsh, X. G. Gong, and S. H. Wei, *Adv. Mater.* 25, 1522 (**2013**).
27. S. Chen, J. H. Yang, X. G. Gong, A. Walsh, and S. H. Wei, *Phys. Rev. B* 81, 245204 (**2010**).
28. J. B. Li, V. Chawla, and B. M. Clemens, *Adv. Mater.* 24, 720 (**2012**).
29. A. Polizzotti, I. L. Repins, R. Noufi, S. H. Wei, and D. B. Mitzi, *Energy and Environmental Science* 6, 3171 (**2013**).
30. W. J. Yin, Y. Wu, S. H. Wei, R. Noufi, M. M. Al-Jassim, and Y. Yan, *Advanced Energy Materials* 4, 1300712 (**2014**).
31. W. M. H. Oo, J. L. Johnson, A. Bhatia, E. A. Lund, M. M. Nowell, and M. A. Scarpulla, *J. Electron. Mater.* 40, 2214 (**2011**).
32. T. Gershon, B. Shin, N. Bojarczuk, M. Hopstaken, D. B. Mitzi, and S. Guha, *Advanced Energy Materials* 5, 1400849 (**2015**).
33. C. M. Sutter-Fella, J. A. Stückelberger, H. Hagendorfer, F. L. Mattina, L. Kranz, S. Nishiwaki, A. R. Uhl, Y. E. Romanyuk, and A. N. Tiwari, *Chem. Mater.* 26, 1420 (**2014**).
34. D. Hironiwa, N. Matsuo, N. Sakai, T. Katou, H. Sugimoto, J. Chantana, Z. Tang, and T. Minemoto, *Japanese Journal of Applied Physics* 53, 106502 (**2014**).
35. J. Kim, H. Hiroi, T. K. Todorov, O. Gunawan, M. Kuwahara, T. Gokmen, D. Nair, M. Hopstaken, B. Shin, Y. S. Lee, W. Wang, H. Sugimoto, and D. B. Mitzi, *Adv. Mater.* 26, 7427 (**2014**).
36. K. Tanaka, M. Oonuki, N. Moritake, and H. Uchiki, *Sol. Energy Mater. Sol. Cells* 93, 583 (**2009**).
37. D. M. Meysing, *Journal of Vacuum Science and Technology, A: Vacuum, Surfaces, and Films* 33, 021203 (**2015**).
38. J. Malmström, *Appl. Phys. Lett.* 85, 2634 (**2004**).
39. S. Lopez-Marino, M. Placidi, A. P. Tomás, J. Llobet, V. I. Roca, X. Fontané, A. Fairbrother, M. E. Rodríguez, D. Sylla, A. P. Rodríguez, and E. Saucedo, *J. Mater. Chem.* 1, 8338 (**2013**).
40. U. Kumar, S. Sikarwar, R. K. Sonker, and B. C. Yadav, *Journal of Inorganic Organometallic Polymer* 26, 1231 (**2016**).
41. Z. Shi and A. H. Jayatissa, *Progress in Natural Science: Materials International* 27, 550 (**2017**).
42. M. Gajdoš, K. Hummer, G. Kresse, J. Furthmuller, and F. Bechstedt, *Physical Review B* 73, 045112-1-9 (**2006**).
43. J. T. Watjen, J. Engman, M. Edoff, and C. Platzer-Björkman, *Appl. Phys. Lett.* 100, 3 (**2012**).
44. D. Colombara, E. V. C. Robert, A. Crossay, A. Taylor, M. Guennou, M. Arasimowicz, J. C. B. Malaquias, R. Djemour, and P. J. Dale, *Sol. Energy Mater. Sol. Cells* 123, 220 (**2014**).
45. G. Suresh Babu, Y. B. Kishore Kumar, P. Uday Bhaskar, and V. Sundara Raja, *Sol. Energy Mater. Sol. Cells* 94, 221 (**2010**).
46. T. Tanaka, A. Yoshida, D. Saiki, K. Saito, Q. Guo, M. Nishio, and T. Yamaguchi, *Thin Solid Films* 518, 29 (**2010**).
47. H. Katagiri, K. Saitoh, T. Washio, H. Shinohara, T. Kurumadani, and S. Miyajima, *Sol. Energy Mater. Sol. Cells* 65, 141 (**2001**).
48. K. Moriya, K. Tanaka, and H. Uchiki, *Japanese Journal of Applied Physics* 46, 5780 (**2007**).
49. H. Katagiri, K. Jimbo, S. Yamada, T. Kamimura, W. S. Maw, T. Fukano, T. Ito, and T. Motohiro, *Applied Physics Express* 1, 041201 (**2008**).
50. A. M. Acevedo, *Solar Energy* 80, 675 (**2006**).
51. X. Mathew, J. P. Enriquez, A. Romeo, and A. N. Tiwari, *Solar Energy* 77, 831 (**2004**).
52. B. Marsen, H. Wilhelm, L. Stienkopf, S. Klemz, T. Untold, R. Sheer, and H. W. Schock, *Thin Solid Film* 519, 7224 (**2011**).
53. P. Jackson, et al., *Physica Status Solidi (RRL)-Rapid Research Letters* 10, 583 (**2016**).
54. E. Shi, L. Zhang, Z. Li, P. Li, Y. Shang, Y. Jia, J. Wie, K. Wang, H. Zhu, D. Wu, S. Zhang, and A. Cao, *Nature* (**2012**).
55. K. A. Bush, et al., *Nature* 2, Article number: 17009 (**2017**).
56. K. Shin, J. B. Yoo, and H. Park, *J. Power Sources* 225, 263 (**2013**).
57. B. C. Yadav, P. Kumar, S. Singh, and R. Kothari, Emerging Energy Alternatives for Sustainable Environment, TERI Press, Chap. 3, pp. 524–536, ISBN: 9788179934111.

Received: 15 July 2017. Accepted: 23 December 2017.

Synthesis and characterization of ZnO nano-particles for solar cell application by the cost effective co-precipitation method without any surfactants

Cite as: AIP Conference Proceedings **2142**, 030008 (2019); https://doi.org/10.1063/1.5122336

Shweta, Krishan Pal, and Khem B. Thapa

AIP Conference Proceedings **2142**, 030008 (2019); https://doi.org/10.1063/1.5122336

Synthesis and characterization of ZnO nano-particles for solar cell application by the cost effective co-precipitation method without any surfactants

Shweta, Krishan Pal and Khem B. Thapa*

Department of Physics, School of Physical and Decision Sciences, Babasaheb Bhimrao Ambedkar University (A Central University), Lucknow-226025 (UP), INDIA

*Corresponding author: khem.bhu@gmail.com

Abstract. The energy problem is the most fascinating problem in this world because the way of success of every country is depending upon the development of the low cost, well-ordered and high efficiency energy source devices.There are several research groups are working to develop the devices for renewable energy sources. So we are going to focusour research on solar cells materialsforrenewable energy sources like Zinc Oxide (ZnO). This material ishighly useful for making the heterojunction solar cell as well as window layer.Other hand ZnO is used for 3rd generation/DSSC. In this direction we have synthesized zinc oxide (ZnO) nanoparticles by low cost co-precipitation method without any surfactants. The synthesized ZnO nanoparticles have done the characterizations like X-Ray Diffraction (XRD), Scanning Electron Microscope (SEM), Energy Dispersive X-ray Spectroscopy (EDS) to evaluate shape, size, reproducibility and morphology of nanoparticles.

Keywords: Zinc Oxide, Doped ZnO, Nano-particle, Solar cell, DSSCs.

INTRODUCTION

Today there is huge demanding of the renewable energy resourcesfor human kinds and people are developed the devices which are made of eco-friendly materials. The researchers and the scientists are working on developing the renewable energy resource that can be used more and more without damaging the environment. A lot of development works had been done in the field of renewable energy technology such as solar cells, fuel cells and biofuels [1]. In renewable energy sources, the solar energy may be an absolute solution to the energy and environment challengingsourceas a carbon neutral energy source.There is already commercialized the solar devices are available in market which are costly and made of the environment harmful materials and the efficiency is achieved near about 25%. They are still required a lot of improvement to fulfill the demand of solar cell having low cost, stability, eco-friendly and high efficiency[1]. It means a common people want a solar cell which has the high efficiency,thecost effectiveness and the eco-friendly of the solar devices.

As we know that Zinc oxide (ZnO) is a very promising material for solar cells applications as it is non-toxic, good thermal stability, excellent chemical and optical properties and low cost [6-8]. The ZnO has a stable wurtzite structure with lattice spacing a=0.325nm and b=0.521nm, direct band gap energy of 3.37eV and excitation binding energy of 60meV (at room temperature), so that excitonic emission processes can persist at and above room temperature [3, 8, 14-16]. The researchers are still not able to controlthe conductivity ofZnO [8]. There are thermal decomposition, spray pyrolysis, chemical vapour decomposition, sol gelandco-precipitation methods for the fabrication of ZnO nanoparticles with uniform morphology and size [9-11]. Among the all these methods, co-precipitation is the best method which can control the shape, size, reproducibility and morphology of nanoparticles and which is a low costmethod[12, 13]. The nano sizeZnO has various applications like UV nano-lasers, nano-generators, gas sensors, biosensors, solar cells, photo detectors, photocatalysts and surface acoustic wave devices due to its unique and superior physical and chemical properties [9,16].The ZnO can be made the highly conductive

Advances in Basic Science (ICABS 2019)
AIP Conf. Proc. 2142, 030008-1–030008-4; https://doi.org/10.1063/1.5122336
Published by AIP Publishing. 978-0-7354-1885-1/$30.00

by doping it with suitable material [18]. Recent achievement had been made by oxide nanocrystallite aggregates in DSCs [2]. A lot of improvement in conversion efficiency was achieved for ZnO based DSCs [2,19-20].

So, nano size ZnOhassynthesized by co-precipitation methodwhich is the best low cost method.We have donethe characterization to evaluate the shape, size, reproducibility and morphology of nanoparticles: X-Ray Diffraction (XRD), Scanning Electron Microscope (SEM), Energy and Dispersive X-ray Spectroscopy (EDS) of the samples. Using these characterizations, we can determine the crystal type, particle shape and size, surface morphology, and porosity.

MATERIAL AND SYNTHESIS METHOD

Laboratory grade Zinc acetate ($Zn(CH_3COO)_2.H_2O$) and Sodium hydroxide (NaOH) were purchased from Thermo fisher, China. These materials are used without any further purification. Distilled water is used Laboratory grade. The ZnOnanoparticles were synthesized by low cost co-precipitation method without any use of surfactants. In this process, $Zn(CH3COO)2\cdot 2H_2O$ (0.2M), and deionized water were mixed vigorously 3 hours at 60^0.After that, 150ml solution of distilled water and NaOH (1M) added drop wise with 1.5ml/minute. At pH=9, we got the white color precipitate which was filtrate by filter paper. Filtrate was washed several times with deionized water and ethanol to remove the byproducts. And dried overnight at 80^0 by simple oven. The three samples are prepared and named A, B, C, where sample A is pureZnO without calcinated temperature, sample B and C are calcinated at 600^0 and 800^0Crespectively.

CHARACTERIZATION

The synthesized ZnO powder is done XRD characterization which was performed using the X-ray diffractometer (X-pert Powder) in the diffraction ranges of angle $20 \leq 2\theta \leq 80^0$, with monochromatic CuKα radiation (λ= 1.5418^0Angstrom) source. And SEM (JEOL) was taken the image of the ZnO.

RESULT AND DISCUSSION

In this section, we have divided into two parts: (i) XRD analysis and (ii) SEM and EDS

(i) XRD analysis: Figure1 shows the XRD patterns of ZnO in pure (Green), calcinated at 600^0C (Red) and 800^0C (Blue) in the open atmosphere which was prepared by co-precipitation method. The diffraction peaks of ZnOnano particles correspond to the indices(100), (002), (101), (102), (110), (103), (112) and (201) planes [21].The XRD patterns of ZnOnanoparticles (NPs)were calcinated at different temperatures confirm that all peaks shows the Wurtzite structure of ZnO as shown in JCPDS card no. 36-1451 [22]. The 2θvalues are located at 31.7518, 34.4014 and 36.2366° forstrong peak of the crystalplanes (100), (002) and (101) lines shown in the Figure 2 (a), 2 (b), and 2 (c) respectively.There is no identified the other impurity peaks in crystalline material of theZnO. However,

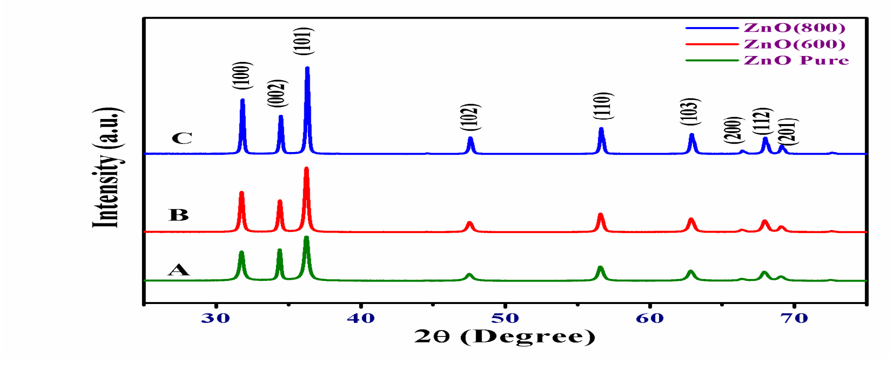

Figure 1: XRD patterns of ZnONPs synthesized by co-precipitation method (a) A sample (b) B sample and (b) C sample.

The diffraction peaks become stronger and sharper when the calcination temperatures increase. Such properties are also improved crystallinity of the material. This result is justified with Ref.[19]. The average crystallite size,pureZnOand calcinated at 600^0C ZnONPs,isfound same i.e. 28.15nm and the average crystalline size of the calcinated at 800^0C ZnO NPs is found 22.54nm which were calculated by Debye Scherer formula as the precursor of zinc acetate dihydrate. After study the all possess of ZnO NPs structures, lattice parameters are calculated and found a=0.3248nm and c=0.5205nm. These results are good agreement with previously reported papers [9, 19].

(ii) SEM and EDS analysis: Figure 2 shows the SEM images of surface morphology of the ZnO NPs and the EDS analysis of the constituent percentage elements of ZnO NPs on glass substrate which was prepared a thin film of the synthesized ZnO powder by master blade method. The SEM analysis shows that the morphology of ZnO NPs is spherical and short-rodshape, and there are no more differences in the shape of pure ZnO NPs and calcinatedZnO NPs at different temperatures. The surfaces of the film are rough and micro-porous which helps to absorption the photons at the obtained energy band gap such ZnO NPs may be used in solar application. The EDS analysis at atomic scale are shown in the Table1.

The strong peaks are observed for Zinc (Zn) and Oxygen (O) element. The peaks of the Zn and O in the elemental constitution of the A sample are found atomic percentage 26.30% and 73.70% respectively. This study were confirmed the formation of ZnO NPs in the co-precipitation method without any surfactants.

Table 1: EDS analysis of ZnO NPs at different calcinated temperature.

Elements present	A sample	B sample	C sample
Oxygen (O)	73.70%	63.02%	69.99%
Zinc (Zn)	26.30%	36.98%	30.01%
Total	100%	100%	100%

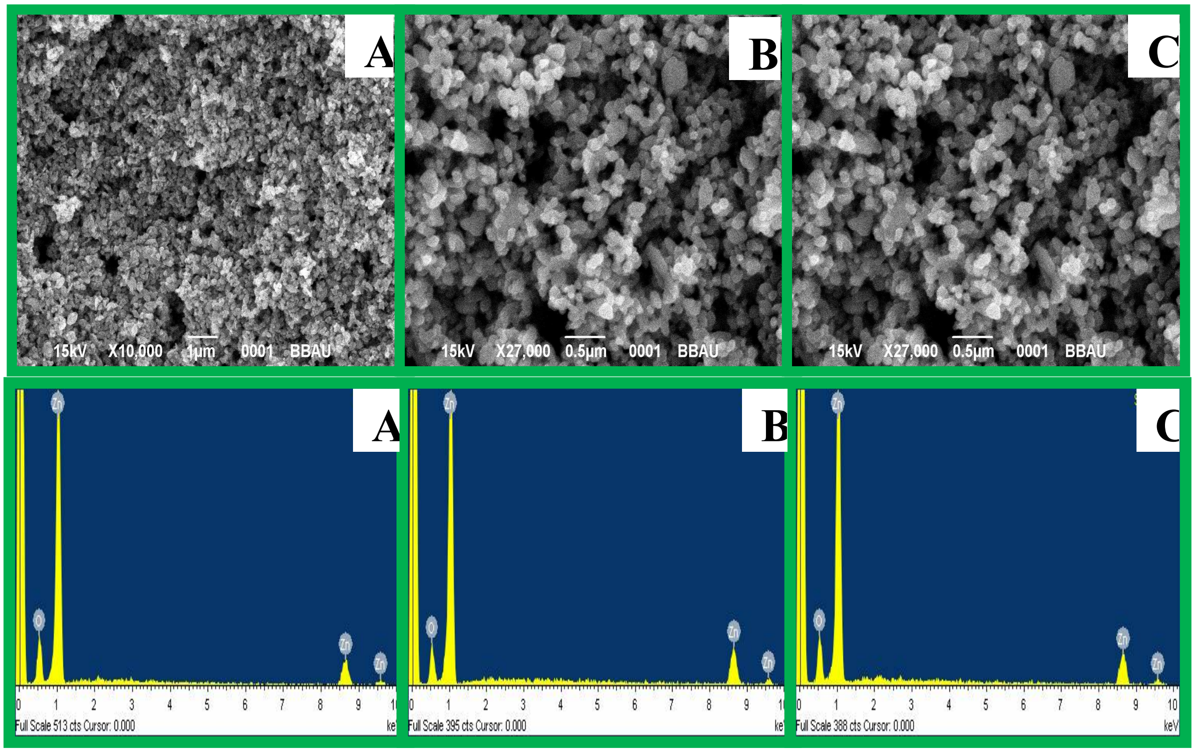

Figure 2: SEM and EDS images of A, B & C samples at pure, 600^0C and 800^0C calcinated temperature.

CONCLUSION

The ZnO NPs were synthesized by cost effective co-precipitation method without any surfactant. The XRD data were demonstrated that the ZnO has pure hexagonal wurtzite and polycrystalline structure with the lattice parameters a=0.3248nm and c=0.5205nm. The present study showed that the ZnO NPs can be synthesized by low cost co-precipitation method without any surfactant. The crystallinity properties of ZnOwere tuned by thecalcinated temperatures. Such powder of the ZnO NPs may be used in the hetero-junction solar cell as a window layer and third generation solar cell. It may be beneficial to synthesis the low costsolarcellcommercially.

ACKNOWLEDGEMENT

The authors would like to thanks to Prof. B. C.Yadav and Dr A. K. Yadav, Department of Physics, BabasahebBhimraoAmbedkar University (A Central University) Lucknow, for the Laboratories help to synthesize the samples.

REFERENCES

1. Qifeng Zhang, Christopher S. Dandeneau, Xiaoyuan Zhou, and Guozhong Cao, Adv. Mater.**21**, 4087–4108 (2004).
2. Qifeng Zhang, Kwangsuk Park and Guozhong Cao, Material Matters**5.2**, 32-42 (2010).
3. Avnish Kumar Arora, Sarita Devi, VivekSheelJaswal et al., Orient. J. Chem.**30**, 1671-1679 (2014).
4. Robina Ashraf, SairaRiaz, Muhammad Khaleeq-ur-Rehman and ShahzadNaseem, Advances in Nano, Biomechanics, Robotics and Energy Research, 287-297 (2013).
5. Chapter 3: Synthesis of Zinc Oxide Nanoparticles, 114-128.
6. Jia Huang, Zhigang Yin and QingdongZheng, Energy Environ. Sci. **4**, 3861–3877 (2011).
7. S.R.Brintha and M.Ajitha, IOSR Journal of Applied Chemistry **8**, 66-72 (2015).
8. Anderson Janotti and Chris G Van de Walle, Rep. Prog. Phys.**72**, 1-29 (2009).
9. A. JafarAhamed and P. Vijaya Kumar, J. Chem. Pharm. Res.**8(5)**, 624-628 (2016).
10. Y Yang, H Chen, B Zhao and X Bao, Journal of Crystal Growth**263(1–4)**, 447–453 (2004).
11. RudeeratSuntako, Bull. Mater.Sci. **38**, 1033–1038 (2015).
12. Muhammad FajriRomadhan, NurgahaEdhiSuyatma and FahimMuchammadTaqi, Indones. J. Chem. **16 (2)**, 117 – 123 (2016).
13. Reynolds D C, Look D C and Jogai B Solid State Commun.**99**, 873-875 (1996).
14. Bagnall D M, Chen Y F, Zhu Z, Yao T, Koyama S, Shen M Y and Goto T, Appl. Phys. Lett.**70**, 2230-2232 (1997).
15. Zahra MonsefKhoshhesab, Mohammad Sarfaraz and Mohsen AsadiAsadabad, Synthesis and Reactivity in Inorganic, Metal-Organic, and Nano-Metal Chemistry, **41**, 814–819 (2011).
16. Sanjeev Kumar, Fouran Singh and A. Kapoor, International Journal of Recent Trends in Electrical & Electronics Engg.**4**, 25-29 (2014).
17. Zhong Lin Wang, J. Phys.: Condens. Matter **16**, R829–R858 (2004).
18. Zhang, Q. F., Chou, T. R., Russo, B., Jenekhe, S. A., Cao and G. Z. Angew., Chem. Int. Ed.,**47**, 2402-2406 (2008).
19. Mohammad Shohel, Muhammed Shah Miran, Md. Abu Bin Hasan Susan and M. Yousuf A. Mollah, Research on Chemical Intermediates **42**, 5281–5297(2016).
20. M.H. Rashid, M. Raula, R.R. Bhattacharjee and T.K. Mandal, J. Colloid Interface Sci. **339**, 249 (2009).

Journal of Physical Science, Vol. 32(2), 27–39, 2021

Co-precipitation Synthesis with a Variation of the Sulphur Composition of Kesterite Phase Cu_2ZnSnS_4 (CZSS) without Annealing Process

Krishan Pal,[1] Dheeraj Kumar Maurya,[2] Priyanka Chaudhary,[1] Khem Bahadur Thapa,[1*]
and Bal Chandra Yadav[1]

[1]Department of Physics, School of Physical and Decision Sciences,
Babasaheb Bhimrao Ambedkar University (A Central University),
Lucknow-226025 (UP), India
[2]Electro-materials Research Laboratory, Centre for Nanoscience and Technology,
Pondicherry University, Puducherry-605014, India

[*]Corresponding author: khem.bhu@gmail.com

To cite this article: Pal, K. et al. (2021). Co-precipitation synthesis with a variation of the sulphur composition of kesterite phase Cu_2ZnSnS_4 (CZSS) without annealing process. *J. Phys. Sci*., 32(2), 27–39. https://doi.org/10.21315/jps2021.32.2.3

To link to this article: https://doi.org/10.21315/jps2021.32.2.3

ABSTRACT: *Commercially available compound CuInGa (S, Se) can be replaced with emerging quaternary compound Cu_2ZnSnS_4 (Copper Zinc Tin Sulphur or CZSS) for photovoltaic applications due to the high absorption coefficient and optimum bandgap. Unstable sulphur and the co-existence of binary and ternary phases in CZSS are the main obstacles for a single-phase kesterite quaternary compound. To overcome these issues, the researchers are synthesising the CZSS in presence of sulphur and selenium environment. The sulphurization and selenization are the constraints for the synthesis of CZSS and these processes make it costlier. In the present work, the wet-chemical method (i.e., co-precipitation method) was used to synthesise CZSS without vacuum annealing where the sulphur constituent was controlled by changing the stoichiometric ratio. X-ray diffraction (XRD) and Raman analysis confirm that the synthesised CZSS was in polycrystalline and single-phase kesterite nature. The average crystallite sizes for thiourea 16, 18, 20 mmol were found 15 nm, 17 nm and 17 nm, respectively. Surface morphology of the as-prepared film was identified by scanning electron microscope (SEM) and optical bandgap of the film was obtained ~1.33 eV by UV-visible (UV-vis) analysis. The 18 mmol of thiourea with stoichiometric ratio 4:2:2:9 is found the best optimisation for synthesising the CZSS without vacuum annealing by the co-precipitation method. Thus, the thin film of such synthesised CZSS may be employed for the low-cost photovoltaic application.*

Keywords: Cu_2ZnSnS_4, co-precipitation, without annealing, kesterite, photovoltaic

1. INTRODUCTION

In the last three decades, Cu_2ZnSnS_4 (CZSS) nanomaterials have attracted enormous attention by promising development for solar energy conversion due to high absorbent ($>10^4 cm^{-1}$), low cost, environment-friendly, non-toxic and sustainable earth-abundant elements. CZSS has a tunable bandgap of about 1.4 eV to 1.6 eV, which is very close to the optimum value as an absorber layer in solar cells.[1–3] According to the Shockley and Queisser limit, the bandgap range, 1.4 eV to 1.6 eV, is suitable for thin-film photovoltaic cells. On the other hand, CZSS is the counterpart of CuInGa (S, Se) (CIGS) because both Zn (+2) and Sn (+4) have similar properties to In (+6). But the co-existence of binary and ternary phases, the synthesis of CZSS puts a lot of hurdles in its development.[4] An effort has been laid by researchers to overcome the phase problem by sulphurization process in inert or vacuum atmosphere.[5,6] Such process also has a constraint of cost and time consumption. So, the exploration of novel methods for the CZSS synthesis has gained much attention across the globe.

To overcome the problems of the sulphurization process in an inert or vacuum atmosphere, many researchers have been used other methods for synthesising CZSS nanomaterial for wide applications such as photovoltaic, hydrogen generation and light emitting diode (LED), etc.[7] Co-precipitations, sol-gel, solvothermal, hot-injection, one-pot syntheses and microwave-assisted methods are widely adopted for purpose of the photovoltaic application.[5,6,8–11] In a design of a photovoltaic device, the CZSS material is used as an absorber layer.

According to previously reported results, the disadvantage of the device structure, Mo/Absorber layer/buffer layer/nanostructured metal oxide/metal grids, is highlighted with regard to the thermal instability in the absorber layer, which can be only controlled by buffer interface.[12] In addition to this limitation, photovoltaic cells in this configuration have erosion reaction between CZSS and Mo at back contact, and the surface instability of CZSS has increased during the heat treatment.[13] This drawback can be overcome by the deposition of metal oxide on a smooth surface of a substrate with subsequent annealing at high temperatures to prevent the direct contact of CZSS and the conducting substrate. It is evident from previous studies that, nanorods are the best substitute for metal grids.[14,15] Hence, the TiO_2 thin layer was offered the highest conversion efficiency of 0.25%.[16] Hamady et al. trying to develop a novel approach of InGaN Schottky based solar cell device to make the efficiency 22%, theoretically.[17] The CZSS may be a better option in place of GaN in this device.

In the present work, we have described a facile and low-cost synthesis of wurtzite CZSS Nanocrystals (NCs) without vacuum annealing or sulphurization by the co-precipitation method where ethanol and water were used as a solvent. The co-precipitation method is done at room temperature without any surfactants and noble gases as well as vacuum process. Besides, this method does not require annealing the synthesised samples. As compared to other methods, this method is simple and economical. The formation of kesterite CZSS NCs, ethanol solvent plays an important role in the CZSS phase transition from a tetragonal structure and the balanced stoichiometry ratio of the compound optimizes sulphur content. The novelty in this work lies in the synthesis of NCs CZSS material by an economically cheaper co-precipitation method without any sulphurization and selenization because the sulphurization and the selenization processes in the NCs CZSS synthesis are imparted huge toxicity to the environment. Hence, the NCs are evident that the surface-to-volume ratio enhances the properties of the material. The high absorption coefficient and optimum bandgap of NCs CZSS can be synthesised by the co-precipitation method without sulphurization or vacuum annealing. The cost-effective thin film of CZSS NCs can be very useful to enhance the efficiency of the photovoltaic cells.

2. EXPERIMENTAL METHODS

2.1 CZSS NCs Powder Synthesis

The metallic Cu, Zn, and Sn cations were taken as the cupric (II) chloride ($CuCl_2.2H_2O$, Thermo Fisher Scientific India Pvt. Ltd., Maharashtra, India, 98.5%), zinc (II) acetate ($Zn[CH_3COOH]_2.2H_2O$, Thermo Fisher Scientific India Pvt. Ltd., Maharashtra, India, 98.5%), Stannous or tin (II) chloride ($SnCl_2$, Thermo Fisher Scientific India Pvt. Ltd., Maharashtra, India, 97%) and the sulphur anion was taken as thiourea (NH_2CSNH_2, Sarabhai Chemicals [India] Pvt. Ltd., Ahmedabad, India [reagent grade], 98%). In a typical experimental procedure, the preparation of metal precursor cupric (II) chloride (8 mmol, 0.5455 gram [gm.]), zinc (II) acetate (4 mmol, 0.3512 gm.), tin (II) chloride (4 mmol, 0.3034 gm.) were dissolved in 200 ml ethanol in a beaker. The reaction mixture was stirred continuously for 10 min at 400 round per minute (rpm). After that, thiourea (20 mmol, 0.6090 gm.) was added in 200 ml ethanol as a sulphur precursor and stirred well for 5 min, and mixed within the first beaker quickly. The reaction mixture was stirred continuously for 3.5 h and found a transparent homogeneous solution. Then, the mixture was transferred into an oven for 3 h at 210°C temperature and subsequently, it was cooled down to room temperature to obtain black colour precipitation. This precipitation was further centrifuged at 7,000 rpm for 15 min and washed several times by distilled water and ethanol, respectively. The schematic diagram is shown in Figure 1. Finally, it was dried at 80°C in the oven and it was crushed into a fine powder using a mortar pestle, named sample A. Similar process was taken for 18 mmol (0.5480 gm.) and 16 mmol (0.4871 gm.) of sulphur in the salt thiourea and prepared the fine powder, named as samples B and C, respectively.

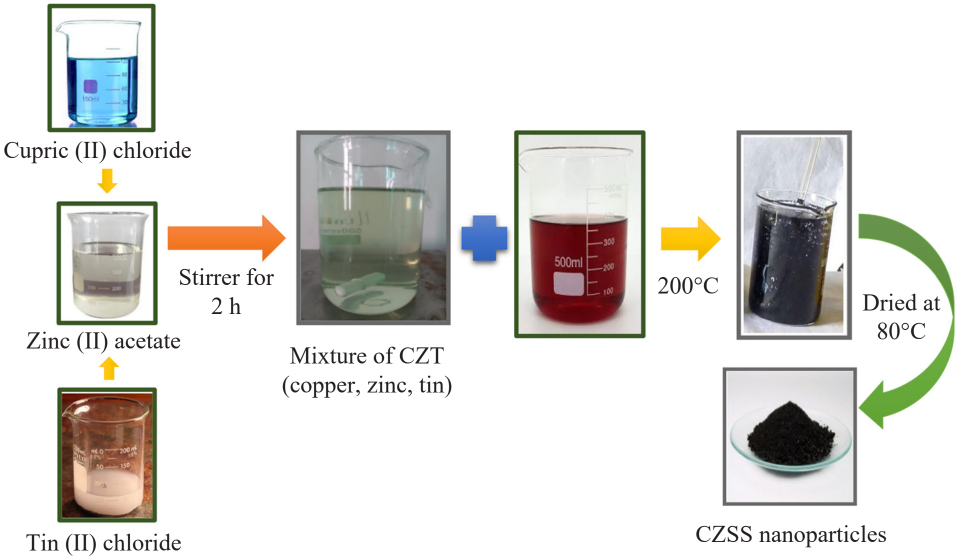

Figure 1: Schematic diagram for synthesis process of CZSS NCs.

2.2 Growth and Formation Mechanism

Generally, in this synthesis process, metal salts react with ethanol and form the metal alkoxide [M(Tu)m]-OR. Then, the nanocrystals are generated during the polycondensation reactions. In this process, thiourea reacts with metal ions and forms the metal thiourea complexes. The metal thiourea complexes are subsequently subjected to alcoholysis and condensation reactions with ethanol at 210°C and formed the CZSS nanocrystals. The probable reaction mechanisms are followed as:

$$M - X + \mathrm{Tu} \rightarrow [M(\mathrm{Tu})m] - X \tag{1}$$

$$[M(\mathrm{Tu})m] - X + ROH \rightarrow [M(\mathrm{Tu})m] - OR + H - X \tag{2}$$

$$M - X + \mathrm{Tu} \rightarrow [M(\mathrm{Tu})m] - X \tag{3}$$

$$[M(\mathrm{Tu})m] - X + ROH \rightarrow [M(\mathrm{Tu})m] - OR + H - X \tag{4}$$

$$[M(\mathrm{Tu})m] - X + [M(\mathrm{Tu})m] - OR \rightarrow [M(\mathrm{Tu})m] - O - [M(\mathrm{Tu})m] + R - X \tag{5}$$

$$[M(\mathrm{Tu})m] - O - [M(\mathrm{Tu})m] + R - X \rightarrow Cu_xS + ZnS + Sn_xS + SnO_2 + Volatile(matter) \tag{6}$$

$$Cu_xS + ZnS + Sn_xS \rightarrow Cu_2ZnSnS_4 \tag{7}$$

$$Cu_xS + ZnS + SnO_2 \rightarrow Cu_2ZnSnS_4 \tag{8}$$

The representation of the symbols (M, X, Tu, and R, x) in these equations are represented as M = metal ions (Cu^{2+}, Zn^{2+}, Sn^{2+}), X = anions (CH_3COO^- or Cl^-), Tu = thiourea and R = organic molecular chains of ethanol, x = quantity of elements. The gases CS_2, CO_2, NO_2, SO_2, H_2O, and NH_4Cl are volatile materials and generated during the synthesis process at 210°C. In organic solvents, thiourea–metal complexes [M(Tu)m]–X is easily generated from thiourea and metal ions (Cu^{2+}, Zn^{2+}, Sn^{2+}), and several complexes are reported with different stoichiometry.[18–19] In traditional non-aqueous nanoparticle synthesis routes, the oxygen in the formation of a metal–oxygen–metal bond is provided by the solvent or by the organic constituent of the precursor.[20] Generally, *M–O* bonds, *M–S* bonds, and *O–M–S* bonds of the thiourea–metal complex [M(Tu)m]–O–[M(Tu)m] system (as shown in Equations from 1–8) have coexisted in the precursor Sol-Gel method.[18]

2.3 Thin Film Preparation

The soda-lime glass (SLG) substrate was used to deposit the CZSS thin film by spin coater (HSC-8000) and this was used to analyse the scanning electron microscope (SEM). Before the deposition of the CZSS solution, the SLG substrate was cleaned by an ultrasonic bath in distilled water and ethanol and was dried at 80°C in an oven. The CZSS solution was prepared in ethylene glycol (EG) and found a homogeneous solution after ultra-sonication. The CZSS solution was deposited by spin coater at 1,000 rpm for 30 sec and was repeated this process three to five times to get the best thickness of the film. The CZSS film was dried in the oven at every process of deposition.

3. CHARACTERISATION TECHNIQUES

The structural characterisation of the CZSS NCs was analysed by Bruker D8 Advance X-ray diffractometer with 0.154056 nm wavelength of X-ray (Cu K-α radiation) in the angle range 20° to 70°. For optical properties, the spectroscopic measurements have measured the spectra of UV-visible (UV-vis) absorption using a UV-vis spectrophotometer (ThermoFisher Scientific, Massachusetts, USA, Evolution 201). Raman scattering patterns were performed by the Raman spectrometer model (HORIBA France SAS, Loos, France Jobin-Yvon Lab RAMHR 800UV) and the wavelength 514 nm of the Raman spectrometer was used. The surface morphology of CZSS NCs was performed by SEM-JEOL (JEOL Ltd., Tokyo, Japan, JSEM-6490LV).

4. RESULTS AND DISCUSSION

4.1 X-ray Diffraction (XRD) Analysis

Figure 2 shows the XRD pattern of CZSS NCs in the range of diffraction angle 20° to 70°. The XRD pattern exhibits the signature of prominent peaks at angles (2θ) in 28.5°, 47.3° and 56.2° corresponds to the planes (112), (200) and (312), respectively. The XRD pattern of CZSS confirms standard tetragonal kesterite Cu_2ZnSnS_4 crystal structure with JCPDS card no. 26-0575. The XRD pattern reveals a minor presence of impurities or deformations in sample C because the low peak intensity corresponds to the plane (312). It is cleared from the XRD patterns of samples A and B that these samples are having less impurity as compared to sample C. This result suggests that sample A and sample B are free from any such impurities witnessing the formation of a pure kesterite phase. There is either a loss in crystallinity or a decrease in crystallite size because intensity and peak positions are varied slightly from sample A to sample C. The average crystalline size was to be found 15 nm, 17 nm and 17 nm, respectively by Debye-Scherrer's formula.

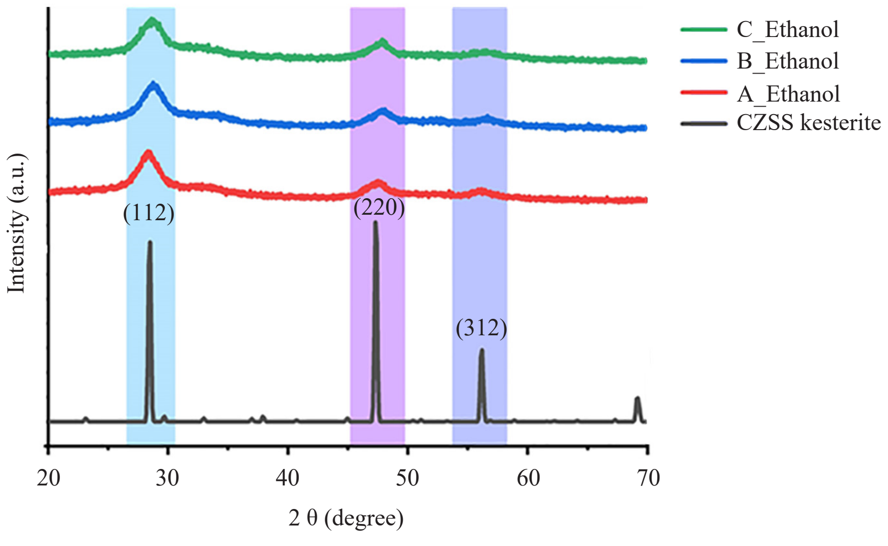

Figure 2: XRD patterns of CZSS samples A, B and C with the variation of concentration of sulphur, comparative with standard CZSS kesterite.

According to Cheng et al., their study showed that strong peaks of Cu_3SnS_4, Cu_4SnS_4, CuS, Cu_2S, SnS, SnS_2 were not found in XRD patterns which is similar to our XRD results.[19] So, it confirms that the synthesised CZSS NCs are in the pure quaternary phase in nature. However, at a first glance, XRD patterns of CZSS, CSS and ZnS are indistinguishable because the peak (220) in the CSS and ZnS has the same as the peak (220) in the CZSS. For adequate phase formation identifications in CZSS samples, further analysis is required. Therefore, Raman spectroscopy of the samples A, B, and C has been done to differentiate the phases of CZSS, CSS, and ZnS materials.

4.2 Raman Spectroscopy

The presence of spatial distributions of various chalcogenide phases can be distinguished by Raman spectroscopy. Minute differences in the phonon densities of states between the different chalcogenide phases can be distinguished from the shifting peaks in the Raman scattering of the samples. According to Himmrich and Haeuseler, CZSS and its phases have distinguished by studying the Raman spectra and identified a strong peak at 336 cm^{-1} and two weak peaks at 285 cm^{-1} and 365 cm^{-1}.[21] Recently, lots of review literature reports on the Raman spectrum of CZSS have been published where the most intense peak position is found at 332–339 cm^{-1} and weak peak positions at 251–288 cm^{-1} and 368–374 cm^{-1}.[22–23] The strong Raman peak of the CZSS is associated with the strong Raman peak of the ternary chalcogenide compounds Cu_2SnS_3 and Cu_3SnS_4.[24]

Figure 3 shows the Raman spectrum of chalcogenide CZSS nanocrystals, which was synthesised through the homemade simple method without any surfactant. In this figure, Raman spectra are compatible with the XRD results because XRD data was confirmed that the prepared CZSS NCs are tetragonal kesterite structures. In the Raman spectrum, this confirmation is justified by high intensity (major) peaks at 328 cm^{-1}, 332 cm^{-1}, 333 cm^{-1} with two shoulder peaks at 288 cm^{-1} and 351 cm^{-1}, 352 cm^{-1}, 355 cm^{-1} for prepared samples A, B and C, respectively. Generally, quaternary compounds of the metal sulphides form unstable sulphur and co-existence of binary and ternary phases. From the Figure 3, it can be observed a good peak results for the case without annealing of the samples. The reason is that the access quantity of sulphur has been taken in optimisation conditions. In this process, the excess sulphur supply evaporates sulphur and maintains the stoichiometric ratio. Some minor peaks are identified with less intensity at 475 cm^{-1} and 575 cm^{-1}. These minor peaks confirm that there may be the phases of Cu_2SnS_3 and ZnO.[25] But XRD characteristics already verified that such compounds do not exist.

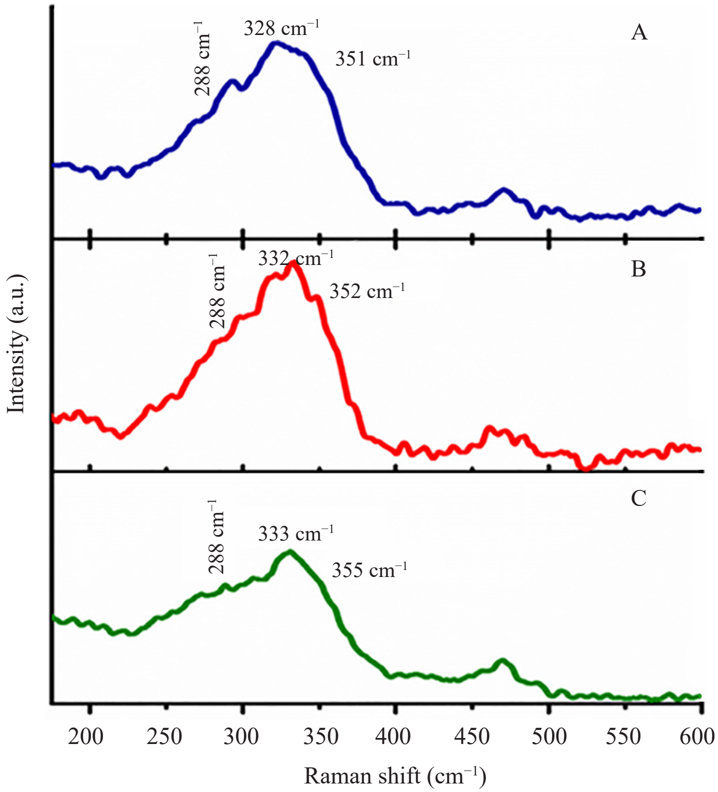

Figure 3: Raman spectra of CZSS kesterite (NCs) synthesised from Cu^{2+}, and Sn^{2+} at 210°C while varying the S:M ratio. The sulfur source thiourea was varied from 16 mmol, 18 mmol, 20 mmol, i.e., samples A, B and C, respectively.

From Figure 3, we confirm that the peak intensities of Raman spectroscopy are shown lower and broader. The broadening of peaks in nanocrystalline materials is usually described by the phonon confinement model as explained by XRD results due to crystalline size (15 nm to 17 nm). The phonon confinement leads to a break-up of selection rules; it also means that the non-zone-centre phonons will participate in scattering.[21] This usually can be seen in an asymmetric broadening of peaks. However, it is common to observe that the peaks are shifted towards the higher wavenumbers (e.g., 332 cm^{-1} to 333 cm^{-1}). According to the review literature, the peak of sample A has the wave number 328 cm^{-1}, which is out of the wavenumber range 331 cm^{-1} to 339 cm^{-1}.[22–23] So, we can say that this sample A is not in a pure form of stoichiometric range. So, it may not be useful for photovoltaic applications. The inhomogeneity in the structure is due to the disordered cation within the sublattice that is detected by peak shifting towards the higher angle side. Peaks related to secondary phases such as Cu_2S, SnS, SnS_2, ZnS, Cu_2SnS_3;

and Cu_3SnS_4 were not detected. Some of these compounds (ZnS, Cu_2SnS_3 and Cu_3SnS_4) have found partially overlapping peaks with CZSS. After analysing the XRD and Raman characterisations, we conclude that sample B has given the best results due to the proper stoichiometric ratio for a stable CZSS compound. The morphology of the samples is studied by SEM.

4.3 SEM Analysis

For the SEM analysis, we have mounted the sample on a mounting stand with the help of carbon tape. After mounted the sample, the platinum (Pt) was coated. Figure 4(a), 4(b) and 4(c) show the surface morphology of CZSS NCs thin film with the variation of sulphur quantity. The morphology of sample A shows spherical type nanoparticles that are distributed roughly on the SLG substrate and identified the more cracks in the film. There are more agglomerated crystals and it is identified agglomeration. In samples B and C, it has been observed that the size and shape NCs are changed. In these samples, the agglomerations are less and the films are less cracked compared to sample A.

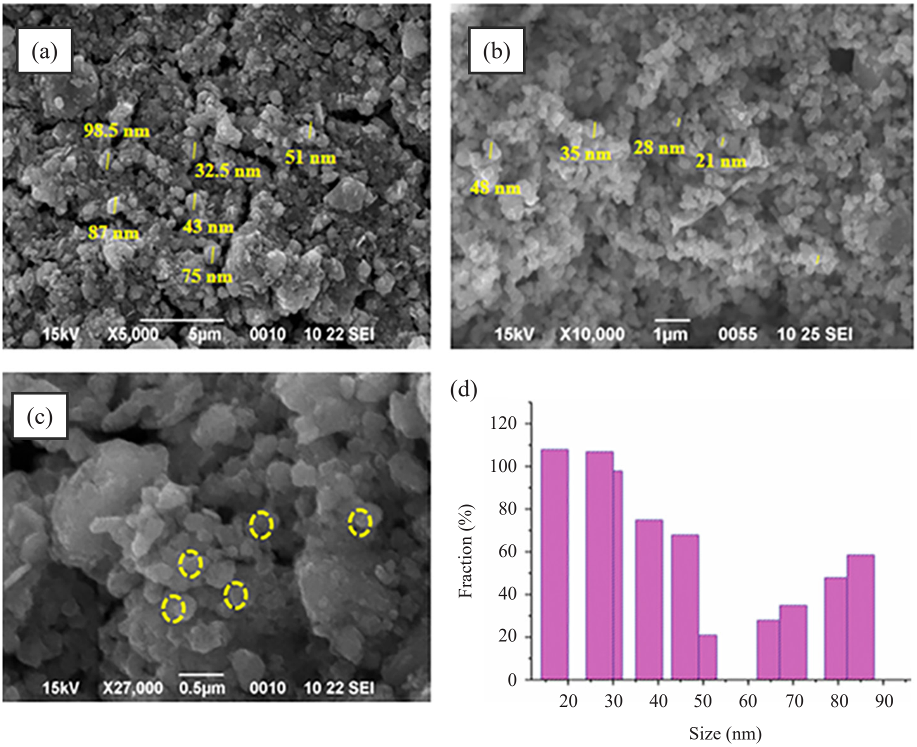

Figure 4: (a), (b), (c) SEM images of CZSS powder thin film with samples A, B and C, respectively, and (d) size distribution with fraction percentage.

The problem of cracking in the film is due to the solvent evaporation rate, which may be removed by changing the evaporation rate. Here, agglomeration is generated due to the anisotropic growth of materials during film fabrication. During the synthesis process, anisotropic growth is being found due to the selective binding nature of ligands. The obtained result confirms that the crystal growth has improved from sample A to sample C as the variation of sulphur is increased. Here, we have analysed the surface morphology at different resolutions because the surface is not showing the clean surface at the same resolution. Figure 4(d) explains the size distribution of the CZSS nanocrystals of sample B with the fraction percentage. This figure confirms that how the size of the NCs distributed in the film. Due to having a good phase and morphology in sample B, the optical bandgap was analysed only to see the suitability for the application of the photovoltaic cells.

4.4 Optical Analysis

The good phase and morphology in the sample B were analysed by the XRD and Raman analysis. So, we have decided to characterise the optical analysis of sample B only by UV-vis spectrometer. The optical bandgap of sample B is shown in Figure 5. The energy of the optical bandgap was analysed by using the formula $\alpha = A(h\nu - E_g)^{1/2}/h\nu$.

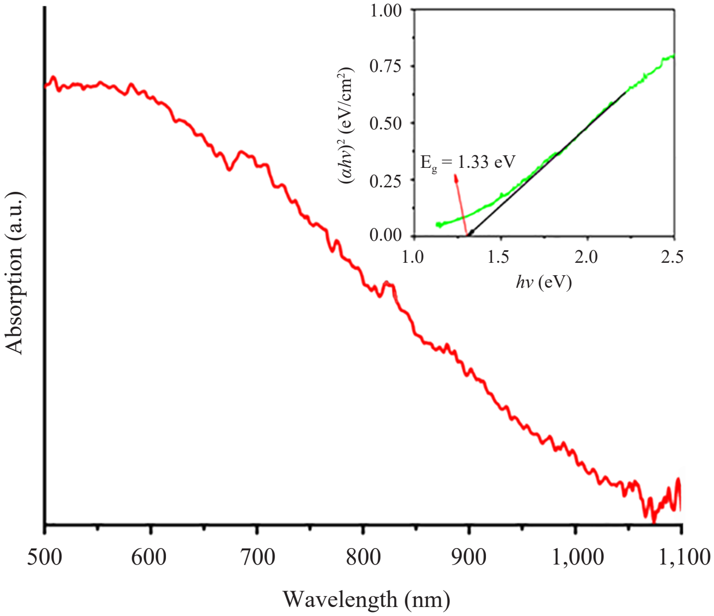

Figure 5: UV-vis absorption spectrum of the CZSS NCs. Inset shows the plot of $(\alpha h\nu)^2$ vs. $h\nu$.

After analysing, the bandgap is to be found 1.33 eV, which is suitable for photovoltaic cell application. Shockley and Queisser theoretically announced that such bandgap limit should be ≈1.5 eV for the highly efficient photovoltaic cell. So, the calculated bandgap of sample B is covered in this range and sample B is highly suitable for a photovoltaic cell. Besides this, the XRD analysis has been shown that the Cu_2SnS_3 and ZnO phases do not exist which is confirmed by the optical spectroscopy characteristics. The novelty in this work lies in the synthesis of CZSS NCs by an economically cheaper co-precipitation method without any sulphurization and salinization processes. In the absence of sulphurization and salinization processes, it imparts less toxicity to the material as well as the environment. The nanocrystals of CZSS have enhanced the surface to volume ratio properties of the synthesised material. The single quaternary phase, good surface morphology, suitable optical bandgap in the sample B having CZSS nanocrystals may be a very useful material for photovoltaic cell application.

5. CONCLUSION

In this article, we synthesised the CZSS nanocrystals with sulphur variation of the 16 mmol, 18 mmol and 20 mmol thiourea by the co-precipitation method. The spin coater was used to fabricate the thin-films as samples A, B, C and such thin films have been used to analyse the surface morphology of all samples. After the XRD, Raman, and SEM characterisations of the samples A, B and C, it was confirmed that the sample B with 18 mmol thiourea concentration was found the best optimisation with the polycrystalline kesterite phase having the better morphology than the samples A and C. The average crystalline size of sample B was found at 17 nm. The calculated optical band gap of the sample B by UV-vis characterisation was showed the suitable for electron-hole generations. These exciting results demonstrate that the synthesised CZSS NCs by co-precipitation method without sulphurization may be fulfilled the promise of a low-cost thin film for photovoltaic cell application. The novelty of this work lies in the synthesis of CZSS nanocrystals by co-precipitation method without any sulphurization and selenization processes, which is less toxic to the material as well as the environment. By the characterisations analysis of the CZSS NCs of sample B, it has been revealed that the thin film of the CZSS NCs is the economically cheapest and the best material for photovoltaic cell applications.

6. ACKNOWLEDGEMENTS

Mr. Krishan Pal would like to thank University Grant Commission (UGC), New Delhi, India for the financial support through the Rajiv Gandhi National fellowship (F1-17.1/2015-16/RGNF-2015-17-SC-UTT-25302).

7. REFERENCES

1. Katagiri, H. (2005). Cu_2ZnSnS_4 thin film solar cells. *Thin Solid Films*, 480−481, 426−432. https://doi.org/10.1016/j.tsf.2004.11.024
2. Katagiri, H. et al. (2008). Enhanced conversion efficiencies of Cu_2ZnSnS_4-based thin film solar cells by using preferential etching technique. *Appl. Phys. Express*, 1, 041201. https://doi.org/10.1143/APEX.1.041201
3. Zhou, Y. L. et al. (2011). Hierarchical Cu_2ZnSnS_4 particles for a low-cost solar cell: Morphology control and growth mechanism. *J. Phys. Chem. C.*, 115, 19632−19639. https://doi.org/10.1021/jp206728b
4. Collord, A. D. & Hillhouse, H. W. (2015). Composition control and formation pathway of CZTS and CZTGS nanocrystal inks for kesterite solar cells. *Chem. Mater.*, 27, 5, 1855–1862. https://doi.org/10.1021/acs.chemmater.5b00104
5. Sun, Y. et al. (2013). Reaction routes for the formation of a Cu_2ZnSnS_4 absorber material from homogenous ethanol-based solution. *RSC Adv.*, 44, 22095–22101. https://doi.org/10.1039/C3RA42746C
6. Diamond, A. M. et al. (2012). Copperalloyed ZnS as a p-type transparent conducting material. *Phys. Status Solidi A.*, 209(11), 2186–2194. https://doi.org/10.1002/pssa.201228181
7. Bai, X., Milton, F. P. & Gun'ko, Y. K. (2019). Optical properties, synthesis, and potential applications of Cu-based ternary or quaternary anisotropic quantum dots, polytypic nanocrystals, and core/shell heterostructures. *Nanomaterials*, 9, 85–121. https://doi.org/10.3390/nano9010085
8. Su, Z. et al. (2014). Fabrication of Cu_2ZnSnS_4 solar cells with 5.1% efficiency via thermal decomposition and reaction using a non-toxic sol-gel route. *J. Mater. Chem. A*, 2, 500–509. https://doi.org/10.1039/C3TA13533K
9. Liu, W. C. et al. (2013). Facile hydrothermal synthesis of hydrotropic Cu_2ZnSnS_4 nanocrystal quantum dots: Band-gap engineering and phonon confinement effect. *J. Mater. Chem.*, 1, 3182–3186. https://doi.org/10.1039/C3TA00357D
10. Guo, Q., Hillhouse, H. W. & Agrawal, R. (2009). Synthesis of Cu_2ZnSnS_4 nanocrystal ink and its use for solar cells. *J. Am. Chem. Soc.*, 131, 11672–11673. https://doi.org/10.1021/ja904981r
11. Li, M. et al. (2012). Synthesis of pure metastable wurtzite CZTS nanocrystals by facile one-pot method. *J. Phys. Chem. C.*, 116, 26507−26516. https://doi.org/10.1021/jp307346k
12. Pal, K. et al. (2019). Current challenges and future prospects for a highly efficient (> 20%) kesterite CZTS solar cell: A review. *Sol. Energy Mat. Sol. Cells*, 196, 138–156. https://doi.org/10.1016/j.solmat.2019.03.001

13. Scragg, J. J. et al. (2013). Effects of back contact instability on Cu_2ZnSnS_4 devices and processes. *Chem. Mater.*, 25, 3162–3171. https://doi.org/10.1021/cm4015223
14. Pandey, G. & Srivastava, S. K. (2006). A novel synthetic method for the preparation of CuS, and CdS nanochains. *Synthesis and Reactivity in Inorganic, Metal-Organic and Nano-Metal Chemistry*, 36, 663–666. https://doi.org/10.1080/15533170600962455
15. Shrivastava, S. et al. (2010). Study of structural and electronic properties of metallic nanowires: Bi, Na, Cu, Pb. *Journal of Physics: Conference Series*, 245, 012089–012093. https://doi.org/10.1088/1742-6596/245/1/012089
16. Yan, R. et al. (2018). Solution-processed Cu_2ZnSnS_4 thin film with mixed solvent and its application in superstrate structure solar cells. *RSC Adv.*, 8, 11469–11477. https://doi.org/10.1039/C8RA01095A
17. Hamady, S. O. S. et al. (2019). Development of novel thin film solar cells: Design and numerical optimisation. *J. Phys. Sci.*, 30(2), 199–205. https://doi.org/10.21315/jps2019.30.s2.17
18. Smolander, K. et al. (1994). Monomeric (dipropionato-*O*)(dithiourea-*S*) zinc(II). *Acta Crystallogr. Sect. C*, 50, 1900–1902. https://doi.org/10.1107/S0108270194004397
19. Cheng, A. J. et al. (2011). Imaging and phase identification of Cu_2ZnSnS_4 thin films using confocal Raman spectroscopy. *J. Vac. Sci. Technol. A*, 29(5), 051203–051214. https://doi.org/10.1116/1.3625249.
20. Niederberger M. (2007). Nonaqueous sol-gel routes to metal oxide nanoparticles, *Acc. Chem. Res.*, 40(9), 793–800. https://doi.org/10.1021/ar600035e.
21. Himmrich, M. & Haeuseler, H. (1991). Far infrared studies on stannite and wurtzstannite type compounds. *Spect. Chim. Acta Part A: Mol. Spect.*, 47(7), 933–942. https://doi.org/10.1016/0584-8539(91)80283-O
22. Wang, K. et al. (2010). Thermally evaporated Cu_2ZnSnS_4 solar cells. *Appl. Phys. Lett.*, 97, 143508–143511. https://doi.org/10.1063/1.3499284
23. Woo, K., Kim, Y., & Moon, J. (2012). A non-toxic, solution-processed, earth-abundant absorbing layer for thin-film solar cells. *Energy Environ. Sci.*, 5, 5340–5345. https://doi.org/10.1039/C1EE02314D
24. Fernandes, P. A., Salomeand, P. M. P., & da Cunha, A. F. (2010). A study of ternary Cu_2SnS_3 and Cu_3SnS_4 thin films prepared by sulfurizing stacked metal precursors. *J. Phys. D: Appl. Phys.*, 43(21), 215403–215411.
25. Rakhshani, A. E. (2020). Sn-rich CZTS films spin-coated from methanol-based sol-gel solution: Annealing effect on microstructure and optoelectronic properties. *J Solgel Sci Technol.*, 94, 270–278. https://doi.org/10.1007/s10971-020-05262-7.

IOP Publishing *Mater. Res. Express* **6** (2019) 066209 https://doi.org/10.1088/2053-1591/ab1057

Materials Research Express

CrossMark

RECEIVED
28 December 2018

REVISED
1 March 2019

ACCEPTED FOR PUBLICATION
15 March 2019

PUBLISHED
29 March 2019

PAPER

Graphene layers on semi-finite 1D asymmetric periodic structure of Si/Glass materials with defect of nematic liquid crystal for a sensor device

Pawan Singh, Khem B Thapa , Narinder Kumar, Krishan Pal and Devesh Kumar

Department of Physics, School of Physical and Decision Sciences, Babasaheb Bhimrao Ambedkar University, Lucknow, India

E-mail: khem.bhu@gmail.com

Keywords: nematic liquid crystal (NLC), graphene (G), absorption, semifinite 1D asymmetric periodic structure, sensor

Abstract

In this work, the effective absorption property of graphene layers on one-dimensional periodic structure (1DPS) of Si/Glass materials with nematic liquid crystal (NLC) as a defect has been studied theoretically. The graphene sheets are stuck on the one end of Si as well as Glass of the semifinite periodic structure of Si/Glass materials. Now the nematic liquid crystal (NLC) is embedded with the semifinite periodic structure of Si/Glass materials containing graphene layers. Using the transfer matrix method (TMM), the transmission and absorption behavior of graphene layers on semi-finite 1D asymmetric periodic structure of Si/Glass materials with a defect of nematic liquid crystal have been studied. Our results suggest that defect layer of nematic liquid crystal (NLC) in the semi-finite 1D asymmetric periodic structure with graphene layers (G),$(\mathrm{Si}|\mathrm{Glass})^{m}|\mathrm{G}|\mathrm{NLC}|\mathrm{G}|(\mathrm{Si}|\mathrm{Glass})^{n}$ with $m = 3$ & $n = 5$, may be used as sensor device due to high absorption behavior for a specific director angle of molecules of the nematic liquid crystal (NLC). Besides this, the absorption behavior of the structure for TE mode, $(\mathrm{Si}|\mathrm{Glass})^{3}|\mathrm{G}|\mathrm{NLC}|\mathrm{G}|(\mathrm{Si}|\mathrm{Glass})^{5}$, is more effective in comparison to the absorption behavior of the structure for TM mode at normal incidence wave.

1. Introduction

Photonic crystal (PC) belong to a unique class of periodic structure of dielectric materials that control the propagation of electromagnetic wave and exhibit photonic band gap (PBG) regions in the transmission of PC. Photonic Band Gap (PBG) are special regions which do not allow to propagate the electromagnetic wave in that region due to the contrast of refractive index and spatially periodicity of the dielectric materials. Therefore, PCs are divided into three categories depending on the periodic modulation of refractive index; one-dimensional photonic crystal (1DPC), two-dimensional photonic crystal (2DPC) and three-dimensional (3DPC). The behavior of PBG depends on the refractive indices of dielectric materials and geometrical parameters of PCs [1]. PC with a defect layer lead to a variety of applications in different ways due to their unique optical properties [2, 3]. The periodic structure of dielectric materials with tunable defect layer can be used in tunable optical devices. The transmission properties of PCs and the photonic band gap (PBG) can be enhanced by changing the geometrical parameters of dielectric materials [4].

Nonlinear optical properties of the liquid crystal (LC) can be used in electro-optics devices, widely [5–7]. The defect layer of nematic liquid crystal (NLC) in one-dimensional periodic structure shows all-optical switching behavior of PC [8]. To understand switching property of LC, nonlinear differential equation of director has been solved and obtained the relation between intensity ratio (I/I_{fr}) and maximum director angle of LCs [9]. InLC as defect layer in a periodic structure, when the intensity (I) of the electromagnetic wave reaches to threshold intensity, Freedericksz transition (I_{fr}), LC molecules switch according to intensity ratio (I/I_{fr}) and execute tunable transmission of one-dimensional periodic structure [10, 11]. It is well known that LC has nonlinear optical and electronic properties, graphene (G) also novel optical and electronic properties [12].

Broadband reflector of 1D photonic crystal containing TiO_2/SiO_2 material at visible region

Cite as: AIP Conference Proceedings **2220**, 020068 (2020); https://doi.org/10.1063/5.0002138

Asish Kumar, Pawan Singh, Krishan Pal, Narendra Kumar, and Khem B. Thapa

Absorption and bandwidth properties of graphene based 1D-photonic crystal for THz devices

Cite as: AIP Conference Proceedings **2220**, 020084 (2020); https://doi.org/10.1063/5.0001755

Roshni Maurya, Pawan Singh, Prabal P. Singh, Krishan Pal, Girijesh N. Pandey, and Khem B. Thapa

AIP Conference Proceedings **2220**, 020084 (2020); https://doi.org/10.1063/5.0001755

AIP Conference Proceedings

Low cost synthesis of ZnO nano-particles, and characterization study for the device of water disinfection

Cite as: AIP Conference Proceedings **2220**, 020170 (2020); https://doi.org/10.1063/5.0002142

Varsha Gautam, Krishan Pal, Narendra Kumar, Girijesh N. Pandey, B. Suthar, Khem B. Thapa, and S. P. Ojha

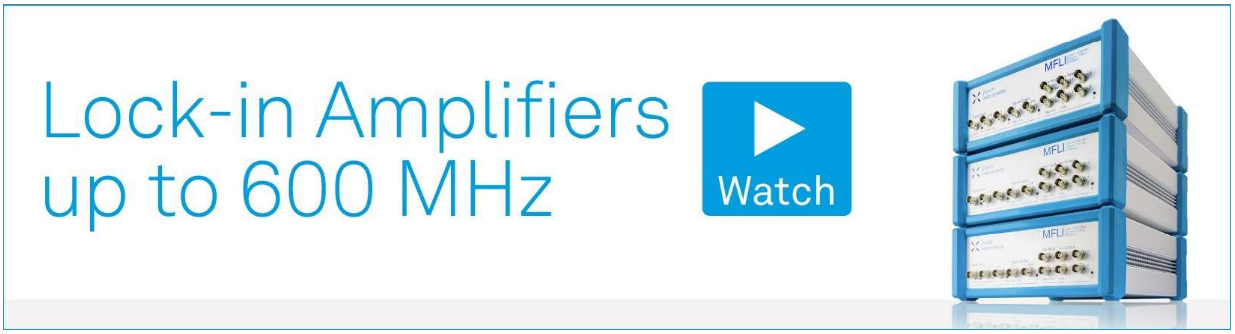

AIP Conference Proceedings **2220**, 020170 (2020); https://doi.org/10.1063/5.0002142 **2220**, 020170

Chapter

Embedded Liquid Crystal Defect with Graphene Layers in Asymmetric One-Dimensional Photonic Crystal as Sensor Application

By Pawan Singh, Krishan Pal, Khem B. Thapa, Narinder Kumar, Devesh Kumar

Book Advances in Photonic Crystals and Devices (https://www.taylorfrancis.com/books/mono/10.1201/9781351029421/advances-photonic-crystals-devices?refId=ec6b45f8-78e7-47aa-9da1-f7523190d751)

Edition	1st Edition
First Published	2019
Imprint	CRC Press
Pages	22
eBook ISBN	9781351029421

ABSTRACT

< Previous Chapter (chapters/edit/10.1201/9781351029421-7/properties-electromagnetic-density-mode-acoustically-perturbed-photonic-crystal-ayush-aman-yogesh-sharma-surendra-prasad-vivek-singh)

Next Chapter > (chapters/edit/10.1201/9781351029421-9/tunable-broadband-reflector-using-one-dimensional-photonic-crystal-containing-metamaterial-symmetrically-introduced-magnetized-cold-plasma-defect-asish-kumar-khem-thapa-narendra-kumar-anil-yadav)